Oxidation catalysis under green chemistry conditions

Yun Wang

Université Fédérale
Toulouse Midi-Pyrénées

THÈSE

En vue de l'obtention du

DOCTORAT DE L'UNIVERSITÉ DE TOULOUSE

Délivré par l'Université Toulouse 3 - Paul Sabatier

Présentée et soutenue par

Yun WANG

Le 7 novembre 2019

Catalyseurs d'oxydation en conditions de chimie verte : métaux non toxiques, eau oxygénée, transformation de la biomasse, recyclage par greffage

---

Ecole doctorale : **SDM - SCIENCES DE LA MATIERE - Toulouse**

Spécialité : **Chimie Organométallique et de Coordination**

Unité de recherche :
LCC - Laboratoire de Chimie de Coordination

Thèse dirigée par
Dominique AGUSTIN et Pascal GUILLO

Jury

M. Alexander SOROKIN, Rapporteur
Mme Anna COMPANY CASADEVALL, Rapporteure
Mme Montserrat GOMEZ, Examinatrice
M. Ahmad MEHDI, Examinateur
M. Dominique AGUSTIN, Directeur de thèse
M. Pascal GUILLO, Co-directeur de thèse

Remerciements

Ces travaux de recherche ont été réalisés au sein de Laboratoire de Chimie de coordination (LCC) et au laboratoire de recherche situé à l'IUT A Paul Sabatier de Castres.

Je remercie tout d'abord le Syndicat Mixte de la Communauté d'Agglomération Castres – Mazamet, l'IUT A Paul Sabatier et la région Occitanie pour le financement de ma bourse de thèse. Je remercie aussi le LCC et le Département de Chimie de l'IUT à Castres pour leur soutien matériel.

J'exprime mes sincères remerciements à mes directeurs de thèse, Dr. Dominique Agustin et Dr. Pascal Guillo, pour m'avoir fourni cette opportunité de travailler sur un sujet de recherche passionnant et m'avoir guidé dans mes travaux avec patience.

Merci aux responsables de l'équipe de recherche, Prof. Rinaldo Poli et Dr. Eric Manoury, pour leurs suggestions constructives. Merci à Dr. Jean-Claude Daran pour la détermination par Rayons-X des nombreuses structures. Je remercie Dr. Florence Gayet pour les analyses DLS ainsi que la préparation des échantillons pour les analyses TEM faites par Vincent Collière. J'exprime mes remerciements au Dr. Yannick Coppel pour les analyses RMN solide.

Evidemment, je remercie tous les membres de jury d'avoir pris part à la soutenance. Notamment les docteurs Alexander Sorokin et Anna Company Casadevall pour avoir accepté d'être les rapporteurs de ce manuscrit. Je n'oublie pas les évaluateurs, les Professeurs Montserrat Gómez et Ahmad Mehdi qui ont accepté d'évaluer mes travaux de recherches. Tous les membres du jury ont donné leurs avis précieux sur la correction du manuscrit.

Dans la vie de tous les jours à Castres, de nombreux jeunes chercheurs ont travaillé au laboratoire. Les échanges étaient intéressants et fructueux, du point de vue scientifique et humain. Pour cela, je tiens à remercier plus particulièrement mon compatriote Xuming Zhang pour son aide précieuse à la détermination des tailles des nanoparticules, mon collègue de paillasse Abdelhak Lachguar pour les discussions scientifiques, ainsi que la délégation croate (Dr. Jana Pisk et les étudiantes Maja Hanic, Sanja Renka, Arijeta Bafti, Marta Razum, Josipa Mihalinec) pour leur bonne humeur.

Je tiens à remercier l'ensemble d'équipe G, les personnels du LCC et du Département chimie de IUT Castres qui m'ont aidé tout au long de ma thèse.

Enfin, j'exprime la plus grande gratitude à mes parents pour leur support afin que je puisse faire mes études en France sans soucis.

Table of contents

List of abbreviations

LCC : Laboratoire de Chimie de Coordination
OAT: Oxygen Atom Transfer
TBHP: *tert*-Butyl HydroPeroxide
NDO: Naphthalene DiOxygenase
NADP: Nicotinamide Adenine Dinucleotide Phosphate
OEC: Oxygen Evolving Center
MMO: Methane MonoOxygenase
Cyt: Cytochrome
Tren: tris(2-aminoethyl)amine
HFIP: HexaFluoroIsoPropanol
POM: PolyOxoMetalates
HPAs: HeteroPolyAcids
ODS: Oxidative DeSulfurization
PS: PolyStyrene
SBA: Santa Barbara Amorphous-15
MCM-41: Mobil Composition of Matter No. 41
MCF: Mesostructured Cellular Foam
APTES: (3-Aminopropyl)triethoxysilane
DPM: Dipyridylmethylene
BPMEN: N,N′-dimethyl-N,N′-bis(pyridin-2-ylmethyl)ethane-1,2-diamine
OTf: Trifluoromethanesulfonate
CO: CycloOctene
COE: CycloOctene Epoxide
H_2ases: Dihydrogenases
LCBM: Laboratoire de Chimie et Biologie des Métaux
SiO_2@CN: Silica particles functionalized by pending nitrile functions
SiO_2@COOH: Silica particles functionalized by pending carboxylic functions
m-CPBA: Meta-ChloroPeroxyBenzoic Acid
DCE: 1,2-DiChloroEthane
Me_3tacn: 1,4,7-Trimethyl-1,4,7-triazacyclononane
CP: Cross-Polarization
p-Ts: Para-toluenesulfonate
TEOS: TetraEthyl OrthoSilicate
TESPN: 3-(Triethoxysilyl)propionitrile
TEM: Transmission Electron Microscope
DLS: Dynamic Light Scattering
IR: Infrared Spectroscopy

NMR: Nuclear Magnetic Resonance
MAS: Magic Angle Spinning
CH: CycloHexene
CHO: CycloHexene Oxide
CHD: CycloHexaneDiol
Chol: Cyclohexene-1-ol
CHone: CycloHexen-1-one
TON: TurnOver Number
TOF: TurnOver Frequency
CYol: Cyclohexanol
CYone: Cyclohexanone
SiO_2@PW: Silica particles grafted with $H_3PW_{12}O_{40}$
SiO_2@PMo: Silica particles grafted with $H_3PMo_{12}O_{40}$
PPI: Poly(Propylene Imine)
DMF: N, N-Dimethylformamide
DMSO: Dimethyl sulfoxide
ATR: Attenuated Total Reflection
GC: Gas Chromatography
HPAN: HeteroPolyANion

Résumé en français

Introduction

Dans le contexte actuel de prise de conscience de protection de l'environnement, des méthodes permettant de remplacer les procédés chimiques traditionnels par des procédés plus « propres » sont à l'étude. Parmi les 12 principes de la chimie verte, la catalyse est un principe exploré dans ce manuscrit.

Au sein de l'équipe G (Ligands, Architectures Complexes et Catalyse) du LCC et plus particulièrement sur le site de Castres, un aspect important des thématiques de recherche d'une partie de l'équipe est de développer de nouveaux catalyseurs pour plusieurs types de réactions, notamment des réactions d'oxydation.

Pour cela, différentes stratégies sont explorées :

- l'utilisation de complexes métalliques de Mo, V et W basés sur des ligands tridentes ONO et ONS ainsi que des polyoxométallates (POMs) pour des réactions d'(ép)oxydation sans utiliser de solvants organiques.
- le développement de complexes de Fe et de Mn basés sur des ligands polyazotés avec une seconde sphère de coordination modifiée afin de créer un réseau de liaison H avec H_2O_2 pour des réactions de transfert d'atome d'oxygène.

Plus précisément, ces travaux de thèse se sont focalisés sur des réactions d'(ép)oxydations catalysées. Différentes approches ont été explorées pour obtenir :

(i) des informations sur les paramètres à améliorer pour rendre plus efficace le processus de transfert d'atome d'oxygène.

(ii) des procédés d'oxydations plus respectueux de l'environnement.

Parmi les différentes conditions de réactions d'époxydation catalytiques décrites dans la littérature, l'utilisation de complexes métalliques de Mn et Fe comme catalyseurs, avec H_2O_2 comme oxydant, permet la formation sélective d'époxydes sans formation de *cis*-diol lorsque la réaction est réalisée en présence d'acide carboxylique comme co-réactif. Des métalloenzymes de type oxygénase ont montré la même réactivité pour ces mêmes processus d'oxydation grâce à la présence de réseaux de liaisons H dans la seconde sphère coordination des sites actifs.

A partir de ces résultats, deux stratégies ont été envisagées pour remplacer l'acide acétique dans les réactions d'époxydation :

(i) Introduire sur des complexes métalliques une seconde sphère de coordination capable de créer un réseau de liaisons H avec H_2O_2 et faciliter son activation par le centre métallique. Cette étude fait partie du Chapitre 2.

(ii) Utiliser des objets (ici des particules de silice fonctionnalisées) possédant des fonctions COOH pour remplacer l'acide acétique. Idéalement, ces objets pourraient être réutilisables. Cette étude est décrite Chapitre 3.

Afin de pouvoir réutiliser les catalyseurs, une autre stratégie a été explorée. Celle-ci consiste en l'immobilisation de catalyseurs moléculaires sur un support solide (ici des nanoparticules de silice fonctionnalisées). Concernant les types de catalyseurs, des polyoxométallates commerciaux efficaces pour les réactions d'(ép)oxydation (déjà étudiés par notre équipe mais d'une autre manière) ont été sélectionnés. L'immobilisation de ces polyoxométalates sur des particules de silice est aussi un des objectifs de ces travaux qui est présenté Chapitre 4.

Cette thèse est une combinaison de ces trois stratégies qui vont être présentées dans les différents chapitres.

Chapitre 2. Influence de la seconde sphère coordination en catalyse d'oxydation

La seconde sphère coordination de complexes métalliques (notamment de type fluoroalcool) pourrait favoriser l'activation et la stabilisation d'intermédiaires réactionnels impliqués dans les processus de réactions de transfert d'atome d'oxygène (voir schéma 1).

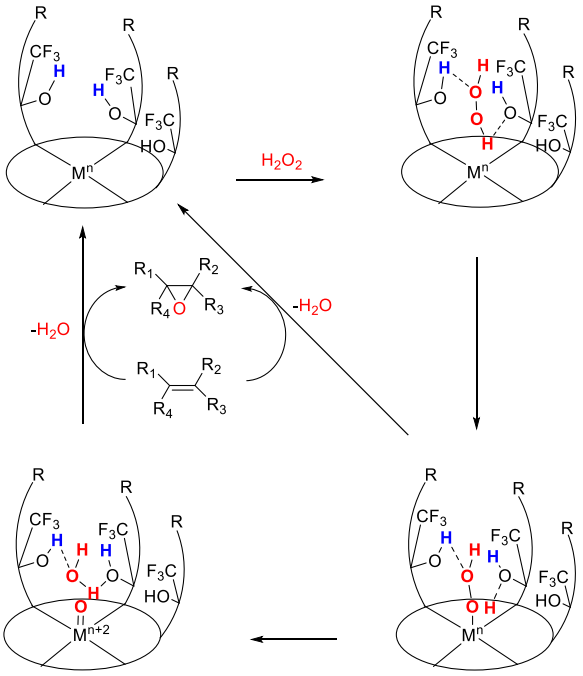

Schéma 1 – Cycle catalytique possible pour une réaction d'époxydation catalysée par un complexe métallique avec des fonctions fluoroalcools.

Pour évaluer cette hypothèse, trois familles de ligands polyazotés (fonctionnalisés avec des groupes fluoroalcools ou méthyles (schéma 2)) et les complexes métalliques correspondants ont été synthétisés. Ces synthèses, ainsi que l'étude de leur réactivité pour des réactions d'époxydation et de photoréduction du proton, sont décrites dans ce chapitre.

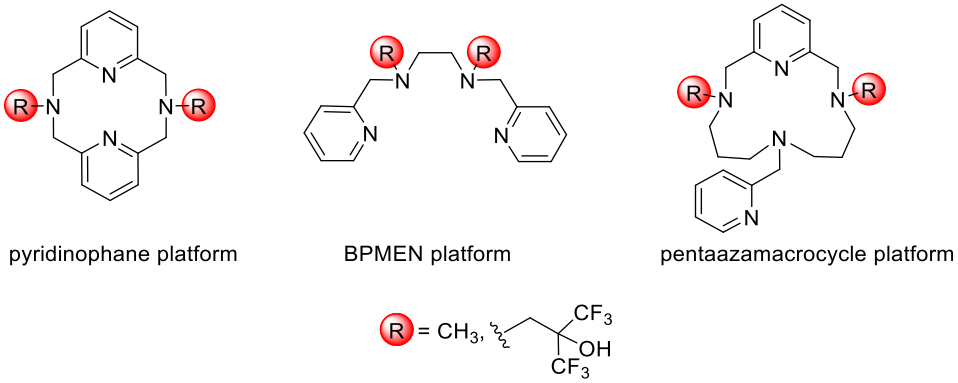

Schéma 2 – Différents ligands envisagés.

Platforme pyridinophane

Les ligands L^1 et L^2, basés sur le ligand pyridinophane (L^1 = version méthyle du ligand pyridinophane, L^2 = version fluoroalcool du ligand pyridinophane) ont été synthétisés avec succès (Schéma 3).

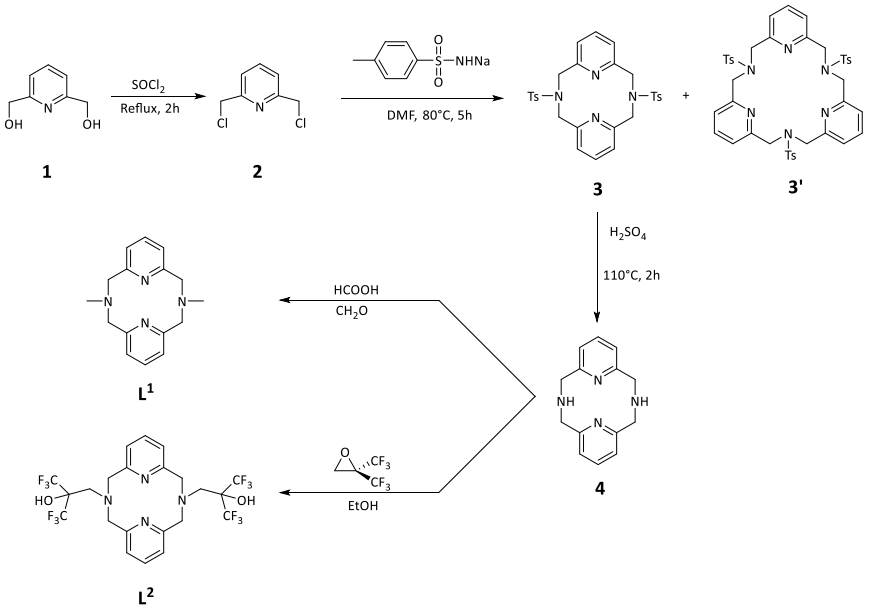

Schéma 3 – Synthèse des ligands L^1 et L^2.

Ces deux ligands ont été notamment caractérisés par RMN ^1H et ^{13}C ainsi que par diffraction des rayons X (Figure 1).

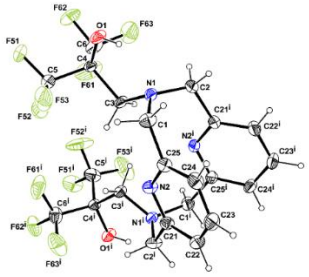

Figure 1 – Structure du ligand L^2.

A partir de **L²**, six nouveaux complexes ont été synthétisés, isolés et caractérisés, notamment par diffraction des rayons X (Schéma 4 et Figure 2). Concernant le complexe [(**L²**)$FeCl_2$]($FeCl_4$), quelques soient les conditions réactionnelles, $FeCl_4^-$ est toujours présent. Concernant les complexes de manganèse, lorsque la réaction est réalisée avec $MnCl_2$, un complexe mononucléaire de Mn est obtenu. Par contre, l'utilisation de $Mn(OTf)_2$ comme précurseur conduit à la formation du complexe (**L²**)Mn_2 possédant deux centres manganèse pour un ligand et ce quelques soient les conditions utilisées.

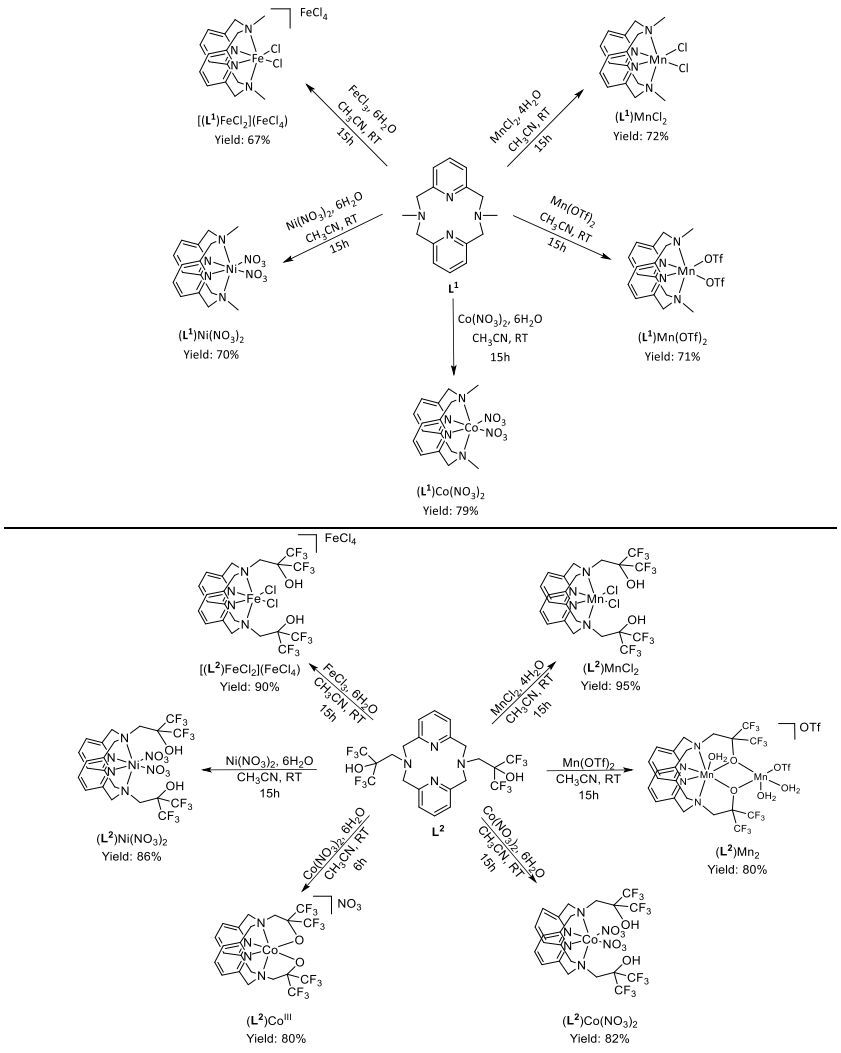

Schéma 4 – Complexes obtenus avec **L¹** et **L²**.

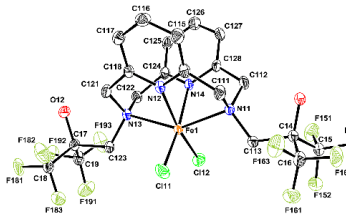

$[(L^2)FeCl_2](FeCl_4)$

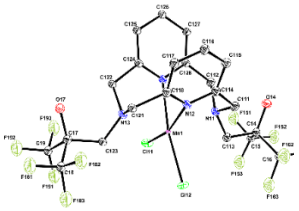

$(L^2)MnCl_2$

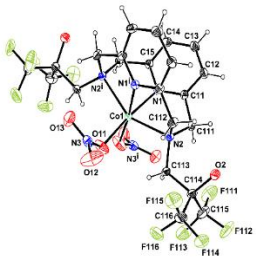

$(L^2)Co(NO_3)_2$

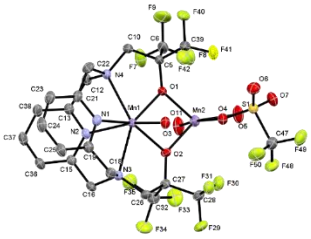

$(L^2)Mn_2$

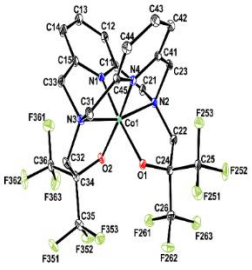

$(L^2)Co^{III}$

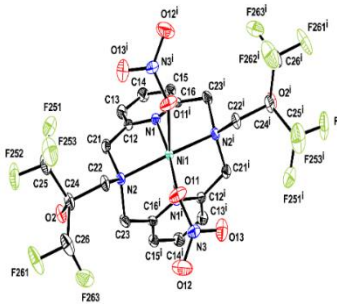

$(L^2)Ni(NO_3)_2$

Figure 2 – Structures des complexes obtenus avec L^2.

$(L^2)Ni(NO_3)_2$ et $(L^2)Co(NO_3)_2$ ont été obtenus sans difficulté. Cependant, dans le cas du complexe de cobalt, un temps de réaction prolongé entraine la formation d'un complexe de Co^{III}, $(L^2)Co^{III}$, par déprotonation des fonctions fluoroalcools suivie de leur coordination sur le centre métallique.

L'obtention des structures cristallographiques de ces six complexes (Figure 2) a confirmé leur formation.

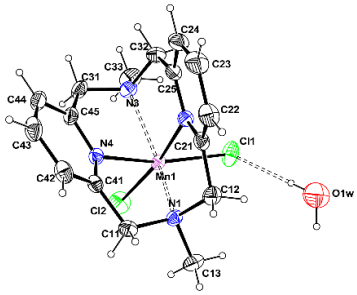

$(L^1)MnCl_2$

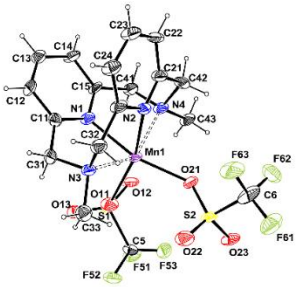

$(L^1)Mn(OTf)_2$

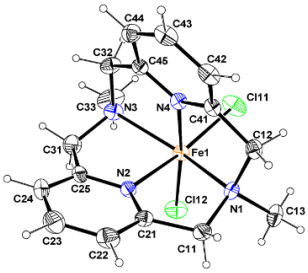

$[(L^1)FeCl_2](FeCl_4)$

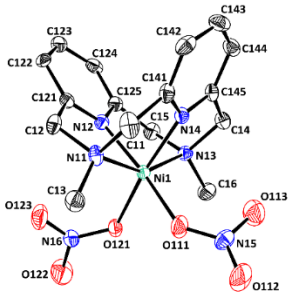

$(L^1)Ni(NO_3)_2$

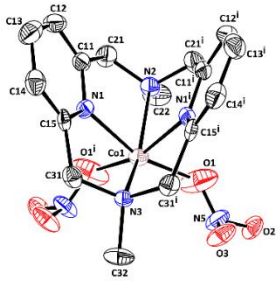

$(L^1)Co(NO_3)_2$

Figure 3 – Structures des complexes obtenus avec L^1.

Avec le ligand **L¹**, une réactivité similaire a été observée et cinq complexes ((**L¹**)Mn(OTf)$_2$, (**L¹**)MnCl$_2$, (**L¹**)Ni(NO$_3$)$_2$, (**L¹**)Co(NO$_3$)$_2$ et (**L¹**)Co(NO$_3$)$_2$) ont été obtenus. Il est à noter que contrairement au ligand **L²**, le complexe de Co^{II} n'évolue pas en Co^{III}.

Plateforme BPMEN

Les ligands **L³** et **L⁴** ont été synthétisés comme représenté dans le schéma 5. Ces deux ligands ont été caractérisés par RMN et diffraction des rayons X pour **L⁴**.

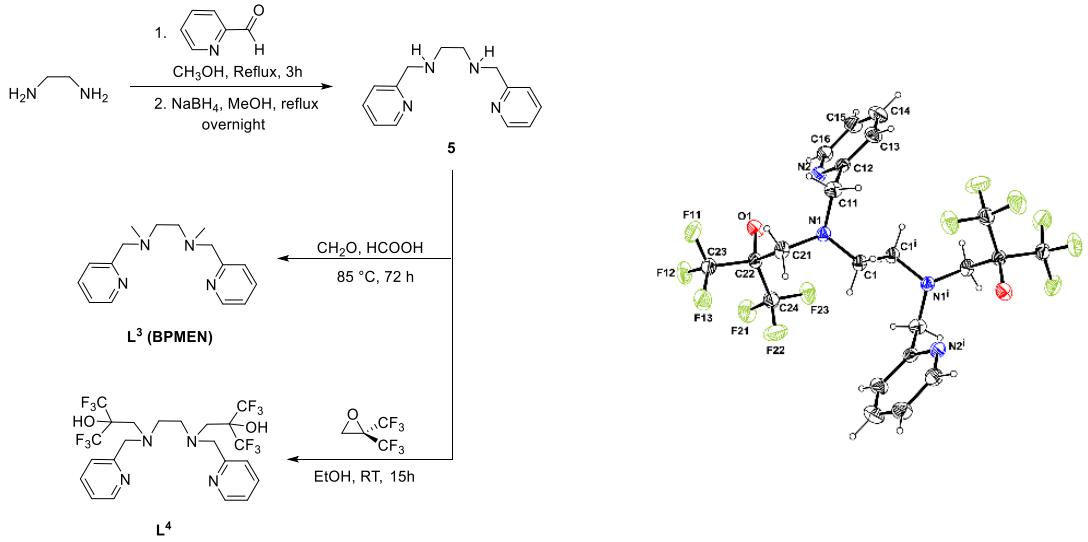

Schéma 5 – Synthèse des ligands **L³** et **L⁴** et structure de **L⁴**.

Plusieurs complexes ont été isolés avec **L³** et ils seront décrits dans le chapitre 3. Cependant, avec le ligand **L⁴**, aucun complexe n'a été obtenu.

Plateforme pentaazamacrocycle

Il est espéré que les complexes possédant un ligand macrocyclique pentaazoté puissent être actifs dans des processus de transfert d'atomes d'oxygène à l'aide de la seconde sphère coordination. La voie de synthèse est décrite dans le schéma suivant :

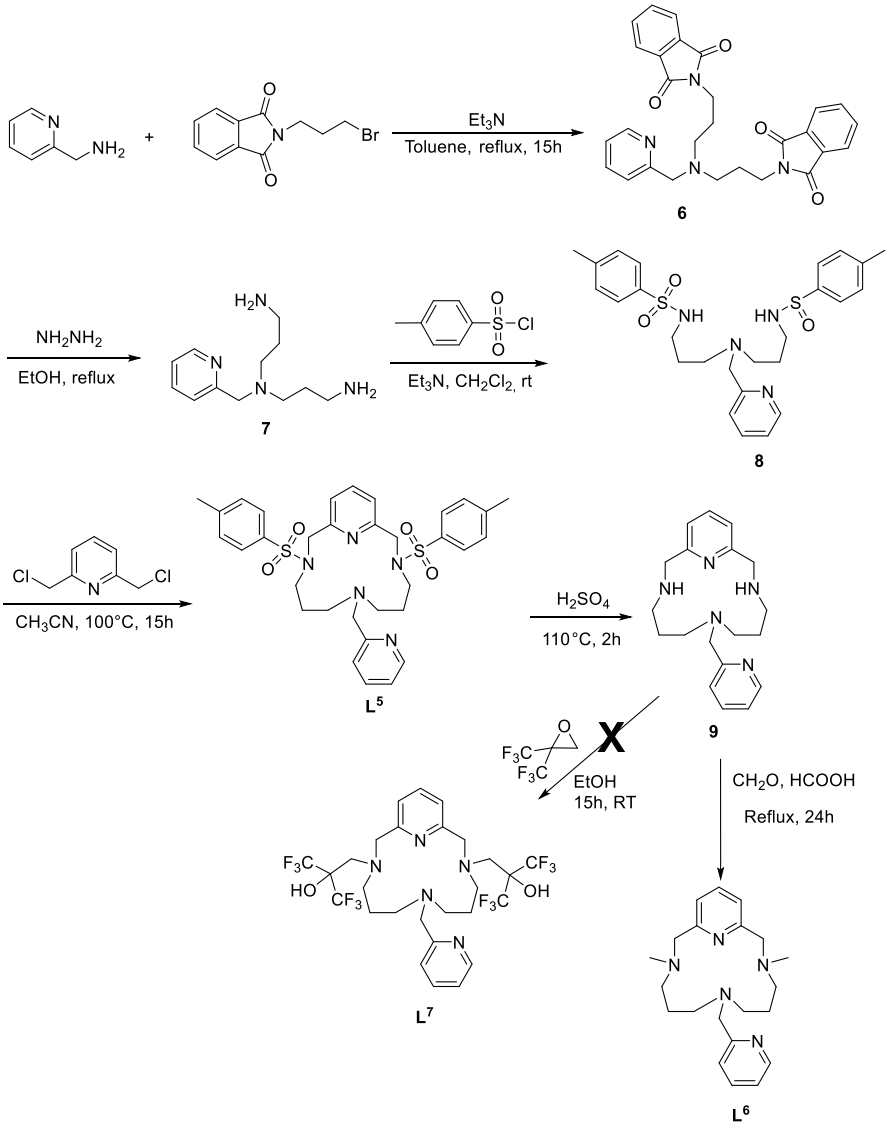

Schéma 6 – Synthèse des ligands L^5 et L^6.

Avec cette procédure, L^5 et L^6 ont été obtenus, mais l'accès à L^7 s'est avéré impossible.

Tests catalytiques avec les complexes dérivés des ligands L^1 et L^2.

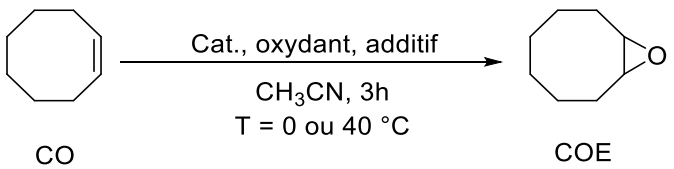

Schéma 7 – catalyse d'oxydation du cyclooctène.

Afin de tester l'activité catalytique des complexes dérivés des ligands L^1 et L^2, le cyclooctène (CO) a été choisi comme substrat modèle et H_2O_2 comme oxydant. Les conditions décrites dans la littérature (0°C, 1.5 équivalent de H_2O_2) ont été reproduites.

Table 1- Oxydation du cyclooctène avec et sans complexes métalliques. [a]

	Catalyseur	T (°C)	CH_3COOH (equiv.)	oxydant	CO Conv[b]	COE sel[c]
0-1	no	0	0	H_2O_2	0	0
0-2			14		0	0
0-3		40	0		0	0
0-4			14		8	<1
1-1	(L^1)$MnCl_2$	0	0	H_2O_2	2	0
1-2				TBHP	2	10
1-3			14	H_2O_2	0	0
1-4				TBHP	1	0
2-1	(L^2)$MnCl_2$	0	0	H_2O_2	0	0
2-2				TBHP	0	0
2-3		40		H_2O_2	12	0
2-4				TBHP	21	0
3-1	(L^2)Mn_2	0	0	H_2O_2	3	0
3-2			14		39	0
3-3		40	0		11	0
3-4			14		3	3
4-1	[(L^2)$FeCl_2$]($FeCl_4$)	0	0	H_2O_2	6	9
4-2			14		6	4
4-3		40	0		33	13
4-4			14		26	6
5-1	[(L^1)$FeCl_2$]($FeCl_4$)	0	0	H_2O_2	11	2
5-2			14		10	1
5-3		40	0		17	4
5-4			14		19	5

[a] Conditions expérimentales: t=3h
Cat. /oxydant/CO/CH_3COOH=1/150/100/1400 avec CH_3COOH;
Cat. /oxydant/CO=1/150/100 sans CH_3COOH;
[b] n CO converti/n CO engagé (in%) en fin de réaction.
[c] n COE formé/ n CO converti en fin de réaction.

Les résultats montrent que quelques soient les conditions testées, même en présence d'acide acétique, une faible conversion du cyclooctène est observée.

Etude de l'activité catalytique des Ni et Co complexes pour la photoréduction du proton.

Inspirée par les enzymes de type hydrogénases réalisant la réduction de H^+ en H_2, la capacité des complexes de Co et de Ni à réaliser cette réaction a été testée. Plus particulièrement, le rôle des fonctions fluoroalcools en tant que relais de protons a été évalué. En utilisant un complexe d'iridium comme photosensibilisateur et la triéthylamine comme donneur sacrificiel d'électrons, les résultats présentés dans la figure suivante ont été obtenus :

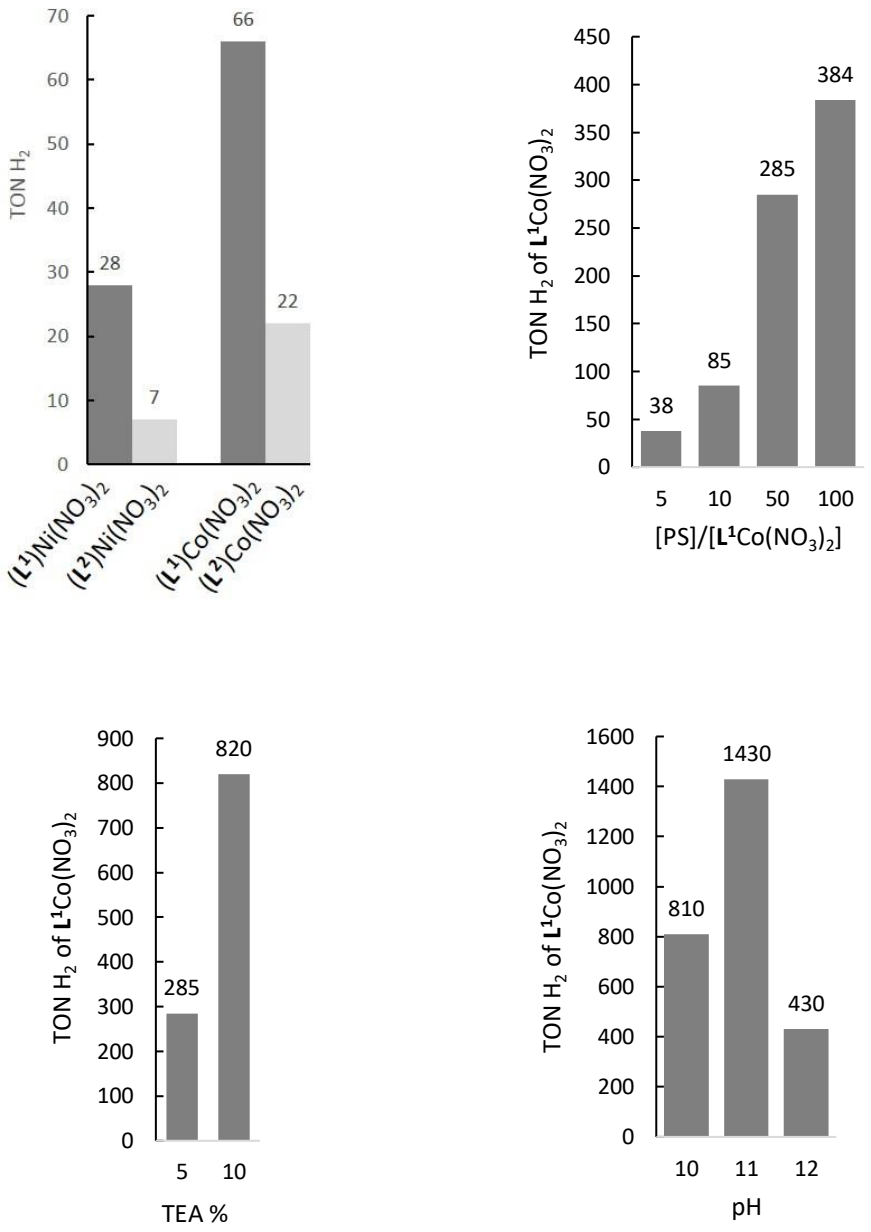

Figure 4 - En haut à gauche : formation de H_2 catalysée par (**L¹**)$Ni(NO_3)_2$, (**L²**)$Ni(NO_3)_2$, (**L¹**)$Co(NO_3)_2$, (**L²**)$Co(NO_3)_2$. Conditions : H_2O/CH_3CN 1:1, [cat] = 50 µM, [PS] = 500 µM, pH = 10, TEA, 5%. En haut à droite : Effet du ratio [PS]/[(**L¹**)$Co(NO_3)_2$] sur la formation de H_2. Conditions : H_2O/CH_3CN 1:1, [(**L¹**)$Co(NO_3)_2$] = 10 µM, pH = 10, TEA 5%. En bas à gauche : Effet de la concentration du donneur d'électron sur la formation de H_2 photocatalysée par (**L¹**)$Co(NO_3)_2$. Conditions: H_2O/CH_3CN 1:1, [(**L¹**)$Co(NO_3)_2$] = 10 µM, [PS]/[(L1)Co(NO3)2] = 50, pH = 10. En bas à droite : Effet du pH sur la formation de H_2 photocatalysée par (**L¹**)$Co(NO_3)_2$. Conditions: H_2O/CH_3CN 1:1, [(**L¹**)$Co(NO_3)_2$] = 10 µM, [PS]/[(**L¹**)$Co(NO_3)_2$] = 50, TEA 10%. PS = Photosensibilisateur, TON H_2 = nH_2/ncat.

Ces résultats montrent que les ligands de type pyridinophane sont adaptés à la photoproduction de H_2. Plus particulièrement, le complexe de Co avec un groupe méthyle montre un TON élevé et est plus actif que le complexe de Ni. Aucun effet positif des groupements fluoroalcools n'a pu être mis en évidence.

Chapitre 3 – Remplacement de l'acide acétique par des (nano)particules de silice SiO_2@COOH pour des réactions d'(ép)oxydation avec des complexes de Mn et de Fe basés sur le ligand BPMEN.

Ce chapitre décrit la stratégie développée pour substituer l'acide acétique, co-réactif volatile utilisé pour favoriser la formation d'époxydes lors de réactions d'oxydation d'alcènes, par des billes de silice fonctionnalisées par des fonctions carboxyliques pendantes. La synthèse et la caractérisation de ces billes de silice ainsi que leur utilisation en catalyse d'(ép)oxydation y sont décrites.

Synthèse de complexes métalliques basés sur le ligand BPMEN (L^3)

Pour étudier l'influence du contre ion sur l'activité catalytique lors de l'utilisation des billes de silice fonctionnalisées, trois complexes de Mn^{II} avec différents anions et un complexe de Fe^{III} ont été synthétisés selon la procédure décrite dans le schéma 8.

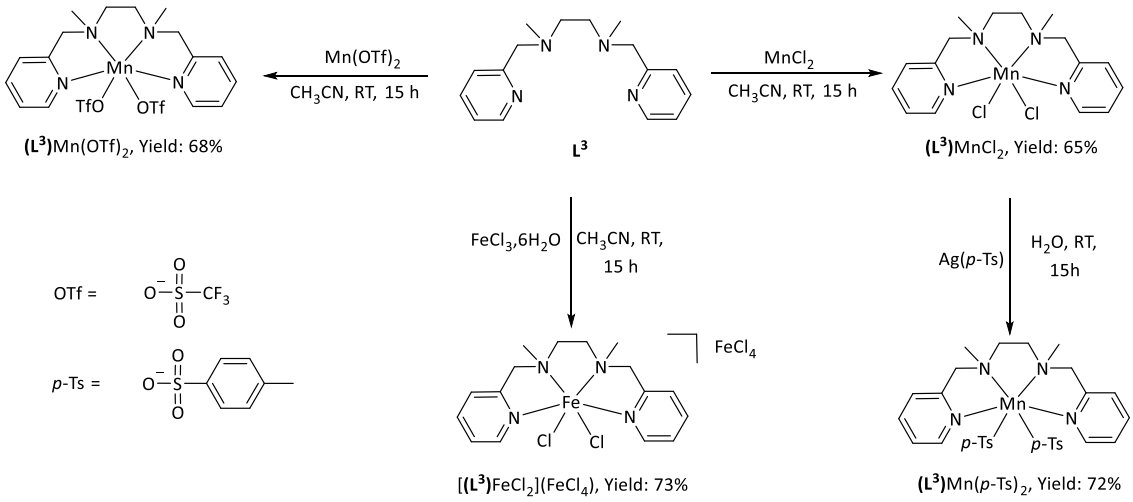

Schéma 8- Synthèse des complexes de Mn et de Fe.

L'obtention de leurs structures cristallographiques a notamment permis de confirmer leur formation (Figure 5).

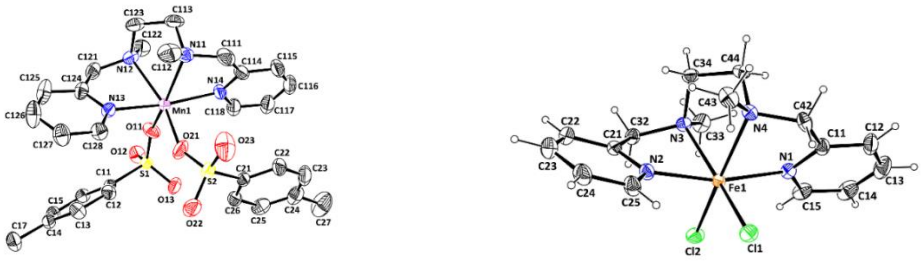

$(L^3)Mn(p\text{-}Ts)_2$ $[(L^3)FeCl_2](FeCl_4)$

Figure 5- Structures de $(L^3)Mn(p\text{-}Ts)_2$ et $[(L^3)FeCl_2](FeCl_4)$.

Synthèse de la silice fonctionnalisée (SiO_2@COOH)

Les particules de silice **SiO_2@COOH** ont été obtenues en trois étapes :

1. Hydrolyse de $Si(OEt)_4$ (TEOS) en particules de SiO_2.
2. Fonctionnalisation des particules de SiO_2 en **SiO_2@CN** par le 3-(Triethoxysilyl)propionitrile (TESPN).
3. Hydrolyse de **SiO_2@CN** en **SiO_2@COOH.**

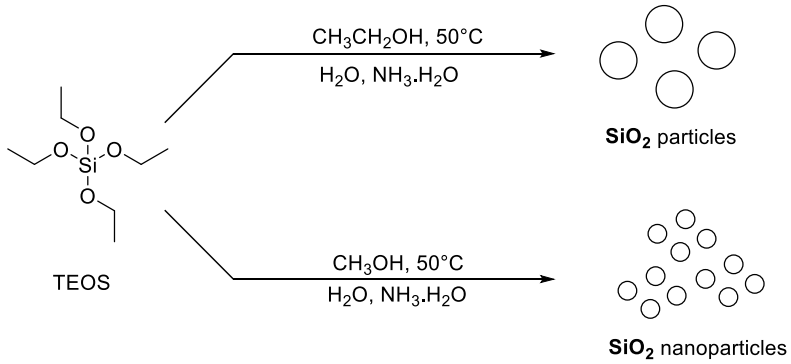

Schéma 9- Synthèse des (nano)particules de SiO_2.

Dans notre cas, deux lots de particules de silice avec des tailles différentes ont été synthétisées dans deux solvants différents (EtOH et MeOH). Quand la polarité du solvant augmente, la taille des particules de SiO_2 diminue. Ces deux différentes tailles de silice seront comparées dans les catalyses d'oxydation.

L'étape suivante est la fonctionnalisation de **SiO_2** en **SiO_2@CN** puis l'hydrolyse de la fonction nitrile en acide carboxylique (Voir schéma suivant).

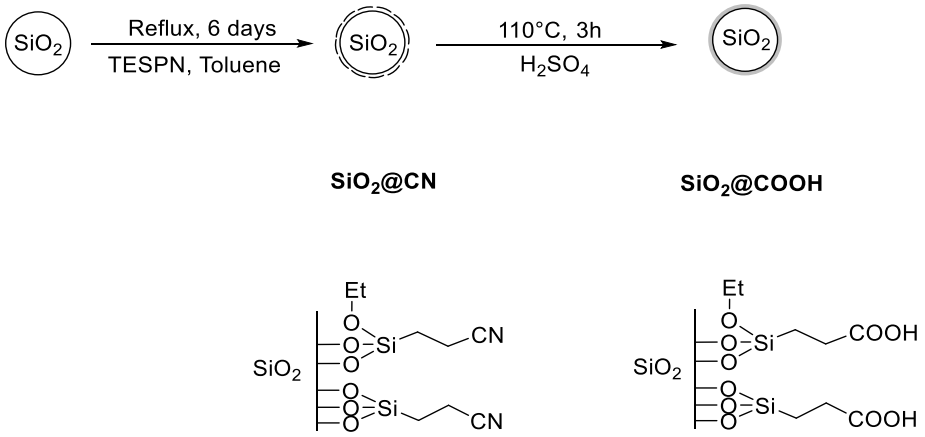

Schéma 10- synthèse de **SiO_2@CN** et **SiO_2@COOH.**

Caractérisation par TEM

Les tailles des particules de silice ont été calculées par rapport aux images des TEM et seront comparées avec les résultats de DLS. Pour les particules synthétisées dans l'éthanol, les tailles sont environ de 430-440 nm alors que des tailles de 62-66 nm ont été observées pour les particules de silice synthétisées dans le méthanol.

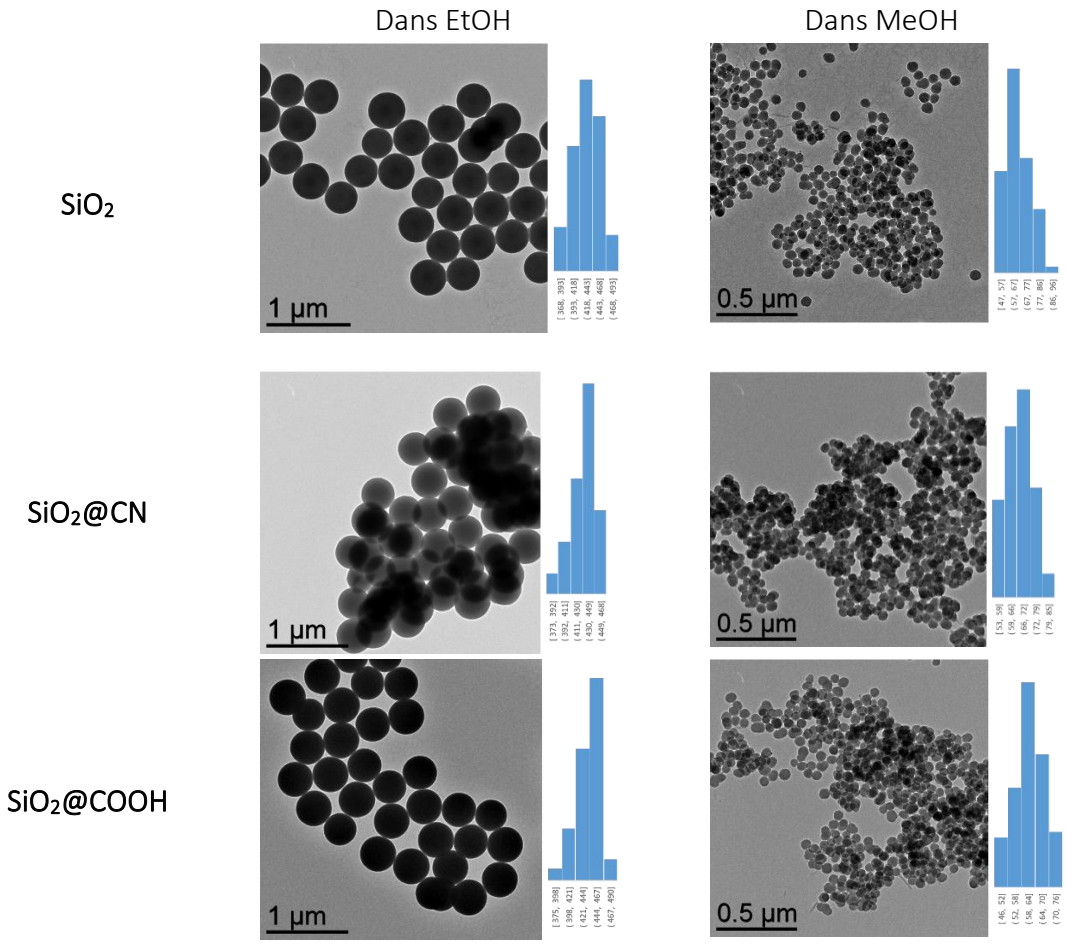

Figure 6- Images de TEM de **SiO_2**, **SiO_2@CN** et **SiO_2@COOH**.

Caractérisation par DLS

La monodispersité est un paramètre important pour étudier l'homogénéité de la taille et pour calculer le taux de couverture des billes de silice non-poreuses **SiO_2@CN** et **SiO_2@COOH**. Une agglomération est observée en DLS, ne permettant pas d'observer les mêmes tailles que sur les images de TEM. Pour les silices réalisées dans EtOH, des tailles entre 400-450 nm sont observées, alors que des tailles de 68-190 nm sont obtenues pour les billes de silice synthétisées dans MeOH.

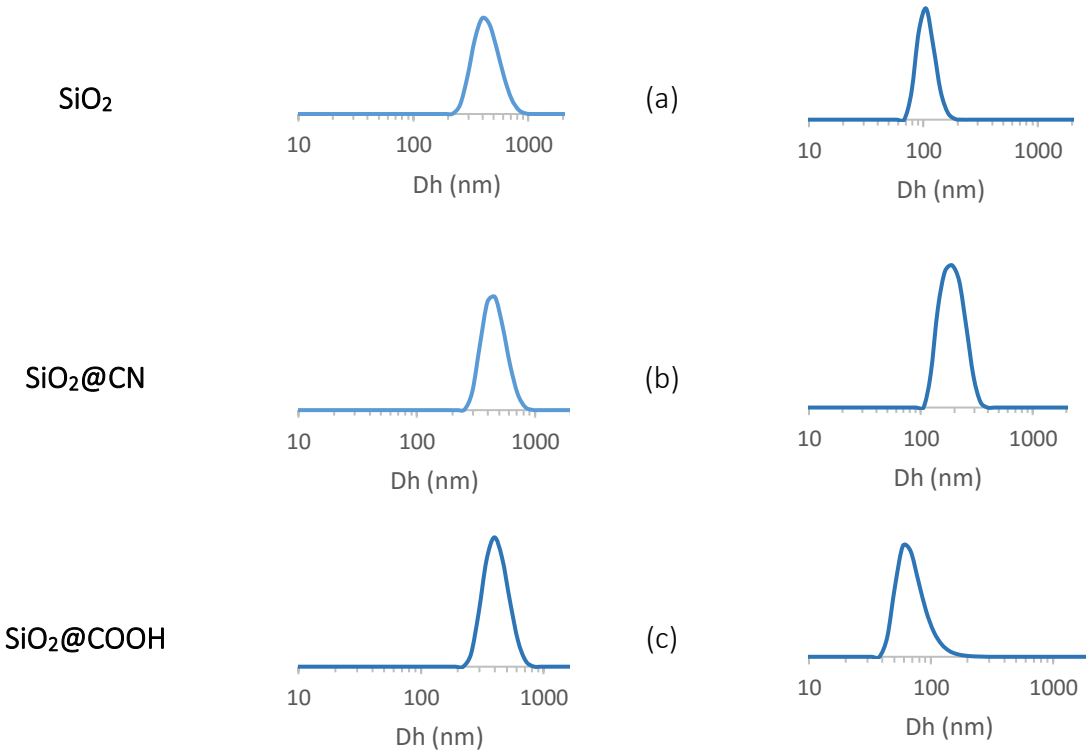

Figure 7- distribution des diamètres hydrodynamique de **SiO_2** (a), **SiO_2@CN** (b) et **SiO_2@COOH** (c).

Caractérisation par spectroscopie infrarouge.

Les vibrations classiques de **SiO_2** ont été observées par IR. Dans le cas de **SiO_2**, la bande à 793 cm^{-1} correspond à la vibration symétrique Si-O-Si, celle à 945 cm^{-1} à Si-OH, celle à 1060 cm^{-1} à Si-O-Si asymétrique. Dans la zone 3700-2930 cm^{-1} sont observées les vibrations associées aux vibrations-OH.

Pour **SiO_2@CN**, les vibrations à 2250 cm^{-1} correspondent à-CN et celles à 2832 cm^{-1} aux vibrations de-CH. La présence de fonctions carboxyliques peut être détectée par la vibration de C=O pour **SiO_2@COOH** à 1712 cm^{-1}. Le taux de couverture des fonctions des billes de silice préparées dans EtOH étant faible, les vibrations sont donc difficiles à observer directement par IR. Cependant, ces vibrations peuvent être observées en faisant la différence de spectres entre **SiO_2@CN** ou **SiO_2@COOH** avec **SiO_2**.

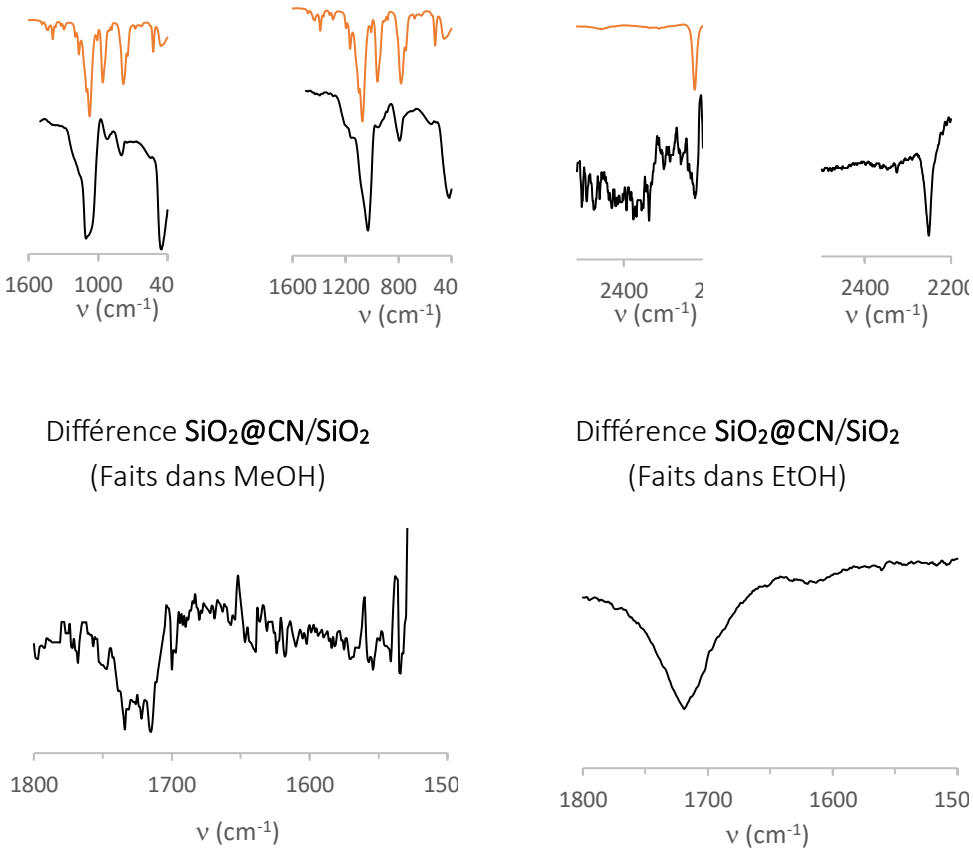

Figure 8- Différence des spectres IR des fonctions caractéristiques entre **SiO_2@CN**, **SiO_2@COOH** et **SiO_2**.

Caractérisation par RMN solide.

La RMN est une autre méthode pour confirmer l'existence des organosilanes à la surface de particules de SiO_2.

^{1}H MAS NMR

Plusieurs signaux ont été observés, tels que silanols et H_2O physisorbée (3.5-5 ppm), groupements éthoxy (3.3-3.6 ppm) et méthoxy (1.1-1.3 ppm) ainsi que CH_2 greffés (0.7-0.9 (Si-CH_2), 6.5-6.8 (CH_2-N) 4.0-4.1 (CH_2)). Malheureusement, certains signaux sont larges et superposés. Les spectres sont simplement indicatifs.

^{13}C CP-MAS NMR

Les signaux des spectres RMN ^{13}C MAS correspondent aux fonctions organiques greffées sur la surface de **SiO_2**. Ces signaux correspondent au silane de TESPN, une situation similaire est observée dans le cas de COOH après hydrolyse de la fonction nitrile. Cette méthode confirme le greffage de -CN et la transformation de -CN en -COOH. Les spectres sont présentés dans la figure 9.

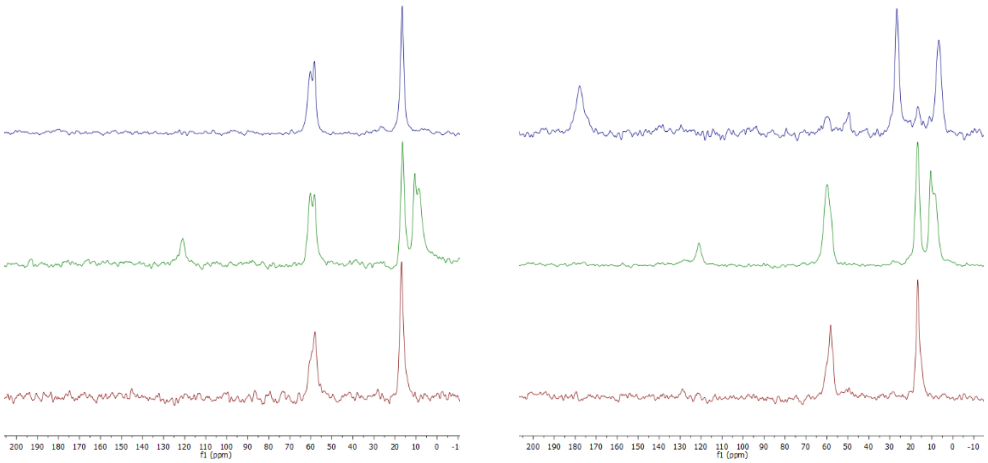

Figure 9 - Spectres RMN ^{13}C MAS de **SiO_2** (bas), **SiO_2@CN** (milieu) et **SiO_2@COOH** (haut). Partie gauche pour les billes de SiO_2 faites dans EtOH et partie droite pour les billes de SiO_2 faites dans MeOH.

^{29}Si NMR CP MAS

Les spectres ^{29}Si CP MAS donnent les informations sur les Si de cœur et les Si du silane organique. Les signaux à -93, -101 et -111 ppm de SiO_2 cœur sont observés dans tous les spectres et correspondent à Q_2, Q_3 et Q_4 (Q_n= $Si(OSi)_n(OH)_{4-n}$). Deux signaux de l'organosilane greffé sont observés vers -60 et -70 ppm (T_2 et T_3). L'observation des signaux T_2 et T_3 confirme la présence de fonction organosilane sur la surface SiO_2.

Quantification par ^1H RMN

Dans le cas de SiO_2 et SiO_2 fonctionnalisées, l'analyse élémentaire ne permet pas de quantifier les fonctions organiques réellement greffées. Cependant, en dissolvant la silice dans un milieu basique, les fragments résiduels peuvent être quantifiés à l'aide un étalon interne (dans notre cas l'acide benzoïque est utilisé). Les résultats suivants ont été obtenus :

Table 2 – Nombre de fonctions (F) (mmol) par g d'échantillon, calcul par ^1H RMN.

Solvant utilisé pour la synthèse	S	ρ(f) (mmol F/g S)			
		OCH_2CH_3	OCH_3	CN	COOH
Ethanol	**SiO_2**	0.43	-	-	-
	SiO_2@CN	0.64		0.29	
	SiO_2@COOH	0.45			0.04
Méthanol	**SiO_2**	1.18	0.05	-	-
	SiO_2@CN	1.85	0.04	1.40	-
	SiO_2@COOH	0.08	0.05	-	0.31

La silice synthétisée dans le méthanol possède un plus nombre de fonctions que la silice obtenue dans l'éthanol. Durant l'étape d'hydrolyse de la fonction nitrile en carboxylique avec H_2SO_4, la plupart de ces fonctions sont perdues.

Basés sur les résultats de quantification obtenus par RMN ^1H, les taux de couverture sont ainsi calculés (voir tableau suivant) :

Table 3- Nombre de fonction (mol) par nm^2.

Solvant utilisé pour la synthèse	SiO_2@CN	SiO_2@COOH
Ethanol	20.6	2.8
Méthanol	16.6	3.2

Remplacement de CH_3COOH par SiO_2@COOH dans les réactions d'oxydation avec les complexes de Mn et de Fe

La faisabilité de remplacement de CH_3COOH par **SiO_2@COOH** est testée sur deux types de réactions : l'(ép)oxydation d'oléfines et l'oxydation d'alcool.

Oxydation du cyclooctène (CO)

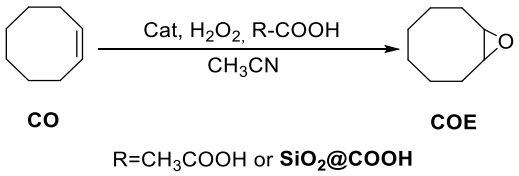

Schéma 11- catalyse d'oxydation du cyclooctène.

Le cyclooctène est sélectionné comme un modèle simple pour réaliser les premiers tests et pour comparer l'activité de **SiO_2@COOH**. L'influence de la taille des billes de **SiO_2@COOH** sur la réactivité est également étudiée. Les résultats sont présentés dans la figure 10:

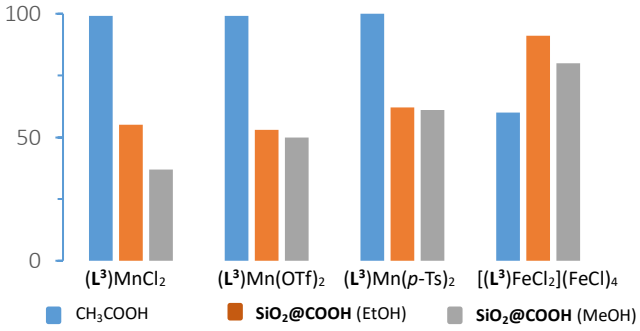

Figure 10 - Comparaison de la conversion de CO entre différents catalyseurs et différentes conditions.

En présence du co-réactif, une conversion du CO est observée dans toutes les conditions. L'acide acétique est plus adapté aux complexes de Mn, donnant une meilleure conversion que les réactions réalisées avec **SiO_2@COOH**. La situation inverse est observée dans le cas du complexe de Fe. Les anions peuvent aussi influencer sur le rendement. Des résultats similaires sont obtenus entre les deux lots de **SiO_2@COOH**.

Oxydation du cyclohexène (CH)

Le cyclohexène (CH) est un substrat intéressant qui peut être utilisé comme une matière première lors de la synthèse de l'acide adipique. En plus, la réactivité du CH est plus complexe que celle du CO. Deux types de réactions peuvent en effet se produire : l'(ép)oxydation et l'oxydation allylique.

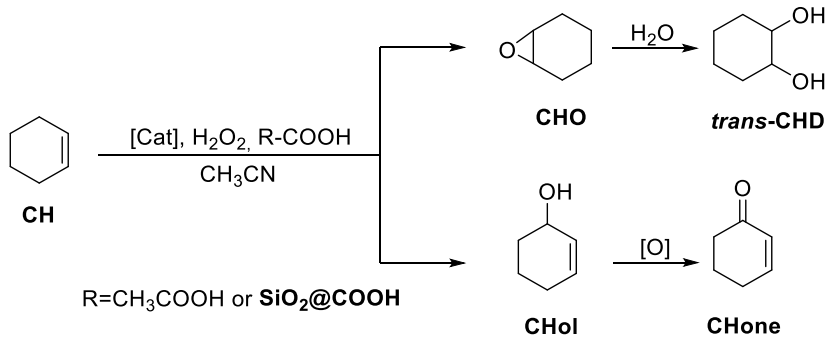

Schéma 12- Catalyse d'oxydation du cyclohexène.

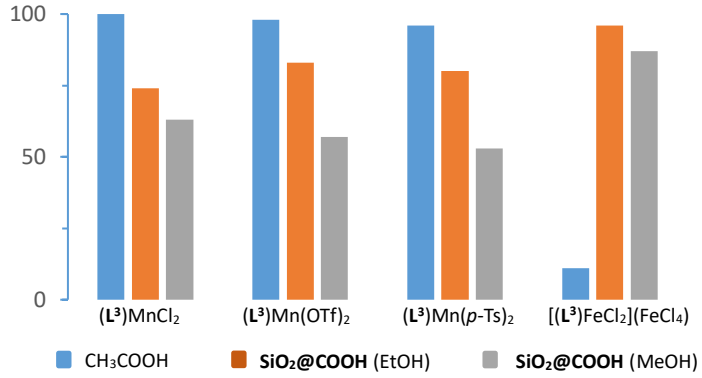

Figure 11- Conversion de CH entre différents catalyseurs et différentes conditions.

Dans les cas des réactions catalysées par les complexes de Mn avec CH_3COOH, des conversions supérieures à 95% ont été observées. Le produit principal est CHO, une faible quantité de cyclohexane diol est observée lors des tests catalytiques avec $(L^3)Mn(OTf)_2$ et $(L^3)Mn(p\text{-}Ts)_2$. Lorsque SiO_2@COOH est utilisé, les conversions sont inférieures à celles obtenues avec CH_3COOH et CHO est le seul produit observé avec $(L^3)Mn(OTf)_2$ et $(L^3)Mn(p\text{-}Ts)_2$. Une petite quantité de CHD est observée avec SiO_2@COOH (faite dans EtOH), et de CHol et Chone avec SiO_2@COOH (faite dans MeOH).

Dans le cas du complexe de Fe, avec CH_3COOH comme co-réactif les produits souhaités ne sont pas obtenus. Cependant, en utilisant SiO_2@COOH comme co-réactif, une conversion remarquable mais non sélective est observée. L'oxydation allylique et l'époxydation ont été observées simultanément.

Oxydation du cyclohexanol (CYol)

L'oxydation de CYol est plus simple car un seul produit est attendu (CYone).

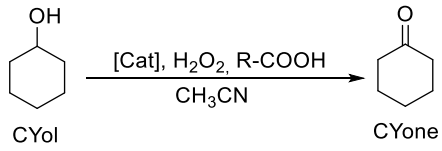

R-COOH=CH_3COOH or **SiO_2@COOH**

Schéma 13- catalyse d'oxydation du cyclohexanol.

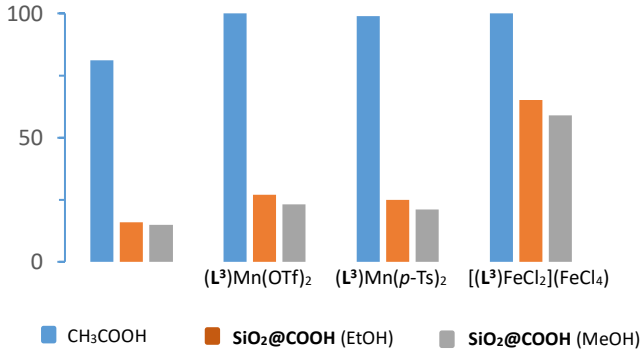

Figure 12- Conversion de CYol entre différents catalyseurs et différentes conditions.

Pour toutes ces réactions de catalyse, en présence de CH_3COOH, les conversions de CYol et les sélectivités vers CYone sont élevées. (L^3)$Mn(OTf)_2$ et(L^3)Mn(*p*-Ts)$_2$ sont plus actifs que (L^3)$MnCl_2$. Les réactions catalysées par les complexes de Mn avec **SiO_2@COOH** donnent de faibles conversions. Une conversion modérée est obtenue dans le cas de la réaction avec le complexe de Fe.

Conclusion

Il est possible de remplacer l'acide acétique, CH_3COOH, par les billes de silice fonctionnalisées avec des fonctions carboxyliques pour les réactions d'(ep)oxydation d'oléfines. L'étude montre que la réactivité est faible avec les billes de silice sur le modèle de CO et CH avec les complexes de Mn. Dans le cas de l'oxydation du cyclohexanol, une meilleure conversion est obtenue avec l'acide acétique par rapport aux billes de silice. La taille n'a pas une influence sur la réactivité. Cependant, la charge de fonctions carboxyliques est 100 fois moindre avec les billes qu'avec l'acide acétique. Dans les réactions de catalyse avec l'acide acétique avec la même charge de fonctions carboxyliques que les billes de silice, aucune conversion des substrats n'est observée. Même si avec les billes de silice, la réaction est moins active, ce travail est la première étape pour remplacer ou réduire le solvant organique et les réactifs volatils.

Chapitre 4- (Ep)oxydation d'oléfines et d'alcools en conditions sans solvant organique par des catalyseurs recyclables basés sur les polyoxométallates $[PM_{12}O_{40}]^{3-}$ (M= Mo or W) greffés ioniquement sur des nano billes de silice fonctionnalisées par des groupements amine.

Dans ce chapitre, avec l'objectif d'accéder à des catalyseurs recyclables, des billes de silice fonctionnalisées par des fonctions amine pendantes ont été synthétisées et caractérisées. Leur utilisation pour des réactions d'(ép)oxydation avec TBHP comme oxydant et des conditions sans solvant sont également décrites.

Synthèse des objets catalytiques

La voie de synthèse des catalyseurs est décrite dans le schéma 14. Les billes de silice ont été synthétisées par hydrolyse de TEOS (tetraéthylorthosilicate) dans le méthanol en présence d'ammoniaque et d'eau. La fonctionnalisation de ces billes par l'APTES dans le toluène a ensuite permis l'introduction des fonctions amine nécessaires au greffage ionique des POM $H_3PM_{12}O_{40}$ (M= Mo or W) et ainsi l'accès aux catalyseurs désirés.

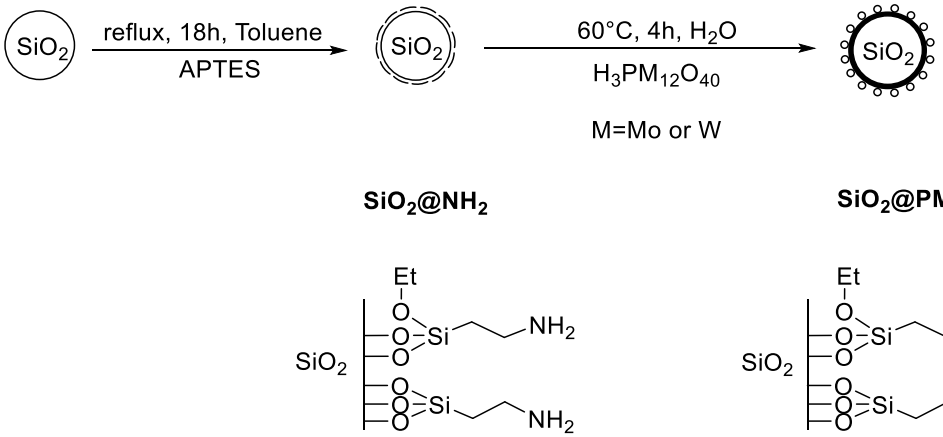

Schéma 14- Synthèse des POMs greffés sur les nanoparticules de silice.

Caractérisations

Pour étudier leurs morphologies et leurs propriétés, tous les objets obtenus (SiO_2, $SiO_2@NH_2$, $SiO_2@PMo$ et $SiO_2@PW$) ont été caractérisés par différentes méthodes, telles que : RX sur poudre, TEM, DLS, IR, RMN solide et liquide.

RX poudre

D'après les diffractogrammes obtenus (Figure 13), une structure non cristalline est observée pour les billes contenant les polyoxométallates greffés. Cela indique que les billes et les POMs n'ont pas une structure cristalline.

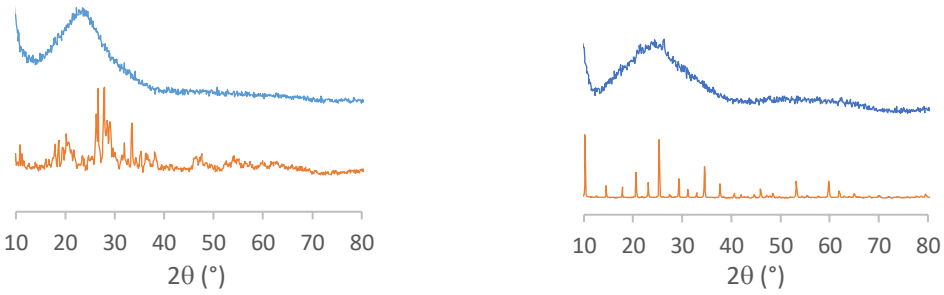

(a) (b)

Figure 13- comparaison des diffractogrammes- $H_3PMo_{12}O_{40}$ (orange) avec (a)- **SiO_2@PMo** (Bleu) et (b)- $H_3PW_{12}O_{40}$ (orange) avec **SiO_2@PW** (Bleu).

Analyse par DLS

Les mesures de DLS sont classiquement utilisées pour déterminer le rayon hydrodynamique des particules colloïdales. Les mesures ont été effectuées sur **SiO_2**, **SiO_2@NH_2**, **SiO_2@PW** and **SiO_2@PMo**. Dans le cas de SiO_2, les particules sont stables et dispersées de manière homogène dans la solution (Figure 14 (a)). Les diamètres sont d'environ 70 nm.

Dans le cas de **SiO_2@NH_2**, à cause de la nature des fonctions NH_2 pendantes, une agglomération est observée au cours du temps. Le diamètre observé est d'environ 340 nm (Figure 14 (b)).

Pour **SiO_2@PM**, au cours du temps, la taille évolue de 190 nm à 220 nm pour **SiO_2@PW** et de 450 nm à 3900 nm pour **SiO_2@PMo**. Ces mesures ont prouvé que **SiO_2@PM** a tendance à s'agglomérer au cours du temps.

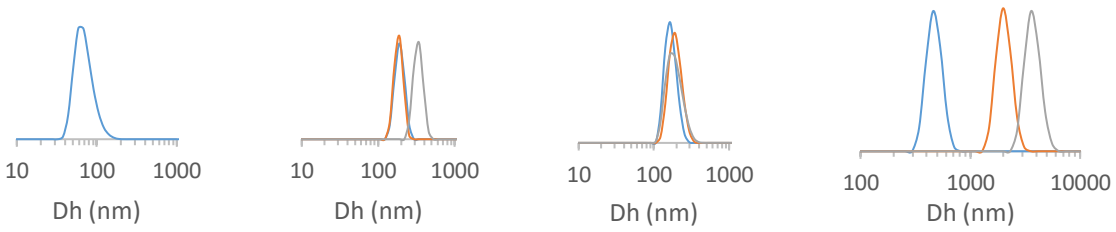

(a) (b) (c) (d)

Figure 14- (a) distribution (Dh) en nombre de SiO_2, (b-d) évolution de Dh de **SiO_2@NH_2**, **SiO_2@PW** et **SiO_2@PMo** au cours du temps avec différentes couleurs (bleu- orange- gris).

Analyse par TEM

Les images obtenues par TEM démontrent la monodispersité des billes de silice. Un diamètre de 75,9 nm a été mesuré pour SiO_2 et **SiO_2@NH_2**, 80,6 nm et 82,9 nm pour **SiO_2@PW** et **SiO_2@PMo**. Ces images de TEM démontrent également que les structures des billes de SiO_2 n'ont pas été modifiées pendant les fonctionnalisations successives.

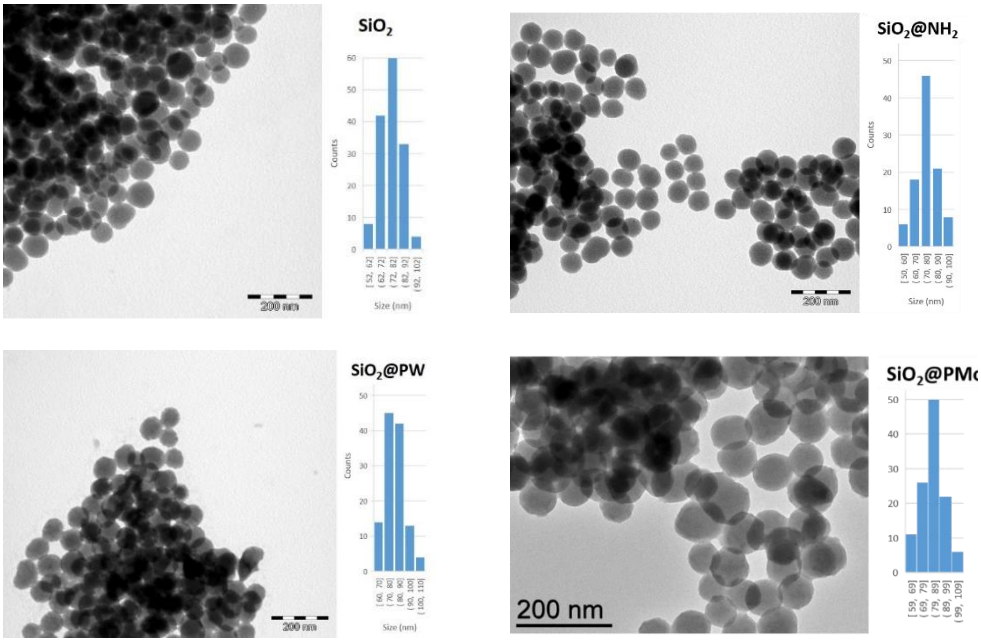

Figure 15- Images de TEM et distribution des diamètres de **SiO_2**, **SiO_2@NH_2**, **SiO_2@PW** et**SiO_2@PMo**.

Dans les cas de **SiO_2@PW** et **SiO_2@PMo**, une interaction entre des billes de silice est observée. Ce phénomène peut être probablement expliqué par l'interaction intermoléculaire des POMs.

Spectroscopie infrarouge

Tous les échantillons ont été caractérisés par spectroscopie IR et les vibrations caractéristiques de SiO_2 ont été observées. Par ailleurs, pour **SiO_2@PM**, la différence des spectres **SiO_2@PM/SiO_2** a mis en évidence les vibrations de la partie POM telles que : P-O, M=O, M-O-M (M=W ou Mo).

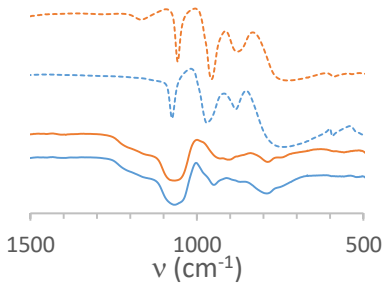

Figure 16- De haut en bas : vibrations IR de **$H_3PMo_{12}O_{40}$**, **$H_3PW_{12}O_{40}$**, et différence de spectres (**SiO_2@PMo**- **SiO_2@NH_2**), (**SiO_2@PW**- **SiO_2@NH_2**).

RMN solide multinucléaire

La spectroscopie IR n'a cependant pas fourni assez d'informations pour prouver l'existence des fonctions pendantes sur SiO_2. La RMN a alors été utilisée pour obtenir ces informations.

RMN ^{1}H MAS

Les fonctions pendantes à la surface de SiO_2 (molécule d'eau, méthoxy, éthoxy, CH_2 des organosilanes) ont été observées dans les spectres RMN.

RMN ^{13}C CP-MAS

La RMN ^{13}C CP-MAS a permis de mettre en évidence la présence des amines pendantes à la surface des billes de silice, notamment par différence des spectres de **SiO_2** et de **SiO_2@PM**.

RMN ^{31}P MAS

La RMN ^{31}P MAS a quant à elle confirmée la présence des POMs ($PW_{12}O_{40}$ et $PMO_{12}O_{40}$) à la surface des billes.

La combinaison de tous ces résultats prouve que les billes de silice ont été fonctionnalisées par les groupements amino alkyle et que les POMs y sont greffés, très probablement de manière ionique.

Quantification du nombre de fonctions sur les billes de silice

Pour quantifier le nombre de fonctions à la surface des billes de silice, deux méthodes ont été utilisées : la RMN ^{1}H liquide avec l'acide benzoïque comme étalon interne et l'analyse élémentaire. L'exploitation et la combinaison des résultats obtenus par ces deux techniques ont permis d'accéder aux données suivantes :

Table 4 - $\rho(NH_2)$ et $\rho(PM)$ valeurs et surface couverture $\mu(NH_2)$.

Sample	$\rho(NH_2)^1$ (^{1}H NMR)	$\rho(PM)^1$ (^{31}P NMR)	$\rho(NH_2)^1$ (EA)	$\rho(PM)^1$ (EA)	$\mu(NH_2)^2$
SiO_2@NH_2	0.52	-	0.53	-	6.8
SiO_2@PW	0.33	0.15	0.31	0.14	6.8
SiO_2@PMo	0.40	0.12	0.41	0.12	6.7

[1] mmol de fonctions/g échantillon [2] nombre de fonctions/nm^2

Les catalyseurs supportés synthétisés et caractérisés, l'étape suivante a consisté à tester leur activité catalytique pour des réactions d'(ép)oxydation en conditions sans solvant.

Catalyse

Les POMs commerciaux (notamment $H_3PW_{12}O_{40}$ et $H_3PMo_{12}O_{40}$) ont montré une excellente activité en catalyse homogène d'époxydation. La plupart des réactions catalysées par ces catalyseurs décrites dans la littérature sont réalisées dans des solvants organiques et les catalyseurs ne sont pas réutilisables. Avec l'approche décrite dans ce travail, les billes de silice non poreuses et amino fonctionnalisées ont été sélectionnées comme supports solides réutilisables. Ces POMs greffés ont été testés sur plusieurs substrats tels que le cyclooctène, le cyclohexène, le limonène et le cyclohexanol. Pour tester leur durabilité, ces catalyseurs ont été

recyclés et testés 3 fois dans les mêmes conditions. Des résultats intéressants ont été obtenus et sont présentés dans le paragraphe suivant.

(Ep)oxydation du cyclooctène (CO)

Le cyclooctène (CO) a été sélectionné comme modèle pour réaliser les premiers tests. Les réactions sont réalisées à 80°C avec un ratio TBHP/CO= 1.5 et POM/substrat = 0,07% pour W et 0,058% pour Mo.

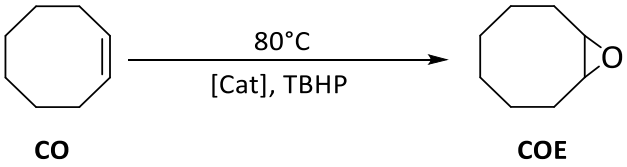

Schéma 15- catalyse d'oxydation de CO.

Table 5- Résultats d'époxydation de CO catalysée par les POMs et les POMs supportés.[1]

Catalyseur	Cycle	CO Conv.[2]	COE Sel.[3]	TON[4]
$H_3PW_{12}O_{40}$	1	64	14	807
SiO_2@PW	1	72	41	981
	2	75	38	987
	3	77	37	968
$H_3PMo_{12}O_{40}$	1	99	44	1712
SiO_2@PMo	1	98	71	1693
	2	96	72	1620
	3	93	69	1598

[1] Conditions : 80°C. POM/TBHP/CO=0.070/150/100 pour W, 0.058/150/100 pour Mo ; *t*=24h.

[2] n CO converti/n CO engagé (%) après 24h.

[3] n COE formé/ nCO converti (%) à 24h.

[4] n CO transformé /nPOM à 24h.

Dans ces conditions, pour les réactions catalysées par **SiO_2@PW**, les conversions et sélectivités en faveur du COE sont supérieures à celles observées lorsque la réaction est catalysée par $H_3PW_{12}O_{40}$. Après 3 cycles de recyclage, aucune diminution de la conversion et de la sélectivité n'a été observée. Dans les cas du Mo, **SiO_2@PMo** présente une conversion similaire à celle de $H_3PMo_{12}O_{40}$, mais la sélectivité en faveur de COE est meilleure. Ce phénomène peut être expliqué par la diminution d'acidité pendant le greffage, l'ouverture de cycle d'époxyde est alors moins favorisée. Les résultats sont présentés dans le tableau précédent.

Oxydation du cyclohexène (CH)

Le cyclohexène (CH) peut être utilisé comme un précurseur d'acide adipique et un modèle simplifié de limonène. Dans cette réaction, plusieurs produits ont été observés tels que : les produits d'époxydation (**CHO** puis hydrolyse en **CHD**) et les produits d'oxydation allylique (CHol et CHone).

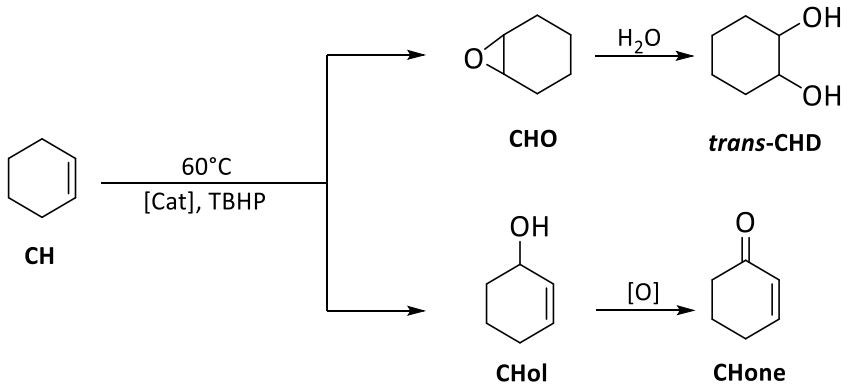

Schéma 16- catalyse d'oxydation du CH.

Table 6- Résultats d'époxydation de CH catalysée par les POMs libres et les POMs supportés.[1]

Catalyseur	Run	CH Conv[2]	CHO Sel[3]	CHD sel[3]	CHol sel[3]	CHone sel[3]	TON[4]
$H_3PW_{12}O_{40}$	1	31	< 1	4	3	3	11307
SiO_2@PW	1	45	1	2	4	5	21458
	2	43	1	2	2	3	20649
	3	26	3	3	7	7	12373
$H_3PMo_{12}O_{40}$	1	91	< 1	40	3	2	52728
SiO_2@PMo	1	80	13	26	5	2	46732
	2	74	15	22	6	3	42487
	3	60	26	20	4.9	2	36345

[1]Conditions : 80°C. POM/TBHP/CH=0.014/150/100 pour W, 0.0116/150/100 pour Mo ; *t*=48h.
[2]nCH converti/nCH engagé (%) après 48h. [3]n produit formé/ nCH converti (%) à 48h.
[4]nCH transformé /nPOM à 48h.

Après 48h, tous les produits représentés dans le schéma 16 ont été observés par CPG. Dans le cas du W, par rapport aux POMs libres, les POM greffés conduisent à une meilleure conversion et une sélectivité similaire est observée. Cependant, avec **SiO_2@PMo**, les produits principaux sont CHO et CHD alors qu'avec le POM libre, $H_3PMo_{12}O_{40}$, le produit principal d'oxydation est CHD. Ce phénomène est probablement dû à la différence d'acidité. Les résultats sont présentés dans le tableau précédent.

Oxydation du limonène (Lim)

Plusieurs produits peuvent se former lors de la réaction de catalyse d'oxydation du limonène, tels que les produits d'époxydation : LO (*cis* + *trans*), les produits d'ouverture de cycle en présence d'eau : LD (*ax* et *eq*) et les produits d'oxydation allylique (C^{ol} et C^{one}).

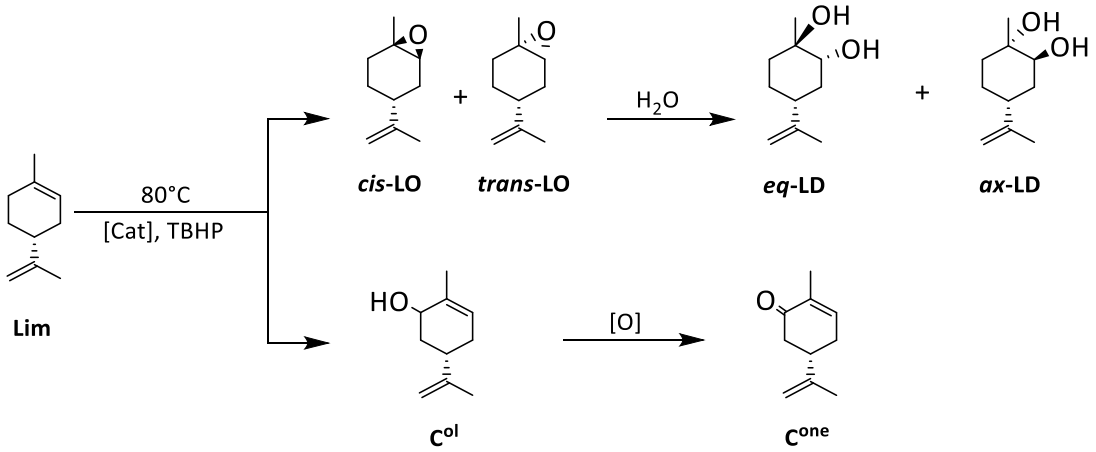

Schéma 17- catalyse d'oxydation du limonène.

Table 7- Résultats d'oxydation de limonène catalysés par les POMs libres et les POMs supportés.[1]

Catalyseur	Run	Lim Conv[2]	*cis*-LO sel[3]	*trans*-LO sel[3]	*ax*-LD sel[3]	*eq*-LD sel[3]	C^{ol} sel[3]	C^{one} sel[3]	TON[4]
$H_3PW_{12}O_{40}$	1	67	0	0	5	3	1	4	1287
SiO_2@PW	1	58	0	3	13	1	8	8	754
	2	59	0	3	13	1	10	8	768
	3	62	0	2	12	2	11	8	754
$H_3PMo_{12}O_{40}$	1	99	0	0	18	10	1	2	1859
SiO_2@PMo	1	91	0	0	36	11	4	3	1721
	2	86	0	0	32	8	6	7	1626
	3	81	0	< 1	20	5	6	6	1526

[1] Conditions : 80°C. POM/TBHP/Lim=0.070/150/100 pour W, 0.058/150/100 pour Mo ; *t*=24h.
[2] nLim convertie/nLim engagé (%) après 24h. [3] n produit formé/ nLim convertie à 24h.
[4] nLim transformé /nPOM à 24h.

Pour SiO_2@PMo, les produits principaux observés sont *ax*- et *eq*-LD. Le carvéol et la carvone sont également observés lors de l'utilisation de SiO_2@PW. Ces résultats sont similaires à ceux obtenus lors des réactions de catalyse d'oxydation du CH. Dans tous les cas, SiO_2@PMo est plus actif que SiO_2@PW.

Oxydation du cyclohexanol (CYol)

Le cyclohexanol (CYol) est un précurseur intéressant de l'acide adipique. Dans cette réaction d'oxydation, la cyclohexanone (CYone) est le seul produit observé.

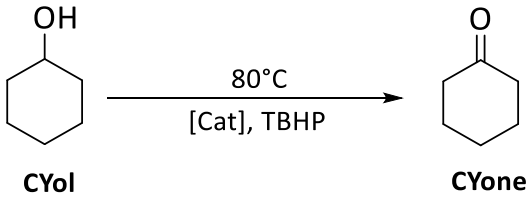

Schéma 18- catalyse d'oxydation du cyclohexanol.

De faibles conversions de CYol ont été observées pour les catalyseurs greffés (10% pour **SiO_2@PW** et 18% pour **SiO_2@PMo** en moyenne). Une conversion modérée est observée avec les POMs libres. Les POM supportés ont été recyclés 3 fois et des résultats similaires ont été observés. Les résultats sont présentés dans le tableau suivant :

Table 8- Résultats d'oxydation du cyclohexanol catalysés par les POMs libres et les POM supportés.[1]

Catalyseur	Cycle	CYol Conversion[2]	CYone Selectivité[3]	TON[4]
$H_3PW_{12}O_{40}$	1	44	34	525
SiO_2@PW	1	11	51	137
	2	8	97	101
	3	7	87	92
$H_3PMo_{12}O_{40}$	1	58	54	728
SiO_2@PMo	1	18	76	228
	2	17	90	207
	3	20	75	249

[1] Conditions : 80°C. POM/TBHP/CYol=0.070/150/100 pour W, 0.058/150/100 pour Mo ; *t*=24h.

[2] n CYol converti/n CYol engagé (%) après 24h.

[3] n CYone formé/ nCYol converti (%) à 24h.

[4] n CYol transformé /nPOM à 24h.

Conclusion générale et perspectives

Conclusion

Durant ce travail, différentes stratégies ont été explorées pour obtenir de nouveaux catalyseurs afin de rendre les procédés plus verts et plus propres.

La première stratégie a consisté à introduire une seconde sphère coordination sur les catalyseurs métalliques déjà décrits comme efficaces pour des réactions de transfert d'atome d'oxygène avec H_2O_2 comme oxydant. Le but est d'obtenir les catalyseurs capables de favoriser l'activation de H_2O_2 par création d'un réseau de liaisons hydrogène impliquant H_2O_2 et la seconde sphère de coordination du catalyseur. Pour cela, des groupements fluoroalcools ont été introduits sur un ligand tétradente de type pyridinophane et les complexes correspondants (Fe^{III}, Mn^{II}, Co^{II}, Ni^{II}) ont été obtenus et caractérisés par plusieurs méthodes. Malheureusement, les complexes de Fe et Mn ne sont pas efficaces pour les réactions de catalyse d'oxydation du cyclooctène avec H_2O_2 comme un oxydant et ce pour les complexes fonctionnalisés par des groupements fluoroalcools ou par des fonctions méthyle devant mettre en évidence l'influence de la seconde sphère de coordination. D'autre part, les complexes de Ni et Co (version méthyle) ont montré une activité intéressante dans la photoproduction d'hydrogène en utilisant un complexe d'iridium photo photosensibilisateur et la triéthylamine comme donneur d'électron.

Dans la deuxième partie de ce travail, pour remplacer l'acide acétique, réactif volatile utilisé comme co-réactif pour favoriser une haute sélectivité en faveur des époxydes lors de réactions d'oxydation d'alcènes, des (nano)billes de silice fonctionnalisées par des silanes à fonction carboxyliques pendantes ont été synthétisées et complètement caractérisées. Ces billes de silice sont une version solide de l'acide acétique. Durant les catalyses, des résultats intéressants ont été obtenus notamment avec un complexe de Fe issu du ligand BPMEN. Un point remarquable est la charge en fonctions carboxyliques de ces billes silice qui est 100 fois moindre qu'avec l'acide carboxylique.

La dernière partie est le greffage de POMs commerciaux sur des nanoparticules de silice fonctionnalisée par des fonctions amines. Ces POMs immobilisés ont été caractérisés puis testés comme catalyseurs d'oxydation en condition sans solvant et avec TBHP comme oxydant sur plusieurs substrats. Deux types de réactions ont été étudiées : des réactions d'(ép)oxydation d'alcènes et d'oxydation d'alcool. Pour les réactions d'(ép)oxydation, des résultats satisfaisants ont été obtenus. Les conversions et sélectivités vers les produits souhaités sont supérieures lors de l'utilisation des catalyseurs greffés par rapport aux POMs non greffés. Cependant, dans le cas de l'oxydation d'alcool, les conversions des POMs non greffés sont meilleures que celles des POMs greffés.

Perspectives

A partir des résultats obtenus, plusieurs perspectives sont envisageables.

Concernant la partie moléculaire, pour mieux comprendre le rôle de seconde sphère coordination dans les processus impliquant un transfert d'atome d'oxygène, de nouveaux ligands fonctionnalisés par des groupements fluoroalcools et d'autres groupements permettant de créer des réseaux de liaisons H avec H_2O_2, sont envisagés. Pour cela, une attention particulière sera portée au design des ligands afin qu'il n'y ait pas de coordination de ces fonctions sur le centre métallique.

Des billes de silice fonctionnalisées par des groupements sulfonates pendants sont également envisagées pour être testés dans les réactions de catalyse d'oxydation. En effet, comme cela a été décrit dans la littérature, dans certains cas, la présence d'un acide fort permet d'obtenir au moins une aussi bonne sélectivité en faveur de l'époxyde par rapport à l'utilisation d'acide acétique. La morphologie des billes de silice sera optimisée pour trouver un meilleur équilibre entre la taille, le nombre de fonctions, la réactivité et la facilité de recyclage.

Les POMs supportés sur les billes de silice seront également testés sur les substrats plus complexes, notamment issus de la biomasse. Il est possible de recycler les catalyseurs et donc de développer le procédé par cette méthode simple. Le greffage d'autres POMs (POM contenant du vanadium) est également envisagé. En effet, ces catalyseurs permettent de réaliser des réactions de catalyse d'oxydation en utilisant l'oxygène moléculaire comme oxydant et donc rendre le procédé plus propre. Enfin, ces catalyseurs pourront être testés en flux continu, en conditions sans solvant.

D'un point de vue général, les méthodes développées dans ce travail sont une première étape pour obtenir des produits à haute valeur ajoutée par des procédés plus respectueux de l'environnement.

General Introduction

In the actual context in which more sustainable processes need to be developed, there is a huge need of cleaner chemical processes. According to the 12 Principles of Green Chemistry, catalysis is one of the possibilities. Finding a catalyzed process does bring a substantial economy of energy in a complete process. This is the main goal envisioned during the three years of this PhD.

Indeed, in team G (Ligands, Complex Architectures and Catalysis) from LCC, and in the part of team based at Castres, one research strategy explored is the development of new catalysts for a large panel of reactions and notably oxidation reactions.

For this, several complexes are studied:

- Mo, V and W metal complexes based on ONO or ONS tridentate ligands and polyoxometalate for organic solvent-free (ep)oxidation.
- Fe and Mn complexes based on polydentate N ligands with second sphere modifications for Oxygen Atom Transfer (OAT) reactions.

More specifically, this work has focused on catalytic (ep)oxidation reactions and different approaches have been explored

(i) to gain information about the parameters that need improvement to access to more efficient OAT catalysts.

(ii) to obtain more sustainable oxidation processes

Among the different catalytic epoxidation reactions described in the literature, Mn and Fe metal complexes are very efficient catalysts when associated with H_2O_2 as oxidant in the presence of carboxylic acid as additive. The latter one is needed to favor the exclusive formation of epoxides. Oxygenase metalloenzymes display the same reactivity of OAT reactions thanks to the presence of an H-bond network in the second coordination sphere of their active sites.

Based on this analysis, two strategies have been envisioned:

(i) The first one, inspired by metalloenzymes, was to introduce a second coordination sphere on metal complexes to remove acetic acid from the process.

(ii) The second one is the replacement of volatile acetic acid by an object (functionalized silica beads) possessing COOH functions that would be ideally recoverable.

In order to recover the catalyst, another strategy was explored, i.e. immobilization of molecular catalysts on a support (functionalized silica beads). Concerning the choice of the catalyst, based on the expertise of the group about commercially available efficient catalysts for oxidation reactions, immobilization of polyoxometalates was targeted.

This PhD thesis is a combination of these three different strategies that will be presented into the following chapters.

The first chapter presents the state of the art of the different strategies explored during this PhD work, i.e.

(i) manganese and iron catalysts based on polydentate N-donor atoms and more specifically the mechanistic aspects that inspired a part of the work.

(ii) Polyoxometalates and their applications in oxidation reactions

In order to evaluate the influence of the second coordination sphere in catalysis, the second chapter deals with (i) the synthesis of metal complexes (metal = Fe(III), Mn(II), Co(II) and Ni(II)) based on polydentate N-donor ligands functionalized either with alkyl groups or fluoroalcohol groups, (ii) the evaluation of Mn and Fe metal complexes for the oxidation of cyclooctene with H_2O_2 as oxidant, (iii) the use of Ni(II) and Co(II) metal complexes for hydrogen photoproduction.

In the third chapter, the replacement of acetic acid, a volatile co-reagent used to favor the exclusive formation of epoxides when Fe or Mn metal complexes with N_4 ligands are used as catalysts with H_2O_2 as oxidant, was targeted. Silica nanobeads functionalized by COOH pendant functions have been synthetized and their application as solid co-reagent during (ep)oxidation reactions has been evaluated.

In the last chapter, in order to access to recoverable catalysts, Mo and W polyoxometalates have been ionically anchored on silica nanobeads functionalized by amino pendant functions. Their catalytic activities for (ep)oxidation reactions with TBHP as oxidant and their recyclability have been studied in solvent-free conditions.

Chapter 1

Bibliographic background

1.1. Introduction

Oxidation reactions represent a core industrial technology for the conversion of chemical feedstocks, such as alkanes and alkenes, into fine chemicals, epoxides, diols, and alcohols.[1] Those transformations are essential for the laboratory-scale synthesis of small molecules. The current use of stoichiometric oxidants including nitric acid,[2] chromic acid and its derivatives,[3] permanganate,[4] osmium tetroxide[5] and hypochlorite (bleach)[6] is remarkably efficient but those processes involve higher costs, formation of toxic waste, and low atom efficiency due to the stoichiometric factor.[7] This is in strong contrast with the extensive use of catalytic methods in most other areas of chemical synthesis. The increasing role of catalysis in organic chemistry in general and the ever-increasing environmental consideration provide a strong incentive to develop sustainable catalytic alternatives to stoichiometric reagents.[8] Among the oxidation reactions, the formation of epoxides *via* the epoxidation of alkenes is important to obtain important products, such as alcohols, diols etc.[9]

Among the different strategies to achieve such transformations, bioinspired catalysts based on iron and manganese display interesting properties when using H_2O_2 as oxidant.[10] Some limitations, such as the necessity of carboxylic acid as additive, still exist.[11] Avoiding this volatile co-reagent by catalysts modifications or replacing it are potential pathways that might lead to more efficient process.

Heterogenization of catalysts on a surface is a valuable strategy to access to recoverable catalysts that also needs to be investigated.

These different options have been explored during this work.

In this bibliographic chapter, in Part 1.2, particular attention would be paid on the influence of the second coordination sphere in oxidation catalysis (from enzymatic to molecular systems). In Part 1.3, polyoxometalates, good candidates for heterogenization, will be described and their applications in oxidation reactions developed.

1.2. From enzymatic systems to bioinspired catalysts and beyond

1.2.1. Iron in biological system

In biological metabolism processes, different strategies are developed to incorporate oxygen atoms into substrates.[12] Thus, metalloenzymes, mainly iron-based, activate molecular dioxygen and generate very strong oxidants through protons and electrons transfer (Scheme 1).[13]

During the O_2 activation, several metal-oxygen adducts are formed, such as M-superoxo, M-peroxo, M-hydroperoxo, M-oxo and M-hydroxo.[14]

The first step is the activation of O_2 by a M(II) metal center leading to the formation of a M(III)-$O_2^{\cdot-}$ superoxo adduct (Scheme 1, a). From this adduct, a hydroperoxo species (M(III)-OOH) is generated following two possible paths:

- through $H^{\cdot}$ addition (Scheme 1, d)
- a reduction step leading to a peroxo compound (M(III)-OO^{-}) followed by a protonation step (Scheme 1, b and c).

Once the hydroperoxo formed, different species can be formed depending on the O-O bond cleavage process:

- Heterolytic cleavage will form a M(V)=O compound (Scheme 1, f)
- homolytic cleavage will generate the radical hydroxyl $HO^{\cdot}$ and a M(IV)=O species (Scheme 1, e).

Both very reactive species can evolve into a hydroxo (M(III)-OH), a stable compound in absence of further reactivity.[15]

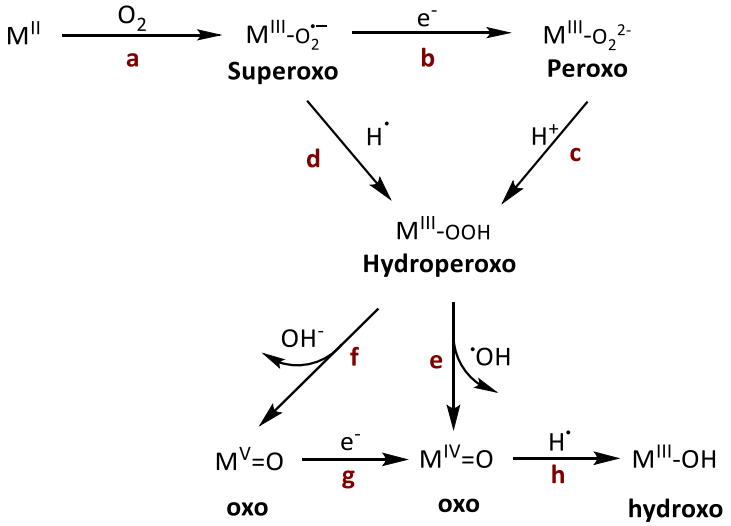

Scheme 1- general processes of O_2 activation by metalloenzyme.

In this context, cytochrome P450 and Rieske oxygenase enzymes are typical representants of heminic and non-heminic enzymes able to activate dioxygen O_2 for selective oxidation of a large panel of substrates.

1.2.1.1. Cytochrome P450

Cytochromes P450 (Cyt P450) are heminic enzymes with a Fe^{III}(porphyrinic) active site chelated by a cysteinate sulfur residue of the protein in axial position,[12a,16] the last coordination place generally being occupied by H_2O (Scheme 2).[17]

Scheme 2 - Example of cysteinato-heme enzyme (left). Simplified symbol of Cyt P450 for oxygen transfer mechanism description (right).

The pathways of Oxygen Atom Transfer (OAT) reactions catalyzed by Cyt P450 have been clearly defined and are detailed in Scheme 3.[18]

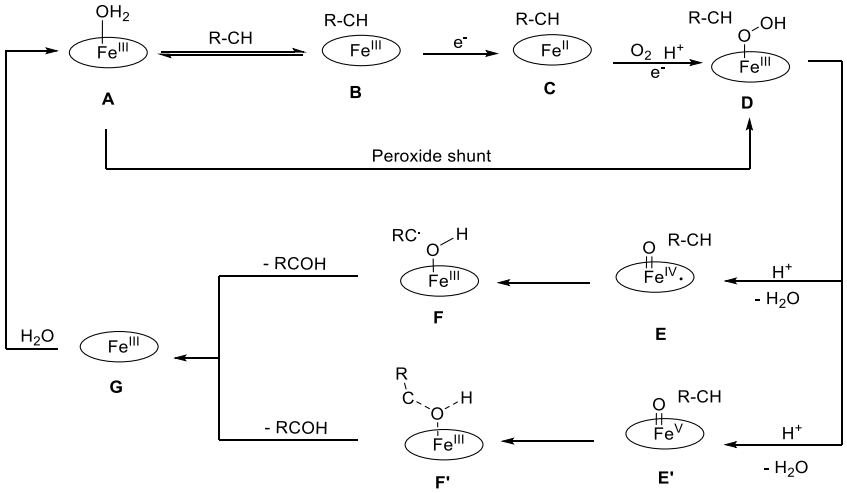

Scheme 3 – mechanism of hydroxylation catalyzed Cyt P450.

The first step (from **A** to **B**) is a reversible exchange of the H_2O molecule from Fe(III)-OH_2 (**A**) by the substrate R-CH, leading to Fe(III)-R-CH (**B**). Then a reduction of (**B**) by NADPH leads to Fe(II)-R-CH (**C**). These compounds do permit the dioxygen activation. After a protonation step, an hydroperoxo intermediate Fe(III)-OOH (**D**) is formed. This key intermediate was isolated and characterized by X-Ray crystallography,[18a, 19] resonance Raman,[20] and Mossbauer spectroscopy [21]. **D** is a very active and unstable species and a second protonation leads to the O-O heterolytic bond cleavage forming a Fe(IV)=O species I with a radical cation delocalized on the porphyrin.[22] **E** can also be considered as a Fe(V)=O species (**E'**) without delocalization of an electron on the porphyrin. Then the oxygen atom will be transferred on the substrate and the complex **A** is reformed. A key step in this mechanism is the selective formation of **E** (or **E'**). Indeed, the formation of the radical hydroxyle HO·, a non-selective strong oxidant, through a O-O homolytic bond cleavage of **D**, has to be avoided. This is realized thanks to the protonation of the distal O atom of this hydroperoxo compound **D** that favors the heterolytic O-O bond cleavage leading to **E** (or **E'**) and the release of a water molecule. It has to be noted that, in horseradish peroxidase, the protonation of this O atom is realized by the distal His residue, i.e. protonation and formation of **E** (or **E'**) are favored by the presence of an amino acid acting as a proton relay in the second coordination

sphere.[23] Moreover, other residues participate to the stabilization of these highly unstable compounds through the formation of H-bond networks.[18a,24]

1.2.1.2. Rieske Oxygenase

In addition to cytochrome P450, the most representative heminic enzyme, some non-heme iron-dependent oxidative enzymes are also able to activate O_2. Although those enzymes do not possess heminic part to stabilize high valent species, the same catalytic activities are displayed.[12b] Among those enzymes, Rieske oxygenases are involved in the oxidative degradation of aromatic compounds, the first step being a regio and stereospecific *cis*-dihydroxylation reaction.[25]

Naphthalene dioxygenase (NDO), probably the best-characterized enzyme of the family, will be taken to explain the mechanism (Scheme 4).[10h,26] This enzyme does catalyse the *cis*-1,2-dihydroxylation of naphthalene through two parts: a reductase part (the Rieske cluster) and an oxygenase part.[27] The reductase part provides electrons from NAD(P)H and transfers them to the oxygenase part to allow O_2 activation by the Fe(II) center. For the active site of oxygenase part, the iron atom is coordinated by a so-called "2-His-1-carboxylate triad" (two histidine residues and an aspartate/glutamate residue), one or two water molecules completing the coordination sphere of the iron center. [27]

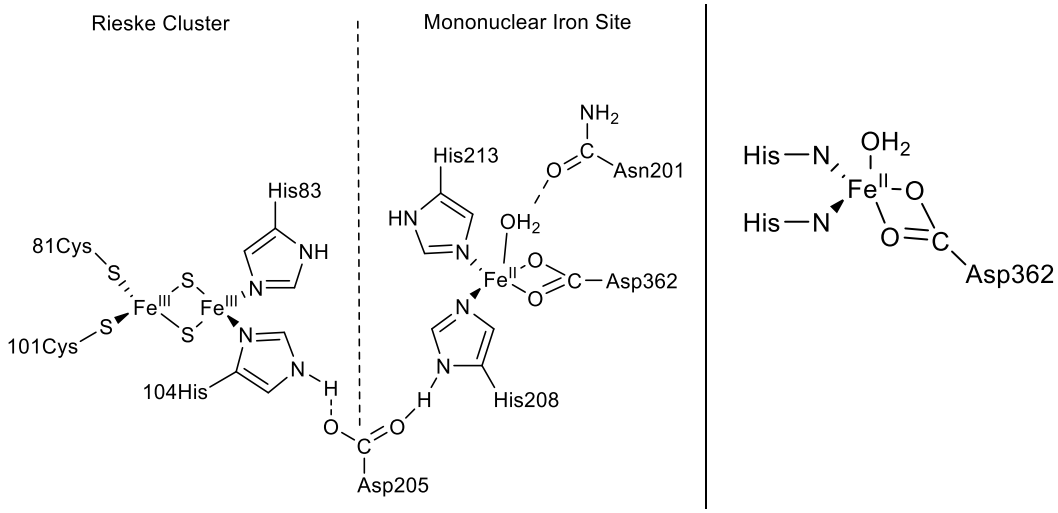

Scheme 4- Reductase and oxygenase parts of NDO (left)[27] and active site of the oxygenase part (right).

Despite considerable recent insight from structural, spectroscopic, and substrate analogue studies, the catalytic cycle of NDO remains to be fully elucidated. A consensual mechanism is presented in Scheme 5.[27,28] As for Cyt P450, succession of reduction and protonation steps are observed leading to metal-oxo intermediates, responsible of the oxidation of the substrate.

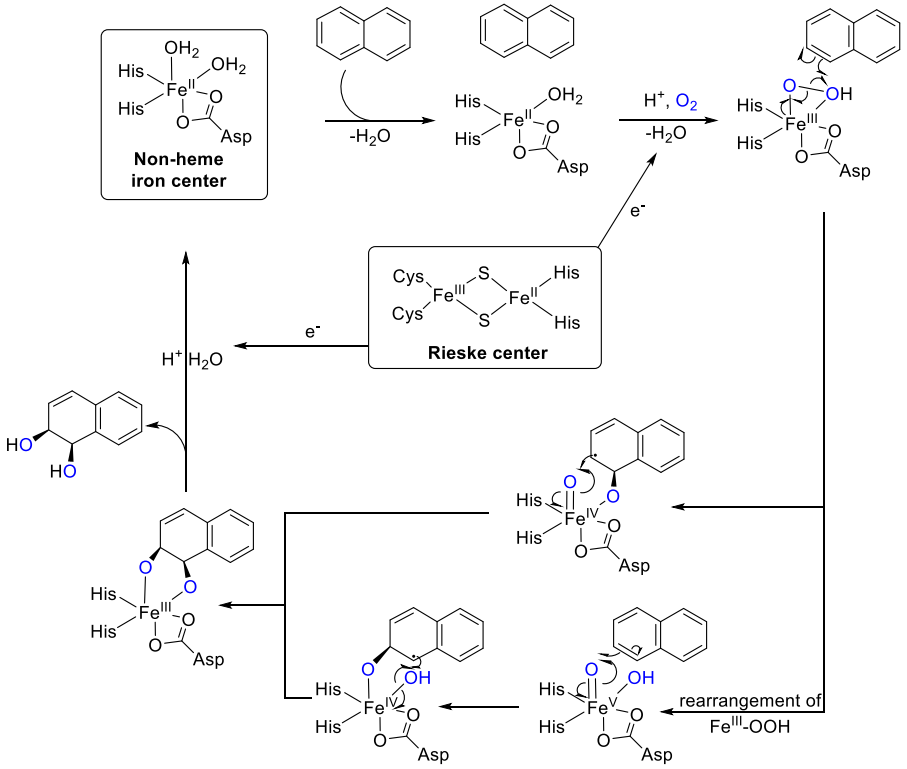

Scheme 5 - Mechanism of naphthalene oxidation catalyzed by NDO.[27]

1.2.2. Manganese complexes in biological systems

Manganese is also involved in various important biological processes, notably in the Oxygen Evolving Center (OEC) of photosystem II.[29] OEC is a $CaMn_4O_5$ cluster surrounded by amino acids residues and water molecules (Scheme 6). This cluster is responsible of water oxidation, generating molecular oxygen through a four-step photocatalytic cycle.[30] Despite the progress made in the past years, the exact mechanism about the O-O bond formation is still a challenge. It is however admitted that high valent manganese species (Mn(V)-oxo or Mn(IV)-O·) are involved in the mechanism.[31]

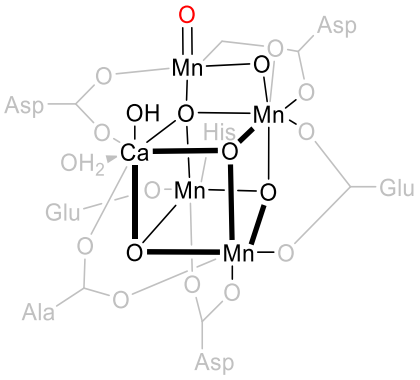

Scheme 6 - Proposed structure of S_4 state during water-splitting process catalyzed by OEC in PS II.

Inspired by the active site of these enzymatic systems- mainly oxygenases- able to access to high valent metal-oxo intermediates involved in the selective oxidation alkenes and alkanes for example, bioinspired molecular complexes have emerged in the literature to try to reproduce such reactions with the same level of selectivity.[32]

More particularly, inspired by the heminic chemistry, most groups focused on Fe and Mn metal complexes with tetradentate N_4-donor atoms. The next section will focus on some of these systems. A particular attention will be devoted to the mechanistic aspects and more particularly to the generation of the highly reactive metal-oxo species.[33]

1.2.3. Fe and Mn bioinspired complexes.

While O_2 is the oxidant in metalloenzymes, most research groups focused on the development of processes based on H_2O_2 or peracids.[34] Indeed, the use of O_2 requires the presence of a reducing agent to convert one oxygen atom into H_2O,[35] which is not the case with H_2O_2 or peracids.

In 2001, inspired by the methane monooxygenase (MMO) enzyme, Jacobsen and coll. reported that H_2O_2 was able to oxidize alkenes into epoxides in presence of $[Fe(BPMEN)(CH_3CN)_2](ClO_4)_2$ at 5 mol% with a selectivity of 40%.[11a] Addition of one equivalent of acetic acid with respect to catalyst as additive in the reactional mixture improved the selectivity to 82%. After this seminal work demonstrated that one additive can enhance the selectivity for epoxidation reactions with metal complexes with a tetradentate N_4-donor ligand, different ligand scaffolds have emerged in the literature

(i) to access to higher selectivity and higher catalytic performances

(ii) to study the mechanism and notably the role of the carboxylic acid additive.

Among the numerous catalysts described in the literature, a selection of a few highly efficient ones is reported in Scheme 7.

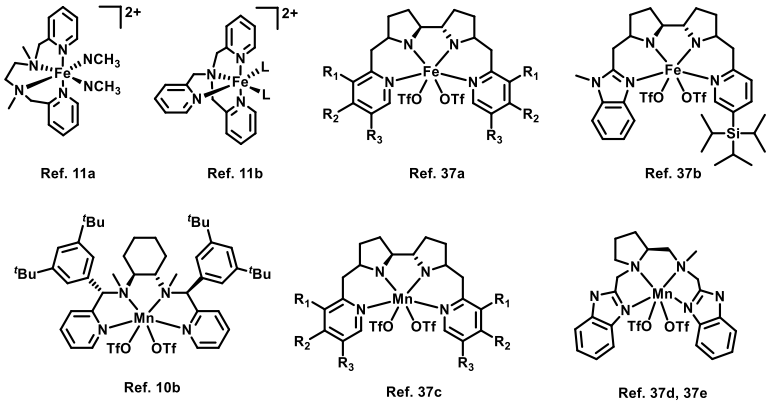

Scheme 7 - Selected iron(II) and manganese(II) complexes for epoxidation.[11a,36]

All these catalysts possess tetradentate N_4 ligand and two *cis*-labile sites. It has to be noted that most of them possess a chiral backbone and enantioselectivities up to

99% were obtained.[36b,36c] They are efficient for epoxidation with H_2O_2 in acetonitrile with the presence of a carboxylic acid or H_2SO_4 in one case.[10b] Without carboxylic acid, a mixture of *cis*-diol and epoxide was observed with ligand-dependent *cis*-diol: epoxide ratios between 1:10 to 1:1. With carboxylic acid, the epoxide was formed exclusively.[11b]

These results questioned the nature of OAT reagent and the role of carboxylic acid. During the two last decades, extensive studies have answered these questions and a summary is presented in Scheme 8.[11b,36a] In both cases, the first step is the generation of a hydroperoxo compound, a sluggish oxidant by itself, evolving into the oxidizing species through O-O cleavage.[26a] As in Cyt P450, this cleavage step is crucial. In absence of carboxylic acid, water molecules assist the O-O bond cleavage and generate the Fe(V)=O(OH) species responsible of the oxidation of the alkene into epoxides and *cis*-diols.[37] In presence of acetic acid, the mechanism is slightly different. Carboxylic acid, acting as proton relay, is responsible of the protonation of the distal oxygen atom of the hydroperoxo compound and the generation of a Fe(V)O(OCOR) species. In this case, the carboxylate group remaining on the Fe center does not allow the formation of the *cis*-diol product and thus leads to exclusive formation of the epoxide.[38]

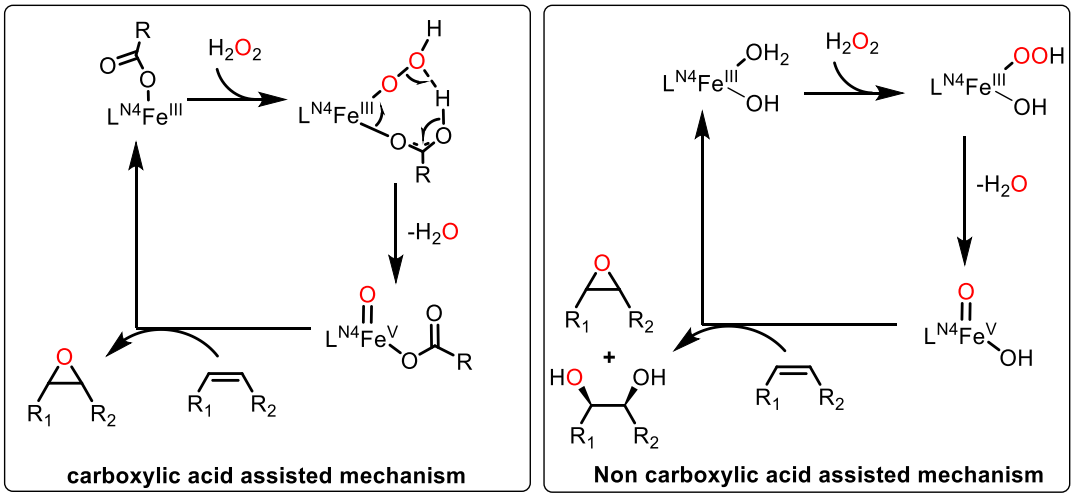

Scheme 8 - Comparison of carboxylic and non-carboxylic assisted mechanism for oxygen atom transfer process.

In addition to the use of H_2O_2 as oxidants, peracids are also used with metal complexes with two *cis* labile sites. The nature of the oxidant has been highly discussed. Using the enantioselectivity as a mechanistic probe for epoxidation reaction, it has been clearly demonstrated that the electrophilic $Fe^V(O)(O_2CR)$ species is the sole possible OAT agent.[11c]

One remaining question was about the metal complexes with one or two *trans* labile sites, inefficient when H_2O_2 is used as oxidant.[39] However, the use of peracids as oxidant leads to the formation of an iron(III)-acylperoxo complex intermediate responsible for epoxidation without conversion into a high-valent iron-oxo species (Scheme 9).[40]

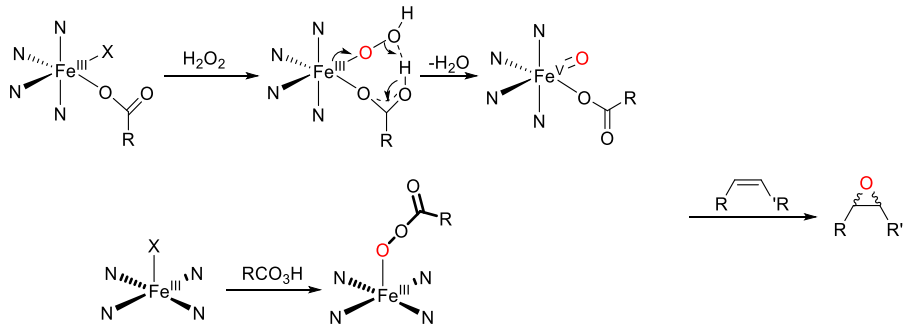

Scheme 9 - Differences between H_2O_2 and peracid epoxidation processes.

However, the reactivity difference between these two systems (*cis vs. trans*) is spectacular. Indeed, the iron(III)-acylperoxo complex is 400 times slower than the $Fe^{V}(O)(O_2CR)$ complex.[41]

These results highlight that the O-O bond cleavage of the peroxo intermediate is crucial for creating a unique powerful oxidation agent.

The controlled access to metal-oxo species is crucial to obtain efficient catalysts with H_2O_2 as oxidant. Based on the results from the literature, the heterolytic O-O bond cleavage of the hydroperoxo intermediate might be the key step to improve the access to more efficient catalysts. More precisely, the selective protonation of the distal oxygen atom of the hydroperoxo through a proton relay is a strategy to explore.

1.2.4. Strategies to favor O-O bond cleavage in metal complexes

In the context of non heminic systems, metal complexes possessing functional groups able to interact with H_2O_2 have been designed to favor the heterolytic O-O bond cleavage.[42]

Ménage and coll. incorporated carboxylic moieties on the BPMEN ligand to mimic the effect of the carboxylic acid. However, a deprotonation followed by a coordination on the Fe center was observed, inhibiting the catalyst. (Scheme 10).[43]

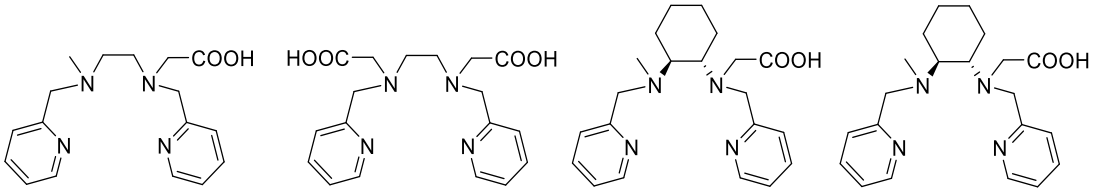

Scheme 10 - ligands developed by Ménage and coll.

In a similar approach, during the PhD time-work, F. Banse and coll. described the first selective formation of a Fe(IV)-oxo intermediate starting from a Fe(II)-metal complex and H_2O_2. Indeed, an amine introduced in the second coordination sphere of a metal complex acted as a proton relay and lead to the exclusive conversion of a Fe(II)-

metal complex into an Fe(IV)-oxo intermediate by H_2O_2 without Fenton reaction (Scheme 11). This result highlights the importance of an H-bond interaction to selectively produce a metal-oxo complex.[44] However, no catalytic activity for this compound has been reported so far.

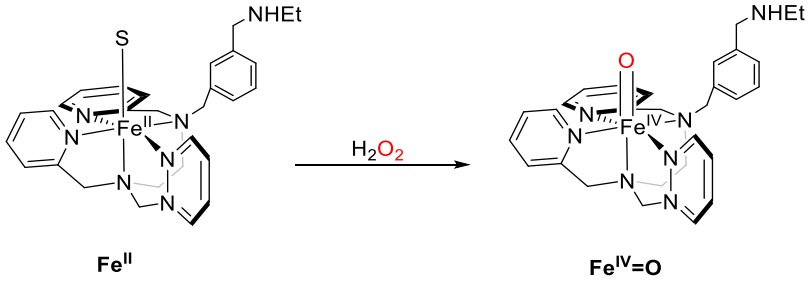

Scheme 11 - Influence of the second coordination sphere on the formation of a $Fe^{IV}O$ intermediate (S=H_2O or MeOH).

1.2.5. Stabilization of high-valent metal-oxo species in metal complexes

In parallel to the development and mechanistic studies in OAT reactions, several groups are interested in the stabilization of highly reactive species, notably by H-bond network.[45] Indeed, many metalloproteins, especially those involved in oxidative processes, have H-bond networks within their active sites that directly interact with the metal-oxo species and stabilize them during the oxidation process. For example, the structure of compound I of cytochrome C peroxidase determined by X-ray diffraction analysis shows a H-bond network involving a structural water molecule and active site amino acid residues interacting with the iron-oxo unit (Figure 1).[46]

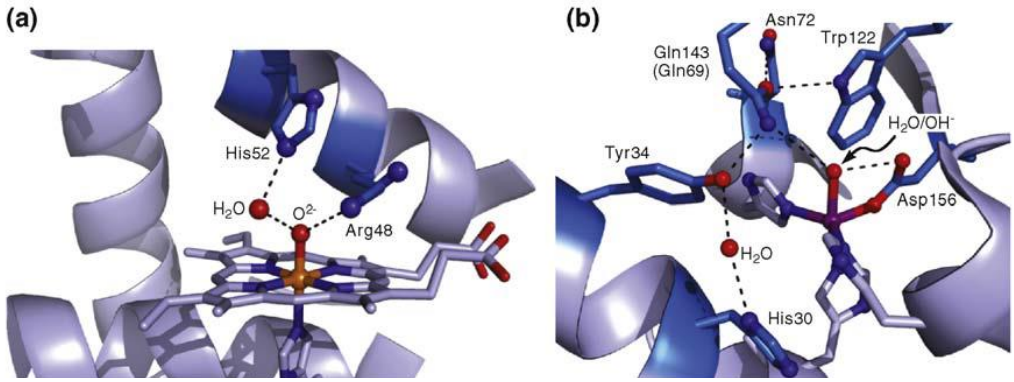

Figure 1 - Stabilization of the active site of a peroxidase stabilized by a H-bond network.

Noticeable advances on non-heme synthetic systems have been reported mainly by the Borovik's group and more recently by the groups of D. Goldberg, A. Fout, C. Scarborough and N. Szymczak[47] whose main synthetic contributions are summarized in scheme 12.

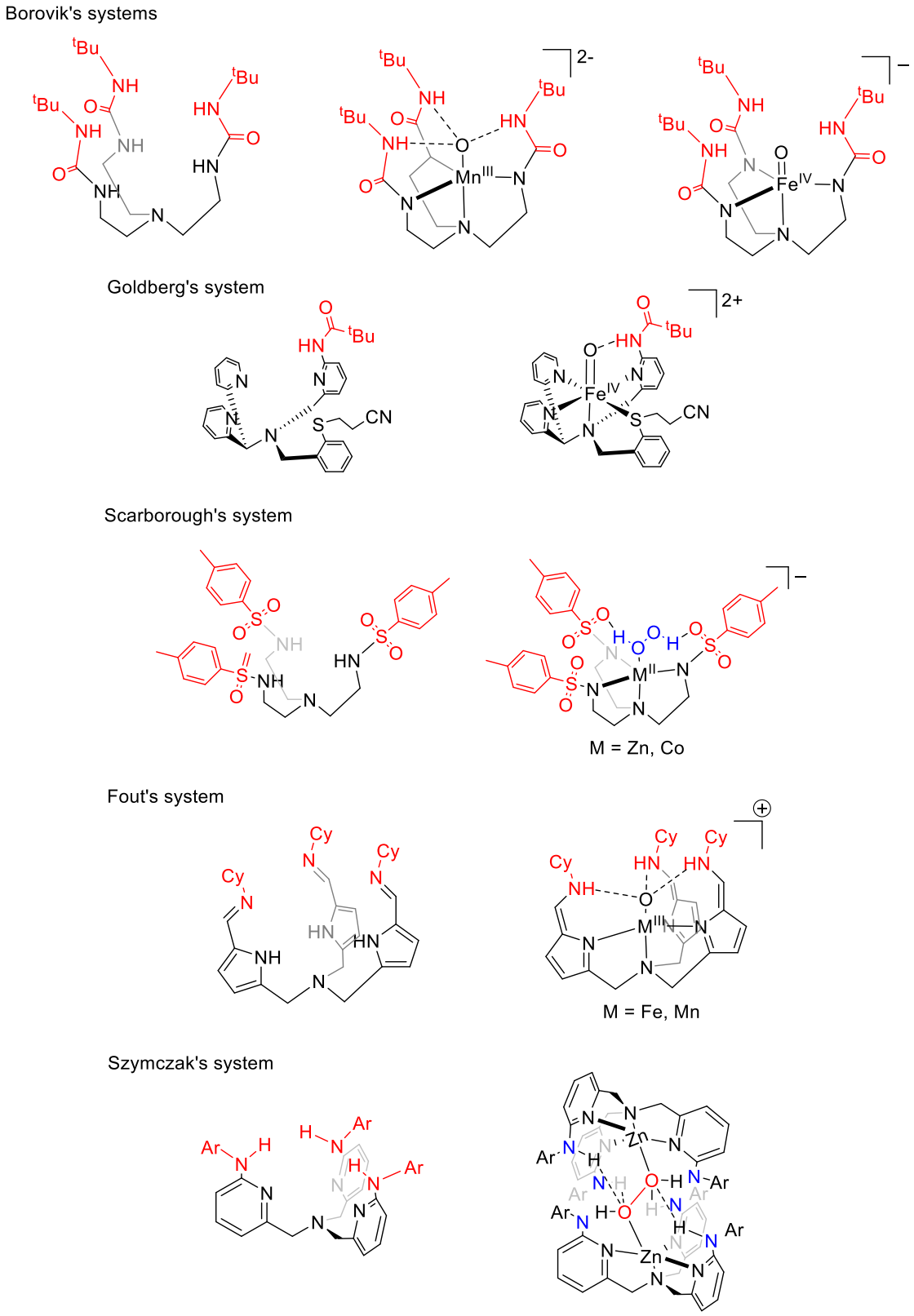

Scheme 12- Systems from the literature stabilizing reactive species. Ligands (left), species isolated (right).

Over the last two decades, the Borovik group has worked with a tripodal urea-based ligand that allows accessing metal complexes with an N_4 primary coordination environment.[48] In the second coordination sphere, a cavity formed by the urea arms installs three N-H groups proximal to the metal center prone to form intramolecular H-bonds to exogenous ligands on the metal center. Thanks to the H-bond donating properties of the N-H functions, very unstable species such as Fe^{IV}-oxo and Mn^{V}-oxo compounds were isolated and characterized by X-ray crystallography. However, the reactivity of these systems toward OAT reactions has not been reported so far.

With the objective to examine the influence of a single H-bond donor on the reactivity of the Fe^{IV}-oxo toward oxygenation reactions, the Goldberg group reported a pentadentate N_4S ligand functionalized by pendant amide group in the second coordination sphere. Using PhIO as oxygen atom donor with 2 mol% catalyst loading, oxidation of thioanisole produced the corresponding sulfoxide solely in 80% yield. Kinetic studies revealed that the presence of amide group provoked a 70-fold rate enhancement in comparison with the amide-free parent compound. [49]

Scarborough's group explored the effect of H-bond acceptors in the second coordination sphere by using the ligand tren (tren = tris(2-aminoethyl)amine) functionalized by tosyl groups. Notably, they characterized Co^{II}-H_2O_2[50b] and Zn^{II}-H_2O_2[50a] adducts, the latter being stable enough to be characterized by X-ray crystallography thanks to second sphere hydrogen bond interactions. The reactivity of the Co^{II} complex is also very interesting. Indeed, the reaction between the Co^{II} complex and H_2O_2 in presence of $[(15\text{-crown-5})Ca](OTf)_2$ leads to the formation of a Co^{III}-OH compound *via* a putative Co^{IV} intermediate that rapidly abstracts an hydrogen atom from the solvent. In this reaction the Ca^{2+} ion induces the oxidation of Co^{II} to Co^{III} by H_2O_2.[50b]

Fout's group reported ligands based on a pyrrolide platform functionalized with imine groups.[51] Upon complexation, a tautomerization process occurred to afford the amine-azafulvene species. This strategy allowed a modulation of the oxidation state of a transition metal center in coordination complexes and this ligand species can serve as both a hydrogen bond donor and acceptor. With these ligands, Mn-oxo and Fe-oxo were obtained, the latter ones being implicated into the catalytic reduction of nitrate and perchlorate anions.[51b]

1.2.6. Fluoroalcohol solvents in OAT reactions

Using molecular metal complexes to activate H_2O_2 or to stabilize reactive intermediates is not the only pathway explored. In the context of alkenes oxidation with H_2O_2 as oxidant, fluorinated alcohol solvents have shown exciting properties.[52] Indeed, catalyst-free oxidation of cyclic alkenes in presence of two equivalents of H_2O_2 led to the exclusive formation of the corresponding epoxide in 100% yield when reaction was

carried out in hexafluoroisopropanol (HFIP) as solvent. The yield diminished to 20% with linear alkenes. [53] Mechanistic studies have identified multiple hydrogen-bonding interactions between the solvent and the oxidant as the crucial factor (Figure 2). In a putative aggregate composed of H_2O_2 and fluorinated alcohol molecules, hydrogen peroxide is coordinated by two alcoholic hydroxyl groups in a cyclic fashion, one fluorinated alcohol acting as a hydrogen bond donor toward the leaving OH group (formally OH^-) and the other one as a hydrogen bond acceptor, deprotonating the hydroxyl group which is transferred to the C=C double bond to form the epoxide. The internal hydrogen bond between the two fluorinated alcohols cooperatively increases the hydrogen bond donor ability of the alcohol molecule which activates the leaving OH group. Through this cooperative hydrogen bond network, O-O bond polarization is achieved generating an electron deficient oxygen atom, ready for electrophilic attack on the alkene double bond. The simultaneous cyclic hydrogen-bond network and proton relay action of the fluorinated alcohol molecules allow an almost barrier-free proton transfer from one O atom to the adjacent one in H_2O_2. However, the substrate scope for efficient epoxidation in fluoroalcohol solvents is limited to electron-rich alkenes; linear alkenes such as 1-octene are poorly converted into their corresponding epoxide. Moreover, the need of a fluoroalcohol as solvent poses limitations, as these materials are prohibitively expensive for large-scale applications.[54]

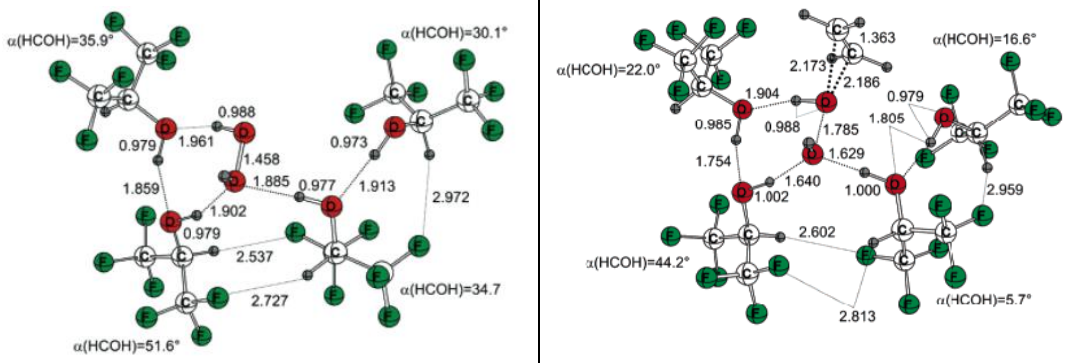

Incorporation of HFIP in H_2O_2 activation process | Transition state of H_2O_2 activation by HFIP

Figure 2- Activation of H_2O_2 by hexafluoroisopropanol (HFIP).

A recent contribution of M. Costas and coll. has also shown that the reactivity of Fe^{II}- and Mn^{II}-metal complexes towards hydroxylation reactions can be modified when carried out in fluoroalcohol solvents. Notably, for C-H oxidation reactions, these solvents engage in hydrogen bonding with the first formed alcohol product, preventing overoxidation to the ketone and allowing highly chemoselective hydrocarbon hydroxylation. These solvents are able moreover to strongly activate adjacent C-H bonds toward electrophilic hydroxylating reagents (Scheme 13).[55]

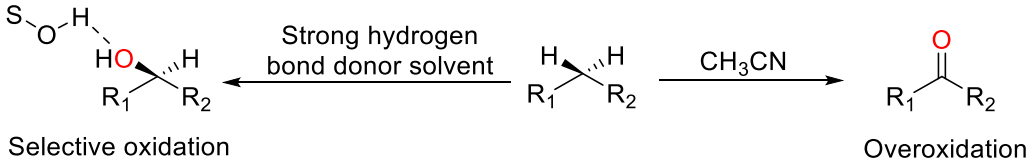

Scheme 13- Influence of fluoroalcohol solvents during hydroxylation reaction.

1.2.7. Fluoroalcohol and metal complexes

Inspired by H-bond network in their second coordination sphere of metalloenzymes, our group has introduced fluoroalcohol groups in the second coordination sphere of a pyridinophane based ligand.[56] With this ligand, first-row metal complexes (metal = Fe(III), Mn(II), Zn(II), Cu(II)) have been synthetized (Scheme 14). No reactivity of these metal complexes has been explored before this PhD work.

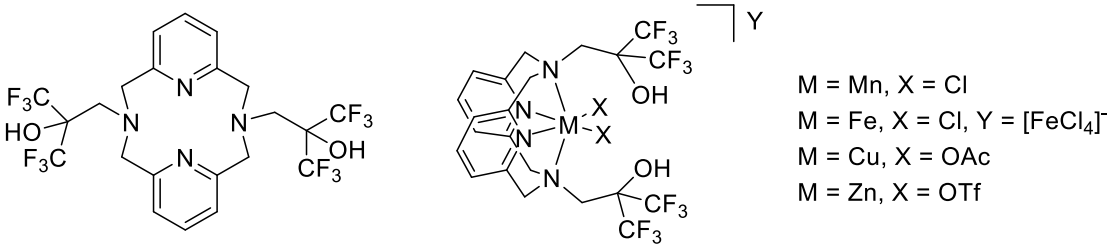

Scheme 14 - Pyridinophane ligand functionalized by fluoroalcohol functions (left) and first row metal complexes (right)

Based on these literature precedents, during this work, introduction of a second coordination sphere, able to create a H-bond network with H_2O_2, on metal complexes was targeted. An interaction between the metal center, H_2O_2 and the second coordination sphere was expected. The goal was to facilitate H_2O_2 activation, and so to favor the formation of a metal-oxo species to finally obtain very efficient catalysts. This approach will be explored in chapter 2.

1.3. Polyoxometalates (POMs)

Polyoxometalates (POMs) are a class of inorganic compounds which are present in different classical research areas.[57] Being used as catalysts in the Chapter 4 of this manuscript, those species will be presented briefly and attention will be focused on their catalytic properties towards (ep)oxidation, considering the processes using free POMs and the supported POMs.

Historically, those compounds are known from a long time. Indeed, the first polyoxometalate $(NH_4)_3PMo_{12}O_{40}$ was found in 1826 by Berzelius[58]. The syntheses of those compounds have been also followed by Marignac.[59] The topic is still active from this time and more studies about their syntheses and the study of their properties have been performed.[60] In the last thirty years, as relevant for the manuscript, POMs have showed an important role as catalysts for organic synthesis.[61]

POMs (in protonated forms) possess strong acidity as well as redox properties.[62] They are environmentally friendly[63] and are good selective oxidation catalysts.[51c] Those properties could be tuned by the nature of the elements used for their synthesis (metal, heteroatom, counterions). Since 1970s, those eco-friendly catalysts became interesting for researchers.[57a,63]

Even if synthesis of POMs, as well as their structure elucidation and catalytic reactivity, have been highly reported in numerous articles, books and reviews,[60a-p,64] we will present very briefly in this chapter the nature of the species. The focus will concern catalytic oxidation, the only chemical transformation we studied in presence of those species.

1.3.1. Structural parameters and definitions

Polyoxometalates (POMs) are deprotonated forms of heteropolyacids (HPAs). Those species consist formally in condensation of different metal oxides in acidic media (primary structure).[65] POMs are surrounded by inorganic or organic cations (secondary structure) and water molecules (tertiary structure).[66] POMs can be expressed as in Figure 3 with the general formula of the primary structure being $[X_aM_bO_c]^{n-}$:

- X is a central templating heteroatom, located from IB group to VIIIA group.
- M is a transition metal (such as Mo, W, V Nb...), generally in its highest oxidation state (d^0 or d^1). They can be called addenda or coordination atoms when added in a second step. The most common ones are W and Mo. V appears occasionally. In general case, Mo (VI) and W(VI) are the most stable form of polyoxometalates.[67]
- X and M atoms are linked together through oxo bridges.
- M is coordinated with terminal oxygen atoms (oxo), leading to octahedral coordination around M.[68]

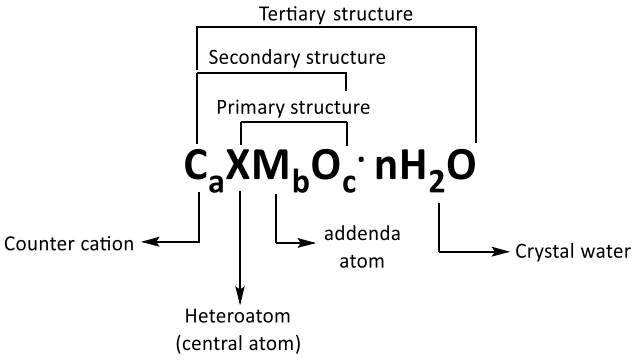

Figure 3 - General features of polyoxometalates.[66]

The primary backbone POM structure is determined by atomic distribution (Table 1).[62] Five main different structures were discovered, their usual names given according to their discoverers: Keggin,[69] Wells-Dawson,[70] Waugh,[71] Anderson[72] and Silverton.[73] The general formulas are described in Table 1 and the structures represented in Figure 4.

Table 1 -Structure of POMs

General formula	Negative charge number	X^{n+}	Usual name
$XM_{12}O_{40}$	8-n	P^{5+}, As^{5+}, Si^{4+}, Ge^{4+}, C^{4+}	Keggin
$X_2M_{18}O_{62}$	6	P^{5+}, As^{5+}	Dawson
XM_9O_{32}	6	Mn^{4+}, Ni^{4+}	Waugh
XM_6O_{24}	12-n	Te^{6+}, I^{7+}	Anderson(A)
$XM_6O_{24}H_6$	6-n	Co^{3+}, Al^{3+}, Cr^{3+}	Anderson(B)
$XM_{12}O_{42}$	8	Ce^{4+}, Tb^{4+}	Silverton

With: M: addenda atom (coordination atom, e.g. W^{6+}, Mo^{6+} etc.); n: positive charge number of central atom X.

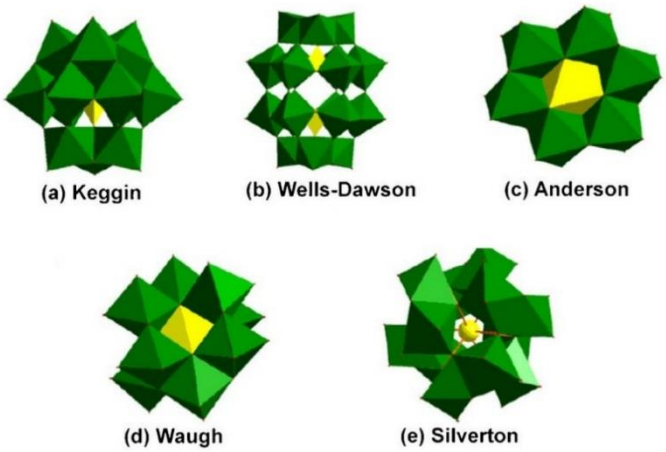

Figure 4 - Different structures of polyoxometalates.[74]

1.3.1.1. Primary structure of Keggin structure POM

Keggin structure POM is the most thermally stable among these five POM structures.[75] It is also the most explored one, especially as catalyst in lots of catalytic reactions.

A Keggin POM possesses three characteristics features[76]:

1. Ideal high Td symmetry.
2. Tetrahedral coordination of central atom X
3. Octahedral coordination of transition metal M

Four type of oxygens are found in Keggin structure (Scheme 15): which correspond to:[77]

1. O_a: 4 μ^4-oxo bridges between X and M
2. O_b: 12 μ^2-oxo bridges between two M (octahedrons sharing one corner)
3. O_c: 12 μ^2-oxo bridges between two M (octahedrons sharing one edge)
4. O_t: 12 terminal oxo bounded with one M.

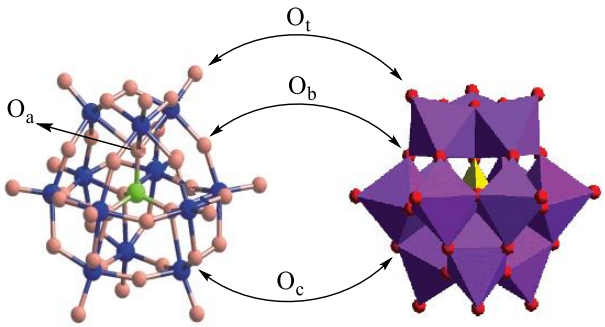

Scheme 15 - Type of oxygens in Keggin structure.[77b]

Due to the high symmetry of those species, IR spectroscopy has been an efficient tool to characterize the POMs since each structure has its own "fingerprint". The explanation will not be detailed herein but M-O bond of different type heteropolyanion connection could be identified, infrared was used frequently to identify primary structure of POM.[77c] Characteristic IR vibrations in the range 600-1100 cm^{-1} belong to $\nu_{as}(P\text{-}O_a)$, $\nu_{as}(M{=}O_t)$, $\nu_{as}(M\text{-}O_b\text{-}M)$, $\nu_{as}(M\text{-}O_c\text{-}M)$ (M= Mo, W, V etc.). [63,78]

Multinuclear NMR has been a very useful tool to characterize those species.[79]

1.3.1.2. Secondary structure

Secondary structure is related to the cations surrounding the POMs. The nature of cations (charge, size) does define different POM properties (crystal lattices, acidity, redox properties, solubility, catalytic reactivity).[80]

XRD analysis was often used to determinate atom arrangement within crystal cell. Diffraction peaks position depend on crystal lattice structure and peak intensity depends on atom position in crystal cell.[81]

1.3.1.3. Addenda atoms

The structures presented consider a complete structure. According to experimental conditions, one (or more) M can be removed from the structures, leading to lacunary species. Those lacunas can be filled by other atoms, called in this part M'. The role of metal M' added to lacunary POM/HPA must not be neglected. Indeed, M' can play an important role in catalytic oxidation reactions. Those metal atoms are active sites that can generate the oxo- or diperoxo-Metal M'(O_2), intermediates responsible of the oxygen atom transfer to the substrate. Let consider three examples.

- The vanadium in $TBA_4[\gamma\text{-}V_2(\mu\text{-}OH)_2SiW_{10}O_{38}]$ TBA = $(n\text{-}C_4H_9)_4N^+$) is the active site in alkene epoxidation.[82]
- The iron in $TBA_4[Fe(H_2O)PW_{11}O_{39}]$ is the active site in the alkanes oxidation.[83]
- The M (M= Ru, Os) in $[(C_8H_{17})_3NCH_3]_4\text{-}[M^{II}(DMSO)_3Mo_7O_{24}]$ is the active site in the oxidation of alcohols.[84]

1.3.2. POM properties

1.3.2.1. Acidic properties

The multiple active sites can explain catalytic activity of HPAs, provided by the nature of POMs and surrounding hydrogen atoms. HPAs can bring active proton to promote acid-catalysed reactions. In contrast, POM can catch active proton or cation from organic substrate, i.e. the terminal oxygen atoms can be active sites in base-catalysed reactions.

Due to electron delocalization, POMs are strong Brönsted acids.[85] Their acidity is related to POM negative charge and oxidation degree of central atom.[86] Most of POMs possess stronger acidity than oxyacid form of their central atom.[87]

HPAs are very soluble in polar solvent, such as H_2O, alcohol, ethers, etc.[88] and weakly soluble in non-polar solvent (e.g. hydrocarbon).[60h] The pKa-measured in polar solvents

(H_2O,[89] Ethanol,[90] and CH_3COOH[91])- showed that HPAs are more acidic in acetic acid than strong inorganic acids, such as HBr, HCl and H_2SO_4.

Regardless of homogenous and heterogeneous catalysis, reactivity of POMs is limited by its acidity determined using different techniques like Hammett acidity,[92] n-butylamine titration,[93] and NH_3-TPD[94].

1.3.2.2. Redox properties

POMs are strong multi-electrons oxidants. Addenda atom - existing in highest oxidation form- can accept electrons without damaging their stability. Thus, POMs are strong oxidants often used as catalysts in oxidation reactions.[63]

Heteroatom, addenda atom and surrounding cations influence significantly its acidic strength. Its acidity is also related to the following parameters:

1. Structure (e.g. acidity of Phosphomolybdic acid Dawson > Keggin structure)
2. Addenda atom (Oxidation ability: V > Mo > W)
3. Electrostatic effect of anionic charge (when negative charge increase, oxidizing ability decrease)
4. Cation can influence on the oxidative ability. When cation is reduced, POMs oxidative ability increases. Oxidative ability of POMs was deeply studied on H_2, CO and organic model substrates[95].

1.3.2.3. Pseudo phase properties

Concept of "pseudo phase" was proposed by Hill in 1989.[96] This theoretical foundation for HPAs application in catalysis was used to explain the excellent catalytic reactivity of HPAs.[97] Generally, catalytic reaction catalyzed by solid catalysts often occur on their surfaces. However, the coordinated water of POM release- during absorption – desorption process- results in a change of secondary structure, creating "free internal spaces" where substrate can enter, providing a bigger contact area within a more flexible structure and boosting the catalytic reaction.

Due to the space increase, small polar molecules (e.g. alcohol, ammonium) can exchange with coordinated water at the interface of POM, transforming POMs from hard material into soft (gel-like) one. Molecules on the surface of POMs can easily exchange with molecules inside the bulk, leading to bigger efficiency and lower activation energy. This "pseudo phase" behavior is applicable to HPAs and water-soluble POMs.

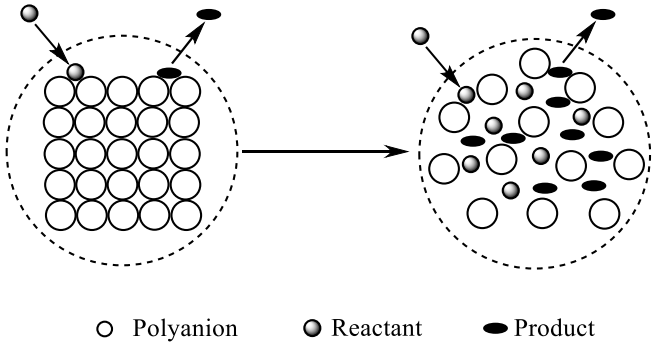

Scheme 16 - Schematic of pseudo phase property.

1.3.2.4. Thermal Stability

POM stability- important parameter for activity and recyclability- is related to their structure[57g]. Keggin structure possess higher stability among all five structures described previously. Keggin HPAs/POMs with high thermal stability are frequently used in gas-phase reaction at high temperature.[98] The thermal stability observed follows the trend: $H_3PW_{12}O_{40} > H_4SiW_{12}O_{40} > H_3PMo_{12}O_{40} > H_4SiMo_{12}O_{40}$.[99] Cation does influence POM stability, following cation order: $K^+ \approx Tl^+ \approx Cs^+ > NH_4^+ > La^{3+} \approx Ce^{3+} > Mg^{2+} > Ca^{2+} \approx Mn^{2+} > H^+ \approx Cd^{2+} > Cu^{2+} \approx Ni^{2+} > Ba^{2+} \approx Co^{2+}$.[100]

1.3.3. Catalytic reactivity of POMs

POMs as catalyst are used mainly in chemical/photochemical/electrochemical oxidation and acid catalysis. Among numerous oxidation reactions, alkenes, alkanes, alcohols and sulfides were the most studied compounds. In acid catalyzed reaction, POM/HPA also proved its activity and lead to interesting results (epoxide ring opening and rearrangements…).

Catalysis with POM/HPA is a mature research field. High efficiency and high stability define them as eco-friendly catalysts.

1.3.3.1 Non grafted POMs in catalysis oxidation reaction.

POM showed excellent reactivity in oxidation reactions. This concerns the research direction of this thesis. Traditional oxidation processes use often strong oxidants, such as peroxyacids,[101] HNO_3,[102] and HIO_4[103] which produce lots of wastes as described previously. Utilization of green oxidants such as O_2, H_2O_2 and TBHP as oxygen source, producing non waste by-products. These cleaner oxidants often demanded catalysts for activation. POMs match perfectly as catalysts with these “green” oxidants.[104]

POMs possess strong oxidative ability and can remain stable after obtained six or more electrons. In catalytic reactions, POMs can be reduced by substrate and oxidized

by oxidant to return to their initial form. The POMs with Keggin structures $Y_n[XM_{12}O_{40}]$ were deeply studied in catalysis.

Oxidative desulfurization (ODS)

General properties of structure and reactivity of oxo complexes of Mo(VI) and W(VI) have been deeply studied. The terminal bonds Mo=O and W=O can react reversibly with H_2O_2, leading to active labile η^2-peroxo complexes without destroying the Keggin structure. This active species acts as an oxidizing agent in ODS reaction.

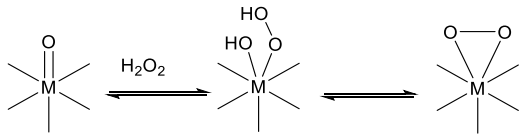

Scheme 17- formation of peroxo moiety in metal-oxygen octahedron of Keggin HPA immobilized on activated carbon (M = W or Mo).

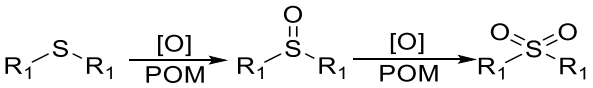

Scheme 18 - general procedure of catalyzed ODS reaction.

Several examples relate this transformation under different conditions. Some active POMs are active in epoxidation reactions: $TPA_3\{[HW_2O_2(O_2)_4(\mu\text{-}O)]_2\}$,[105] $TBA_4(\gamma\text{-}H_4SiW_{10})$, [106] $TBA_3H[\gamma\text{-}SiW_{10}O_{36}(PhPO)_2]$, [107] $\gamma\text{-}V_2SiW_{10}/SiO_2$, [108] $(C_{10}H_{21}N(CH_3)_3)_{11}[La(PW_{11}O_{39})_2]$,[109] and $TBA_{3(}\gamma\text{-}V_2PW_{10})$[110] are also highly active in oxidative desulfurization reactions.

For example, Rujiraworawut et al. tested activity catalytic of a series of POMs ($Na_2HPM_{12}O_{40}$, $H_3PM_{12}O_{40}$, $Na_2HPM_{12}O_{40}$, $(VO)H[PM_{12}O_{40}]$ and $(n\text{-}Bu_4N)_3[PM_{12}O_{40}]$) (M= Mo or W)) using BDT as a model substrate and H_2O_2 as an oxidant. Remarkable results were obtained, up to 95% of conversion was obtained when catalyzed by $Na_2HPW_{12}O_{40}$. This exciting result might be reproduced and used in gas oil desulfurization.[111]

Alcohol oxidation

Oxidation of alcohols to ketones is an important step in organic synthesis for fundamental research and industrial production. Some of them are important intermediates in pharmaceuticals and agricultural chemistry.[112] POMs are remarkable efficient catalysts in alcohols oxidation with H_2O_2, O_2 and TBHP.[113]

Several Mo(VI) and W(VI) complexes were reported as effective catalysts with H_2O_2, and operate *via* a peroxometal mechanism similar than the one with general Mo or W peroxo complexes.[114]

Complex **1** can react with H_2O_2 and lead to a bis(peroxo)oxo-complex (**2**), in CH_3OH. CH_3OH takes one place of M-O bond of dioxo bridge and lead to a M-OOH(CH_3OH) complex. When the alcohol molecule approaches, coordinated solvent is replaced by the substrate. Then ketone is formed, and water molecule is released.

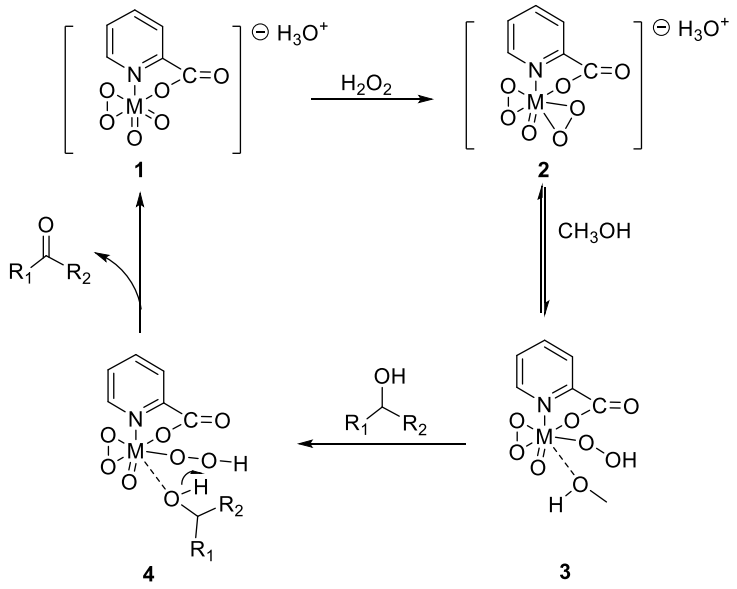

Scheme 19 - Mechanism of alcohol oxidation with peroxocomplexes (M = W or Mo).[115]

Neumann's group reported a new system for alcohol oxidation into ketone and aldehyde using O_2 as oxygen source and $[(C_8H_{17})_3NCH_3]_4[M^{II}(DMSO)_3Mo_7O_{24}]$ as catalyst (M = Ru, Os).[84]

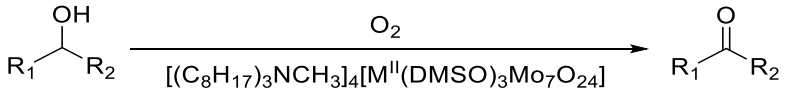

Scheme 20 - catalyzed alcohol oxidation with O_2 as oxidant.

Among most of model substrates are oxidized with this system and exciting results were obtained with most of yields higher than 99%.

Epoxidation of Allylic alcohols

In 2003, Mizuno group reported that $K_2\{[WO(O_2)_2(H_2O)]_2(\mu\text{-}O)\}\cdot 2H_2O$ is an active specie in epoxidation of allylic alcohol reaction with H_2O_2 as oxygen source.[116] This peroxospecies, which can remain stable between pH=2.5 to 7, is a very active species in selective epoxidation of allylic alcohol with H_2O_2.

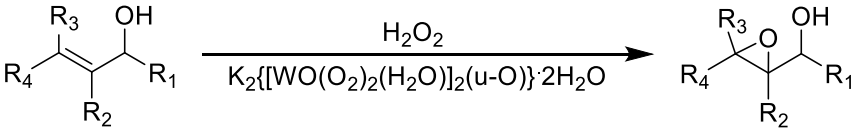

Scheme 21 - epoxidation of allylic alcohol by H_2O_2catalyzed by $K_2\{[WO(O_2)_2(H_2O)]_2(\mu\text{-}O)\}\cdot 2H_2O$.

The activity of the peroxospecies was tested on propen-1-ol, 96% of conversion and 99% of selectivity to 2,3-epoxy-1-propanol were observed. Other substrates were also tested, such as 3-methyl-2-buten-1-ol, isobutenol, hex-2-en-1-ol and yields higher than 90% were obtained. As W- peroxospecies showed an interesting activity in catalytic epoxidation of allylic alcohol reaction, W- peroxospecies in POM could be also an excellent catalyst in the same type of reaction. Potential reactivity of POMs needs to be explored.

Niu et al. reported new series of polyoxotungstates for epoxidation of allylic alcohol reactions, using H_2O_2 as oxidant. Satisfying results were observed.[117] Conversion with catalysts Ni1 to Ni3 are between 94.8% and 97.5%. With Ni catalyst fragment (Glyphosate, $NiCl_2$ and As_2W_{19}) only 4.3 %, 3.3 % and 53.4 % of conversion were observed respectively. With these examples, activity of POM in epoxidation of allylic alcohol reaction were proved.

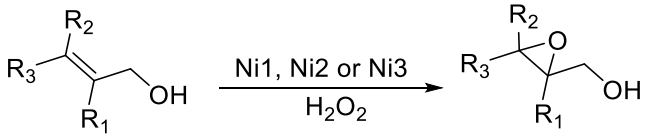

$[\{Ni(H_2O)_5\}\mathbf{x}(AsW_6O_{21})_2\{Ni(OOCCH_2NCH_2PO_3)_2\}_3]$ (**x** = 0 (Ni1), 1 (Ni2 and Ni3))

Scheme 22 - Catalyzed epoxidation reaction by Polyoxotungstates incorporating organophosphonate and nickel.

Epoxidation of alkenes

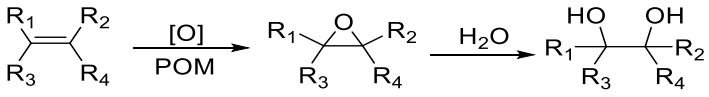

Scheme 23 - oxidation of alkene.

The first stage of alkenes oxidation usually leads to epoxides. In presence of water, hydrolysis can occur and does give the corresponding diol. Both epoxide and diols are interesting substrates, but epoxide is a more important intermediate that can have several industrial applications.

POMs are used extensively with olefins and some results can be highlighted.[61a-c]

Venturello–Ishii systems[118] are famous for epoxidation reaction with H_2O_2. In 1989, Venturello found a new way of alkenes epoxidation in biphasic system in presence of tungstates and phosphates (mixed *in situ*) as precursor of catalyst and H_2O_2 as oxygen source. Under reaction conditions, a peroxo intermediate is formed. The compound of formula $\{PO_4[WO(O_2)_2]_4\}^{3-}$ (isolated and characterized by X-ray) possesses a high activity in epoxidation reactions.

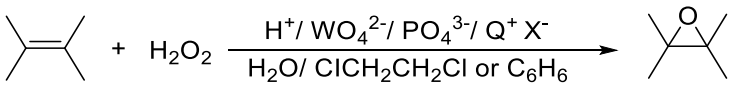

Q^+X^- = onium salt

Scheme 24 - Alkene oxidation with H_2O_2 catalyzed by $\{PO_4[WO(O_2)_2]_4\}^{3-}$.

Ishii group studied more deeply the Venturello system.[119] They used $H_3PW_{12}O_{40}$ or $H_3PMo_{12}O_{40}$ as catalysts, H_2O_2 as oxidant and ammonium salts with long-chain alkyls as phase-transfer agent. Under those conditions, epoxides were observed as minor product, the main products being diols. During the reaction, the proton on POMs was exchanged by the long chain quaternary ammonium cation. As a result, the modified catalyst $[\pi\text{-}C_5H_5N(CH_2)_{15}CH_3]_3PW_{12}O_{40}$ or $[\pi\text{-}C_5H_5N(CH_2)_{15}CH_3]_3PMo_{12}O_{40}$ can shuttle between two phases and accelerate reaction rate. Due to low POM acidity, main product observed is epoxide. This modified catalyst could be prepared before reaction by reacting $H_3PW_{12}O_{40}$ with organic cation.

Based on cation exchange method, POM could be immobilized on surface of any functionalized solid support to make the catalyst reusable, this part will be introduced later.

Catalytic epoxidation mechanism with H_2O_2 and Keggin POM were also deeply studied. Several mechanisms were proposed. The mechanism of H_2O_2 activation by Ti^{IV} containing Keggin structure POM was clarified by Carbo, Kholdeeva and Poblet.[113b] In this case, M' (Ti) was the active site. Two types of mechanisms were proposed (See following scheme). In the case of OAT processes from $PTi(OH)W_{11}O_{39}^{4-}$, two pathways were proposed. The homolytic O-O cleavage is energetically less favorable (path **b**) and the heterolytic O-O bond cleavage leads to high selectivity towards epoxide. Michaelis–Menten-type kinetics for $[Ti_2(OH)_2As_2W_{19}O_{67}(H_2O)]^{8-}$(**2**) catalyzed epoxidation of cyclooctene with H_2O_2 show: procedure **d** from Ti-OH to Ti^{IV}-OOH is a reversible process, the rate limiting step being oxygen transfer from Ti^{IV}-OOH to alkene. Another important factor in oxygen transfer step is the electronic property (nucleophilicity) of alkene.[120]

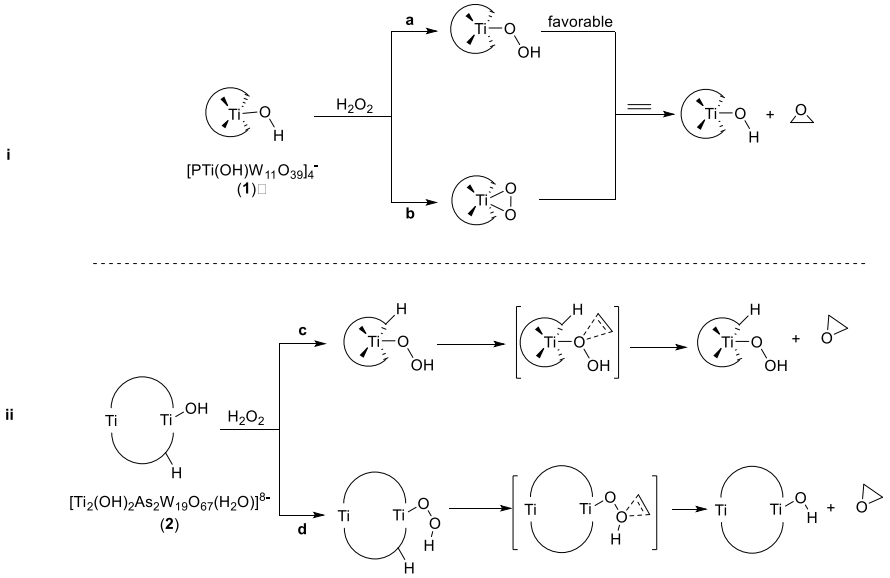

Scheme 25 - Oxygen atom transfer from Ti^{IV}-OOH to alkene.

Another example was reported by Mizuno et al. in 2003. An efficient Keggin POM-$[\gamma\text{-}SiW_{10}O_{34}(H_2O)_2]^{4-}$ synthesized by a protonation of a divacant lacunary $[\gamma\text{-}SiW_{10}O_{36}]^{8-}$ showed excellent reactivity in epoxidation reaction, process being tested on over 10 substrates under different conditions. Yields ≥ 99% were obtained for all tested substrates.[121]

All the reaction examples described previously were done in organic solvents. In order to produce less waste, it is very interesting to reduce or eliminate organic solvent. In the research group, epoxidation of cyclooctene with H_2O_2 catalyzed by an ion exchanged POM ($[PM_{12}O_{40}]^{3-}$, M = (W or Mo)) under solvent-free condition was studied.[113a]

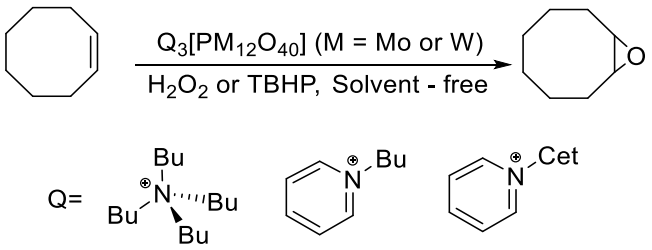

Scheme 26 - Oxidation of cyclooctene with H_2O_2 or TBHP catalyzed by POM.

Under this protocol, the cyclooctene conversion is between 44 to 91 % according to the different loading of catalyst. These systems gave satisfying results, under organic solvent-free conditions and extremely low catalyst loading conditions (less than 0.15% catalyst loading).

1.3.3.2. Catalysis with supported POMs

Since 90s, in the context of Green Chemistry more catalytic processes are explored. From the point of view of the protection of the environment and in terms of economical reason, development of active reusable catalysts, notably POMs, is a hot research aspect.

Most of POMs were supported by an impregnation method. The nature of the solid support, the nature and the loading of POM, and also the temperature of reaction will influence the reactivity. Most of the time, the POMs were immobilized by covalent or ionic interaction on acid or neutral solid supports such as SiO_2[122], activated carbon,[61b] diatomite, [123] molecular sieves, [124] polymer, [125] and mesoporous transition metal oxide.[126] Among those materials, carbonaceous species supports, polymers and SiO_2 were largely used due to several advantages, such as their relatively low-cost , their ability to be easily obtained and to be easily functionalized.

Carbon-based supports

Activated carbon was often used as support because of its high porosity, high specific surface area, high thermostability and facility of fabrication. An interesting example, reported by Genovese and Lian, concerned the activated carbon obtained from pinecones (as source of carbon) activated in KOH solution to obtain porous material. POM was immobilized by physical absorption method.[127]

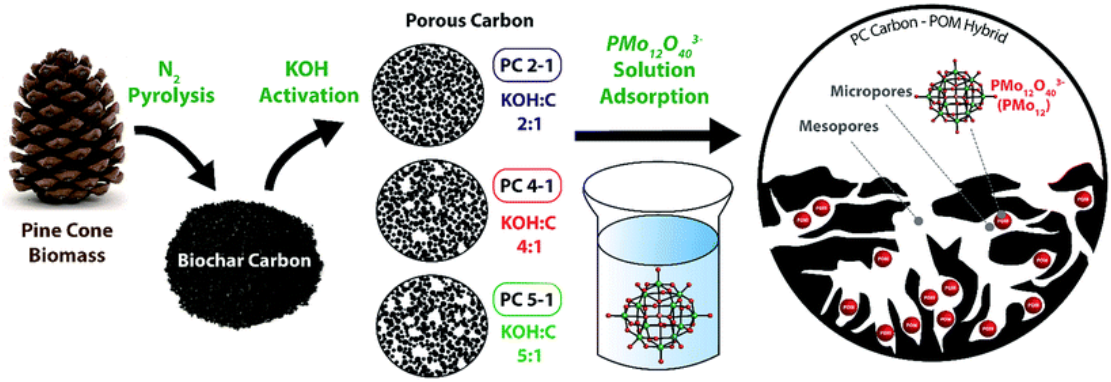

Scheme 27 - Synthesis of porous pine cone biomass carbon and POM grafting.

Kozhevnikov et al. reported oxidative mechanism of desulfurization catalyzed by Keggin-type POMs ($H_3PMo_{12}O_{40}$, $H_3PW_{12}O_{40}$ and $H_4SiW_{12}O_{40}$) immobilized on active carbon surface. H_2O_2 was used as oxidant. Highest conversion of dibenzothiophene (DBT) goes up to 100 % after 0.5 hour.[128]

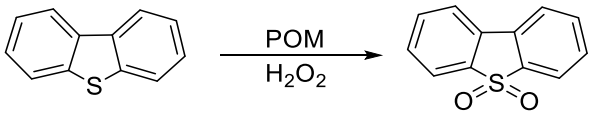

Scheme 28 - Oxidation of DBT to sulfone with H_2O_2 catalyzed by POM.

From a mechanistic point of view, the POM reacts with H_2O_2 and lead to a M-OH(OOH) intermediate complex, then a molecule of water is released to form a M(η^2-O_2) peroxo complex (Scheme 29). The catalytic cycle is described below.

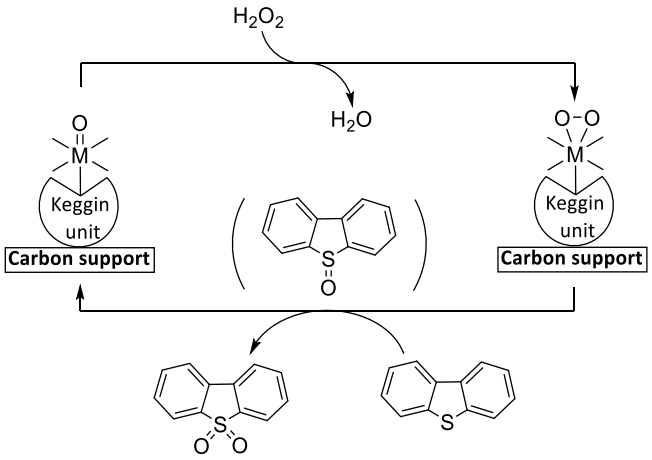

Scheme 29 - Oxidation of DBT with H_2O_2 catalyzed by HPA/C. (M=Mo^{VI} or W^{VI}).

Izumi et al. synthesized POMs supported by physical impregnation on active carbon solid support. The interaction between carbon support and POMs is strong enough to avoid the POM release during the reaction and treatment.[129]

Acidity of POMs was reduced after grafting on support (organic cation replacing proton).[60h] When $H_3PW_{12}O_{40}$ and $H_3PWSi_{12}O_{40}$ were grafted with more than 5 wt.%) on chemically treated carbon support, their structure was maintained. With lower loading, the Keggin structure was destroyed.[130].

Other type of carbonaceous compounds was used as POM supports, like carbon nanotubes,[131] carbon nitride,[132] and graphene oxide[133].

Polymer supports

Organic polymers were deeply studied in fundamental research and industry, due to their tunable abundant structures and functionalities. Some of them are commercial products that can be easily obtained. Various POM immobilized on polymer have been successively prepared in recent years.[134]

For example, in 2012, a supported catalyst based on the ionic interaction between $H_3PW_{12}O_{40}$ and a task-specific synthesized ionic copolymer with stimuli-responsive properties- was reported by group of Leng and Wang. These catalysts were used for benzyl alcohol oxidation with H_2O_2 under solvent-free conditions.[135] 92% yield were obtained in two hours. The amino-free polymeric hybrid object NDMAM-BVIM-PW was

insoluble in benzyl alcohol before the reaction, forming a stable emulsion at 90 °C after the addition of H_2O_2.

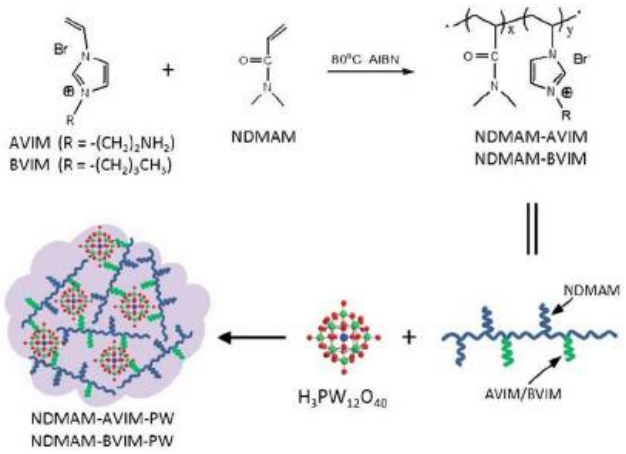

Scheme 30 - Synthesis of polymer-supported POMs.

Sometimes, organic-functionalized cationic polymer does play the role of solid support but also provides a suitable hydrophobicity/hydrophilicity performance for catalysis.[125b, 136] The same group also designed an amphiphilic POM-paired ionic copolymer in order to obtain a good match between the Venturello catalyst $H_3PW_4O_{16}$ and hydrophobic alkyl chains ($–C_{12}H$) and hydrophilic carboxyl groups (–COOH) of the functionalized ionic copolymer (Scheme 31).[136b] The POM immobilized object, DIM-CIM-PW, is designed for alkene epoxidation and displayed a high catalytic activity. The polymer structure offered an amphiphilic microenvironment for the catalyst, playing a shuttle role between alkene substrates in organic phase and H_2O_2 in water phase.

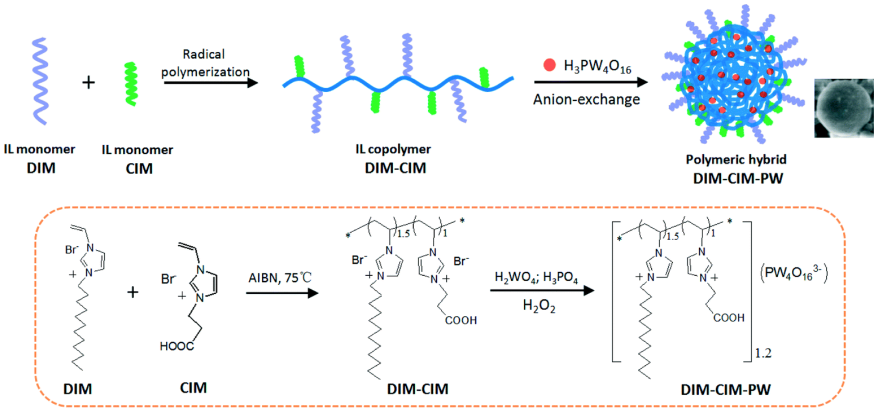

Scheme 31 - Schematic illustration outlining the preparation and structure of the catalyst DIM–CIM–PW.

Polystyrene was also largely used as POM solid state support. Recently, Wang et al. reported a new self-assembled POM-PS (polystyrene) materials. This material can shuttle between micelles, vesicles and linear forms upon concentration.[125b]

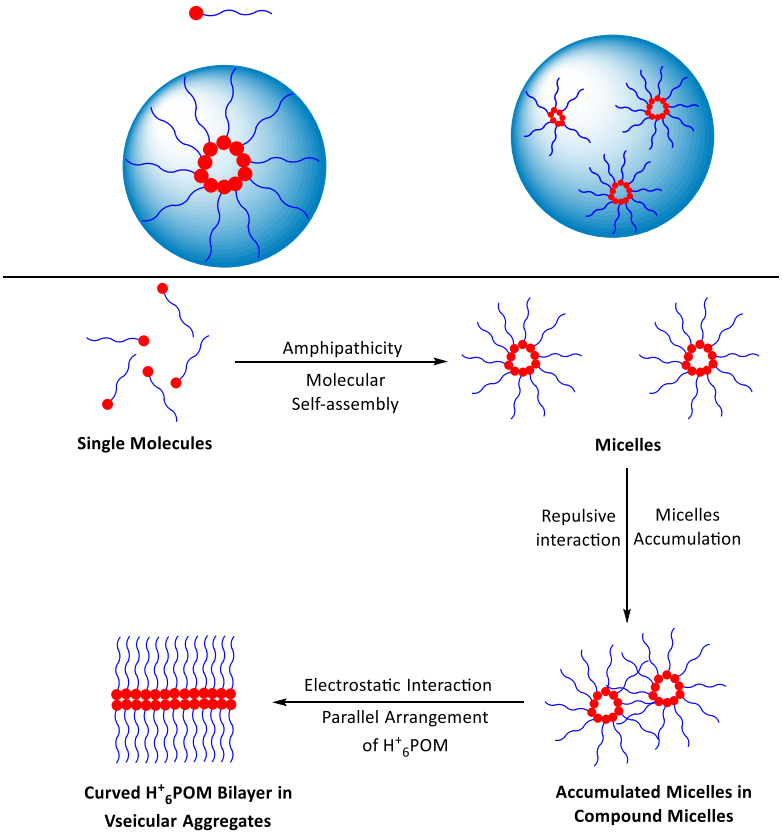

Scheme 32 - Formation mechanisms of various morphologies of the aggregates.

Merrifield resin is an organic polymer that possesses lot of advantages, such as low cost, relative robustness and it could undergo facile functionalization. This polymer was originally designed for peptides synthesis, but it can be also used as support

In the research team, Keggin POM (based on HPAs $H_3PM_{12}O_{40}$ M = Mo or W) were successfully grafted on Merrifield resin by ionic way for adipic acid synthesis.[137]

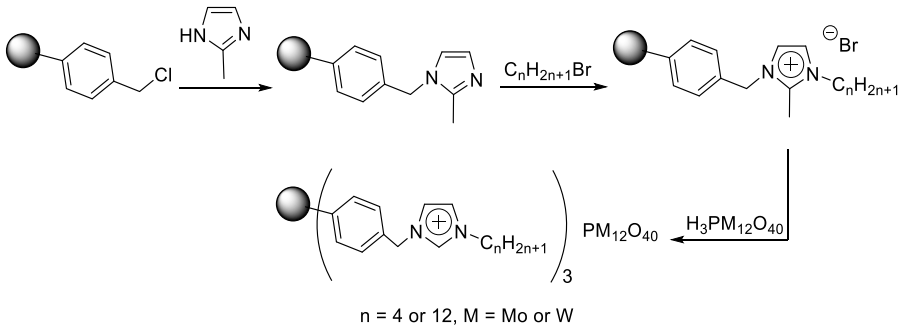

Scheme 33 - synthesis of Merrifield resin supported catalysts.

According to the developed protocol, H_2O_2 was used as oxygen source, POM supported as catalyst with low molar loading and under organic solvent free conditions. Similar conversion of acid adipic were observed between POM – supported and organic salts POM, but with different loading (0.025% for organic salt POM, 0.001 – 0.007% for POM – supported). This new system avoids the use of organic solvent and phase transfer catalysts. It provides a new “green chemistry” approach.

Silica support

Silica is another interesting support to immobilize the ionic catalytic species on the surface.[138] Largely used as catalyst support because of high specific surface area, mesoporous silica (SBA,[139] MCM-41[140] and silica (nano)particles)[141] are interesting solid support candidates.

Mesoporous silica

Several strategies have been explored to prepare POM-immobilized mesoporous silica materials, such as impregnation, [142] sol–gel techniques, [143] electrostatic interactions,[140] ion-exchange,[144] and covalent grafting.[145]

To improve the recyclability and stability of POM catalysts, mesoporous silica with functionalized surface are used with the purpose of creating stronger ionic and covalent chemical bonds with POM. [146]

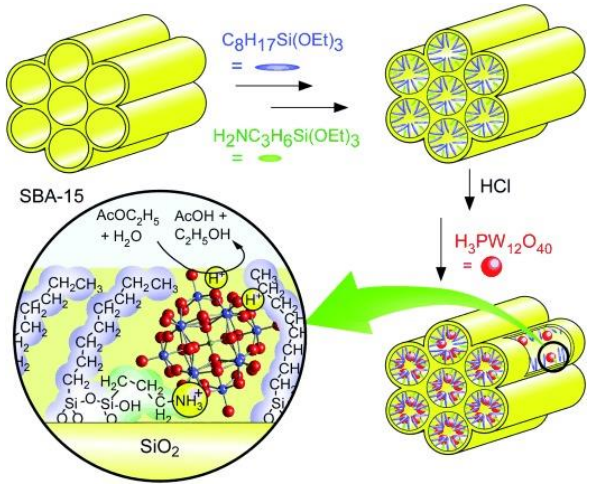

Scheme 34 - Immobilized catalyst of $H_3PW_{12}O_{40}$ in SBA-15. (Copyright (2007) Wiley-VCH).

For example, Inumaru and coworkers reported the construction of water-tolerant solid catalysts by immobilization of $H_3PW_{12}O_{40}$ on hydrophobic organic modified mesoporous silica SBA-15 (Scheme 34).[147] POMs can be homogeneously dispersed in the channels of functionalized silica through electrostatic interaction and POM structure can be preserved. Generally, immobilized POM on mesoporous silica attracted attention due to relative low cost, easy synthesis and easy functionalization.

Villanneau et al. proposed a hybrid siliceous MesoCellular Foam (SBA-15 vs MCF) functionalized by amino and carboxypropyl function solid support for POM immobilization. Three POM-anchored were synthesized (POM-CO_2H@SBA-NH_2, POM-CO_2H@MCF-NH_2 and POM-NH_2@SBA-CO_2H) and were tested for oxidation reactions using H_2O_2 as oxidant and cyclooctene and cyclohexene as substrates. In the case of

cyclooctene oxidation, the best conversion (76%) is obtained by POM-CO_2H@SBA-NH_2. Its recyclability was also assessed for cyclooctene oxidation and a conversion of 81% was measured after the second run.[138]

Silica NPs

Very recently, Zharov et al. reported a new method to immobilize a Pd catalyst on the surface of functionalized silica NPs for catalytic oxidation of benzyl alcohol to benzaldehyde.[148] Although the work does not concern POMs, it was relevant to point it out since it goes in straight line with what will be presented in Chapter 4.

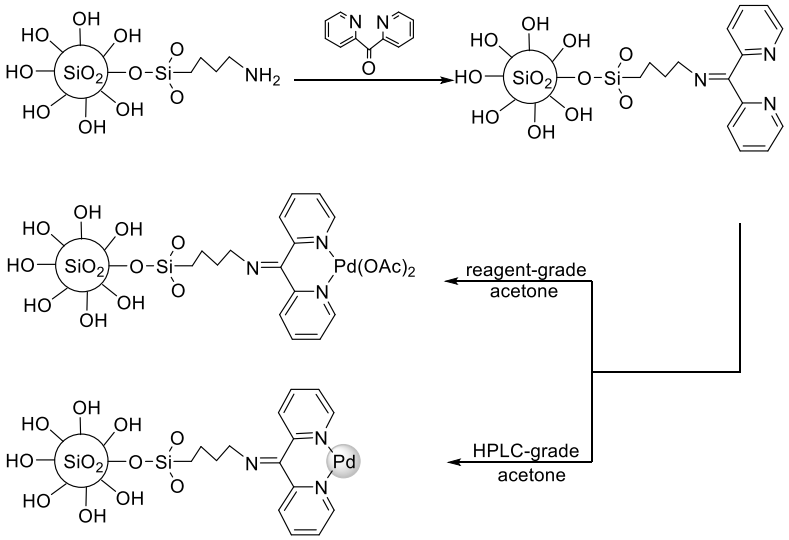

Scheme 35 - Pd catalyst immobilized on silica NPs surface by covalent method.

Amine function (APTES) was grafted on the NPs silica surface, then dipyridylmethylene (dpm) ligand coordinates with Pd precursor. Different form of Pd could be obtained (Pd^{2+} or Pd^0) by varying preparation conditions. In order to compare their reactivity, oxidation of benzyl alcohol to benzaldehyde was selected as a model reaction. Interesting results was obtained with Pd catalyst supported.

Based on these literature precedents, during this work, grafting of POMs on functionalized non porous silica nanobeads in order to recover catalysts was aimed. The goal was to be able to obtain recoverable catalysts active with low catalysts loading and organic solvent-free conditions. This approach will be explored in chapter 4.

1.4. References

[1] R. A. Sheldon, J. K. Kochi, *Metal-Catalyzed Oxidations of Organic Compounds*, 1981.

[2] A. Castellan, J. C. J. Bart, S. Cavallaro, *Catal. Today,* 1991, *9* (3), 237–254.

[3] G. Cainelli, *Chromium Oxidations in Organic Chemistry,* Springer Berlin Heidelberg, Berlin, Heidelberg, 1984.

[4] D. T. Downing, R. S. Greene, *Lipids,* 1968, *3* (1), 96–100.

[5] R. Pappo, Jr., D. S. Allen, R. U. Lemieux, W. S. Johnson, *J. Org. Chem.* 1956, *21* (4), 478–479.

[6] S. Wolfe, S. K. Hasan, J. R. Campbell, *J. Chem. Soc. D*, 1970, 21, 1420-1421.

[7] R. A. Sheldon, *Green Chemistry,* 2007, *9* (12), 1273–1283.

[8] (a) R. Noyori, M. Aoki, K. Sato, *Chem. Commun.* 2003, 1977-1986.
(b) R. Hage, A. Lienke, *Angew. Chem., Int. Ed.* 2006, 45, 206-222.

[9] (a) P. Saisaha, J. J. Dong, T. G. Meinds, J. W. de Boer, R. Hage, F. Mecozzi, J. B. Kasper, W. R. Browne, *ACS Catal.* 2016, *6* (6), 3486–3495.
(b) I. Garcia‐Bosch, M. A. Siegler, *Angew. Chem. Int. Ed.* 2016, *55* (41), 12873–12876.
(c) G. Olivo, O. Lanzalunga, S. Di Stefano, *Adv. Synth. Catal.* 2016, *358* (6), 843–863.

[10] (a) S. Lorenz, B. Plietker, *ChemCatChem*, 2016, 8 (20), 3203–3206.
(b) C. Miao, B. Wang, Y. Wang, C. Xia, Y.-M. Lee, W. Nam, W. Sun, *J. Am. Chem. Soc.* 2016, 138 (3), 936–943.
(c) E. P. Talsi, K. P. Bryliakov, *Coord. Chem. Rev.* 2012, *256* (13), 1418–1434.
(d) K. P. Bryliakov, E. P. Talsi, *Coord. Chem. Rev.* 2014, *276*, 73–96.
(e) R. V. Ottenbacher, E. P. Talsi, K. P. Bryliakov, *Catal. Today* 2016, *278*, 30–39.
(f) G. Olivo, O. Cussó, M. Costas, *Chem. Asian J.* 2016, *11* (22), 3148–3158.
(g) O. Cussó, X. Ribas, M. Costas, *Chem. Commun.* 2015, *51* (76), 14285–14298.
(h) M. Costas, M. P. Mehn, M. P. Jensen, L. Que, *Chem. Rev.* 2004, *104* (2), 939–986.
(i) W. Nam, Y.-M. Lee, S. Fukuzumi, *Acc. Chem. Res.* 2014, *47* (4), 1146–1154.

[11] (a) M. C. White, A. G. Doyle, E. N. Jacobsen, *J. Am. Chem. Soc.* 2001, *123* (29), 7194–7195.
(b) R. Mas-Ballesté, L. Que, *J. Am. Chem. Soc.* 2007, *129* (51), 15964–15972.
(c) O. Cussó, J. Serrano-Plana, M. Costas, *ACS Catal.* 2017, *7*, 5046-5053

[12] (a) I. G. Denisov, T. M. Makris, S. G. Sligar, I. Schlichting, *Chem. Rev.* 2005, *105* (6), 2253–2278.
(b) D. J. Ferraro, L. Gakhar, S. Ramaswamy, *Biochem. Biophys. Res. Commun.* 2005, *338* (1), 175–190.
(c) S. Hayward, T. Cilliers, P. Swart, *Compr. Rev. Food Sci. Food Saf.* 2017, *16* (1), 199–211.
(d) C. Glorieux, P. B. C. Calderon, *Biol. Chem.* 2017, 398 (10), 1095–1108.

[13] K. Ray, F. F. Pfaff, B. Wang, W. Nam, *J. Am. Chem. Soc.* 2014, *136* (40), 13942–13958.

[14] J. Du, C. Xia, W. Sun. *Acta Chim. Sinica*, 2018, 76(5): 329-346.

[15] W. Nam, *Acc. Chem. Res.* 2015, *48* (8), 2415–2423.

[16] (a) D. Kumar, S. P. de Visser, P. K. Sharma, H. Hirao, S. Shaik, *Biochem.* 2005, *44* (22), 8148–8158.
(b) Y. Wang, H. Chen, M. Makino, Y. Shiro, S. Nagano, S. Asamizu, H. Onaka, S. Shaik, *J. Am. Chem. Soc.* 2009, *131* (19), 6748–6762.
(c) Y. Wang, C. Yang, H. Wang, K. Han, S. Shaik, *ChemBioChem.* 2007, *8* (3), 277–281.

[17] (a) X.-X. Li, V. Postils, W. Sun, A. S. Faponle, M. Solà, Y. Wang, W. Nam, S. P. de Visser, *Chem. Eur. J.* 2017, *23* (26), 6406–6418.
(b) S. Shaik, S. Cohen, Y. Wang, H. Chen, D. Kumar, W. Thiel, *Chem. Rev.* 2010, *110* (2), 949–1017.

[18] (a) I. Schlichting, J. Berendzen, K. Chu, A. M. Stock, S. A. Maves, D. E. Benson, R. M. Sweet, D. Ringe, G. A. Petsko, S. G. Sligar, *Science* 2000, *287* (5458), 1615–1622.
(b) W. Nam, *Acc. Chem. Res.* 2007, *40* (7), 522–531.

[19] Y. Zhang, J. D. Biggs, S. Mukamel, *ChemPhysChem.* 2015, *16* (9), 2006–2014.

[20] (a) I. G. Denisov, P. J. Mak, T. M. Makris, S. G. Sligar, J. R. Kincaid, *J Phys Chem A* 2008, *112* (50), 13172–13179.
(b) P. J. Mak, I. G. Denisov, D. Victoria, T. M. Makris, T. Deng, S. G. Sligar, J. R. Kincaid, *J. Am. Chem. Soc.* 2007, *129* (20), 6382–6383.

[21] (a) M. Sharrock, P. G. Debrunner, C. Schulz, J. D. Lipscomb, V. Marshall, I. C. Gunsalus, *Biochim. Biophys. Acta. Protein Struct.* 1976, *420* (1), 8–26.

(b) J. Rittle, M. T. Green, *Science* 2010, *330* (6006), 933–937.
22 Y. Watanabe, H. Nakajima, T. Ueno, *Acc. Chem. Res.* 2007, *40* (7), 554–562.
23 N. C. Gerber, S. G. Sligar, *J. Am. Chem. Soc.* 1992, *114* (22), 8742–8743.
24 S. A. Martinis, W. M. Atkins, P. S. Stayton, S. G. Sligar, *J. Am. Chem. Soc.* 1989, *111* (26), 9252–9253.
25 A. Karlsson, J. V. Parales, R. E. Parales, D. T. Gibson, H. Eklund, S. Ramaswamy, *Science,* 2003, *299* (5609), 1039–1042.
26 (a) P. C.A. Bruijnincx, G. V. Koten, R. J. M. K. Gebbink, *Chem. Soc. Rev.* 2008, *37* (12), 2716–2744.
(b) S. M. Barry, G. L. Challis, *ACS Catal.* 2013, *3* (10), 2362–2370.
27 A. Bassan, M. R. A. Blomberg, P. E. M. Siegbahn, *J Biol Inorg Chem* 2004, *9* (4), 439–452.
28 (a) M. C. Baratto, D. A. Lipscomb, M. J. Larkin, R. Basosi, C. C. R. Allen, R. Pogni, *Int. J. Mol. Sci.* 2019, *20* (14), 3402.
(b) E. G. Kovaleva, J. D. Lipscomb, *Nat. Chem. Biol.*, 2008, 4, 186-193.
29 Y. Umena, K. Kawakami, J.-R. Shen, N. Kamiya, *Nature*, 2011, *473* (7345), 55–60.
30 C. Zhang, C. Chen, H. Dong, J.-R. Shen, H. Dau, J. Zhao, *Science*, 2015, *348* (6235), 690–693.
31 (a) W. Lubitz, E. J. Reijerse, J. Messinger, *Energy Environ. Sci.* 2008, *1* (1), 15–31.
(b) K. J. Young, B. J. Brennan, R. Tagore, G. W. Brudvig, *Acc. Chem. Res.* 2015, *48* (3), 567–574.
(c) N. Cox, D. A. Pantazis, F. Neese, W. Lubitz, *Acc. Chem. Res.* 2013, *46* (7), 1588–1596.
32 D. Shen, C. Saracini, Y.-M. Lee, W. Sun, S. Fukuzumi, W. Nam, *J. Am. Chem. Soc.* 2016, *138* (49), 15857–15860.
33 (a) C. G. Miller, S. W. Gordon-Wylie, C. P. Horwitz, S. A. Strazisar, D. K. Peraino, G. R. Clark, S. T. Weintraub, T. J. Collins, *J. Am. Chem. Soc.* 1998, *120* (44), 11540–11541.
(b) S. Hong, Y.-M. Lee, M. Sankaralingam, A. K. Vardhaman, Y. J. Park, K.-B. Cho, T. Ogura, R. Sarangi, S. Fukuzumi, W. Nam, *J. Am. Chem. Soc.* 2016, *138* (27), 8523–8532.
(c) T. J. Collins, S. W. Gordon-Wylie, *J. Am. Chem. Soc.* 1989, *111* (12), 4511–4513.
34 (a) A. Kejriwal, S. Biswas, A. N. Biswas, P. Bandyopadhyay, *J. Mol. Catal. A: Chem.* 2016, *413*, 77–84.
(b) A. Trehoux, Y. Roux, R. Guillot, J.-P. Mahy, F. Avenier, *J. Mol. Catal. A: Chem.* 2015, *396*, 40–46.
(c) R. V. Ottenbacher, K. P. Bryliakov, E. P. Talsi, *Adv. Synth. Catal.* 2011, *353* (6), 885–889.
35 J. T. Groves, T. E. Nemo, *J. Am. Chem. Soc.* 1983, *105* (18), 5786–5791.
36 (a) O. Cussó, I. Garcia-Bosch, X. Ribas, J. Lloret-Fillol, M. Costas, *J. Am. Chem. Soc.* 2013, *135* (39), 14871–14878.
(b) O. Cussó, M. Cianfanelli, X. Ribas, R. J. M. Klein Gebbink, M. Costas, *J. Am. Chem. Soc.* 2016, *138* (8), 2732–2738.
(c) R. V. Ottenbacher, D. G. Samsonenko, E. P. Talsi, K. P. Bryliakov, *ACS Catal.* 2016, *6* (2), 979–988.
(d) B. Wang, S. Wang, C. Xia, W. Sun, *Chem. Eur. J. Chemistry,* 2012, *18* (24), 7332–7335.
(e) B. Wang, C. Miao, S. Wang, C. Xia, W. Sun, *Chem. Eur. J. Chemistry,* 2012, *18* (22), 6750–6753.
37 K. Chen, L. Q. Jr, *Angew. Chem. Int. Ed.* 1999, *38* (15), 2227–2229.
38 O. Y. Lyakin, R. V. Ottenbacher, K. P. Bryliakov, E. P. Talsi, *ACS Catal.* 2012, *2* (6), 1196–1202.
39 J. Du, C. Miao, C. Xia, Y.-M. Lee, W. Nam, W. Sun, *ACS Catal.* 2018, *8*, 4528-4538
40 B. Wang, Y. M. Lee, M. Clemancey, M. S. Seo, R. Sarangi, J. M. Latour, W. Nam, *J. Am. Chem. Soc.* 2016, *138*, 2426-2436.
41 J. Serrano‐Plana, A. Aguinaco, R. Belda, E. García‐España, M. G. Basallote, A. Company, M. Costas, *Angew. Chem. Int. Ed.* 2016, *55* (21), 6310–6314.
42 N. Jin, D. E. Lahaye, J. T. Groves, *Inorg. Chem.* 2010, *49* (24), 11516–11524.
43 (a) C. Esmieu, M. V. Cherrier, P. Amara, E. Girgenti, C. Marchi‐Delapierre, F. Oddon,; M. Iannello, A. Jorge‐Robin, C. Cavazza, S. Ménage, *Angew. Chem. Int. Ed.* 2013, *52* (14), 3922–3925.
(b) F. Oddon, E. Girgenti, C. Lebrun, C. Marchi‐Delapierre, J. Pécaut, S. Ménage, *Eur. J. Inorg. Chem.* 2012, *2012* (1), 85–96.
44 K. Cheaib, M. Q. E. Mubarak, K. Sénéchal‐David, C. Herrero, R. Guillot, M. Clémancey, J.-M. Latour, S. P. de Visser, J.-P. Mahy, F. Banse, F. Avenier, *Angew. Chem. Int. Ed*. 2019, *131* (3), 864–868.
45 M. R. DuBois, D. L. DuBois, *Chem. Soc. Rev.* 2009, *38* (1), 62–72.

[46] (a) K. L. Stone, A. Borovik, *Curr. Opin. Chem. Biol.* **2009**, *13* (1), 114–118.
(b) C. A. Bonagura, B. Bhaskar, H. Shimizu, H. Li, M. Sundaramoorthy, D. E. McRee, D. B. Goodin, T. L. Poulos, *Biochem.* **2003**, *42* (19), 5600–5608.

[47] (a) E. W. Dahl, J. J. Kiernicki, M. Zeller, N. K. Szymczak, *J. Am. Chem. Soc.* **2018**, 140, 10075-10079.
(b) E. W. Dahl, H. T. Dong, N. K. Szymczak, *Chem. Commun.* **2018**, 54, 892-895.

[48] (a) Z. Shirin, V. G. Young Jr., A. S. Borovik, *Chem. Commun*. **1997**, 1967-1968.
(b) C. E. MacBeth, A. P. Golombek, V. G. Young Jr., C. Yang, K. Kuczera, M. P. Hendrich, A. S. Borovik, *Science*, **2000**, 289, 938-941.
(c) C. E. MacBeth, R. Gupta, K. R. Mitchell-Koch, V. G. Young Jr., G. H. Lushington, W. H. Thompson, M. P. Hendrich, A. S. Borovik, *J. Am. Chem. Soc.* **2004**, 126, 2556-2567.
(d) R. Gupta, T. Taguchi, B. Lassalle-Kaiser, E. L. Bominaar, J. Yano, M. P. Hendrich, A. S. Borovik, *Proc. Natl. Acad. Sci. U. S. A.* **2015**, 112, 5319-5324.
(e) T. Taguchi, K. L. Stone, R. Gupta, B. Kaiser-Lassalle, J. Yano, M. P. Hendrich, A. S. Borovik, *Chem. Sci.* **2014**, 5, 3064-3071.
(f) T. Taguchi, R. Gupta, B. Lassalle-Kaiser, D. W. Boyce, V. K. Yachandra, W. B. Tolman, J. Yano, M. P. Hendrich, A. S. Borovik, *J. Am. Chem. Soc*. **2012**, 134, 1996-1999.
(g) D. C. Lacy, R. Gupta, K. L. Stone, J. Greaves, J. W. Ziller, M. P. Hendrich, A. S. Borovik, *J. Am. Chem. Soc*. **2010**, 132, 12188-12190.
(h) A. Dey, R. K. Hocking, P. L. Larsen, A. S. Borovik, K. O. Hodgson, B. Hedman, E. I. Solomon, *J. Am. Chem. Soc*. **2006**, 128, 9825-9833
(i) Z. Shirin, B. S. Hammes,; V. G. Young, A. S. Borovik, *J. Am. Chem. Soc.* **2000**, *122* (8), 1836–1837.
(j) R. L. Shook, W. A. Gunderson, J. Greaves, J. W. Ziller, M. P. Hendrich, A. S. Borovik, *J. Am. Chem. Soc.* **2008**, *130* (28), 8888–8889.

[49] (a) S. Sahu, B. Zhang, C. J. Pollock, M. Durr, C. G. Davies, A. M. Confer, I. Ivanovic-Burmazovic, M. A. Siegler, G. N. Jameson, C. Krebs, D. P. Goldberg, *J. Am. Chem. Soc.* **2016**, *138*, 12791-12802.
(b) L. R. Widger, Y. Jiang, A. C. McQuilken, T. Yang, M. A. Siegler, H. Matsumura,; P. Moenne-Loccoz, D. Kumar, S. P. de Visser, D. P. Goldberg, *Dalton Trans.* **2014**, *43*, 7522-7532.
(c) L. R. Widger, C. G. Davies, T. Yang, M. A. Siegler, O. Troeppner, G. N. Jameson, I. Ivanovic-Burmazovic, D. P. Goldberg, *J. Am. Chem. Soc.* **2014**, 136, 2699-2702.

[50] (a) C. M. Wallen, L. Palatinus, J. Bacsa, C. C. Scarborough, *Angew. Chem. Int. Ed.* **2016**, *55*, 11902-11906.
(b) C. M. Wallen, J. Bacsa, C. C. Scarborough, *J. Am. Chem. Soc.* **2015**, *137*, 14606-14609.

[51] (a) Z. Gordon, M. J. Drummond, E. M. Matson, J. A. Bogart, E. J. Schelter, R. L. Lord, A. R. Fout, *Inorg. Chem*. **2017**, 56, 4852-4863
(b) C. L. Ford, Y. J. Park, E. M. Matson, Z. Gordon, A. R. Fout, *Science* **2016**, *354*, 741-743.
(c) Y. J. Park, E. M. Matson, M. J. Nilges, A. R. Fout, *Chem. Commun*. **2015**, 51, 5310--5313.
(d) E. M. Matson, J. A. Bertke, A. R. Fout, *Inorg. Chem*. **2014**, 53, 4450-4458.

[52] S. P. de Visser, J. Kaneti, R. Neumann, S. Shaik, *J. Org. Chem.* **2003**, *68* (7), 2903–2912.

[53] K. Neimann, R. Neumann, *Org. Lett.* **2000**, *2* (18), 2861–2863.

[54] A. Berkessel, J. A. Adrio, *J. Am. Chem. Soc.* **2006**, *128* (41), 13412–13420.

[55] V. Dantignana, M. Milan, O. Cusso, A. Company, M. Bietti, M. Costas, *ACS central science* **2017**, *3*, 1350-1358

[56] P. Guillo, J.-C. Daran, E. Manoury, R. Poli, *ChemistrySelect,* **2017**, *2* (8), 2574–2577.

[57] (a) S. Omwoma, C. T. Gore, Y. Ji, C. Hu, Y.-F. Song, *Coord. Chem. Rev.* **2015**, *286*, 17–29.
(b) Y. Zhou, Z. Guo, W. Hou, Q. Wang, J. Wang, *Catal. Sci. Technol.* **2015**, *5* (9), 4324–4335.
(c) Z.-J. Liu, X.-L. Wang, C. Qin, Z.-M. Zhang, Y.-G. Li, W.-L Chen, E.-B. Wang, *Coord. Chem. Rev.* **2016**, *313*, 94–110.

[58] J. Berzelius, Pogg Ann, **1826**, 6: 369-371.

[59] J. C. Marignac. *Chim.Phys*. **1864**,3,5.

[60] (a) T. Yamase, *Chem. Rev.* **1998**, *98* (1), 307–326.
(b) I. A. Weinstock, *Chem. Rev.* **1998**, *98* (1), 389–390.
(c) I. A. Weinstock, *Chem. Rev.* **1998**, *98* (1), 113–170.
(d) M. Sadakane, E. Steckhan, *Chem. Rev.* **1998**, *98* (1), 219–238.
(e) J. T. Rhule, C. L. Hill, D. A. Judd, R. F. Schinazi, *Chem. Rev.* **1998**, *98* (1), 327–358.
(f) A. Müller, F. Peters, M. T. Pope, D. Gatteschi, *Chem. Rev.* **1998**, *98* (1), 239–272.
(g) N. Mizuno, M. Misono, *Chem. Rev.* **1998**, *98* (1), 199–218.
(h) I. V. Kozhevnikov, *Chem. Rev.* **1998**, *98* (1), 171–198.
(i) W. G. Klemperer, C. G. Wall, *Chem. Rev.* **1998**, *98* (1), 297–306.
(j) D. E. Katsoulis, *Chem. Rev.* **1998**, *98* (1), 359–388.
(k) Y. P. Jeannin, *Chem. Rev.* **1998**, *98* (1), 51–76.
(l) C. L. Hill, Introduction: *Chem. Rev.* **1998**, *98* (1), 1–2.
(m) P. Gouzerh, A. Proust, *Chem. Rev.* **1998**, *98* (1), 77–112.
(o) E. Coronado, C. J. Gómez-García, *Chem. Rev.* **1998**, *98* (1), 273–296.
(p) L. C. W. Baker, D. C. Glick, *Chem. Rev.* **1998**, *98* (1), 3–50.

[61] (a) S.-S. Wang, G.-Y. Yang, *Chem. Rev.* **2015**, 115 (11), 4893–4962.
(b) Y. Zhou, G. Chen, Z. Long, J. Wang, *RSC Adv.* **2014**, 4 (79), 42092–42113.
(c) Q. Chen, C. Shen, L. He, *Acta Crystallogr., Sect. C: Cryst. Struct. Commun.* **2018**, 74 (11), 1182–1201.

[62] X. López, J. A. Fernández, J. M. Poblet, *Dalton Trans*. **2006**, 0 (9), 1162–1167.

[63] H. Firouzabadi, A. A. Jafari, *J. Iran. Chem. Soc.* **2005**, *2* (2), 85–114.

[64] (a)G. Hervé, A. Tézé, R. Contant, General Principles of The Synthesis of Polyoxometalates in Aqueous Solution. In *Polyoxometalate Molecular Science*; J. J. Borrás-Almenar, E. Coronado, A. Müller, M. Pope, Eds.; NATO Science Series; Springer Netherlands: Dordrecht, **2003**; pp 33–54.

[65] G. M. Maksimov, *Russ. Chem. Rev.* **1995**, 64 (5), 445.

[66] A. Balaska, R. Belghiche, M.-H. Samar, T. Chouchane, R. Haseneder, *MATEC Web of Conferences,* **2013**, 5, 04019.

[67] M. T. Pope, Heteropoly and Isopoly Oxometalates, Springer Verlag, New York, **1983**, pp. 23-27.

[68] J. M. Cameron, D. J. Wales, G. N. Newton, *Dalton Trans.* **2018**, *47* (15), 5120–5136.

[69] J F. Keggin, *Proc Roy Soc London*, **1934**, A144: 75

[70] B. Dawson, *Acta Crystallogr.* **1953**, 6, 113

[71] M. T. Pope, A. Müller, *Angew. Chem. Int. Ed.* **1991**, 30 (1), 34–48.

[72] (a) J. S. Anderson, *Nature*, **1937**, 140 (3550), 850.
(b) H. T. Evans, *J. Am. Chem. Soc.* **1948**, *70* (3), 1291–1292.

[73] D. D. Dexter, J. V. Silverton, *J. Am. Chem. Soc.* **1968**, *90* (13), 3589–3590.

[74] X. López, J. J. Carbó, C. Bo, J. M. Poblet, *Chem. Soc. Rev.* **2012**, 41 (22), 7537–7571.

[75] Hattori, H.; Ono, Y. Isopolyanions and heteropolyanions in Heteropolyacids in *Solid Acid Catalysis: From Fundamentals to Applications*; CRC Press, 2015; pp 187-189.

[76] X. López, L. Vilà-Nadal, X. Aparicio-Anglès, J. M. Poblet, *Physics Procedia*, **2010**, 8, 94–103.

[77] (a) S. Ganapathy, M. Fournier, J. F. Paul, L. Delevoye, M. Guelton, J. P. Amoureux, *J. Am. Chem. Soc.* **2002**, 124(26), 7821–7828.
(b) J. M. Poblet, X. López, C. Bo, *Chem. Soc. Rev.* **2003**, 32 (5), 297–308.
(c) C. Rocchiccioli-Deltcheff, M. Fournier, R. Franck, R. Thouvenot, *Inorg. Chem.* **1983**, *22* (2),207–216.

[78] N. I. Kuznetsova, N. V. Kirillova, L. I. Kuznetsova, V. A. Likholobov, *J. Mol. Catal. A: Chem.* **2003**, *204–205*, 591–597.

[79] (a) M. Filowitz, R. K. C. Ho, W. G. Klemperer, W. Shum, *Inorg. Chem.* **1979**, *18* (1), 93–103.

(b) R. Massart, R. Contant, J. M. Fruchart, J. P. Ciabrini, M. Fournier, *Inorg. Chem.* **1977**, *16*(11), 2916–2921.
(c) Y.-G. Chen, J. Gong, L.-Y. Qu, *Coord. Chem. Rev.* **2004**, *248* (1), 245–260.

80 M. Misono, N. Mizuno, K. Katamura, A. Kasai, Y. Konishi, K. Sakata, T. Okuhara, Y. Yoneda, *Bull. Chem. Soc. Jpn.* **1982**, 55 (2), 400–406.

81 S. Reinoso, P. Vitoria, J. M. Gutiérrez-Zorrilla, L. Lezama, L. San Felices, J. I. Beitia, *Inorg. Chem.* **2005**, *44* (26), 9731–9742.

82 Y. Nakagawa, N. Mizuno, *Inorg. Chem.* **2007**, 46 (5), 1727–1736.

83 M. S. S. Balula, I. C. M. S. Santos, M. M. Q. Simões, M. G. P. M. S. Neves, J. A. S. Cavaleiro, A. M. V. Cavaleiro, *J. Mol. Catal. A: Chem.* **2004**, 222 (1), 159–165.

84 A. M. Khenkin, L. J. W. Shimon, R. Neumann, *Inorg. Chem.* **2003**, 42 (10), 3331–3339.

85 I. V. Kozhevnikov, *Appl. Catal., A,* **2003**, *256* (1), 3–18.

86 (a) J. J. Altenau, M. T. Pope, R. A. Prados, H. So, *Inorg. Chem.* **1975**, *14* (2), 417–421.
(b) I. V. Kozhevnikov, *Russ. Chem. Rev.* **1987**, 56 (9), 811.
(c) I. V. Kozhevnikov, K. I. Matveev, *Appl. Catal.* **1983**, 5 (2), 135–150.

87 N. I. Kuznetsova, N. V. Kirillova, L. I. Kuznetsova, M. Y. Smirnova, V. A. Likholobov, *J. Hazard. Mater.* **2007**, 146 (3), 569–576.

88 M. Mahkam, *Drug Delivery*, **2010**, 17 (3), 158–163.

89 A. A. Ivakin, L. D. Kurbatova, L. A. Kapustina, *Zh. Neorg. Khim.***1978**, 23 (9), 2545–2546.

90 S. M. Kulikov, I. V. Kozhevnikov, *Russ. Chem. Bull.* **1981**, *30* (3), 348–353.

91 M. N. Timofeeva, *Applied Catalysis A: General* **2003**, *256* (1), 19–35.

92 F. Cavani, *Catal. Today*, **1998**, *41* (1), 73–86.

93 (a) P. Vázquez, L. Pizzio, C. Cáceres, M. Blanco, H. Thomas, E. Alesso, L. Finkielsztein, B. Lantaño, G. Moltrasio, J. Aguirre, *J. Mol. Catal. A: Chem.* **2000**, 161 (1), 223–232.
(b) L. A. M. Cardoso, W. Alves, A. R. E. Gonzaga, L. M. G. Aguiar, H. M. C. Andrade, *J. Mol. Catal. A: Chem.* **2004**, 209 (1), 189–197.

94 (a) L. Yang, Y. Qi, X. Yuan, J. Shen, J. Kim, *J. Mol. Catal. A: Chem.* **2005**, 229 (1), 199–205.
(b) C. L. Padró, C. R. Apesteguía, *J. Catal.* **2004**, *226* (2), 308–320.

95 N. Mizuno, M. Misono, *J. Mol. Catal.* **1994**, *86* (1), 319–342.

96 R. C. Chambers, C. L. Hill, *Inorg. Chem.* **1989**, 28 (13), 2509–2511.

97 M. Misono, *Chem. Commun.* **2001**, *0* (13), 1141–1152.

98 M. J. Verhoef, P. J. Kooyman, J. A. Peters, H. V. Bekkum, *Microporous Mesoporous Mater.* **1999**, *27* (2), 365–371.

99 (a) I. Kozhevnikov, Sustainable Heterogeneous Acid Catalysis by Heteropoly Acids. in *Handbook of Green Chemistry*, American Cancer Society, **2010**, 153–174
(b) T. Okuhara, N. Mizuno, M. Misono, *Academic Press*, **1996**; Vol. 41, pp 113–252.

100 K. Eguchi, N. Yamazoe, T. Seiyama, *Nippon Kagaku Kaishi*, **1981** (3), 336-342.

101 R. N. McDonald, R. N. Steppel, J. E. Dorsey, *Org. Synth.* **1970**, 50, 15– 18.

102 A. Castellan, J. C. J. Bart, S. Cavallaro, *Catal. Today,* **1991**, *9* (3), 237–254.

103 A. V. Pinto, V. F. Ferreira, M. D. C. F. R. Pinto, *Synth. Commun.* **1985**, *15* (13), 1177–1180.

104 (a) S. Mouanni, D. Amitouche, T. Mazari, C. Rabia, *Appl. Petrochem. Res.* **2019**, *9* (2), 67–75.
(b) Y. Shen, P. Jiang, P. T. Wai, Q. Gu, W. Zhang, *Catalysts,* **2019**, *9* (1), 31.

105 R. Ishimoto, K. Kamata, N. Mizuno, *Angew. Chem. Int. Ed.* **2012**, *51* (19), 4662–4665.

106 K. Kamata, M. Kotani, K. Yamaguchi, S. Hikichi, N. Mizuno, *Chem. Eur. J.* **2007**, *13* (2), 639–648.

107 M. Carraro, L. Sandei, A. Sartorel, G. Scorrano, M. Bonchio, *Org. Lett.* **2006**, *8* (17), 3671–3674.

108 J. Kasai, Y. Nakagawa, S. Uchida, K. Yamaguchi, N. Mizuno, *Chem. Eur. J.* **2006**, *12* (15), 4176–4184.

109 S. Zhao, Y. Jia, Y.-F. Song, *Appl. Catal., A,* **2013**, *453*, 188–194.

110 T. Yamaura, K. Kamata, K. Yamaguchi, N. Mizuno, *Catal. Today,* **2013**, *203*, 76–80.

[111] W. Trakarnpruk, K. Rujiraworawut, *Fuel Process. Technol.* **2009**, *90* (3), 411–414.

[112] S.-S. Wang, Z. Popović, H.-H. Wu, Y. *ChemCatChem,* **2011**, *3* (7), 1208–1213.

[113] (a) B. Guérin, D. M. Fernandes, J.-C. Daran, D. Agustin, R. Poli, *New J. Chem.* **2013**, *37*(11), 3466–3475.
(b) N. S. Antonova, J. J. Carbó, U. Kortz, O. A. Kholdeeva, J. M. Poblet, *J. Am. Chem. Soc.* **2010**, *132*(21), 7488–7497
(c) T. Mallat, A. Baiker, *Chem. Rev.* **2004**, *104* (6), 3037–3058.

[114] G. Li, Y. Ding, J. Wang, X. Wang, J. Suo, *J. Mol. Catal. A: Chem.* **2007**, *262* (1), 67–76.

[115] S. E. Jacobson, D. A. Muccigrosso, F. Mares, *J. Org. Chem.* **1979**, *44* (6), 921–924.

[116] K. Kamata, K. Yamaguchi, S. Hikichi, N. Mizuno, *Adv. Synth. Catal.* **2003**, *345* (11), 1193–1196.

[117] Q. Xu, Y. Li, R. Ban, Z. J. Li, X. Han, P. Ma, V. Singh, J. Wang, J. Niu, *Dalton Trans.* **2018**, *47* (38), 13479–13486.

[118] (a) C. Venturello, R. D'Aloisio, J. C. J. Bart, M. Ricci, *J. Mol. Catal.* **1985**, 32, 107-110.
(b) C. Venturello, E. Alneri, M. Ricci, *J. Org. Chem.* **1983**, *48* (21), 3831–3833.
(c) C. Venturello, M. Gambaro, *Synthesis,* **1989**, *1989* (4), 295–297.

[119] Y. Matoba, H. Inoue, J.-I. Akagi, T. Okabayashi, Y. Ishii, M. Ogawa, *Synth. Commun.* **1984**, *14*(9),865–873.

[120] P. Jiménez-Lozano, I. D. Ivanchikova, O. A. Kholdeeva, J. M. Poblet, J. J. Carbó, *Chem. Commun.* **2012**, *48* (74), 9266–9268.

[121] K. Kamata, K. Yonehara, Y. Sumida, K. Yamaguchi, S. Hikichi, N. Mizuno, *Science,* **2003**, *300*(5621), 964–966.

[122] D. Zhao, J. Feng, Q. Huo, N. Melosh, G. H. Fredrickson, B. F. Chmelka, G. D. Stucky, *Science,* **1998**, *279* (5350), 548–552.

[123] M. Sun, W.-C. Chen, L. Zhao, X.-L. Wang, Z.-M. Su, *Inorg. Chem. Commun.* **2018**, *87*, 30–35.

[124] (a) S.-W. Li, R.-M. Gao, R.-L. Zhang, J. Zhao, *Fuel,* **2016**, *184*, 18–27.
(b) M. Bagherzadeh, H. Hosseini, S. Akbayrak, S. Özkar, *ChemistrySelect,* **2019**, *4* (19), 5911–5917.

[125] (a) Y. Leng, J. Wu, P. Jiang, J. Wang, *Catal. Sci. Technol.* **2014**, *4* (5), 1293–1300.
(b) S.-J. Yu, Y.-K. Han, W. Wang, *Polymer,* **2019**, *162*, 73–79.

[126] L. Li, C. Liu, A. Geng, C. Jiang, Y. Guo, C. Hu, *Mater. Res. Bull.* **2006**, *41* (2), 319–332.

[127] M. Genovese, K. Lian, *J. Mater. Chem. A* **2017**, *5* (8), 3939–3947.

[128] R. Ghubayra, C. Nuttall, S. Hodgkiss, M. Craven, E. F. Kozhevnikova, I. V. Kozhevnikov, *Appl. Catal. B,* **2019**, *253*, 309–316.

[129] (a) Y. Izumi, R. Hasebe, K. Urabe, *J. Catal.* **1983**, *84* (2), 402–409.
(b)M. A. Schwegler, P. Vinke, M. van der Eijk, H. van Bekkum, *Appl. Catal. A,* **1992**, *80* (1), 41–57.

[130] M. E. Chimienti, L. R. Pizzio, C. V. Cáceres, M. N. Blanco, *Appl. Catal. A,* **2001**, *208*(1), 7–19.

[131] F. M. Toma, A. Sartorel, M. Iurlo, M. Carraro, P. Parisse, C. Maccato, S.Rapino, B. R Gonzalez,. H. Amenitsch, T. D. Ros, L. Casalis, A. Goldoni, M. Marcaccio, G. Scorrano, G. Scoles, F. Paolucci, M. Prato, M. Bonchio, *Nature Chem.* **2010**, *2*(10), 826–831.

[132] J. Wu, L. Liao, W. Yan, Y. Xue, Y. Sun, X. Yan, Y. Chen, Y. Xie, *ChemSusChem,* **2012**, *5*(7), 1207–1212.

[133] (a) Y. Kim, S. Shanmugam, *ACS Appl. Mater. Interfaces,***2013**, 5 (22), 12197–12204.
(b) W. Zhang, Q. Zhao, T. Liu, Y. Gao, Y. Li, G. Zhang, F. Zhang, X. Fan, I*nd. Eng. Chem. Res.* **2014,** 53(4), 1437–1441.
(c) K. Liu, T. Chen, Z. Hou, Y. Wang and L. Dai, *Catal. Lett.* **2014**, 144 (2), 314–319.

[134] (a) Y. Han, Y. Xiao, Z. Zhang, B. Liu, P. Zheng, S. He, W. Wang, *Macromolecules,* **2009**, *42* (17), 6543–6548.
(b) R. Yu, X.-F. Kuang, X.-Y. Wu, C.-Z. Lu, J. P. Donahue, *Coord. Chem. Rev.* **2009**, *253* (23), 2872–2890.

(c) Y. Xiao, D. Chen, N. Ma, Z. Hou, M. Hu, C. Wang, W. Wang, *RSC Adv.* **2013**, *3* (44), 21544–21551.
(d) J. Du, M.-D. Cao, S.-L. Feng, F. Su, X.-J. Sang, L.-C. Zhang, W.-S. You, M. Yang, Z.-M. Zhu, *Chem. Eur. J.l* **2017**, *23* (58), 14614–14622.
(e) M. Zhu, J. Peng, H.-J. Pang, P.-P. Zhang, Y. Chen, D.-D. Wang, M.-G. Liu, Y.-H. Wang, *J. Solid State Chem.* **2011**, *184* (5), 1070–1078.

135 Y. Leng, J. Liu, P. Jiang, J. Wang, *RSC Adv.* **2012**, *2*(31), 11653–11656.

136 (a) E. Poli, J.-M. Clacens, Y. Pouilloux, *Catal. Today*, **2011**, *164* (1), 429–435.
(b) Y. M. A. Yamada, C. K. Jin, Y. Uozumi, *Org. Lett.* **2010**, *12*(20), 4540–4543.

137 J. Pisk, D. Agustin, R. Poli, *Molecules,* **2019**, *24* (4), 783.

138 F. Bentaleb, O. Makrygenni, D. Brouri, C. Coelho Diogo, A. Mehdi, A. Proust, F. Launay, R. Villanneau, *Inorg. Chem.* **2015**, *54* (15), 7607–7616.

139 (a) M. Masteri-Farahani, M. Modarres, *J. Mol. Catal. A: Chem.* **2016**, *417*, 81–88.
(b) I. Tamiolakis, I. N. Lykakis, A. P. Katsoulidis, M. Stratakis, G. S. Armatas, *Chem. Mater.* **2011**, *23* (18), 4204–4211.

140 W. Kaleta, K. Nowińska, *Chem. Commun.* **2001**, *0* (6), 535–536.

141 (a) N. M. Okun, T. M. Anderson, C. L. Hill, *J. Am. Chem. Soc.* **2003**, *125* (11), 3194–3195.
(b) M. Green, J. Harries, G. Wakefield, R. Taylor, *J. Am. Chem. Soc.* **2005**, *127* (37), 12812–12813.

142 (a) A. Patel, N. Narkhede, *Catal. Sci. Technol.* **2013**, *3* (12), 3317–3325.
(b) Q. Liu, W. Wu, J. Wang, X. Ren, Y. Wang, *Microporous Mesoporous Mater.* **2004**, *76* (1), 51–60.
(c) F. Zhang, C. Yuan, J. Wang, Y. Kong, H. Zhu, C. Wang, *J. Mol. Catal. A: Chem.* **2006**, *247* (1), 130–137.

143 K. Nowińska, R. Fórmaniak, W. Kaleta, A. Wącław, *Appl. Catal. A,* **2003**, *256* (1), 115–123.

144 J. Wang, H.-O. Zhu, *Catal. Lett.* **2004**, *93* (3), 209–212.

145 (a) R. Zhang, C. Yang, *J. Mater. Chem.* **2008**, *18* (23), 2691–2703.
(b) R. Villanneau, A. Marzouk, Y. Wang, A. B. Djamaa, G. Laugel, A. Proust, F. Launay, *Inorg. Chem.* **2013**, *52* (6), 2958–2965.

146 (a) S. Wu, J. Wang, W. Zhang, X. Ren, *Catal Lett* **2008**, *125* (3), 308–314.
(b) S. Wu, P. Liu, Y. Leng, J. Wang, *Catal Lett* **2009**, *132* (3), 500.

147 K. Inumaru, T. Ishihara, Y. Kamiya, T. Okuhara, S. Yamanaka, *Angew. Chem. Int. Ed.* **2007**, *46*(40), 7625–7628.

148 M. Bornstein, D. M. Parker, A. D. Quast, J. S. Shumaker - Parry, I. Zharov, *ChemCatChem,* **2019**, *11*(17), 4360–4367.

Chapter 2

Influence of the second coordination sphere in catalysis – Introduction of fluoroalcohol groups on metal complexes based on polydentate N-donor ligands

Abstract: This chapter describes the synthesis of three families of polydentate N-donor ligands functionalized with fluoroalcohol or methyl groups and related metal complexes. In order to evaluate the influence of the second coordination sphere in catalytic processes, the complexes based on the pyridinophane family (L^1 = pyridinophane ligand with methyl groups, L^2 = pyridinophane ligands with fluoroalcohol groups) were successfully obtained.

The catalytic activity towards cyclooctene oxidation has been studied in presence of Mn and Fe coordination complexes with L^1 and L^2 ligands, the influence of the second coordination sphere being evaluated on those systems.

The reactivity of Co and Ni coordination complexes toward H_2 photoproduction has also been explored and in this chapter, the results obtained being discussed.

2.1. Introduction

As described in the bibliographic chapter, in all processes including a molecular coordination complex as catalyst, the second coordination sphere can play a crucial rule in the activation and stabilization of substrates and/or intermediates in numerous catalytic processes.[1]

It is noteworthy to pay attention on the oxygen atom transfer (OAT) reactions, especially when the catalytic systems use H_2O_2 as oxidant and Mn or Fe as reactive metal center. After the H_2O_2 activation, the cleavage of the O-O peroxo bond of the created intermediate is crucial to obtain the oxidized species. In literature, acetic acid (CH_3COOH) has been widely used for those reactions and mechanistic studies clearly demonstrated its role during the heterolytic cleavage of the O-O peroxo bond of a hydroperoxo intermediate.[2] In order to overcome the use of acetic acid as co-reagent, the use of Mn- and Fe- metal complexes with ligands bearing well-defined second coordination sphere - able to create a H-bond network with H_2O_2 facilitating its activation - has been envisioned herein. More specifically, the introduction of fluoroalcohol functions has been realized for the reasons described in the bibliographic chapter. A synergy between the metal center and the fluoroalcohol groups should favor the generation of a metal-oxo intermediate able to transfer an oxygen atom on a substrate as described in Scheme 1.

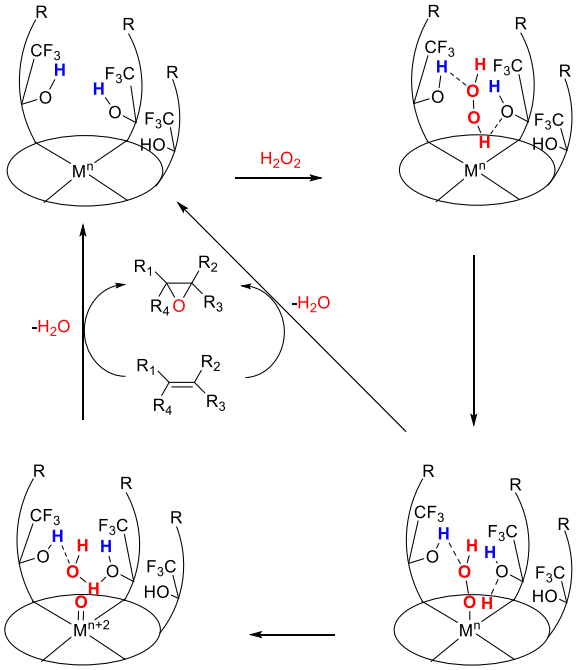

Scheme 1 - Possible catalytic cycle for epoxidation by metal complexes with fluoroalcohol functions.

In summary, the main objective is to develop a new catalytic system for epoxidation reactions with H_2O_2 as oxidant based on the use of a new class of metal complexes combining

1. a non-noble and abundant metal center (iron or manganese),
2. a robust ligand with a nitrogen-containing first coordination sphere
3. a second coordination sphere with functional groups able to create an H-bonding network with H_2O_2.

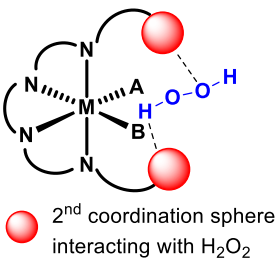

Since most of the iron based catalysts are air sensitive Fe(II)-coordination complexes[3] in the field of bioinspired OAT catalysis, we focused on air stable metal complexes. Indeed, in addition to easier handling procedures, the first step of the catalytic process is the oxidation of the Fe(II) into a Fe(III), the one responsible of the H_2O_2 activation. [2b] Moreover, Fe(III) coordination complexes have proven to be also efficient in OAT catalytic reactions.[4]

Thus, three ligands platforms have been explored in order to introduce the fluoroalcohol functions (Scheme 2). For each platform, introduction of two different R groups (R = CH_3 or R = $CH_2C(OH)(CF_3)_2$) will be targeted in order to compare the systems with/without a second coordination sphere able to interact with H_2O_2.

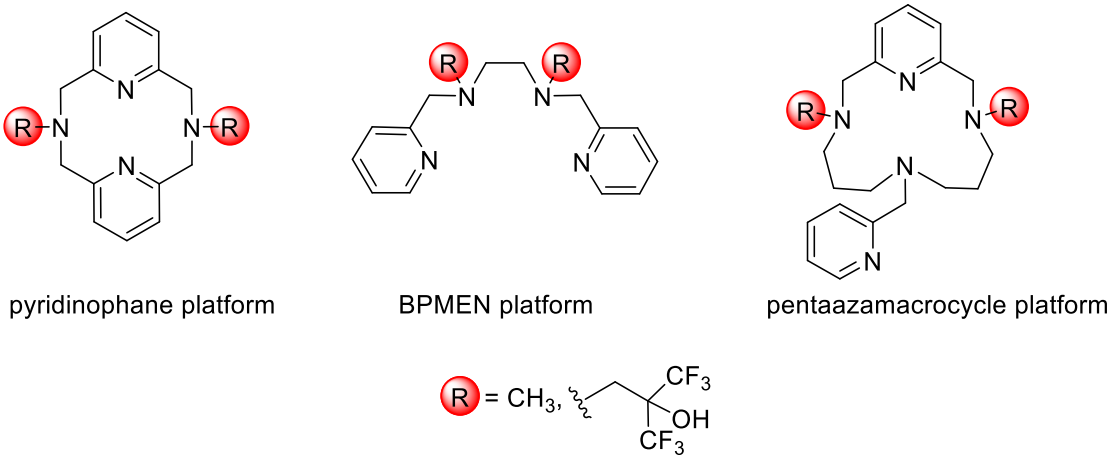

Scheme 2 - Ligands platforms envisioned.

- The first platform is based on the pyridinophane ligand (scheme 2). The choice was motivated by the fact that metal complexes using those ligands have been reported for various applications such as DNA cleavage, [5] H_2O_2 disproportionation, [6] C-C bond formation, [7] *cis*-dihydroxylation, [8] O_2 activation, [9] water oxidation [10] and proton photoreduction.[11] During this PhD worktime, the group of J. Cho has also reported the reactivity of metal complexes (metal = Ni, Co, Mn) based on this ligand for the activation of hydroperoxides[12] and iodosylbenzene[13]. Different first-row metal complexes based on this ligand have also been described, notably by Mirica's group.[14] Finally, based on the reported X-ray structures for these metal complexes, the geometry around the metal center was suitable to expect a strong interaction between the fluoroalcohol group, the metal center and H_2O_2.[15] It has to be noted that the strategy to introduce fluoroalcohol groups has been previously described by the group and some Mn(II) and Fe(III) metal complexes were obtained,[15] but the evaluation of the catalytic activity of these metal complexes has not been realized.
- The second ligand platform explored is based on the BPMEN (*N*,*N*′-dimethyl-*N*,*N*′-bis(pyridin-2-ylmethyl)ethane-1,2-diamine) ligand (Scheme 2). Indeed, this model ligand is extensively used in the field of OAT reactions.[3c, 16] Moreover, in order to evaluate the influence of the fluoroalcohol groups during a catalytic process, an easily

accessible system and modifiable ligand was targeted, making of this ligand an ideal candidate.

- Finally, the last platform envisioned is a pentaazamacrocycle. Indeed, while the two first platforms are suitable for metal complexes with two labile sites, this one should allow the access to metal complexes possessing only one labile site. In the context of OAT reactions, this aspect is of particular interest. Indeed, while metal complexes with two *cis* labile sites have proven to be efficient for OAT reactions,[17] metal complexes with only one vacant site did not display OAT reactivity with H_2O_2 as oxidant, and this even in presence of carboxylic acid as additive.[2b, 18] Indeed, no coordination of the carboxylate on the labile site and no assistance for the O-O bond cleavage can occur. However, with the approach proposed in this chapter, the fluoroalcohol functions introduced in the second coordination sphere of the metal complexes should favor the O-O bond cleavage. Moreover, with complexes bearing tetradentate ligands possessing two *cis* labile sites, and when no carboxylic acids are used, a mixture of *cis*-diols and epoxides has been reported.[2a] With complex containing a pentadentate ligand, the selective epoxide formation is expected.

2.2. Results and discussion

2.2.1. Pyridinophane platform

2.2.1.1. Ligands syntheses

Ligands L^1 and L^2 were synthesized according to literature procedures (Scheme 3).[15,19] Synthesis of the macrocycle **4**, precursor of the ligands L^1 and L^2, was achieved in 3 steps.

- The first one consisted in the reaction between 2,6-bis(chloromethyl)pyridine **2** (obtained from 2,6-pyridinedimethanol (**1**)) and sodium tosylamide in DMF at 80 °C. A mixture of the targeted intermediate **3** and a larger ring with three pyridine groups **3'** is obtained. Selective Soxhlet extraction led to pure compound **3** in 36% yield. Hydrolysis of the tosyl function with concentrated H_2SO_4 allows the access to the precursor **4** in 65% yield.[19]
- The synthesis of ligand L^1 was achieved by methylation of **4** through a reductive amination in presence of excess of formic acid and formaldehyde at reflux overnight.[19]
- A regioselective ring opening of 2,2-bis(trifluoromethyl)oxirane by compound **4** in ethanol during 24h at room temperature led to the exclusive formation of L^2 as a white precipitate. The pure product was obtained by recrystallization in boiling CH_3CN.[15]

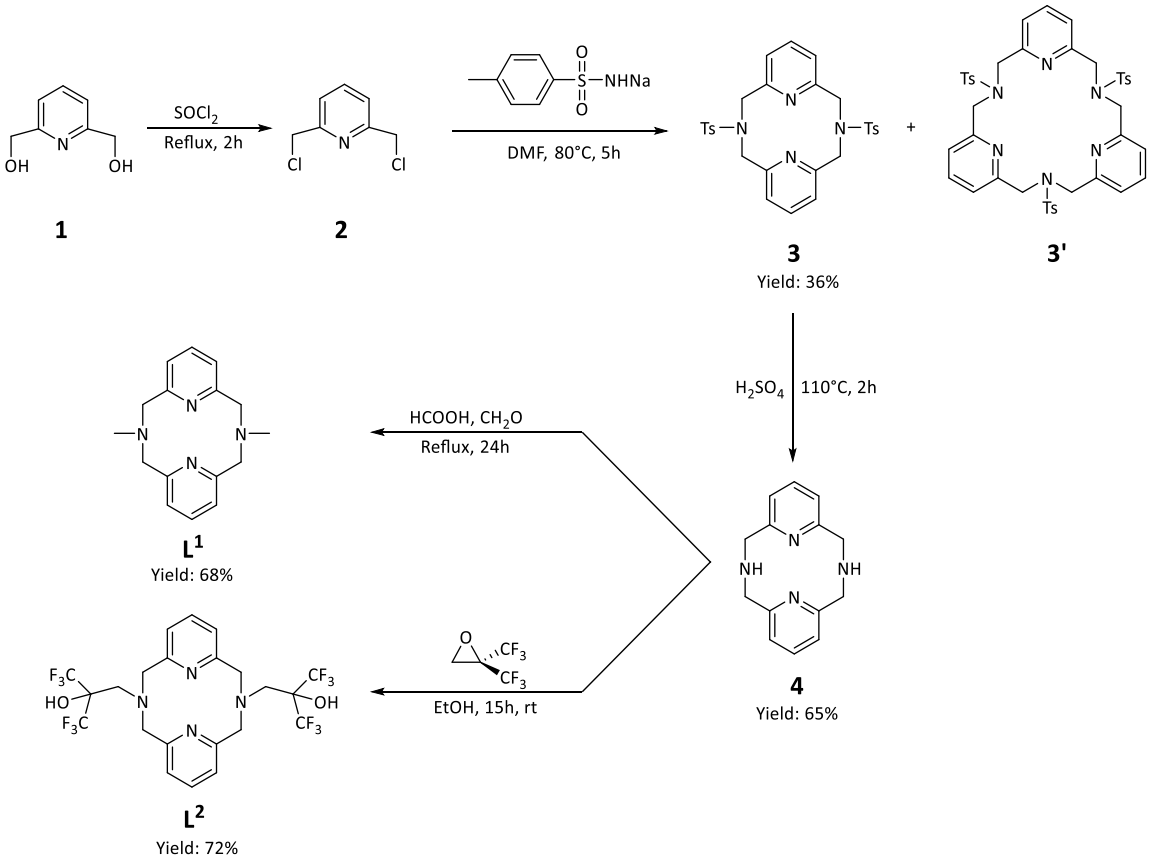

Scheme 3 - synthesis of L^1 and L^2.

The ligands L^1 and L^2 were characterized by ^1H, ^{13}C and ^{19}F (for L^2) NMR. The NMR spectra indicated the formation of symmetrical species. More specifically, only one doublet and one triplet for *m*-H and *p*-H nuclei of the pyridine ring were observed, respectively, in a 2:1 ratio for the ^1H NMR experiments. The X-ray structure of L^2 (Figure 1) indicated a *syn* boat-boat conformation, L^2 being already properly disposed to host metal salts.[15]

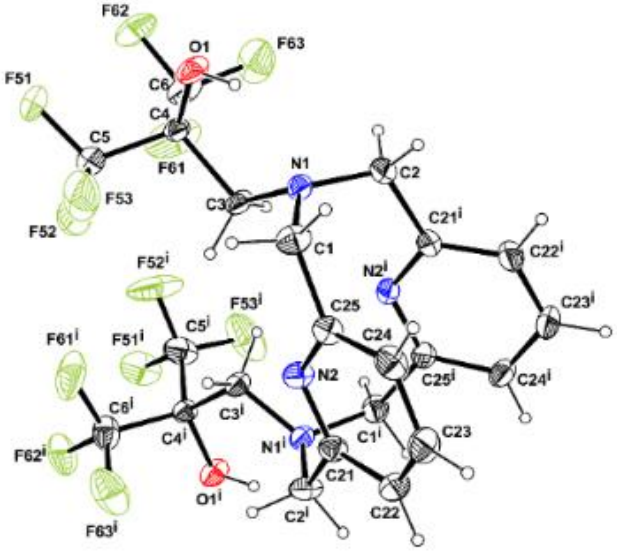

L^2

Figure 1 - Molecular view of L^2 with the atom labelling scheme. Ellipsoids are drawn at the 50% probability level.

2.2.1.2. Metal complexes syntheses

- From L^2

As mentioned previously, prior to this work, several metal complexes (metal = Fe(III), Mn(II), Cu(II), Zn(II)) derived from L^2 have already been synthetized.[15]

- Syntheses of $[(L^2)FeCl_2](FeCl_4)$ and $(L^2)MnCl_2$ have been reproduced and four new first row metal complexes have been obtained according to Scheme 4.
- Ni(II) and Co(II) metal complexes have also been synthetized. Indeed, even if these metal complexes have not been used for oxygen atom transfer reactions, their reactivity has been explored in the context of hydrogen photoproduction (*vide infra*).

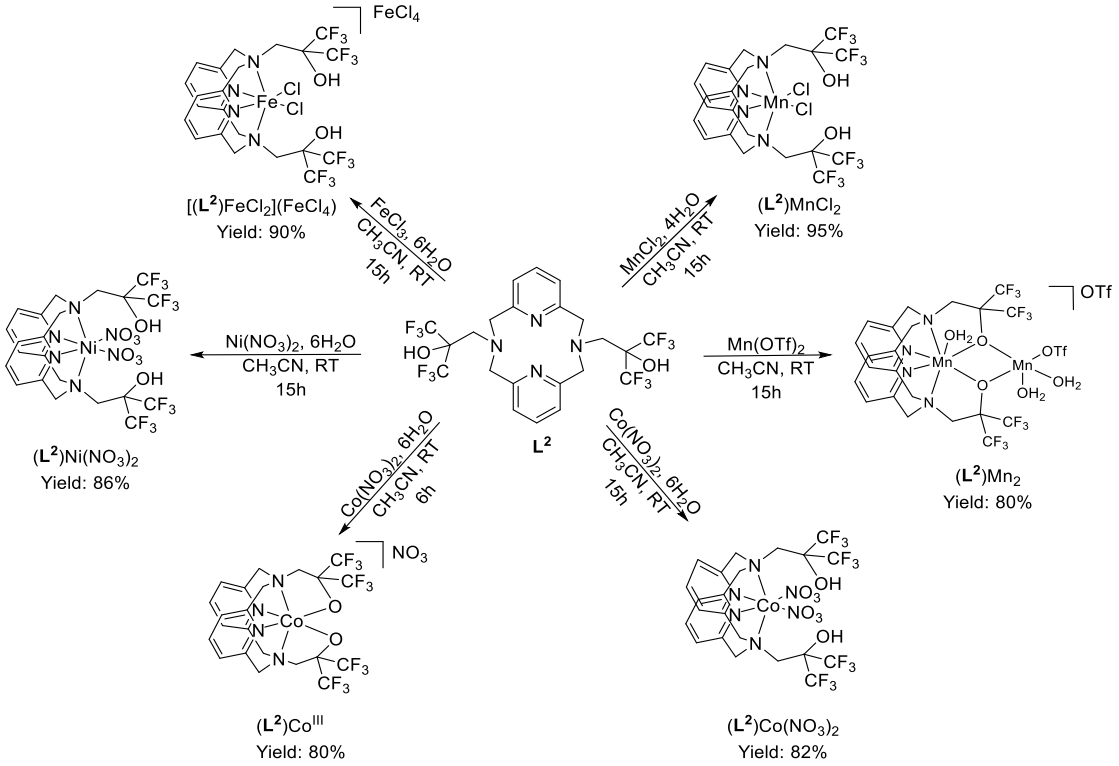

Scheme 4 - Synthetic pathways to access to metal complexes derived from L^2.

With $FeCl_3$

As represented in Scheme 4 and determined by X-ray diffraction analysis, when $FeCl_3$ was used as metal precursor, the isolated compound contained two metals for one ligand, one forming the Fe(III)-metal complex, the second iron being present as counteranion, $FeCl_4^-$. Other metal salt precursors ($Fe(OTf)_3$, $Fe(ClO_4)_3$) have been tested but no metal complexes could be isolated.

With $Mn(OTf)_2$

In order to access to a metal complex surrounded by ligands more labile than Cl^-, L^2 was reacted with $Mn(OTf)_2$ and the only isolated metal complex obtained was the dinuclear metal complex $(L^2)Mn_2$, in which the two deprotonated alcohol functions of the ligand are coordinated

on two Mn centers on a Mn_2O_2 four-member ring arrangement, one Mn center being linked to the nitrogen atoms of the ligand, the second one being non linked. The structure obtained from the X-ray diffraction analysis will be described later. Despite different strategies tested (slow addition of $Mn(OTf)_2$ into a solution of **L²** for example) to avoid the formation of the dinuclear metal complex, the expected monomeric complex (**L²**)$Mn(OTf)_2$ was not obtained.

With $Ni(NO_3)_2$

(**L²**)$Ni(NO_3)_2$ was obtained by reaction between **L²** and one equivalent of $Ni(NO_3)_2$,$6H_2O$ in CH_3CN at room temperature for 15h. After precipitation in diethyl ether, the pure metal complex was obtained in 86% yield as purple crystals through slow diffusion of diethyl ether into an acetonitrile solution of the complex (**L²**)$Ni(NO_3)_2$.

With $Co(NO_3)_2$

Starting at room temperature from $Co(NO_3)_2$,$6H_2O$ as metal precursor, 6 h of reaction were sufficient to lead to the formation of (**L²**)$Co(NO_3)_2$ in 82% yield as purple crystals in the same conditions that for (**L²**)$Ni(NO_3)_2$. A prolonged reaction time induced the formation of a diamagnetic metal complex, isolated as a purple solid (80% yield) indicating the formation of an oxidized Co^{III} metal complex. Indeed, a diamagnetic ^1H NMR spectrum was observed which indicated the formation of a symmetrical compound assigned as (**L²**)Co^{III}. It is proposed that aerobic oxidation of the Co^{II} complex occurred during the reaction time, leading to a Co^{III} metal complex stabilized by the formation of a hexacoordinated Co, environment due to the deprotonation of the fluoroalcohol groups followed by its coordination to the Co center.

Crystals suitable for X-ray diffraction analysis were obtained for all metal complexes described in Scheme 4. Molecular views are presented in Figure 2 and selected bond distances and angles in Table 1. Concerning (**L²**)$MnCl_2$, the quality of the data were sufficient to confirm the formation of the metal complex but did not allow a discussion on the bond distances and angles.

Table 1 - Selected bond distances (Å) and angles (deg.) for (**L²**)$Ni(NO_3)_2$, (**L²**)$Co(NO_3)_2$, (**L²**)Co^{III}, [(**L²**)$FeCl_2$]$FeCl_4$ and (**L²**)Mn_2.

	$(L^2)Ni(NO_3)_2$	$(L^2)Co(NO_3)_2$	$(L^2)Co^{III}$	$[(L^2)FeCl_2]FeCl_4$	$(L^2)Mn_2$
Bonds					
M - N_{py}	1.999(3)	2.071(2)	1.846(1) – 1.848(1)	2.101(3) – 2.124(3)	2.2707(18) – 2.2710(18)
M - N_{amine}	2.239(3)	2.285(2)	1.951(1) – 1.954(1)	2.261(3) – 2.280(3)	2.4063(19) – 2.4337(18)
Angles					
N_{amine}-M-N_{amine}	154.80(13)	150.25(10)	164.74(5)	146.96(9) – 147.37(9)	137.58(6)
N_{Py}-M-N_{Py}	84.94(14)	83.58(11)	92.76(5)	77.30(10) – 77.41(10)	74.01(7)

As previously reported for metal complexes based on the same pyridinophane scaffold, a *syn* boat-boat conformation is observed for all metal complexes.[15] The metal complexes

(L^2)$Ni(NO_3)_2$, (L^2)$Co(NO_3)_2$ and [(L^2)$FeCl_2$]$FeCl_4$ display a distorted octahedral geometry around the metal center with a N_{amine}-M-N_{amine} angle between 147° and 155 ° and a N_{py}-M-N_{py} angle between 77° and 85° (Table 1).

Concerning the Co^{III} metal complex (L^2)Co^{III}, a less distorted octahedral geometry is observed, with notably a N_{amine}-Co-N_{amine} angle of 164.74°. Typical shorter M-N distances are observed in comparison to the Co^{II} metal complex.

Concerning (L^2)Mn_2, due to the presence of two Mn centers, a more distorted octahedral geometry is observed concerning the Mn_1 coordinated by the pyridinophane ligand. Another consequence is an elongation of the Mn_1-N bonds.

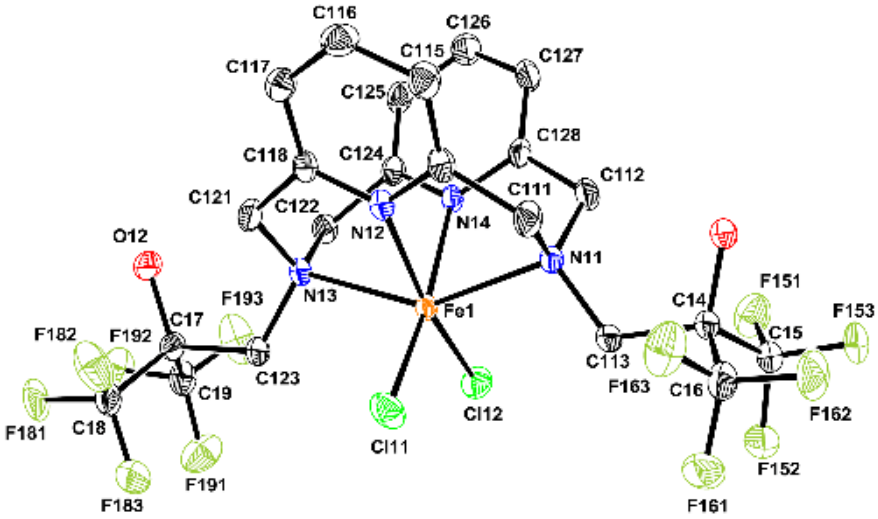

[(L^2)$FeCl_2$]($FeCl_4$)

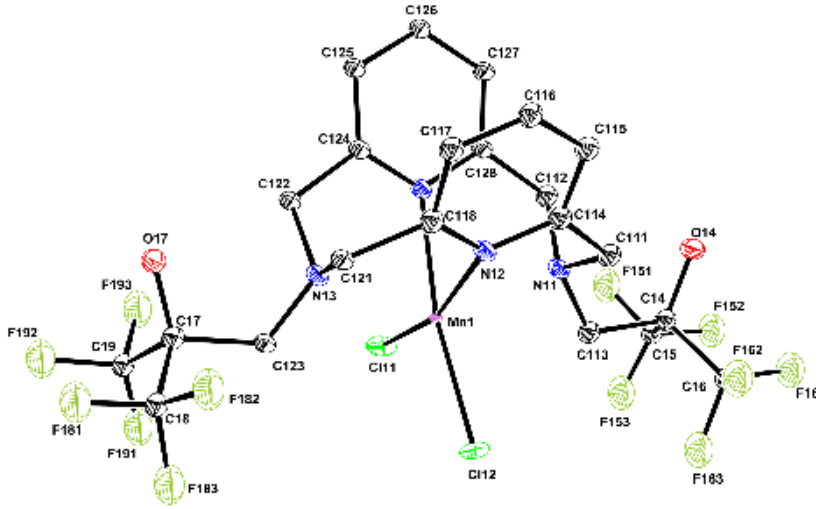

(L^2)$MnCl_2$

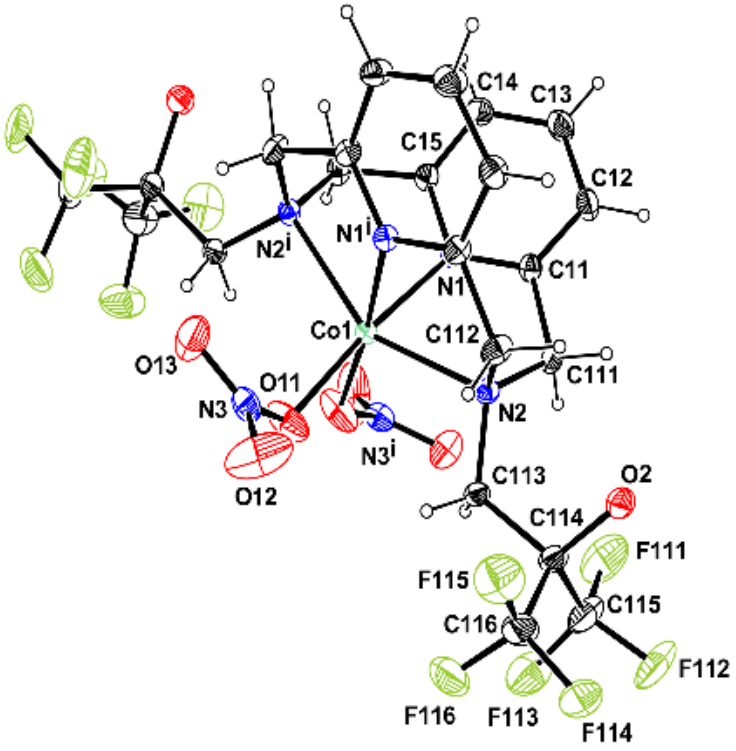

$(L^2)Co(NO_3)_2$

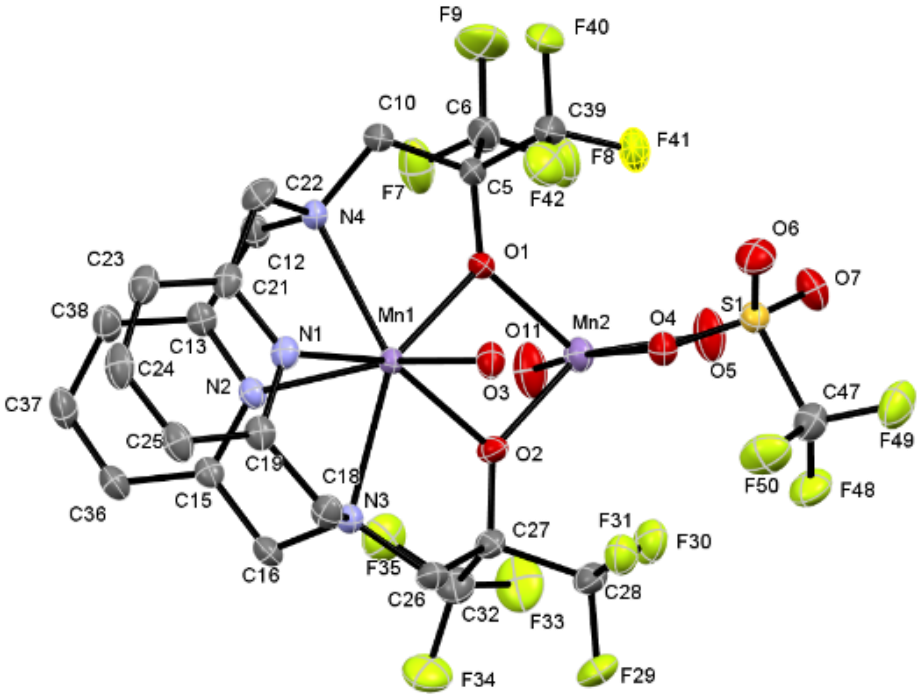

$[(L^2)Mn_2(OTf)]$

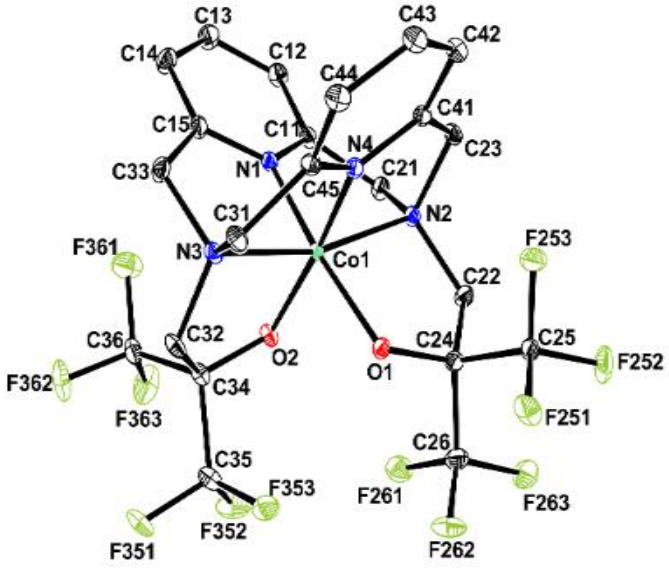

$(L^2)Co(NO_3)_2$

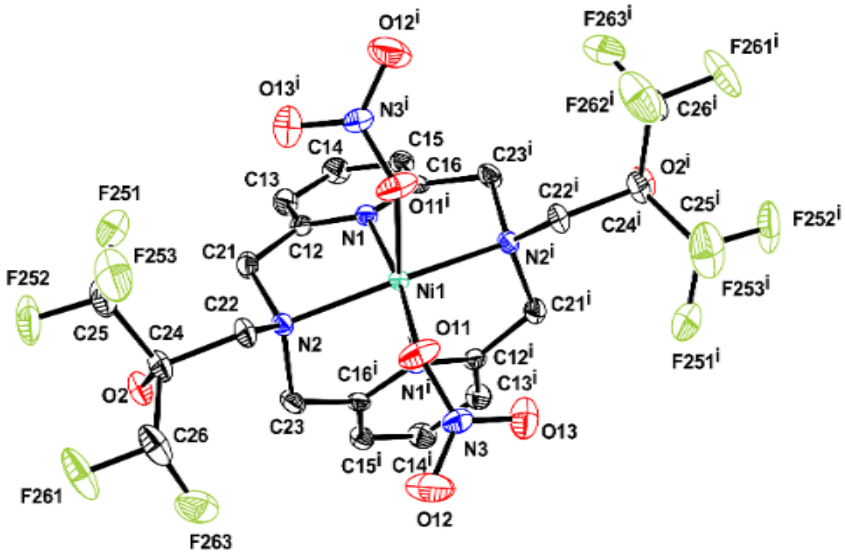

$(L^2)Ni(NO_3)_2$

Figure 2 - Molecular views of $[(L^2)FeCl_2](FeCl_4)$, $(L^2)MnCl_2$, $(L^2)Co(NO_3)_2$, $[(L^2)Mn_2(OTf)]$, $(L^2)Ni(NO_3)_2$ and $(L^2)Co^{III}$ with the atom labelling scheme. Ellipsoids are drawn at the 50% probability level. H atoms (except $(L^2)Co(NO_3)_2$) and solvents molecules have been omitted for the sake of clarity. For $[(L^2)FeCl_2](FeCl_4)$, $FeCl_4$ anion has been omitted for the sake of clarity. For $(L^2)Co^{III}$, NO_3 anion has been omitted for the sake of clarity.

From **L¹**

Once the metal complexes derived from **L²** obtained, analog complexes- with CH_3 groups instead of fluoroalcohol groups- have been synthesized in order to be able to compare their reactivity. Based on the same synthetic strategy used for metal complexes from **L²**, the access to all metal complexes described in Scheme 5 is straightforward and resulted into the addition of the metal precursor in a solution of the ligand in CH_3CN. After stirring at room temperature for 15h, the pure metal complexes were obtained as crystals by diethyl ether diffusion into a concentrated solution of the metal complex in CH_3CN.

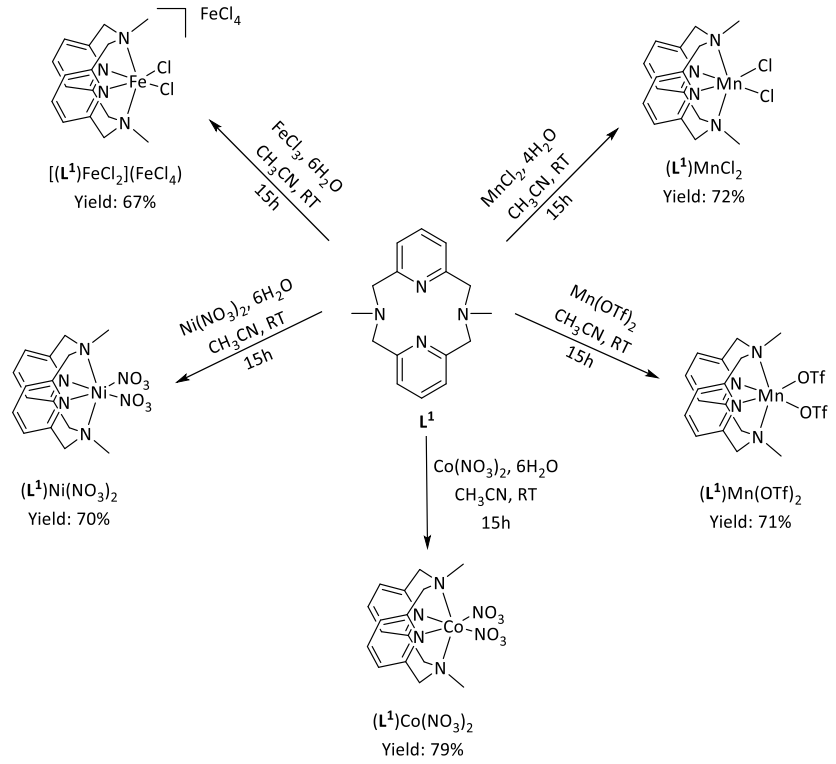

Scheme 5 - Synthetic pathways to access to metal complexes derived from **L¹**.

With Mn(OTf)₂

When $Mn(OTf)_2$ was used as Mn(II) precursor, (**L¹**)$Mn(OTf)_2$ was obtained and not a dinuclear metal complex as previously with **L²**. This result suggests that the reactivity observed with **L²** and $Mn(OTf)_2$ arises from the properties of the fluoroalcohol groups.

With Co(NO₃)₂

Another difference of reactivity between **L¹** and **L²** was observed when **L¹** was reacted with $Co(NO_3)_2$,$6H_2O$. Indeed, even with a 15h reaction time, no oxidation of the Co(II) into a Co(III) center was observed. While a stabilization of the Co(III) center by the deprotonated fluoroalcohol was possible for (**L²**)Co^{III}, it is not possible for (**L¹**)$Co(NO_3)_2$, and thus explain its stability in Co(II) state.

As for metal complexes obtained from **L²**, crystals suitable for X-ray diffraction analysis were obtained for all metal complexes described in Scheme 5 and are presented in Figure 3.

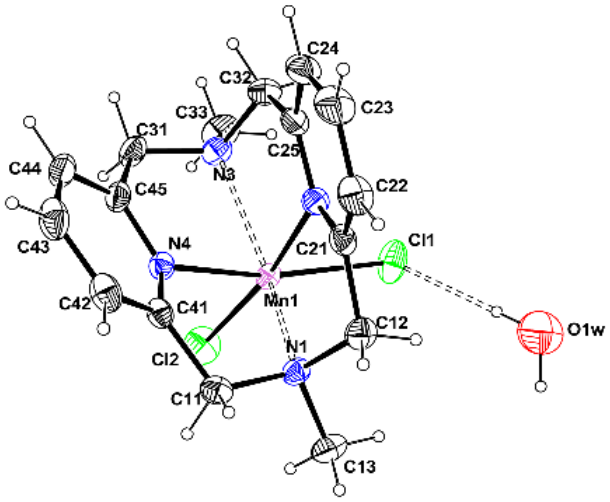

$(L^1)MnCl_2$

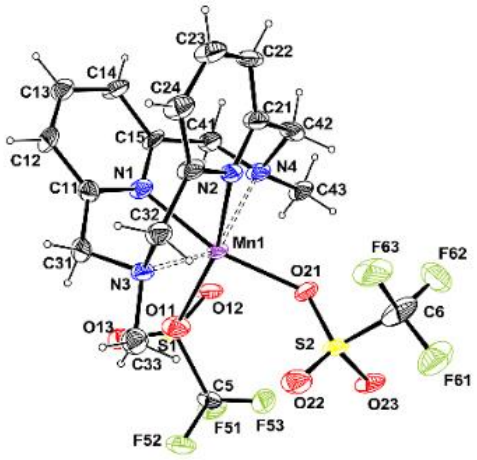

$(L^1)Mn(OTf)_2$

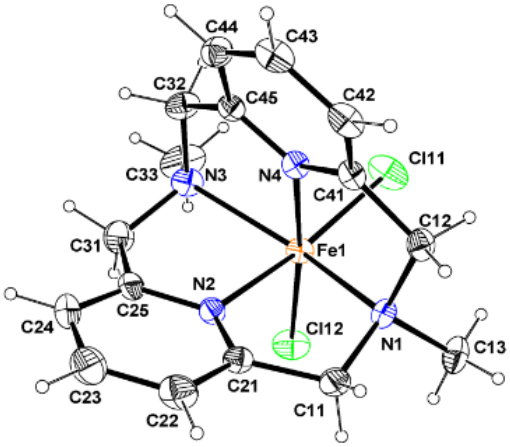

$[(L^1)FeCl_2](FeCl_4)$

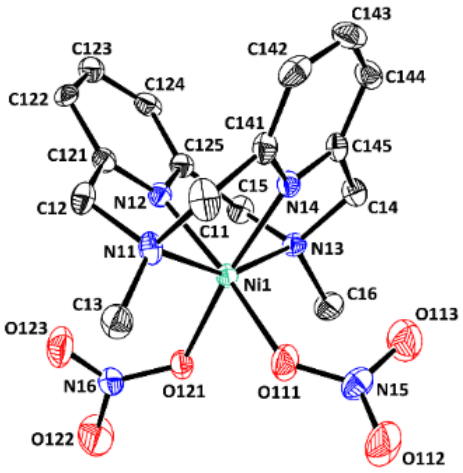

$(L^1)Ni(NO_3)_2$

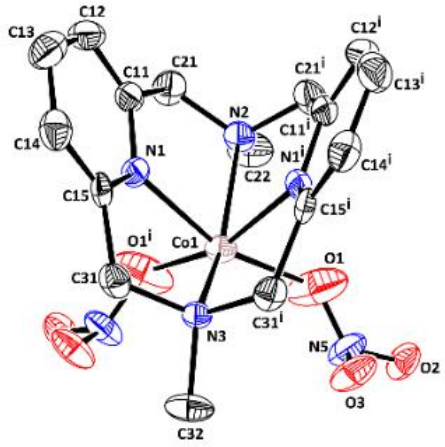

$(L^1)Co(NO_3)_2$

Figure 3 - Molecular views of $(L^1)MnCl_2$, $(L^1)Mn(OTf)_2$, $[(L^1)FeCl_2](FeCl_4)$, $(L^1)Ni(NO_3)_2$ and $(L^1)Co(NO_3)_2$ with the atom labelling scheme. Ellipsoids are drawn at the 50% probability level. For $[(L^1)FeCl_2](FeCl_4)$, $FeCl_4$ anion has been omitted for the sake of clarity. $(L^1)Ni(NO_3)_2$ and $(L^1)Co(NO_3)_2$ H atoms and solvents molecules have been omitted for the sake of clarity.

Table 2- Selected bond distances (Å) and angles (deg.) for $(L^1)Ni(NO_3)_2$, $(L^1)Co(NO_3)_2$, $(L^1)MnCl_2$, $(L^1)Mn(OTf)_2$, and $[(L^1)FeCl_2](FeCl_4)$.

	$(L^1)Ni(NO_3)_2$	$(L^1)Co(NO_3)_2$	$(L^1)MnCl_2$	$(L^1)Mn(OTf)_2$	$[(L^1)FeCl_2](FeCl_4)$
Bonds					
M - N_{py}	1.999(4) – 2.027(4)	2.094(4)	2.2539(14) – 2.2706(14)	2.228(9) – 2.256(8)	2.114(3) – 2.115(3)
M - N_{amine}	2.196(4) – 2.216(4)	2.259(6) - 2.297(5)	2.3460(15) – 2.3800(14)	2.355(8) – 2.366(9)	2.216(3) – 2.232(3)
Angles					
N_{amine}-M-N_{amine}	153.58(15) - 153.95(15)	147.7(2)	139.11(5)	141.5(3)	146.54(10)
N_{Py}-M-N_{Py}	83.69(17) - 84.60(15)	80.4(2)	73.83(5)	78.7(3)	78.08(10)

As for metal complexes derived from **L²**, those obtained from **L¹** possess a distorted octahedral geometry around the metal center. Concerning the two Mn metal complexes, this phenomenon is more significant and longer M-N bond are observed. For (**L¹**)$MnCl_2$, a H-bond involving a water molecule that has co-crystalized and the Cl atoms on the Mn centers is also observed and might explain the elongation of the Mn-N bonds.

It has to be noted that the nature of the substituents (fluoroalcohol or methyl) on the N_{amine} atoms did not significantly influence the bonds distances and angles.

2.2.2. BPMEN platform

2.2.2.1. Synthesis of the ligands

Ligands **L³** (BPMEN) and **L⁴** were synthesized as described in Scheme 6. As reported,[20] N,N'-bis(pyridin-2-ylmethyl)ethane-1,2-diamine (**5**), precursor of **L³** , was obtained in 82% yield by the condensation of ethylenediamine and pyridine-2-carboxaldehyde in methanol.

Then, reductive amination of **5** in presence of formic acid and formaldehyde led to the formation of **L³** in 92% yield as an orange oil. As for ligand **L²**, **L⁴** was obtained *via* a regioselective epoxide ring opening in absolute ethanol and was obtained in 75% yield as a white powder after recrystallization in boiling CH_3CN.

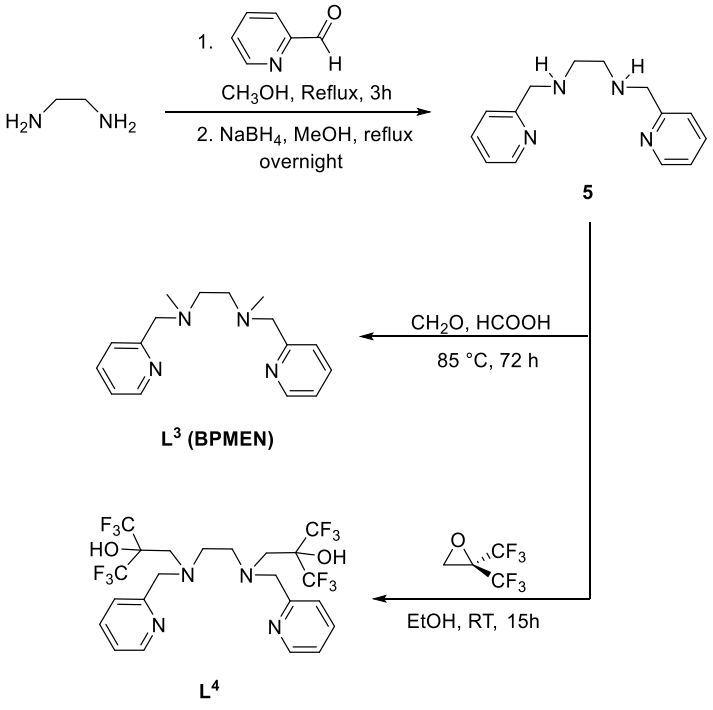

Scheme 6 - Synthesis of ligands **L³** and **L⁴**.

Both ligands **L³** and **L⁴** were characterized by ^{1}H and ^{13}C NMR. ^{19}F NMR and elementary analysis were done for **L⁴**. All analyses confirmed their formation. Suitable crystals for X-ray diffraction analysis were obtained for **L⁴** and its X-ray structure is presented in Figure 4, confirming its formation.

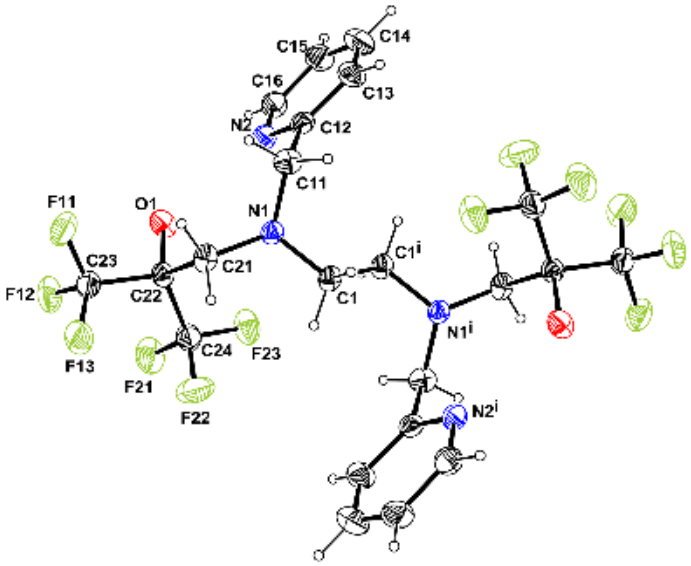

L^4

Figure 4 - Molecular view of ligand L^4 with the atom labelling scheme. Ellipsoids are drawn at the 50% probability level.

In both ligands (L^4 and L^2) structures, similar N-C distances were measured (1.447 to 1.473 Å). Ligand L^2 is already preorganized to coordinate metal precursors. For ligand L^4, due to the flexibility of this ligand, conformational modifications will be necessary to access to the targeted metal complexes during the complexation reactions.

2.2.2.2. Tentative of synthesis of complexes with L^4 ligand

Based on the same strategy used to synthesize metal complexes from L^2, metal salts precursors of Mn(II) and Fe(III) were mixed with L^4 in CH_3CN. Despite different attempts in different conditions (temperature, slow addition of reagents, solvent, concentration…), no metal complexes could be isolated. Due to the well-known chemistry on the BPMEN ligand, this was totally unexpected. Formation of polymeric species might be an explanation. Indeed, looking at the X-ray structure of L^4 (Figure 4), if the ligand possesses the same geometry in solution, two independent coordination sites involving two N atoms and one O atom could allow the formation of polymeric coordination chain (Scheme 7). Unfortunately, none of them has been isolated to confirm this hypothesis.

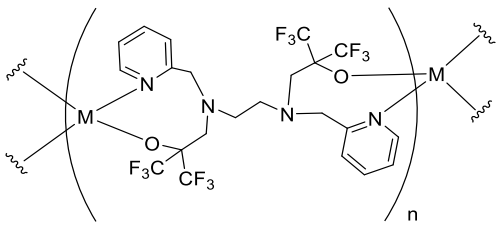

Scheme 7 - Potential polymeric coordination chain from L^4 and metal salts.

The syntheses of metal complexes derived from L^3 have also been realized and will be described in Chapter 3, in which they will be used in catalysis.

2.2.3. Pentaazamacrocycle platform

As explained in the introductive part of this chapter, pentacoordinated metal complexes have been also targeted. Indeed, even if no catalytic activity for OAT reaction has been reported in presence of H_2O_2 as oxidant and using as catalyst metal complexes with only one labile site,[18] it was expected that the fluoroalcohol functions helped in the O-O cleavage step. It would be an additional proof of the effect of the second coordination sphere. The synthetic pathway to access to the targeted ligands L^5 (tosyl functions), L^6 (methyl functions) and L^7 (fluoroalcohol functions) is described in Scheme 8.

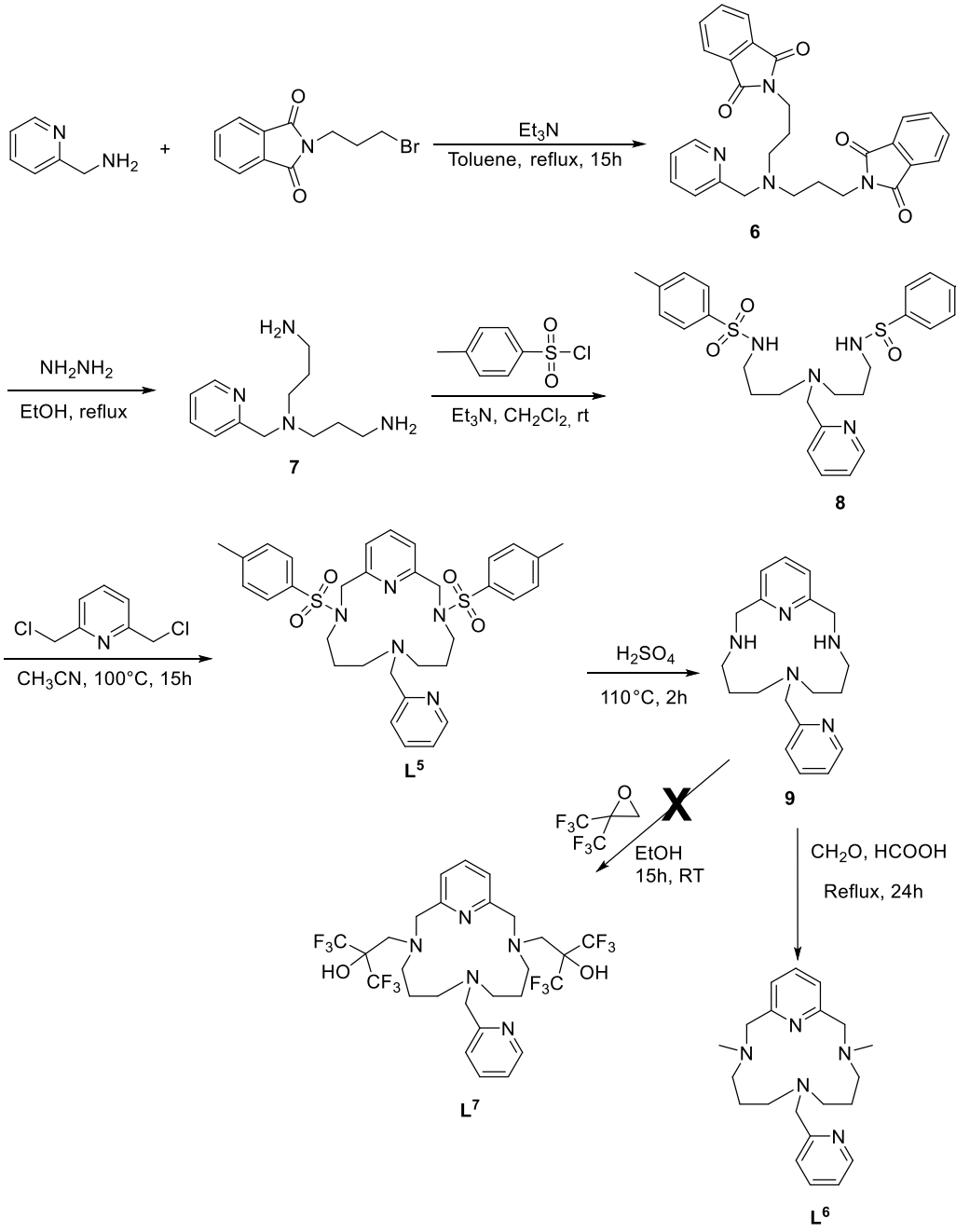

Scheme 8 - Synthetic pathways to access to L^5, L^6 and L^7.

Synthesis of the compound **9** has already been described by reaction between the polyamine **7** and 2,6-pyridinecarboxaldehyde using $Cu(NO_3)_2,6H_2O$ as metal template.[21] Unfortunately, despite numerous attempts to reproduce this procedure, compound **9** has never been obtained. The synthetic pathway described in Scheme 8 has then been envisioned. From a synthetic point of view, this new pathway is less "elegant", but it does allow the access to intermediates such as compound **8** and ligand L^5 that might be interesting as ligands in this project. Indeed, the group of Scarborough has used the ligand H_3Ts_3tren (Ts = tosyl ; tren = tris(2-aminoethyl)amine)) to access to Co^{II}- and Zn^{II}- metal complexes for which H_2O_2 adducts - possible thanks to the creation of a H-bond network between the tosyl groups and H_2O_2- have been isolated (Scheme 9).[22] Compound **8** would be an analog of the H_3Ts_3tren ligand with the replacement of one branch by a pyridine moiety.

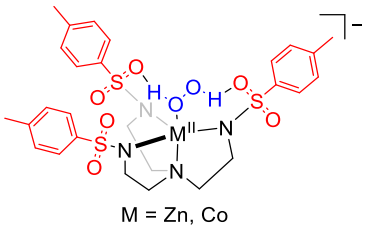

Scheme 9 - Metal-H_2O_2 adducts characterized with H_3Ts_3tren ligand.

Compound **7** was obtained in two steps in 59% overall yield according to a published procedure.[23] Introduction of the tosyl groups to access to **8** was realized according to a modified procedure from the literature.[24] After extraction in basic medium to eliminate unreacted tosyl chloride, **8** was obtained as yellow light oil in 54% yield. The penta-azamacrocycle L^5 was obtained in 39% yield as a pale-yellow powder by reaction between **8** and 2,6-chloromethylpyridine in CH_3CN in presence of Cs_2CO_3. After hydrolysis in concentrated H_2SO_4, the free amine **9** was obtained in 33% yield as an orange oil. Using the same protocol than for L^1 and L^3, methylation of **9** to access to L^6 has been realized through a reductive amination of **9**, giving ligand L^6 in 72% yield as black oil.

Unfortunately, different attempts to obtain L^7 failed. Indeed, reaction between **9** and 2,2-bis(trifluoromethyl)oxirane lead to the formation of mixture of non-separable products. Due to the ease to access to L^2 and L^4, this result was totally unexpected. Addition of $Sc(OTf)_3$ as a Lewis acid to facilitate the opening of the epoxide did not lead to a cleaner reaction.[25]

Due to the difficulties to access to the targeted compound with the fluoroalcohol functions, the reactivity of L^5 has been explored (Scheme 10).

Indeed, as described in the bibliographic chapter, tosyl groups have shown interesting features to stabilize highly reactive intermediates thanks to the formation of H-bond network involving tosyl functions. For the previously ligands described, Ni and Co metal complexes were

the easiest to get suitable crystals for X-ray analysis. Thus, L^5 was reacted with $Ni(NO_3)_2,6H_2O$ and $Co(NO_3)_2,6H_2O$ in CH_3CN at room temperature. Blue metal complexes, $(L^5)Ni(NO_3)_2{\cdot}CH_3CN$ and $(L^5)Co(NO_3)_2{\cdot}CH_3CN$, were isolated in 80% and 85% yield respectively. X-ray structures have been determined for L^5, $(L^5)Ni(NO_3)_2{\cdot}CH_3CN$ and $(L^5)Co(NO_3)_2{\cdot}CH_3CN$ (Figure 5).

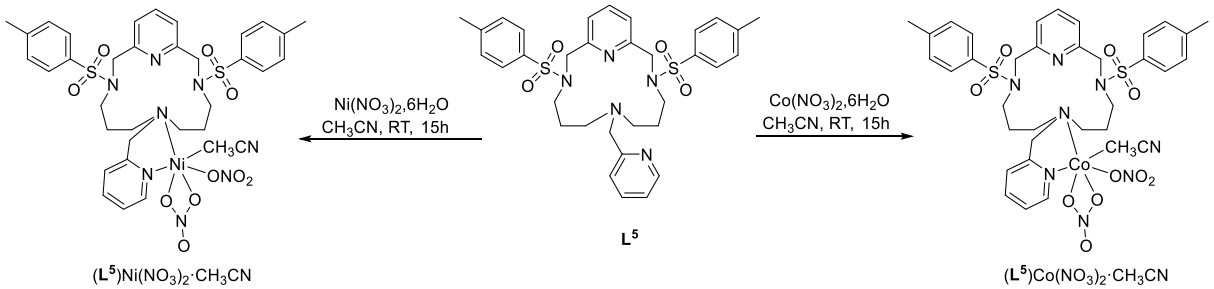

Scheme 10- Syntheses of $(L^5)Ni(NO_3)_2{\cdot}CH_3CN$, $(L^5)Co(NO_3)_2{\cdot}CH_3CN$.

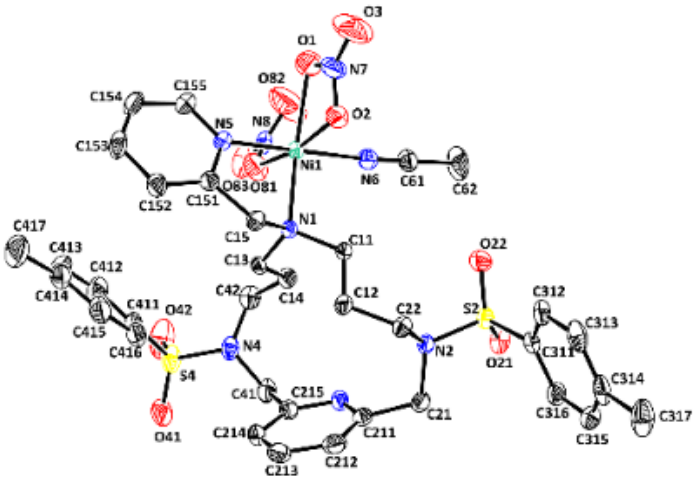

$(L^5)Ni(NO_3)_2{\cdot}CH_3CN$

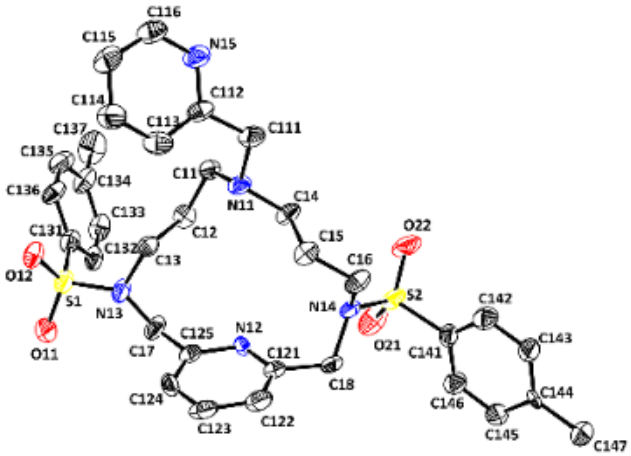

L^5

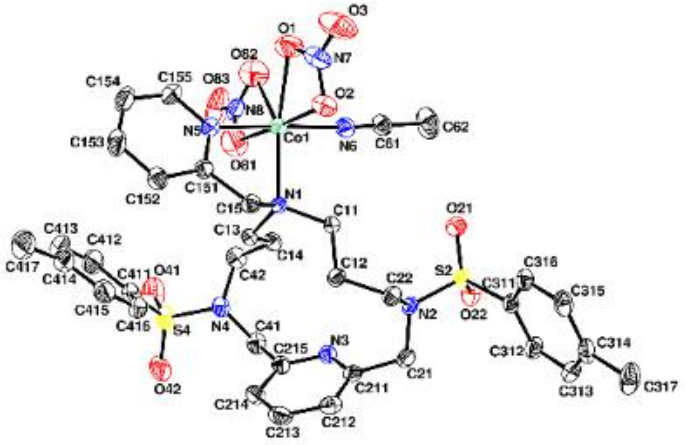

$(L^5)Co(NO_3)_2{\cdot}CH_3CN$

Figure 5 - Molecular views of L^5, $(L^5)Ni(NO_3)_2{\cdot}CH_3CN$ and $(L^5)Co(NO_3)_2{\cdot}CH_3CN$ with the atom labelling scheme. Ellipsoids are drawn at the 50% probability level.

Those structures confirmed the formation of the expected ligand L^5 and the complexation of a metal center. Surprisingly, the metal center is not present in the macrocycle but coordinated to the non tosylated amine and the pending pyridine part of the ligand. Two main hypotheses might explain this way of coordination:

- The presence of the tosyl groups on the nitrogen atoms diminish their ability to coordinate a metal center.
- The steric hindrance of the tosyl groups, blocking the rotation of the nitrogen atoms and thus the lone pair of the nitrogen atoms is not well oriented to coordinate a metal center.

Based on literature precedents, the geometry of this family of ligand seemed to be suitable to coordinate a metal center. Indeed, Zn(II)-, Cu(II)- and Ni(II)-metal complexes derived from L^6 have already been reported.[21] Due to the difficulties to access to the targeted metal complexes from L^5 and L^7, the reactivity of L^6 toward complexation was not evaluated herein.

2.2.4. Catalytic OAT studies with metal complexes from L^1 and L^2

Due to the difficulties met for the syntheses of metal complexes derived from BPMEN and pentaazamocrocycle platforms, we concentrated the catalytic tests on the complexes using ligands $\mathbf{L^1}$ and $\mathbf{L^2}$. Indeed, those ligands could give the possibility to evaluate the influence of the fluoroalcohol functions *vs* methyl ones on the complexes for (ep)oxidation reactions. Thus, activities of [($\mathbf{L^2}$)$FeCl_2$]($FeCl_4$), ($\mathbf{L^2}$)$MnCl_2$, [($\mathbf{L^1}$)$FeCl_2$]($FeCl_4$) and ($\mathbf{L^1}$)$MnCl_2$ were compared ($\mathbf{L^1}$ with methyl groups, $\mathbf{L^2}$ with fluoroalcohol groups).

The substrate chosen was cyclooctene (CO), a simple model due to the few expected oxidation products. As previously reported in the literature for the oxidation of alkenes, with H_2O_2 as oxidant, acetic acid was used as additive to favor the heterolytic cleavage of the O-O bond during the catalytic cycle and to avoid the formation of *cis*-diol products.[2]

Based on the developed approach, it is expected that acetic acid would be necessary with metal complexes derived from ligand $\mathbf{L^1}$ to access the epoxide selectively. However, for metal complexes derived from $\mathbf{L^2}$, the presence of fluoroalcohol functions being introduced to help the heterolytic cleavage of the O-O bond, no acetic acid should be required.

In order to confirm this hypothesis, different combinations have been studied to identify the influence of each parameter.

The conditions of reactions are based on literature, being realized in acetonitrile with 1 mol% catalyst and 1.5 equiv. of oxidant (scheme 11).[26]

In order to study the influence of the temperature, reactions were carried out at two temperatures, 40 °C and 0 °C. Because ($\mathbf{L^1}$)$Mn(OTf)_2$ is known to be very efficient for H_2O_2 disproportionation,[6] and in order to limit this phenomenon, H_2O_2 has been slowly added through a syringe pump. All reactions were followed by GC using acetophenone as internal standard which is stable, soluble only in organic phase during the catalysis and not overlapping with the reactive and products. All reactions were duplicated.

Without catalyst

Catalyst-free reactions were realized, and results summarized in Table 3 (Entries 0-1 to 0-4). No (or low) CO conversion in absence of catalysts, even in presence of acetic acid, demonstrated the necessity of a catalyst.

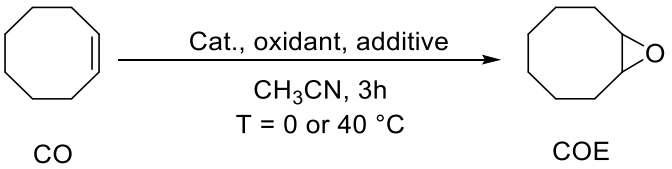

Scheme 11 - catalytic oxidation of cyclooctene.

Table 3- Catalytic oxidation of cyclooctene with/without metal complexes from L^1 and L^2. [a]

Entry	Catalyst	T (°C)	CH_3COOH (equiv.)	oxidant	CO Conv[b]	COE sel[c]
0-1	no	0	0	H_2O_2	0	0
0-2			14		0	0
0-3		40	0		0	0
0-4			14		8	<1
1-1	(L^1)$MnCl_2$	0	0	H_2O_2	2	0
1-2				TBHP	2	10
1-3			14	H_2O_2	0	0
1-4				TBHP	1	0
2-1	(L^2)$MnCl_2$	0	0	H_2O_2	0	0
2-2				TBHP	0	0
2-3		40		H_2O_2	12	0
2-4				TBHP	21	0
3-1	(L^2)Mn_2	0	0	H_2O_2	3	0
3-2			14		39	0
3-3		40	0		11	0
3-4			14		3	3
4-1	[(L^2)$FeCl_2$]($FeCl_4$)	0	0	H_2O_2	6	9
4-2			14		6	4
4-3		40	0		33	13
4-4			14		26	6
5-1	[(L^1)$FeCl_2$]($FeCl_4$)	0	0	H_2O_2	11	2
5-2			14		10	1
5-3		40	0		17	4
5-4			14		19	5

[a] Experimental conditions: t=3h
Cat. /oxidant/CO/CH_3COOH=1/150/100/1400 for the case with CH_3COOH;
Cat. /oxidant/CO=1/150/100/ for the case without CH_3COOH;
[b] n CO converted/n CO engaged (in%) at the end of the reaction.
[c] n COE formed/ n CO converted at the end of the reaction.

2.2.4.1. With manganese complexes

- (L^1)$MnCl_2$ *vs.* (L^2)$MnCl_2$

- At 0°C

Without acetic acid

(L^1)$MnCl_2$ did not display catalytic activity for CO epoxidation using H_2O_2 at 0°C (entries 1-1). Using (L^2)$MnCl_2$ with fluoroalcohol functions, no significant enhancement of the activity was observed (Table 4, entries 2-1 and 2-3).

With acetic acid

The reaction was carried out in presence of 14 equivalents of CH_3COOH (same conditions that some described in the literature).[26] The absence of CO conversion with (L^1)$MnCl_2$ is not

linked to absence/presence of acetic acid. As mentioned previously, ($\mathbf{L^1}$)Mn(OTf)$_2$ being active towards H_2O_2 disproportionation,[6] might explain the absence of CO conversion when ($\mathbf{L^1}$)$MnCl_2$ is used as catalyst even in presence of acetic acid, the disproportionation reaction being faster than CO oxidation.

In order to evaluate the activity of those metal complexes with other peroxides, *tert*-butyl hydroperoxyde (TBHP) was used as oxidant. In the same conditions, no substrate conversion was detected at 0 °C.

- At 40°C

When reaction was carried out at 40 °C, 20% of conversion was observed using ($\mathbf{L^2}$)$MnCl_2$ as catalyst but no selectivity in favor of the epoxide COE was measured and no other products were detected in the conditions used.

- ($\mathbf{L^2}$)Mn_2

Despite the fact that ($\mathbf{L^2}$)Mn_2 was not the expected metal complex, its reactivity toward CO oxidation has been evaluated. In absence of acetic acid, a very low conversion and no selectivity in favor of COE were observed (Table 4, entries 3-1 and 3-3). In presence of acetic acid, at 0 °C, close to 40% of CO conversion were obtained but no COE was detected (Table 4, entry 3-2). The "free" Mn seem to be responsible of the activity.

2.2.4.2. With iron complexes

- [($\mathbf{L^2}$)$FeCl_2$]($FeCl_4$) *vs.* [($\mathbf{L^1}$)$FeCl_2$]($FeCl_4$)

When reaction was realized in presence of [($\mathbf{L^1}$)$FeCl_2$]($FeCl_4$) at 0 °C, a low CO conversion (10%) and a low selectivity in favor of the epoxide COE were observed (Table 4, entry 5-1). The presence of 14 equiv. of acetic acid did not improve the catalytic activity (entry 5-2). When the reaction was carried out at 40 °C, a slight enhancement of the CO conversion was observed but no better selectivity (Table 4, entries 5-3 and 5-4).

Using [($\mathbf{L^2}$)$FeCl_2$]($FeCl_4$) with the fluoroalcohol functions, at 0 °C, no significant difference with [($\mathbf{L^1}$)$FeCl_2$]($FeCl_4$) was observed, in presence or absence of acetic acid (Table 4, entries 4-1 and 4-2). At 40 °C, in comparison to [($\mathbf{L^1}$)$FeCl_2$]($FeCl_4$), a slight enhancement of the catalytic activity was observed, 33% (Table 4, entry 4-3) *vs.* 17% (Table 4, entry 5-3) of conversion. In both cases, the presence of acetic acid did not improve the CO conversion and a very low selectivity towards COE was measured. It has to be noted that a slight effect of the fluoroalcohol functions is observed. However, the conversion and the selectivity are very low and did not compete at all with systems described in the literature for which complete conversion and selectivity close to 100% are observed.[3f]

2.2.4.3. Discussion about catalytic results

Based on X-ray structures, the geometry of the metal complexes seemed initially well suited to favor an interaction between the metal center, H_2O_2 and the fluoroalcohol functions. However, these metal complexes displayed no (or very low) catalytic activity towards CO oxidation. One possibility might be that metal complexes based on pyridinophane ligands are not suited for oxidation reactions. Indeed, the metal complexes without fluoroalcohol (($\mathbf{L^1}$)$MnCl_2$ and [($\mathbf{L^1}$)$FeCl_2$]($FeCl_4$)) did not show catalytic activity for CO oxidation even in presence of acetic acid. However, Che and coll. reported [($\mathbf{L^1}$)$FeCl_2$]($FeCl_4$) as an efficient catalyst for the *cis*-dihydroxylation reaction with oxone® as oxidant.[8b] These results seem to indicate that the access to high valent metal-oxo species able to realize this type of transformation is possible. Another possibility is that the fluoroalcohol functions coordinate on the metal center during the catalytic cycle, leading to a six-coordinated metal center without vacant site necessary to generate the oxidizing metal oxo intermediate, the latter resulting from the activation of H_2O_2. The hypothesis is supported by the formation of metal complex [($\mathbf{L^2}$-2H)Fe](ClO_4) (Figure 6) obtained from reaction between $\mathbf{L^2}$ and $Fe(ClO_4)_3$ in acetonitrile. Isolation of this metal complex was difficult but crystals suitable for X-ray diffraction have been obtained and demonstrated the formation of a stable Fe(III)-metal complex with the deprotonated fluoroalcohol coordinated on the Fe(III) center.

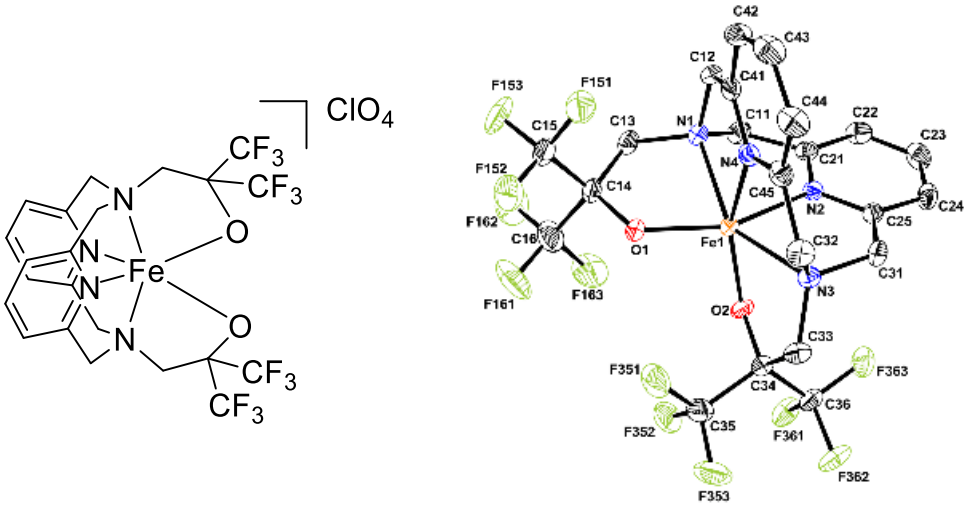

[($\mathbf{L^2}$-2H)Fe](ClO_4)

Figure 6 - Potential Fe(III) metal complex formed during catalytic experiments and molecular views of [($\mathbf{L^2}$-2H)Fe](ClO_4) with the atom labelling scheme. Ellipsoids are drawn at the 50% probability level. H atoms and ClO_4 anion have been omitted for the sake of clarity.

2.2.5. Catalytic hydrogen photoproduction studies with Ni- and Co-metal complexes

As described in the introduction part of this chapter, the pyridinophane family has been used in many types of catalysis, including H^+ photoreduction.[11] With the will to evaluate the influence of the second coordination sphere in catalytic process, this specific activity is very interesting to study.

Indeed, from a "societal" point of view, the development of methods for the storage of renewable energies, their optimization and the efficient conversion of solar energy into fuels is a great challenge.[1b,1c,191,2] One strategy consists on focusing separately on the half reactions of the overall water splitting reaction, *i.e.* water oxidation and proton reduction. For proton reduction, photocatalytic systems are typically based on the association of:

- a photosensitizer, achieving light harvesting and initial charge separation,
- a catalyst with the presence of a sacrificial electron donor.

Concerning the catalyst design, referring to dihydrogenases (H_2ases) - enzymes able to reduce efficiently H^+ into H_2 -the local environment engendered by the second coordination sphere does establish non-covalent interactions, mainly by the presence of a hydrogen-bond network.[27] In the field of molecular catalysis inspired by those systems, one of the best example is the work of DuBois and co-workers who designed Ni-based electrocatalysts for proton reduction possessing amine sites in the second coordination sphere.[1d] This amine group acted as a proton relay, and remarkable rate enhancements for this reaction were achieved. In this context, in order to develop molecular complexes possessing a second coordination sphere able to enhance the reactivity of a targeted catalytic reaction, Co and Ni metal complexes with fluoroalcohol groups on ligands are attractive. Indeed, in addition to their remarkable strength of H-bond donation, fluorinated alcohols are significantly more acidic than nonfluorinated ones (pKa of hexafluoroisopropanol = 9.3).[28] These functional groups are thus interesting candidates to act as proton relay for proton reduction. The catalytic process will thus be examined by comparison between complexes possessing methyl or fluoroalcohol moieties in the ligand.

For this purpose, a collaboration with the Chemistry and Biology of Metals Laboratory (Laboratoire Chimie et Biologie des Métaux, LCBM) in Grenoble has been established. Indeed, this group possesses a recognized expertise notably in the field of dihydrogen (photo)production, more particularly with Ni and Co metal complexes. Metal complexes ($\mathbf{L^1}$)$Ni(NO_3)_2$ and ($\mathbf{L^1}$)$Co(NO_3)_2$, were synthetized and characterized at the LCC and their activity for the photoproduction of H_2 was evaluated at the LCBM by Emmanouil Giannoudis, PhD student working under the supervision of Murielle Chavarot-Kerlidou.

- Electrochemistry

Cyclic voltammograms of all metal complexes were recorded (in CH_3CN using a glassy carbon as working electrode and a saturated calomel as reference electrode and Bu_4NPF_6 as supporting electrolyte) in order to get information about the potential ability of the metal complexes to produce H_2 under photochemical conditions. A summary of the potentials is presented in Table 5 and voltammograms in Figure 7.

Table 5 - Electrochemical properties of metal complexes (L^1)$Ni(NO_3)_2$, (L^2)$Ni(NO_3)_2$, (L^1)$Co(NO_3)_2$ and (L^2)$Co(NO_3)_2$. Glassy carbon and SCE were the working and reference electrodes, scan rate=100 $mV.s^{-1}$. Potentials are quoted versus SCE. R = Reversible, Q = Quasi-reversible, I = Irreversible.

Metal Complex	Ligand reduction or M^I/M^0	M^{II}/M^I	NO_3^- loss	M^{II}/M^{III}
(L^1)$Ni(NO_3)_2$	-2.04 (R)	-1.69 (I)	-1.50 (I)	
(L^2)$Ni(NO_3)_2$	-2.39 (I)	-1.77 (I)	-1.57 (I)	
(L^1)$Co(NO_3)_2$	-1.95 (Q)	-1.68 (I)	-1.25 (I)	
(L^2)$Co(NO_3)_2$	-2.28 (R)	-1.63 (I)	-1.39 (I)	+0.36 (Q)

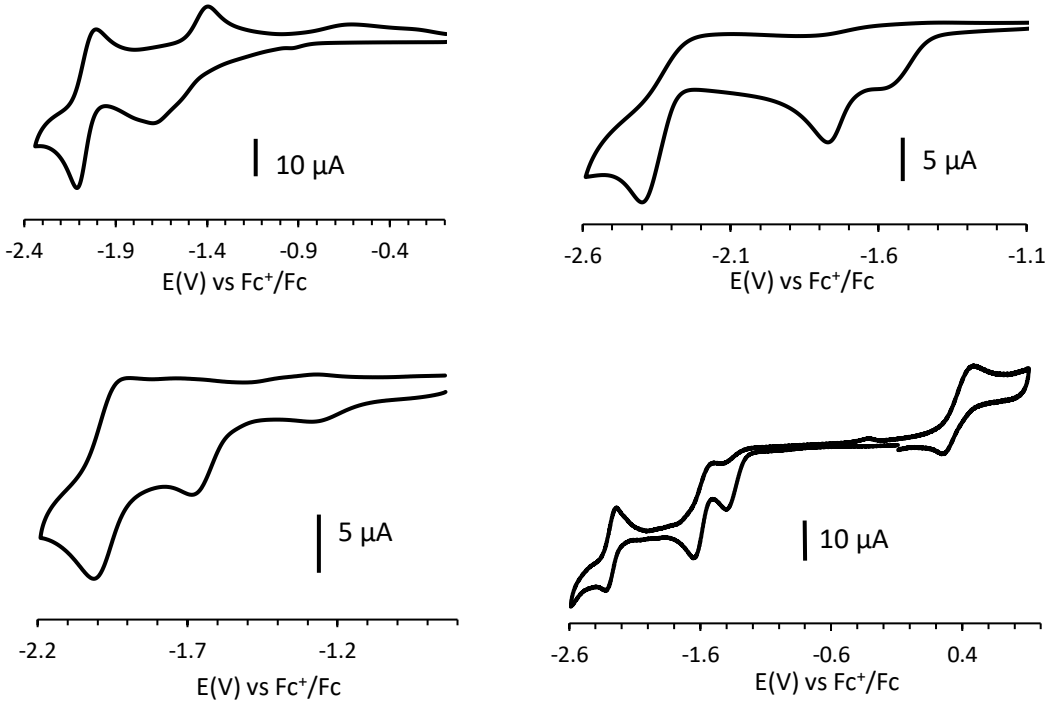

Figure 7 - Cyclic voltammograms of (L^1)$Ni(NO_3)_2$ (top left), (L^2)$Ni(NO_3)_2$ (top right), (L^1)$Co(NO_3)_2$ (bottom left) and (L^2)$Co(NO_3)_2$ (bottom right). Experimental conditions: Bu_4NPF_6 (0.1M) as supporting electrolyte in CH_3CN, using a glassy carbon as working and SCE as reference electrodes. Scan rate of 100 $mV.s^{-1}$.

Based on X-ray structures, nitrate anions are coordinated to metal center in all structures in solid state. For all metal complexes, an irreversible reduction is observed between -1.25 and -1.6 V *vs.* Fc^+/Fc might be attributed to the reduction of the metal center with a nitrate anion coordinated to the metal center. After nitrate decoordination, an irreversible reduction (-1.63 to -1.77 V *vs.* Fc^+/Fc) attributed to the M^{II}/M^I cationic couple is observed. Reduction of the ligand or of the M^I metal center is observed between -1.95 and -2.40 V *vs.* Fc^+/Fc. Influence of the fluoroalcohol function on the cathodic potential is not obvious and no trend can be defined. (L^1)$Ni(NO_3)_2$ and (L^1)$Co(NO_3)_2$ with Me groups exhibit similar reduction potentials for M^{II}/M^I couple (-1.68 and -1.69 V *vs.* Fc^+/Fc respectively). Similar behavior for Ni^{II} and Co^{II} metal complexes has been observed for pentadentate nitrogen-based ligands.[29]

The metal complexes in this study present lower reduction potentials M^{II}/M^I than similar ones described by Mirica et al. i.e. metal complexes based on a similar pyridinophane platform

(^{t}Bu groups on the amine instead of Me and fluoroalcool groups in this work).[30] The values for those complexes are in the range of the ones described for metal complexes based on pentadentate nitrogen based ligands reported as efficient for H_2 photoproduction.[29]

- Photocatalytic H_2 production

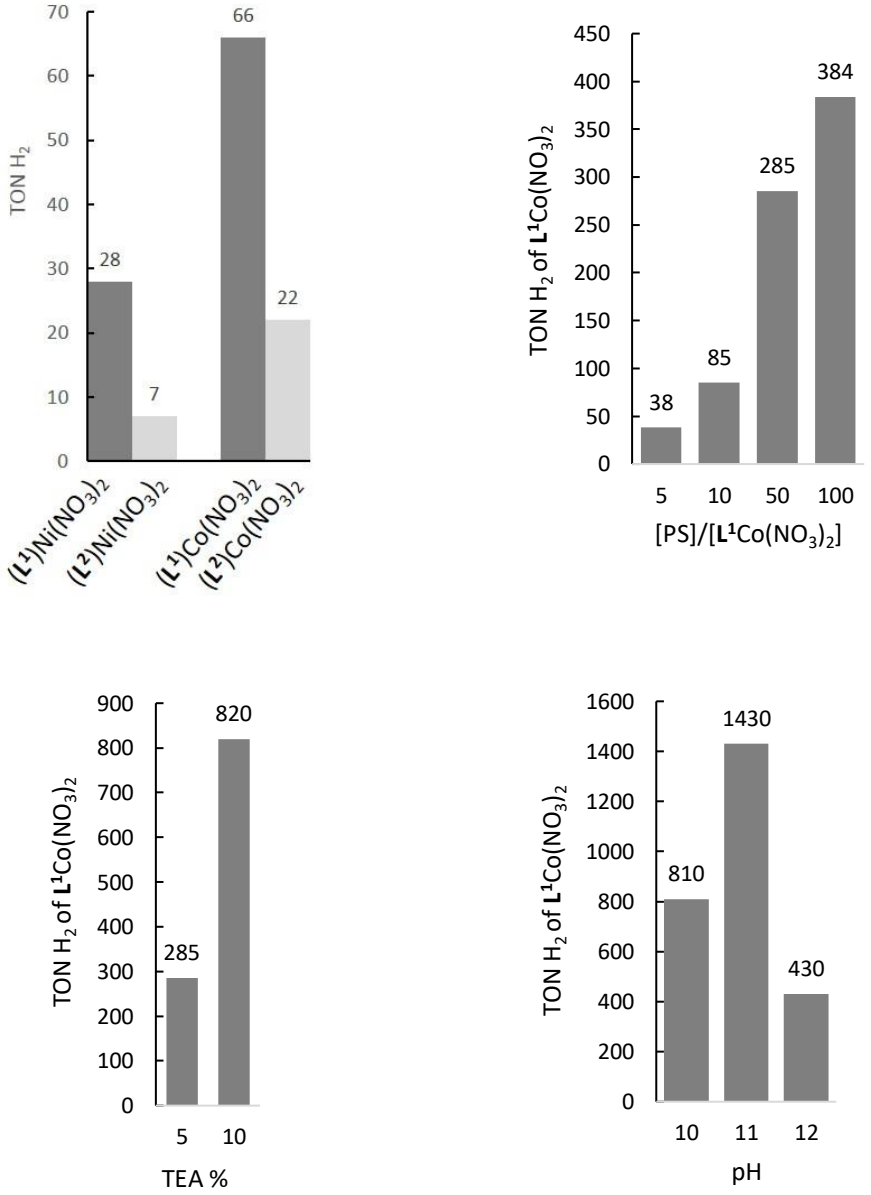

Figure 8 - Top left: Photocatalytic H_2 formation by (**L¹**)Ni$(NO_3)_2$, (**L²**)Ni$(NO_3)_2$, (**L¹**)Co$(NO_3)_2$, (**L²**)Co$(NO_3)_2$. Conditions: H_2O/CH_3CN 1:1, [cat] = 50 µM, [PS] = 500 µM, pH = 10, TEA, 5%. Top right: Effect of [PS]/[(**L¹**)Co$(NO_3)_2$] ratios on photocatalytic H_2 formation. Conditions: H_2O/CH_3CN 1:1, [(**L¹**)Co$(NO_3)_2$] = 10 µM, pH = 10, TEA 5%. Bottom left: Effect of electron donor concentration on photocatalytic H_2 formation by (**L¹**)Co$(NO_3)_2$. Conditions: H_2O/CH_3CN 1:1, [(**L¹**)Co$(NO_3)_2$] = 10 µM, [PS]/[(**L¹**)Co$(NO_3)_2$] = 50, pH = 10. Bottom right: Effect of pH on photocatalytic H_2 formation by (**L¹**)Co$(NO_3)_2$. Conditions: H_2O/CH_3CN 1:1, [(**L¹**)Co$(NO_3)_2$] = 10 µM, [PS]/[(**L¹**)Co$(NO_3)_2$] = 50, TEA 10%. PS = Photosensitizer, TON H_2 = n_{H_2}/n_{cat}.

Photocatalytic hydrogen production was examined for metal complexes. Based on literature,[29] $[Ir(ppy)_2(bpy)](PF_6)$, with a higher reduction potential (-1.95 V *vs.* Fc^+/Fc) than the reduction potential of M^{II}/M^{I} metal complexes was chosen as photosensitizer. Triethylamine was selected as sacrificial donor and a mixture of H_2O-CH_3CN as reactional mixture. Under conditions detailed in Figure 8 (top left), after irradiation with a 150 W Xenon lamp, Co-based complexes displayed a higher efficiency toward H_2 photoproduction. A maximum of 66 TON were obtained with $(\mathbf{L^1})Co(NO_3)_2$ bearing no fluoroalcohol functions. In comparison, under the same conditions, Ni-based complex $(\mathbf{L^1})Ni(NO_3)_2$ displayed only 28 TON. Based on these results, optimized conditions have been explored using the most promising system $(\mathbf{L^1})Co(NO_3)_2$.

Increasing the photosensitizer/catalyst ratio has a positive effect on the H_2 production. However, a PS/cat ratio higher than 50 did not lead to a dramatic TON increase (Figure 8, top right). Indeed, whereas a TON value of 285 was obtained with a 5-fold excess of PS towards the catalyst, only 384 TON were reached by doubling this ratio. This might indicate that the reduction of the Co center is controlling the H_2 production rate. The effect of the electron donor, *i.e.* triethylamine, was examined (Figure 8, bottom left). Doubling the concentration of triethylamine led to a 3-fold increase of TON toward H_2 production (820 *vs.* 285 TON).

In a next step, the effect of the pH during the experiments was outlined (Figure 8, bottom right). Indeed, while an increase of the pH from 10 to 12 resulted in a decrease of H_2 production from a factor 2, an increase of only 1 unit of the pH (11 *vs.* 10) double the TON for H_2 production. In these optimized conditions, 1430 TON were achieved whereas in the initial conditions, only 66 TON were observed.

Under these conditions, the $(\mathbf{L^1})Co(NO_3)_2$ with Me substituents is the most efficient and twice more TON are obtained with this complex in comparison to the one obtained with $(\mathbf{L^2})Co(NO_3)_2$ possessing fluoroalcohol substituents (Figure 9).

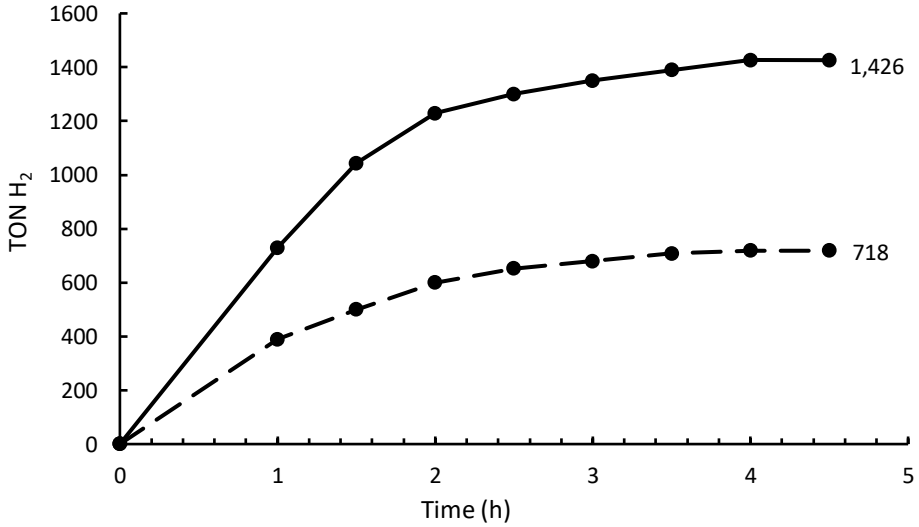

Figure 9 - TON comparison between $(\mathbf{L^1})Co(NO_3)_2$ (solid line) and $\mathbf{L^2}Co(NO_3)_2$ (dashed line). Conditions: H_2O/CH_3CN 1:1, [**cat**] = 10 µM, [PS]/[**cat**] = 50, TEA 10%. PS = Photosensitizer, TON $H_2 = n_{H_2}/n_{cat}$.

Moreover, in order to determine if the formation of hydrogen was due to the catalytic activity of molecular complexes or nanoparticles formed from these molecular complexes,

mercury was added into the solution. Nanoparticles with mercury form amalgams, inefficient for H_2 production. If the starting metal complexes are still present under their molecular form, there are no alloys and similar catalytic activity is observed. In this study, addition of mercury did not influence the reactivity of ($\mathbf{L^1}$)$Co(NO_3)_2$ and similar TON are obtained. These results seem to demonstrate a molecular pathway to produce H_2, excluding the formation of nanoparticles, or at least not a high conversion of the molecular catalyst into nanoparticles. This is also supported by the absence of induction period before H_2 production.

These results demonstrate that pyridinophane ligands are suitable for H_2 photoproduction and Co^{II} metal complexes with Me groups exhibit high TON. Higher activity for Co^{II} complexes in comparison to Ni^{II} complexes has already been described in the literature.[29] Both metal complexes having similar reduction potentials, other considerations that redox potentials have to be considered. Under photochemical conditions, in presence of Et_3N, reduction of M^{II} into a M^{I} species then subsequent protonation of these species generate a M^{III}-species that will produce H_2 after a step of protonation. It is highly possible that under these conditions, Ni and Co metal complexes do not exhibit the same reactivity. More particularly, the formation of the M^{III}-H intermediate has to be realized under basic conditions that might be unfavorable.

Concerning the functionalization of the amine functions, metal complexes with Me functionalization are much more efficient than their homolog with fluoroalcohol functions. A positive effect of the fluoroalcohol functions was hoped, notably with a role of proton relay as it has been previously reported for metal complexes possessing pendant amine groups.

However, with ($\mathbf{L^2}$)$Ni(NO_3)_2$ and ($\mathbf{L^2}$)$Co(NO_3)_2$, a deprotonation of the fluoroalcohol groups then subsequent coordination on the metal center is highly possible, precluding its further reactivity. In the context of H_2 photoproduction, complex ($\mathbf{L^1}$)$Co(NO_3)_2$ based on Co^{II} metal center has proven very efficient in the tested conditions with up to 1400 TON obtained. However, the addition of fluoroalcohol groups acting as H-donor groups in the second coordination sphere did not lead to an enhancement of the catalytic activity as expected.

2.3. Conclusion

The introduction of fluoroalcohol groups on the pyridinophane and BPMEN ligands has been successfully realized. However, using the same synthetic strategy, functionalization of the pentaazamacrocycle ligand failed and simple reasons cannot explain this difference of reactivity between the different families of ligands.

Concerning the access to metal complexes, no metal complexes based on the BPMEN ligand with the fluoroalcohol groups have been isolated (probably due to the formation of polymeric structures) but first-row metal complexes based on the pyridinophane ligand were easily accessible.

($\mathbf{L^2}$)$MnCl_2$ and [($\mathbf{L^2}$)$FeCl_2$]($FeCl_4$), possessing fluoroalcohol groups, display a weak activity towards CO oxidation even in presence of acetic acid. The homologs with methyl groups (($\mathbf{L^1}$)$MnCl_2$ and [($\mathbf{L^2}$)$FeCl_2$]($FeCl_4$)) are also inactive for CO oxidation. It seems that peroxides are not powerful enough oxidants to generate a metal-oxo compound to realize an OAT reaction with this family of metal complexes.

($\mathbf{L^1}$)$Co(NO_3)_2$ with methyl groups display an interesting activity for hydrogen photoproduction using trimethylamine as sacrificial reductant and $[Ir(ppy)_2(bpy)](PF_6)$ as photosensitizer and up to 1400 TON were reached. However, no positive effect of the fluoroalcohol groups has been observed.

Based on the different X-ray structures obtained, it seems highly probable that during catalytic processes explored (oxidation reaction or H_2 photoreduction), a deprotonation of the fluoroalcohol functions followed by a coordination on the metal center occurred and thus inhibit the reactivity of the metal centers.

Motivated by literature reports that have demonstrated that fluoroalcohol solvents allow the selective oxidation of alkanes into alcohols, efforts need to be pursued to access to metal complexes possessing fluoroalcohol groups. In the future, one possibility might be to introduce these groups such as they cannot coordinate on the metal center.

2.4. Experimental part

2.4.1. Materials

All manipulations were carried out under air. Distilled water was used directly from a Milli-Q purification system (Millipore). Acetonitrile, ethanol, chloroform, dichloromethane, diethyl ether, DMF (synthesis grade, Aldrich) were used as solvents and employed as received. Thionyl chloride (99%, Merck), 2,6-pyridinedimethanol (98%, Apollo Scientific), Sulfuric acid (95%-98%, Aldrich), Sodium Hydroxide (98%, Aldrich), formic acid (95%-97%, Aldrich), formaldehyde (37 wt.% in H_2O, Aldrich), 2,2-bis(trifluoromethyl)oxirane (97%, Apollo Scientific), picolinaldehyde (99%, Aldrich), ethylenediamine (99.5%, Aldrich), Sodium borohydride (98%, Aldrich), $MnCl_2{\cdot}4H_2O$ (98%, Strem chemicals), $Zn(OTf)_2$ (98%, Strem Chemicals) Manganese triflate (95%, Aldrich), Iron(III) chloride hexahydrate (97%, Aldrich), $Co(NO_3)_2{,}6H_2O$ (99%, Strem Chemicals), $Ni(NO_3)_2{,}6H_2O$ (99.9%, Strem Chemicals), silver chloride (99%, Aldrich), *cis*-cyclooctene (95%, Alfa Aesar), cyclooctene oxide (99%, Aldrich), and TBHP (70% in water, Aldrich) were used as received.

2.4.2. Methods

NMR Spectroscopy: The ^{1}H and $^{13}C\{^{1}H\}$ NMR spectra were recorded with a Bruker NMR III HD 400 MHz spectrometer. The $^{19}F\{^{1}H\}$ NMR spectra were recorded with a Bruker Avance 400 FT-NMR spectrometer. The resonances were calibrated relative to the residual solvent peaks and are reported with positive values downfield from TMS.

Elemental analysis: Elemental analyses (EA) were performed by the LCC microanalysis service

UV-Visible analysis: UV-Visible spectra were recorded on a CARY60 spectrometer from Agilent.

Gaz Chromatographic: The catalytic reactions were followed by gas chromatography on an Agilent 7820A chromatograph equipped with an FID detector, a DB-WAX capillary column (30m × 0.32mm × 0.5µm) and autosampler. Authentic samples of reactants (cyclooctene) and some potential products (cyclooctene oxide, *cis*-1.2-cyclohexanediol) were used for calibration. The CO conversion and the COE formation were calculated from the calibration curves ($r^2 = 1$) and an internal standard.

2.4.3. Synthesis

- Synthesis of sodium tosylamine (TsNHNa) [19]

To a stirred, refluxing solution of freshly prepared NaOEt (23.8 g, 0.35 mol) in absolute ethanol (400 mL) was added solid 1 *p*-toluenesulfonamide (60 g, 0.35 mol). The mixture was refluxed for 2 h and then cooled. The white precipitate was collected by filtration, washed with absolute EtOH, and dried in vacuo to give sodium tosylamide (TsNHNa) in 90% yield.

- Synthesis of 2,6-bis(chloromethyl)pyridine (**2**)[31]

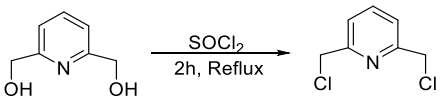

2,6-pyridinedimethanol (**1**) (12 g, 86.2 mmol) was dissolved in thionyl chloride ($SOCl_2$) (100 mL, 1.38 mol) at 0°C. The solution was left under stirring for 1 hour at room temperature then stirred under reflux for 2 hours. 100 mL of H_2O were slowly added into the mixture leading to the appearance of a pale-yellow precipitate. After filtration of the precipitate, a saturated solution of Na_2CO_3 was slowly added into the dark filtrate solution until the pH of the solution reached pH=12 and the formation of a white precipitate. After filtration, **2** (10.8 g, 90% yield) was isolated as a white solid.

^{1}H NMR (400 MHz, $CDCl_3$) δ 7.79 (t, *J* = 7.8 Hz, 1H, Ar- H), 7.47 (d, *J* = 7.7 Hz, 2H, Ar- H), 4.69 (s, 4H, CH_2).

- Synthesis of 3,7-ditosyl-3,7-diaza-1,5(2,6)-dipyridinacyclooctaphane (**3**)[19]

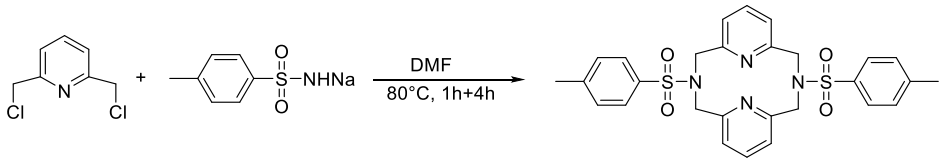

To 2.41 g (12.5 mmol) of sodium tosylamide in suspension in 200 mL of DMF at 80°C, 2.2 g (12.5 mmol) of 2,6-bis(chloromethyl)pyridine (**2**) dissolved in 25 mL of DMF were added dropwise over 5 minutes. After stirring at 80 °C for 1 h, 2.41 g (12.5 mmol) of sodium tosylamide solid were added into the mixture. After stirring at 80 °C 4 h, the solvent was removed by rotary evaporator and the resulting off-white solid was washed by water, absolute ethanol then acetone. The crude product was purified by Soxhlet extractor with acetone for 3 days. After evaporation of the acetone, **3** (2.47g, 36% yield) was isolated as a white solid.

^{1}H NMR (400 MHz, DMSO-d_6) δ 7.94 (d, *J* = 8.3 Hz, 4H, Ar-H), 7.54 (d, *J* = 7.8 Hz, 4H, Ar-H), 7.50 (t, *J* = 7.7 Hz, 2H, Ar-H), 7.05 (d, *J* = 7.7 Hz, 4H, Ar-H), 4.45 (s, 8H, CH_2), 2.49 (s, 6H, CH_3).

- Synthesis of 2,11-Diaza[3,3](2,6)pyridinophane (**4**)[19]

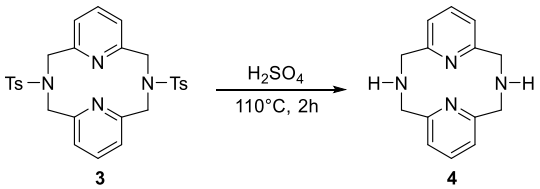

A solution of 2.4 g (10 mmol) of **3** dissolved in 50 mL of H_2SO_4 (98 wt.%) was stirred under reflux for 2 hours. The solution was diluted with 50 mL of H_2O at 0°C and NaOH was added into the mixture until a white precipitate appeared (pH≈12). After extraction with $CHCl_3$ (3x50 mL), drying of the organic phase over Na_2SO_4 and evaporation under vacuum, **4** (1.56 g, 65% yield) was obtained as a white solid.

^{1}H NMR (400 MHz, $CDCl_3$) δ 7.11 (t, *J* = 7.6 Hz, 2H, Ar-H), 6.55 (d, *J* = 7.6 Hz, 4H, Ar-H), 4.02 (s, 8H, CH_2).

- Synthesis of N,N'-Dimethyl-2,11-diaza[3,3](2,6)pyridinophane **L¹** [19]

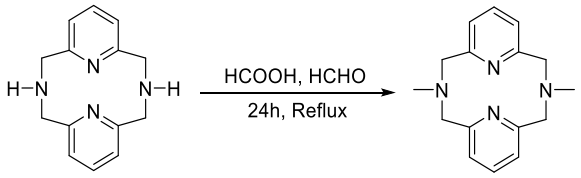

4 **L¹**

0.25 g (1.0 mmol) of 2,11-Diaza[3,3](2,6)pyridinophane (**4**) was mixed with 4.4 g (54.3 mmol) of 37% formaldehyde and 3.1 g (67.3 mmol) of formic acid. The resulting mixture was stirred under reflux for 24 h and after cooling to room temperature, the solution was basified with NaOH until a white precipitate appeared (pH≈12). After extraction with CH_2Cl_2 (3x50 mL), drying of the organic phase over Na_2SO_4 and evaporation under vacuum, **L¹** (0.18 g, 68% yield) was obtained as a white solid.

^{1}H NMR (400 MHz, DMSO-d_6) δ 7.17 (t, *J* = 7.6 Hz, 2H, Ar-H), 6.74 (d, *J* = 7.6 Hz, 4H, Ar-H), 3.70 (s, 8H, CH_2), 2.62 (s, 6H, CH_3).

^{13}C{^{1}H} NMR (101 MHz, DMSO-d_6) δ 157.35 (C_q-Py), 135.54(CH-Pr), 122.53, 65.63, 48.74.

- Synthesis of **L²** [15]

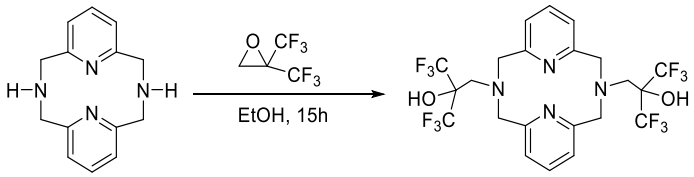

4 **L²**

To 0.239 g (0.995 mmol) of 2,11-diaza[3.3](2,6)pyridinophane (**4**) in 10 mL of ethanol at 0°C, 537 mg (2.98 mmol) of 2,2-bis(trifluoromethyl)oxirane were added and a white precipitate appeared immediately. After stirring at 25 °C for 15 h, the solution was evaporated under reduce pressure. A light yellow powder was collected and was recrystallized by slow diffusion of diethyl ether into a solution of **L²** in acetonitrile. After filtration, **L²** (0.43 g, 72% yield) was obtained as a white powder.

^{1}H NMR (400 MHz, THF- d_8) δ 7.90 (s, 2H, OH), 7.17 (t, *J* = 8Hz, 2H, Ar-H), 6.67 (d, *J* = 8Hz, 4H, Ar-H), 4.11 (s, 8H, CH_2), 3.76 (s, 4H, CH_2).

^{13}C{^{1}H} NMR (101 MHz, THF-d_8) δ 158.6 (CH-Py), 137.0 (CH-Py), 123.6 (CF_3), 122.0 (CH-Py), 75.3(C_q-OH), 64.2 (CH_2 ring), 57.2 (**CH_2**-C_q-OH).

- Synthesis of ($\mathbf{L^1}$)$Ni(NO_3)_2$

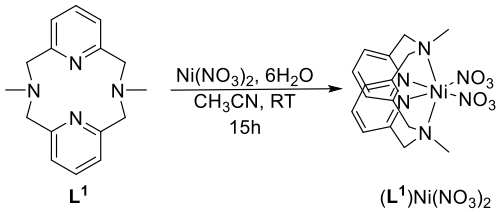

After dissolution of $\mathbf{L^1}$ (100 mg, 0.373 mmol) in acetonitrile (5 mL), $Ni(NO_3)_2$,$6H_2O$ (163 mg, 0.559 mmol) was added and the resulting blue solution was stirred at 25 °C for 15 h. After evaporation under reduced pressure, the complex was dissolved in a minimum of acetonitrile, precipitated in diethyl ether and isolated as a blue solid after filtration. Crystals of ($\mathbf{L^1}$)$Ni(NO_3)_2$ (133 mg, 79%) were obtained by slow diffusion of diethyl ether into a solution of ($\mathbf{L^1}$)$Ni(NO_3)_2$ in acetonitrile.

Anal. Calcd for ($\mathbf{L^1}$)$Ni(NO_3)_2 \cdot 1.5H_2O$, $C_{16}H_{23}NiN_6O_{7.5}$: C, 40.20; H, 4.85; N,17.58. Found: C, 40.22; H, 4.58; N, 17.65.

- Synthesis of ($\mathbf{L^1}$)$Co(NO_3)_2$

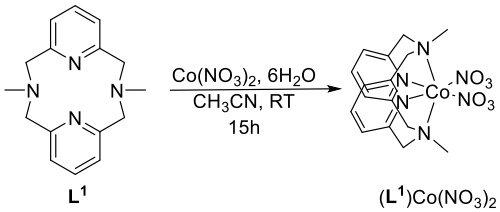

After dissolution of $\mathbf{L^1}$ (100 mg, 0.373 mmol) in acetonitrile (5 mL), $Co(NO_3)_2$,$6H_2O$ (130 mg, 0.447 mmol) was added and the resulting pink/purple solution was stirred at 25 °C for 15 h. After evaporation under reduced pressure, the complex was dissolved in a minimum of acetonitrile, precipitated in diethyl ether and isolated as a purple solid after filtration. Crystals of ($\mathbf{L^1}$)$Co(NO_3)_2$ (120 mg, 70%) were obtained by slow diffusion of diethyl ether into a solution of ($\mathbf{L^1}$)$Co(NO_3)_2$ in 1:1 acetonitrile: ethanol mixture.

Anal. Calcd for ($\mathbf{L^1}$)$Co(NO_3)_2$, $C_{16}H_{20}CoN_6O_6$: C, 42.58; H, 4.47; N,18.62. Found: C, 42.80; H, 4.19; N, 18.93.

- Synthesis of ($\mathbf{L^1}$)$MnCl_2$

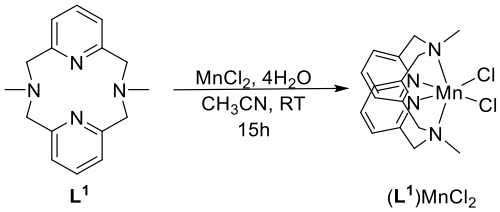

After dissolution of $\mathbf{L^1}$ (100 mg, 0.373 mmol) in CH_3CN (5 mL), $MnCl_2$,$4H_2O$ (88 mg, 0.447 mmol) was added and the resulting white solution was stirred at 25 °C for 15 h. After evaporation under reduced pressure, the complex was dissolved in a minimum of CH_3CN, precipitated in Et_2O and isolated as a white solid after filtration. Crystals of ($\mathbf{L^1}$)$MnCl_2$ (106 mg, 72%) were obtained by slow diffusion of Et_2O into a solution of ($\mathbf{L^1}$)$MnCl_2$ in CH_3CN.

- Synthesis of ($\mathbf{L^1}$)Mn(OTf)$_2$

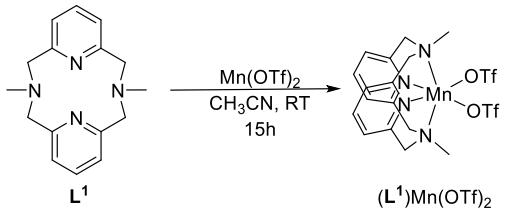

$\mathbf{L^1}$ ($\mathbf{L^1}$)Mn(OTf)$_2$

After dissolution of $\mathbf{L^1}$ (100 mg, 0.373 mmol) in CH_3CN (5 mL), Mn(OTf)$_2$ (158 mg, 0.447 mmol) was added and the resulting white solution was stirred at 25 °C for 15 h. After evaporation under reduced pressure, the complex was dissolved in a minimum of CH_3CN, precipitated in Et_2O and isolated as a white solid after filtration. Crystals of ($\mathbf{L^1}$)Mn(OTf)$_2$ (93 mg, 71%) were obtained by slow diffusion of Et_2O into a solution of ($\mathbf{L^1}$)Mn(OTf)$_2$ in CH_3CN.

Anal. Calcd for ($\mathbf{L^1}$)Mn(OTf)$_2$, $C_{18}H_{20}F_6MnN_4O_6S_2$: C, 34.79; H, 3.24; N, 9.02. Found: C, 34.57; H, 2.83; N, 8.90.

- Synthesis of [($\mathbf{L^1}$)FeCl$_2$](FeCl$_4$)

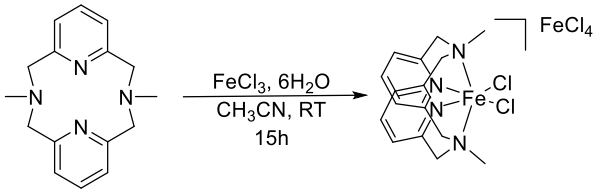

$\mathbf{L^1}$ [($\mathbf{L^1}$)FeCl$_2$](FeCl$_4$)

After dissolution of $\mathbf{L^1}$ (100 mg, 0.373 mmol) in CH_3CN (5 mL), $FeCl_3$,$6H_2O$ (541 mg, 0.894 mmol) was added and the resulting red solution was stirred at 25 °C for 15 h. After evaporation under reduced pressure, the complex was dissolved in a minimum of CH_3CN, precipitated in Et_2O and isolated as a orange solid after filtration. Crystals of [($\mathbf{L^1}$)FeCl$_2$](FeCl$_4$) (154 mg, 67%) were obtained by slow diffusion of Et_2O into a solution of [($\mathbf{L^1}$)FeCl$_2$](FeCl$_4$) in CH_3CN.

- Synthesis of **5** [20]

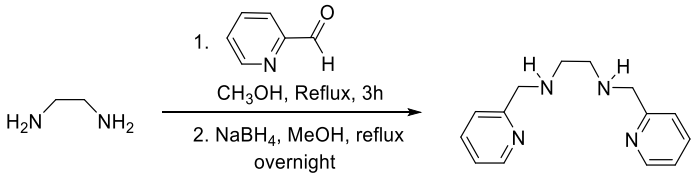

5

A solution of 2-pyridinecarboxaldehyde (1.18 g, 1 mmol) in methanol (8 mL) was added into a solution of ethylenediamine (0.32 g, 5.32 mmol) in methanol (8 mL) and the solution was stirred under reflux for 3 hours. $NaBH_4$ (0.5 g 0.91 mmol) was slowly added and the mixture was stirred under reflux overnight. After removal of the solvent under vacuum, the crude product was dissolved in 30 mL of H_2O and **5** was extracted by $CHCl_3$ (4x50 mL). After drying of the organic phase over Na_2SO_4, **5** (1.19 g, 92% yield) was obtained as an orange oil.

^{1}H NMR (400 MHz, $CDCl_3$) δ 8.53 (d, *J* = 4.9 Hz, 2H, Ar-H), 7.63 (td, *J* = 7.6, 1.8 Hz, 2H, Ar-H), 7.31 (d, *J* = 7.8 Hz, 2H, Ar-H), 7.14 (m, 2H, Ar-H), 3.91 (s, 4H, CH_2), 2.82 (s, 4H, CH_2).

- Synthesis of **L³** (BPMEN) [20]

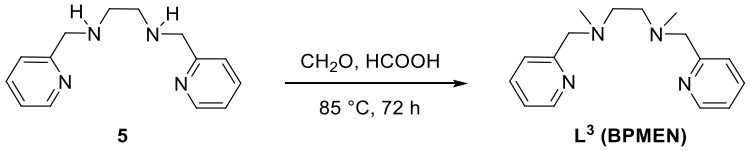

5 **L³ (BPMEN)**

N,N'-bis(pyridin-2-ylmethyl)ethylenediamine (**5**) (2 g, 8.25 mmol) was added into a solution containing 1 mL of water, formic acid (4.5 mL, 119 mmol) and formaldehyde 37 wt.% in solution (4.5 mL, 120 mmol). The mixture was heated at 85°C under stirring for 72h. A concentrated solution of NaOH was added into the mixture until the solution reached pH≈12. After extraction by $CHCl_3$ (3x50 mL), drying of the organic phase over Na_2SO_4 and removal of the solvent under reduced pressure, **L³** (1.83 g, 82% yield) was obtained as an orange oil.

^{1}H NMR (400 MHz, DMSO-d_6) δ 8.46 (d, *J* = 4.6Hz, 2H, Ar-H), 7.72 (td, *J* = 7.6, 1.8 Hz, 2H, Ar-H), 7.40 (d, *J* = 7.8, 2H, Ar-H), 7.22 (m, 2H, Ar-H), 3.60 (s, 4H, CH_2), 2.53 (s, 4H, CH_2), 2.16 (s, 6H, CH_3).

^{13}C{1H} NMR (101 MHz, DMSO-d_6) δ 159.74 (C_q-Py), 149.09 (C_H-Py), 136.81 (C_H-Py), 123.04 (CH-Py), 122.45 (CH-Py), 63.96 (**C**H_2-CH_2), 55.40 (**C**H_2-C_q), 42.96 (CH_3).

- Synthesis of **L²**

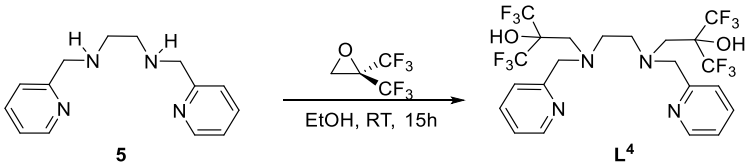

5 **L⁴**

To a solution of N,N'-bis(pyridin-2-ylmethyl)ethylenediamine (**5**) (0.24 g, 1 mmol) in ethanol absolute (10 mL) at 0°C, 2,2-bis(trifluoromethyl)oxirane (0.54 g, 3 mmol) was added and the mixture was stirred overnight at room temperature. After removal of the solvent reduced pressure, the pale-yellow powder obtained was recrystallized by diffusion of diethyl ether into a solution of **L⁴** in acetonitrile. **L⁴** (0.45 g, 75% yield was obtained as a white solid.

^{1}H NMR (400 MHz, DMSO-d_6) δ 9.16 (s, 2H, OH), 8.50 (d, 2H, *J* = 4.8 Hz, Ar-H), 7.79 (t, 2H, *J* = 7.7 Hz, Ar-H), 7.32 (t, 2H, *J* = 7.5 Hz, Ar-H), 7.27 (d, 2H, *J* = 7.7 Hz, Ar-H), 3.89 (s, 4H, CH_2), 3.25 (s, 4H, CH_2), 2.67 (s, 4H, CH_2).

^{13}C{^{1}H} NMR (101 MHz, DMSO-d_6) δ 158.90 (C_q- Ar), 148.71 (CH- Ar), 137.81 (CH- Ar), 123.29 (CH- Ar), 123.13 (C_H- Ar), 60.46 (CH_2 - N), 55.25 (**C**H_2 - C_q- CF_3), 52.94 (**C**H_2- CH_2- N).

- Synthesis of [(**L²**)$FeCl_2$]($FeCl_4$)[15]

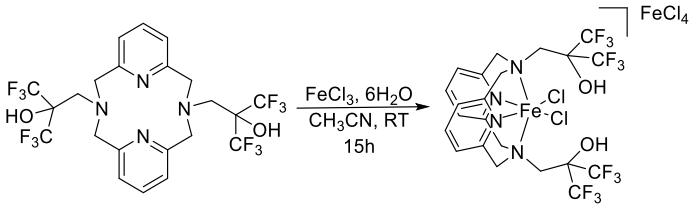

L² [(**L²**)$FeCl_2$]($FeCl_4$)

After dissolution of **L²** (100 mg, 0.167 mmol) in boiling acetonitrile (5 mL), $FeCl_3$,$6H_2O$ (135 mg, 0.500 mmol) was added and the resulting orange solution was stirred at 25 °C for 15 h. After evaporation under reduced pressure, the product was dissolved in 0.5 mL of acetonitrile and precipitated in 5 mL of diethyl ether. After filtration, [(**L²**)$FeCl_2$]($FeCl_4$) (139 mg, 90%) was obtained as a yellow solid. Crystals of [(**L²**)$FeCl_2$]($FeCl_4$) suitable for X-ray diffraction analysis were obtained by slow diffusion of diethyl ether into a solution of [(**L²**)$FeCl_2$]($FeCl_4$) in acetonitrile.

Anal. Calcd for $C_{22}H_{20}Cl_6F_{12}Fe_2N_4O_2$: C, 28.57; H, 2.18; N, 6.06. Found: C, 28.59; H, 2.09; N, 5.81.

- Synthesis of (**L²**)$MnCl_2$ [15]

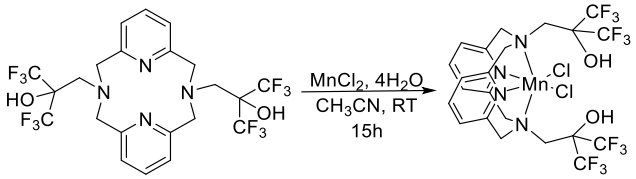

L² (**L²**)$MnCl_2$

After dissolution of **L²** (100 mg, 0.167 mmol) in boiling acetonitrile (5 mL), $MnCl_2$,$4H_2O$ (33 mg, 0.167 mmol) was added and the resulting solution was stirred at 25 °C for 15 h. After evaporation under reduced pressure, the solid was dissolved in 0.5 mL of acetonitrile and precipitated in 5 mL of diethyl ether. After filtration, (**L²**)$MnCl_2$ (115 mg, 95%) was obtained as a very pale yellow solid. Crystals of (**L²**)$MnCl_2$ suitable for X-ray diffraction were obtained by slow diffusion of diethyl ether into a solution of (**L²**)$MnCl_2$ in acetonitrile.

Anal. Calcd for **2**.$2H_2O$, $C_{22}H_{24}Cl_2F_{12}MnN_4O_4$: C, 34.66; H, 3.17; N,7.35. Found: C, 34.53; H, 2.98; N, 7.28.

- Synthesis of (**L²**)Mn_2

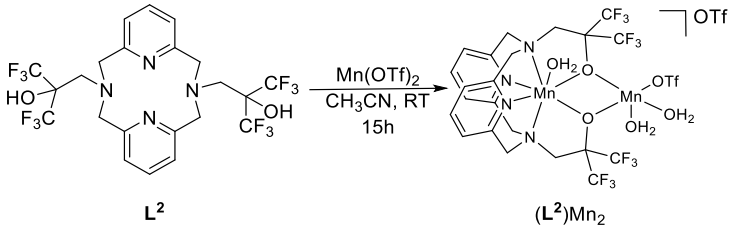

L² (**L²**)Mn_2

After dissolution of **L²** (100 mg, 0.167 mmol) in boiling acetonitrile (5 mL), $Mn(OTf)_2$ (59 mg, 0.167 mmol) was added and the resulting solution was stirred at 25 °C for 15 h. After evaporation under reduced pressure, the solid was dissolved in 0.5 mL of acetonitrile and precipitated in 5 mL of diethyl ether. After filtration, (**L²**)Mn_2 (74 mg, 80%) was obtained as a

very pale yellow solid. Crystals of ($\mathbf{L^2}$)Mn_2 suitable for X-ray diffraction were obtained by slow diffusion of diethyl ether into a solution of ($\mathbf{L^2}$)$MnCl_2$ in acetonitrile.

- Synthesis of ($\mathbf{L^2}$)$Ni(NO_3)_2$

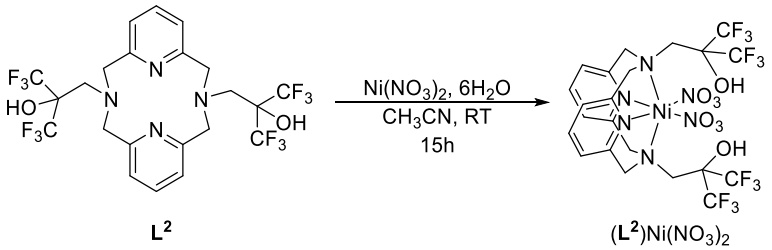

$\mathbf{L^2}$ ($\mathbf{L^2}$)$Ni(NO_3)_2$

After dissolution of $\mathbf{L^2}$ (100 mg, 0.250 mmol) in acetonitrile (5 mL), $Ni(NO_3)_2$,$6H_2O$ (145 mg, 0.500 mmol) was added and the resulting blue solution was stirred at 25 °C for 15 h. After evaporation under reduced pressure and trituration a blue solid was obtained. Crystals of ($\mathbf{L^2}$)$Ni(NO_3)_2$ (168 mg, 86%) were obtained by slow diffusion of diethyl ether into a solution of ($\mathbf{L^2}$)$Ni(NO_3)_2$ in acetonitrile.

Anal. Calcd for ($\mathbf{L^2}$)$Ni(NO_3)_2 \cdot H_2O$, $C_{22}H_{22}F_{12}N_6NiO_9$: C, 32.98; H, 2.77; N, 10.49. Found: C, 32.87; H, 2.48; N, 10.32.

- Synthesis of ($\mathbf{L^2}$)$Co(NO_3)_2$

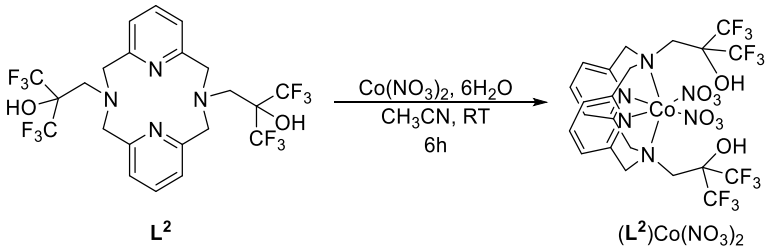

$\mathbf{L^2}$ ($\mathbf{L^2}$)$Co(NO_3)_2$

After dissolution of $\mathbf{L^2}$ (100 mg, 0.167 mmol) in boiling acetonitrile (5 mL), $Co(NO_3)_2$,$6H_2O$ (58 mg, 0.200 mmol) was added and the resulting pink solution was stirred at 25 °C for 6 h. After evaporation under reduced pressure, the complex was dissolved in a minimum of acetonitrile, precipitated in diethyl ether and isolated as a purple solid after filtration. Crystals of ($\mathbf{L^2}$)$Co(NO_3)_2$ (107 mg, 82%) were obtained by slow diffusion of diethyl ether into a solution of ($\mathbf{L^2}$)$Co(NO_3)_2$ in acetonitrile.

HR-MS (ESI): m/z calcd for $C_{22}H_{19}N_4O_2CoF_{12}[M - 2NO_3 - H]^+$: 658.0648 Da; found: 658.0651 Da. m/z calcd for $C_{22}H_{19}N_4O_2CoF_{12}[M - 2NO_3]^{2+}$: 329.5363 Da; found: 329.5362 Da.

- Synthesis of ($\mathbf{L^2}$)Co^{III}

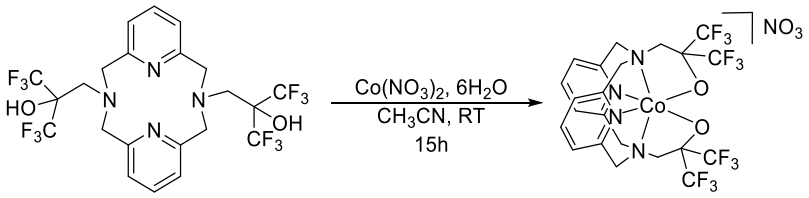

$\mathbf{L^2}$ ($\mathbf{L^2}$)Co^{III}

After dissolution of $\mathbf{L^2}$ (100 mg, 0.167 mmol) in boiling acetonitrile (5 mL), $Co(NO_3)_2$,$6H_2O$ (58 mg, 0.200 mmol) was added and the resulting pink solution was stirred at 25 °C for 15 h. After evaporation under reduced pressure, the complex was dissolved in a minimum of acetonitrile, precipitated in diethyl ether and isolated as a purple solid after filtration. Crystals of ($\mathbf{L^2}$)Co^{III} (93 mg, 80%) were obtained by slow diffusion of diethyl ether into a solution of ($\mathbf{L^2}$)Co^{III} in acetonitrile.

^{1}H NMR (400 MHz, MeOD,) δ = 8.08 (t, J = 8 Hz, 2H, *p*-H Py), 7.67 (d, *J* = 8 Hz, 2H, *m*-H Py), 7.46 (d, *J* = 8 Hz, 2H, *m*-H Py), 5.57 (d, *J* = 16 Hz, 2H, CH_2-ring), 5.22 (d, *J* = 20 Hz, 2H, CH_2-ring), 5.11 (d, *J* = 16 Hz, 2H, CH_2-ring), 5.10 (d, *J* = 20 Hz, 2H, CH_2-ring), 4.37 (d, *J* = 8 Hz, 2H, CH_2-arm), 4.00 (d, *J* = 8 Hz, 2H, CH_2-arm).

^{13}C{^{1}H} NMR (400 MHz, MeOD, 25 °C) δ = 163.3 (*o*-H Py), 161.7 (*o*-H Py), 142.3 (*p*-H Py), 125.0 (q, *J* = 291 Hz, CF_3), 124.4 (q, *J* = 292 Hz, CF_3), 124.0 (*m*-H Py), 121.7 (*m*-H Py), 92.4 (quint, *J* = 27 Hz, C-O), 75.6 (CH_2-ring), 72.6 (CH_2-ring), 66.4 (CH_2(C)).

Anal. Calcd for ($\mathbf{L^2}$)Co^{III} ·⅓CH_3CN, $C_{68}H_{57}Co_3F_{36}N_{16}O_{15}$: C, 37.14; H, 2.61; N, 10.19. Found: C, 37.49; H, 2.13; N, 10.09.

- Synthesis of **6** [23]

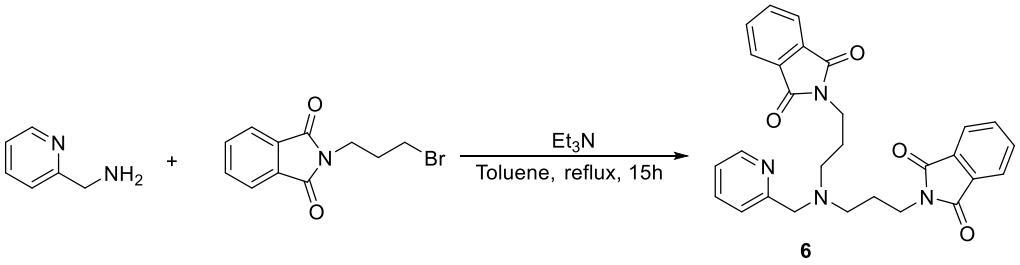

6

2-(Aminomethyl)pyridine (3.2g, 0.03 mol), Et_3N (8.4 mL, 0.06 mol) and N-(3-Bromopropyl)phthalimide (16.1g, 0.06 mol) were added in 50 mL of toluene and the mixture was stirred under reflux for 15h. The white precipitate formed was removed by filtration and the solvent was evaporated under reduced pressure. After recrystallization in EtOH, **6** (9.9 g, 68% yield) was obtained as a white solid.

^{1}H NMR (400 MHz, $CDCl_3$) δ 8.42 (d, 1H, *J* = 4.9 Hz, Ar- H), 7.82 (m, 4H, Ar- H), 7.71 (m, 4H, Ar- H), 7.62 (dd, 1H, *J* = 7.5, 1.8 Hz, Ar- H), 7.55 (d, 1H, *J* = 7.8 Hz, Ar- H), 7.15 (m, 1H, Ar- H), 3.74 (m, 6H, CH_2), 2.60 (t, 4H, CH_2), 1.88 (m, 4H, CH_2).

- Synthesis of **7** [23]

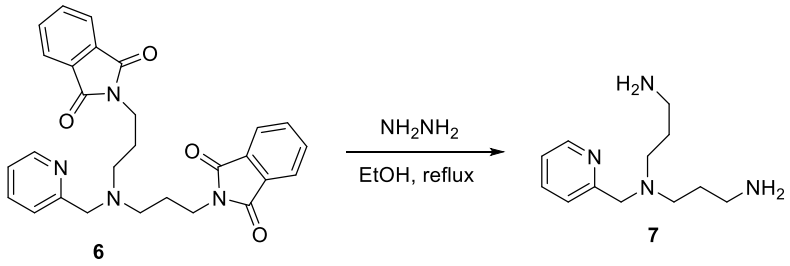

6 **7**

Hydrazine monohydrate (1.63 mL, 0.036 mol) was added into a solution of **6** (8.1 g, 16.8 mmol) in 50 mL of absolute EtOH. The solution was stirred under reflux for 4 h and a white solid appeared. After the addition of 15 mL of concentrated HCl (37 wt.%) and stirring for 1 h under reflux, the solid formed was filtered off and washed by cold EtOH. A concentrated NaOH solution was added until pH ≥ 12 and **7** was extracted with $CHCl_3$ (3x50 mL). After drying of the organic phase over Na_2SO_4, concentration under reduced pressure, **7** (3.25 g, 87%) was obtained as yellow oil.

^{1}H NMR (400 MHz, $CDCl_3$) δ 8.36 (d, *J* = 4.7 Hz, 1H, Ar- H), 7.48 (td, *J* = 7.6, 1.8 Hz, 1H, Ar-H), 7.27 (d, *J* = 7.9 Hz, 1H, Ar- H), 6.98 (ddd, *J* = 7.5, 4.9, 1.2 Hz, 1H, Ar-H), 3.55 (s, 2H, CH_2), 2.56 (t, *J* = 6.8 Hz, 4H, CH_2), 2.37 (t, *J* = 7.0 Hz, 4H, CH_2), 1.64 (s, 4H, NH_2), 1.48 (m, 4H, CH_2).

- Synthesis of **8**

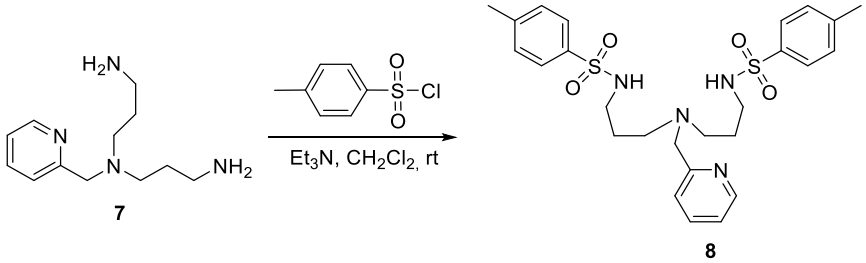

7 **8**

To a solution of tosyl chloride (4.07 g, 21.35 mmol) and Et_3N (2.08 g, 20.56 mmol) in 150 mL of CH_2Cl_2 at 0°C, **7** (2.08 g, 9.35 mmol) dissolved in 20 mL of CH_2Cl_2 was slowly added. After stirring at room temperature for 15 h, the solvent was removed under vacuum and the resulting solid was dissolved in water. The pH was adjusted to 13 by addition of a concentrated NaOH solution and **8** was extracted by $CHCl_3$ (3 x 50 mL). After drying of the organic phase over Na_2SO_4, concentration under reduced pressure, **8** (4.42 g, 92%) was obtained as yellow light solid.

^{1}H NMR (400 MHz, $CDCl_3$) δ 8.81-6.8 (m, 12H, Ar-H), 3.57 (s, 2H, CH_2), 2.96 (m, 4H, CH_2), 2.45-2.34 (m, 10H, CH_2, CH_3), 1.59 (m, 4H, CH_2).

- Synthesis of **L⁵**

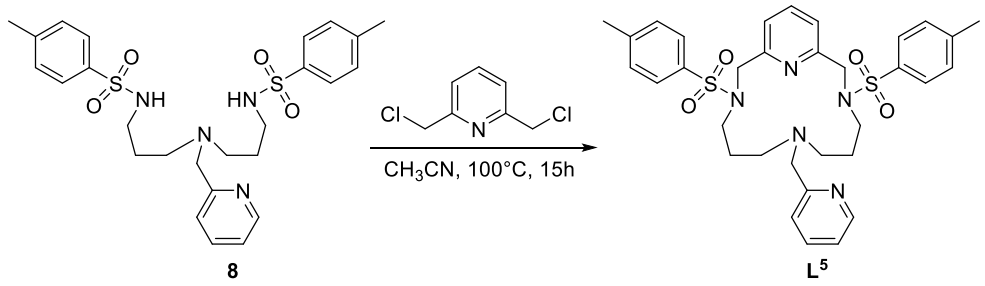

8 **L⁵**

A solution of 2,6-bis(chloromethyl)pyridine (1.6 g, 8.9 mmol) in 50 mL of CH_3CN was slowly added to a solution of **8** (4.5675 g, 8.9 mmol) and Cs_2CO_3 (5.96 g, 18.3 mmol) in 360 mL of CH_3CN at reflux. After stirring at reflux overnight, the precipitate was filtered off and the solution was concentrated until 10 mL of solution remains in the flask. 50 mL of Et_2O were added to precipitate impurities and after filtration, solvents were removed under vacuum. After drying of the organic phase over Na_2SO_4, concentration under reduced pressure, **L⁵** (4.06 g, 72%) was obtained as a light-yellow powder.

^{1}H NMR (400 MHz, $CDCl_3$) δ 8.83-6.87 (m, 15H, Ar-H), 4.31 (s, 4H, CH_2), 3.57 (s, 2H, CH_2), 3.96 (m, 4H, CH_2), 2.40 (s, 6H, CH_3), 2.08 (s, 4H, CH_2), 1.21 (m, 4H, CH_2).

- Synthesis of **9**

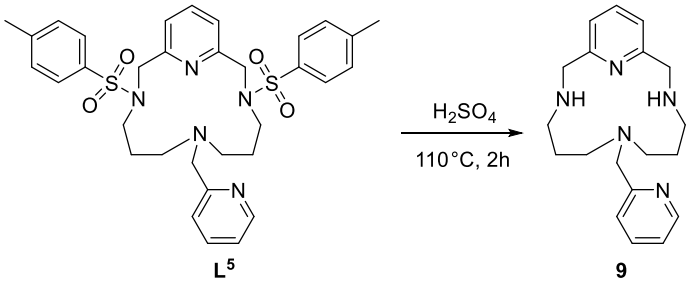

L⁵ **9**

A solution of **L⁵** (3 g, 4.73 mmol) in 24 mL of concentrated H_2SO_4 (96 wt.%) was stirred at 110 °C for 2 h. After the addition of 25 mL of H_2O at 0 °C and addition of NaOH pellets until pH ≈ 12, the solution was extracted by $CHCl_3$ (3 x 50 mL). After drying of the organic phase over Na_2SO_4 and concentration under reduced pressure, **9** (1.26 g, 86%) was obtained as yellow oil.

^{1}H NMR (400 MHz, $CDCl_3$) δ 8.40 (d, *J* = 4.8 Hz, 1H, Ar- H), 7.71 (t, *J* = 7.6 Hz, 1H, Ar- H), 7.39 (td, *J* = 7.7, 1.8 Hz, 1H, Ar- H), 7.23 (d, *J* = 7.6 Hz, 2H, Ar- H), 7.06 (ddd, *J* = 7.5, 4.9, 1.2 Hz, 1H, Ar- H), 6.71 (dt, *J* = 7.91H, 1H, Ar- H), 3.70 (s, 4H), 3.49 (s, 2H), 2.33 (m, 4H), 2.26 (m, 4H, CH_2), 1.51 (m, 4H, CH_2).

- Synthesis of L^6

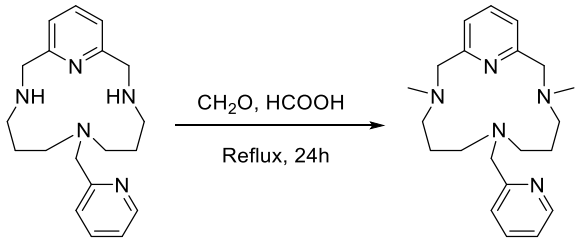

9 **L^6**

A solution of **9** (530 mg, 1.63 mmol) in formic acid (4.07 mL, 0.11 mol) and formaldehyde 37 wt.% (6.51 mL, 0.087 mol) was stirred under reflux for 24 h. After addition of NaOH pellets until pH ≈12, the solution was extracted by $CHCl_3$ (3 x 50 mL). Drying of the organic phase over Na_2SO_4 and concentration under reduced pressure affords L^6 (420 mg, 72%) as a yellow solid.

^{1}H NMR (400 MHz, $CDCl_3$) δ 8.40 (d, *J* = 4.8 Hz, 1H, Ar- H), 7.71 (t, *J* = 7.6 Hz, 1H, Ar- H), 7.39 (td, *J* = 7.7, 1.8 Hz, 1H, Ar- H), 7.23 (d, *J* = 7.6 Hz, 2H, Ar- H), 7.06 (ddd, *J* = 7.5, 4.9, 1.2 Hz, 1H, Ar- H), 6.71 (d, *J* = 7.9 Hz, 1H, Ar- H), 3.70 (s, 4H, CH_2), 3.49 (s, 2H, CH_2), 2.41 (s, 6H, CH_3), 2.33 (m, 4H, CH_2), 2.26 (m, 4H, CH_2), 1.51 (m, 4H, CH_2).

- Synthesis of (L^5)$Ni(NO_3)_2$·CH_3CN

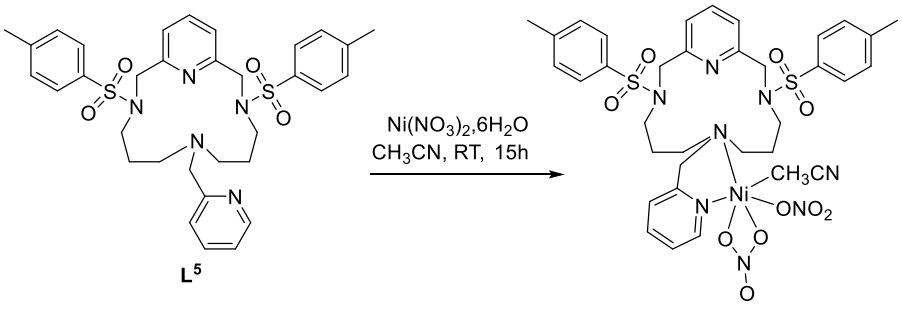

L^5 (L^5)$Ni(NO_3)_2$·CH_3CN

After dissolution of L^5 (50 mg, 78.9 µmol) in acetonitrile (5 mL), $Ni(NO_3)_2$,$6H_2O$ (23 mg, 78.9 µmol) was added and the resulting blue solution was stirred at 25 °C for 15 h. After evaporation under reduced pressure and trituration, a blue solid was obtained. Crystals of (L^5)$Ni(NO_3)_2$·CH_3CN (54 mg, 80%) were obtained by slow diffusion of diethyl ether into a solution of $L^5Ni(NO_3)_2$ in acetonitrile.

Anal. Calcd for (L^5)$Ni(NO_3)_2$·$3CH_3CN$, $C_{39}H_{48}N_{10}NiO_{10}S_2$: C, 49.85; H, 5.15; N, 14.91. Found: C, 49.70; H, 5.15; N, 14.62.

- Synthesis of (L^5)$Co(NO_3)_2 \cdot CH_3CN$

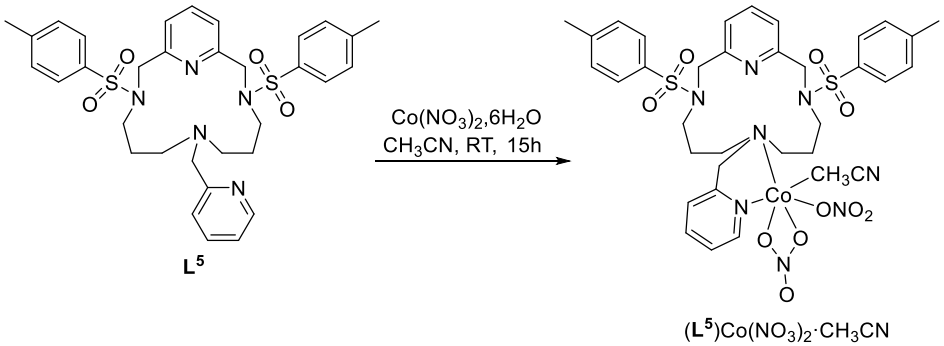

After dissolution of L^5 (100 mg, 158 µmol) in acetonitrile (5 mL), $Co(NO_3)_2,6H_2O$ (46 mg, 158 µmol) was added and the resulting purple solution was stirred at 25 °C for 15h. After evaporation under reduced pressure and trituration, a purple solid was obtained. Crystals of (L^5)$Co(NO_3)_2 \cdot CH_3CN$ (115mg, 85%) were obtained by slow diffusion of diethyl ether into a solution of (L^5)$Co(NO_3)_2$ in acetonitrile.

Anal. Calcd for (L^5)$Co(NO_3)_2 \cdot 3CH_3CN$, $C_{37}H_{45}CoN_9O_{10}S_2$: C, 49.44; H, 5.05; N, 14.02. Found: C, 49.36; H, 5.15; N, 14.56.

2.4.4. Catalytic experiments

General procedure of catalysis

1 mmol of cyclooctene, 0.01 mmol of complexes ((L^1)$MnCl_2$, (L^2)$MnCl_2$, (L^2)Mn_2, [(L^2)$FeCl_2$]($FeCl_4$) or [(L^1)$FeCl_2$]($FeCl_4$)), 14 mmol CH_3COOH (in the case presence of CH_3COOH) and some drops of an internal standard (acetophenone) were mixed in 2ml CH_3CN at room temperature. 0.13 mL of H_2O_2 (35 wt.% in H_2O) diluted in 0.87 mL of CH_3CN were slowly added into the mixture during 2h at 0°C (or 40°C). Then the mixture was left at 0°C (or 40°C) for 1 hour.

2.4.5. Crystal data

L^2

Identification code	L^2
Empirical formula	$C_{22}H_{20}F_{12}N_4O_2$
Formula weight	600.42
Temperature, K	173(2)
Wavelength, Å	0.71073
Crystal system	Monoclinic
Space group	C 2/c
a, Å	18.3276(6)
b, Å	10.2640(3)
c, Å	12.8121(4)
α,°	90.0
β,°	101.309(1)
γ,°	90.0
Volume, $Å^3$	2363.35(13)
Z	4
Density (calc), Mg/m^3	1.687
Abs. coefficient, mm^{-1}	0.174
F(000)	1216
Crystal size, mm^3	0.50 x 0.30 x 0.30
Theta range, °	2.285 to 26.368
Reflections collected	17884
Indpt reflections (R_{int})	2412 (0.0231)
Completeness,%	99.6
Absorption correction	Multi-scan
Max.- min. transmission	0.7464- 0.7191
Refinement method	F^2
Data /restraints/parameters	2412 / 0 / 182
Goodness-of-fit on F^2	1.047
R1, wR2 [$I>2\sigma(I)$]	0.0394, 0.1040
R1, wR2 (all data)	0.0417, 0.1062
Residual density, $e.Å^{-3}$	0.266 /-0.379

$[(\mathbf{L^2})FeCl_2](FeCl_4)$

Identification code	$[(\mathbf{L^2})FeCl_2](FeCl_4)$
Empirical formula	$[C_{22}H_{18}F_{12}FeN_4O_2](FeCl_4),CH_3CN$
Formula weight	892.96
Temperature, K	173(2)
Wavelength, Å	0.71073
Crystal system	Triclinic
Space group	P-1
a, Å	11.082(2)
b, Å	11.298(2)
c, Å	15.453(3)
α,°	97.311(5)
β,°	105.602(5)
γ,°	113.977(5)
Volume, $Å^3$	1640.1(6)
Z	2
Density (calc), Mg/m^3	1.808
Abs. coefficient, mm^{-1}	1.312
F(000)	888
Crystal size, mm^3	0.50 x 0.42 x 0.23
Theta range, °	2.486 to 25.677
Reflections collected	27900
Indpt reflections (R_{int})	6197 (0.0247)
Completeness,%	99.4
Absorption correction	Multi-scan
Max.- min. transmission	0.7454- 0.5939
Refinement method	F^2
Data /restraints/parameters	6197 / 0 / 443
Goodness-of-fit on F^2	1.037
R1, wR2 [$I>2\sigma(I)$]	0.0293, 0.0765
R1, wR2 (all data)	0.0335, 0.0797
Residual density, $e.Å^{-3}$	0.896 /-0.405

$(\mathbf{L^2})Co(NO_3)_2$

Identification code	$(\mathbf{L^2})Co(NO_3)_2$
Empirical formula	$C_{22}H_{20}CoF_{12}N_6O_8,(C_2H_3N)_2$
Formula weight	865.48
Temperature, K	173(2)
Wavelength, Å	0.71073
Crystal system	Orthorhombic
Space group	P b c n
a, Å	a = 14.3235(6)
b, Å	b = 14.2732(8)
c, Å	c = 16.7406(7)
α,°	90.0
β,°	90.0
γ,°	90.0
Volume, $Å^3$	3422.5(3)
Z	4
Density (calc), Mg/m^3	1.680
Abs. coefficient, mm^{-1}	0.626
F(000)	1748
Crystal size, mm^3	0.37 x 0.31 x 0.2
Theta range, °	2.353 to 26.372
Reflections collected	31307
Indpt reflections (R_{int})	3497 (0.0427)
Completeness,%	99.6%
Absorption correction	Multi-scan
Max.- min. transmission	1.0 / 0.636
Refinement method	F^2
Data /restraints/parameters	3497 / 0 / 250
Goodness-of-fit on F^2	1.060
R1, wR2 [$I>2\sigma(I)$]	0.0496, 0.1330
R1, wR2 (all data)	0.0526, 0.1355
Residual density, $e.Å^{-3}$	1.043 /-0.472

$(L^2)Mn_2$	
Identification code	$(L^2)Mn_2$
Empirical formula	$C_{24}H_{24}F_{18}Mn_2N_4O_{11}S_2$
Formula weight	1060.47
Temperature, K	180(2)
Wavelength, Å	0.71073
Crystal system	Triclinic
Space group	P-1
a, Å	11.4949(6)
b, Å	11.6887(6)
c, Å	16.3927(8)
α,°	76.108(4)
β,°	72.132(4)
γ,°	66.136(5)
Volume, $Å^3$	1899.99(17)
Z	2
Density (calc), Mg/m^3	1.854
Abs. coefficient, mm^{-1}	0.922
F(000)	1056
Crystal size, mm^3	0.22 x 0.1 x 0.04
Theta range, °	2.90 to 26.37
Reflections collected	27775
Indpt reflections (R_{int})	7535 (0.0278)
Completeness,%	96.7
Absorption correction	Semi-empirical from equivalents
Max. and min. transmission	0.9991 and 0.9296
Refinement method	Full-matrix least-squares on F^2
Data /restraints/parameters	7535 / 9 / 568
Goodness-of-fit on F^2	1.060
R1, wR2 [I>2σ(I)]	0.0334, 0.0803
R1, wR2 (all data)	0.0439, 0.0859
Residual density, $e.Å^{-3}$	0.418 /-0.649

$(L^2)Co^{III}$

Identification code	$(L^2)Co^{III}$
Empirical formula	$C_{22}H_{18}CoF_{12}N_4O_2$, NO_3, C_2H_3N
Formula weight	760.40
Temperature, K	100(2)
Wavelength, Å	0.71073
Crystal system	Triclinic
Space group	P-1
a, Å	10.0657(6)
b, Å	11.9497(7)
c, Å	13.6144(8)
α,°	111.644(2)
β,°	102.086(2)
γ,°	104.218(2)
Volume, $Å^3$	1391.31(14)
Z	2
Density (calc), Mg/m^3	1.815
Abs. coefficient, mm^{-1}	0.747
F(000)	764
Crystal size, mm^3	0.500 x 0.500 x 0.450
Theta range, °	1.707 to 31.584°.
Reflections collected	56910
Indpt reflections (R_{int})	9305 (0.124)
Completeness,%	100.0
Absorption correction	Multi-scan
Max.- min. transmission	0.688 / 0.719
Refinement method	F^2
Data /restraints/parameters	9305 / 0 / 434
Goodness-of-fit on F^2	1.153
R1, wR2 [$I>2\sigma(I)$]	0.0375, 0.1025
R1, wR2 (all data)	0.0506, 0.1216
Residual density, $e.Å^{-3}$	0.667 /-1.924

$(L^2)Ni(NO_3)_2$

Identification code	$(L^2)Ni(NO_3)_2$
Empirical formula	$C_{11}H_9F_6N_3Ni_{0.5}O_4$, C_2H_3N
Formula weight	431.62
Temperature, K	173(2)
Wavelength, Å	0.71073
Crystal system	Orthorhombic
Space group	P b c n
a, Å	14.1997(4)
b, Å	14.1216(5)
c, Å	16.6794(5)
α,°	90.0
β,°	90.0
γ,°	90.0
Volume, $Å^3$	3344.60(18)
Z	8
Density (calc), Mg/m^3	1.714
Abs. coefficient, mm^{-1}	0.708
F(000)	1744
Crystal size, mm^3	0.5 x 0.35 x 0.08
Theta range, °	3.436 to 26.371
Reflections collected	16228
Indpt reflections (R_{int})	3351(0.0248)
Completeness,%	97.6
Absorption correction	Multi-scan
Max.- min. transmission	1.0 / 0.876
Refinement method	F^2
Data /restraints/parameters	3351 / 0 / 250
Goodness-of-fit on F^2	1.061
R1, wR2 [$I>2\sigma(I)$]	0.0531, 0.1469
R1, wR2 (all data)	0.0622, 0.1561
Residual density, $e.Å^{-3}$	1.204 /-1.240

(L^1)$MnCl_2$

Identification code	(L^1)$MnCl_2$
Empirical formula	$C_{16}H_{23}C_{l2}MnN_4O$
Formula weight	413.22
Temperature, K	173(2)
Wavelength, Å	0.71073
Crystal system	Orthorhombic
Space group	P b c a
a, Å	13.2081(4)
b, Å	15.4897(6)
c, Å	17.9688(7)
α,°	90
β,°	90
γ,°	90
Volume, $Å^3$	3676.2(2)
Z	8
Density (calc), Mg/m^3	1.493
Abs. coefficient, mm^{-1}	1.020
F(000)	1712
Crystal size, mm^3	
Theta range, °	2.267 to 30.590
Reflections collected	32736
Indpt reflections (R_{int})	5617 (0.0433)
Completeness,%	100.0
Absorption correction	Semi-empirical from equivalents
Max. and min. transmission	0.7461 and 0.6821
Refinement method	Full-matrix least-squares on F^2
Data /restraints/parameters	5617 / 3 / 225
Goodness-of-fit on F^2	1.068
R1, wR2 [I>2σ(I)]	0.0333, 0.0784
R1, wR2 (all data)	0.0538, 0.0940
Residual density, $e.Å^{-3}$	0.427 and-0.430

$(L^1)Mn(OTf)_2$

Identification code	$(L^1)Mn(OTf)_2$
Empirical formula	$C_{18}H_{20}F_6MnN_4O_6S_2$
Formula weight	621.44
Temperature, K	293(2)
Wavelength, Å	0.71073
Crystal system	Monoclinic
Space group	P 21/c
a, Å	10.496(2)
b, Å	15.475(5)
c, Å	15.358(6)
α,°	90
β,°	90
γ,°	90
Volume, $Å^3$	2494.7(13)
Z	4
Density (calc), Mg/m^3	1.655
Abs. coefficient, mm^{-1}	0.783
F(000)	1260
Crystal size, mm^3	
Theta range, °	3.287 to 26.372
Reflections collected	13176
Indpt reflections (R_{int})	4937 (0.0896)
Completeness,%	99.5
Refinement method	Full-matrix least-squares on F^2
Data /restraints/parameters	4937 / 0 / 332
Goodness-of-fit on F^2	1.027
R1, wR2 [$I>2\sigma(I)$]	0.0982, 0.2281
R1, wR2 (all data)	0.1544, 0.2774
Residual density, $e.Å^{-3}$	1.457 /-1.182

[(L^1)$FeCl_2$]($FeCl_4$)	
Identification code	[(L^1)$FeCl_2$]($FeCl_4$)
Empirical formula	$C_{16}H_{20}Cl_6Fe_2N_4$
Formula weight	592.76
Temperature, K	173(2)
Wavelength, Å	0.71073
Crystal system	Monoclinic
Space group	C 2/c
a, Å	15.2405(5)
b, Å	12.8915(4)
c, Å	23.7521(9)
α,°	90
β,°	94.296(2)
γ,°	90
Volume, $Å^3$	4653.5(3)
Z	8
Density (calc), Mg/m^3	1.692
Abs. coefficient, mm^{-1}	1.947
F(000)	2384
Crystal size, mm^3	0.500 x 0.300 x 0.050
Theta range, °	1.720 to 26.372
Reflections collected	28722
Indpt reflections (R_{int})	4765 (0.1316)
Completeness,%	99.7
Absorption correction	Semi-empirical from equivalents
Max.- min. transmission	0.7458 / 0.5256
Refinement method	Full-matrix least-squares on F^2
Data /restraints/parameters	4765 / 0 / 255
Goodness-of-fit on F^2	1.071
R1, wR2 [$I>2\sigma(I)$]	0.0473, 0.1202
R1, wR2 (all data)	0.0553, 0.1277
Residual density, $e.Å^{-3}$	0.838 /-0.879

$(L^1)Ni(NO_3)_2$

Identification code	$(L^1)Ni(NO_3)_2$
Empirical formula	$(C_{16}H_{20}N_6NiO_6)_3$
Formula weight	1353.27
Temperature, K	180(2)
Wavelength, Å	0.71073
Crystal system	Orthorhombic
Space group	$P2_12_12_1$
a, Å	14.7861(3)
b, Å	b = 14.9288(5)
c, Å	24.7529(6)
α,°	90.0
β,°	90.0
γ,°	90.0
Volume, $Å^3$	5463.9(3)
Z	4
Density (calc), Mg/m^3	1.645
Abs. coefficient, mm^{-1}	1.115
F(000)	2808
Crystal size, mm^3	0.18 x 0.09 x 0.09
Theta range, °	3.166 to 26.372
Reflections collected	31234
Indpt reflections (R_{int})	10860 (0.0278)
Completeness,%	99.4
Absorption correction	Multi-scan
Max.- min. transmission	1.0 / 0.849
Refinement method	F^2
Data /restraints/parameters	10860 / 0 / 791
Goodness-of-fit on F^2	1.045
R1, wR2 [$I>2\sigma(I)$]	0.0397, 0.0969
R1, wR2 (all data)	0.0497, 0.1038
Flack's parameter	0.471(19)
Residual density, $e.Å^{-3}$	1.144 /-0.419

($\mathbf{L^1}$)$Co(NO_3)_2$

Identification code	($\mathbf{L^1}$)$Co(NO_3)_2$
Empirical formula	$C_{16}H_{20}CoNO_6$
Formula weight	451.31
Temperature, K	173(2)
Wavelength, Å	0.71073
Crystal system	Orthorhombic
Space group	P n m a
a, Å	8.5732(4)
b, Å	14.1425(8)
c, Å	15.2253(8)
α,°	90.0
β,°	90.0
γ,°	90.0
Volume, $Å^3$	1846.01(17)
Z	4
Density (calc), Mg/m^3	1.624
Abs. coefficient, mm^{-1}	0.979
F(000)	932
Crystal size, mm^3	0.35 x 0.28 x 0.27
Theta range, °	2.727 to 26.371
Reflections collected	15265
Indpt reflections (R_{int})	1963 (0.0274)
Completeness,%	99.7%
Absorption correction	Multi-scan
Max.- min. transmission	0.746 / 0.636
Refinement method	F^2
Data /restraints/parameters	1963 / 0 / 148
Goodness-of-fit on F^2	1.289
R1, wR2 [$I>2\sigma(I)$]	0.0783, 0.1849
R1, wR2 (all data)	0.0819, 0.1869
Residual density, $e.Å^{-3}$	1.475 /-0.804

L^4

Identification code	L^4
Empirical formula	$C_{28}H_{28}F_{12}N_4O_2$
Formula weight	680.54
Temperature, K	173(2)
Wavelength, Å	0.71073
Crystal system	Monoclinic
Space group	P 21/c
a, Å	10.9664(7)
b, Å	10.8059(6)
c, Å	10.8144(7)
α,°	90
β,°	107.270(2)
γ,°	90
Volume, $Å^3$	1223.75(13)
Z	2
Density (calc), Mg/m^3	1.847
Abs. coefficient, mm^{-1}	0.180
F(000)	696
Crystal size, mm^3	0.320 x 0.260 x 0.180
Theta range, °	2.709 to 26.371
Reflections collected	21533
Indpt reflections (R_{int})	2502 (0.0273)
Completeness,%	99.5
Refinement method	Full-matrix least-squares on F^2
Data /restraints/parameters	2502 / 0 / 182
Goodness-of-fit on F^2	0.993
R1, wR2 [$I>2\sigma(I)$]	0.0339, 0.0846
R1, wR2 (all data)	0.0408, 0.0902
Residual density, $e.Å^{-3}$	0.288 /-0.227

L^5	
Identification code	L^5
Empirical formula	$C_{33}H_{37}N_5O_4S_2$
Formula weight	631.79
Temperature, K	173(2)
Wavelength, Å	1.54184
Crystal system	Orthorhombic
Space group	P c a 21
a, Å	16.6530(19)
b, Å	9.4834(12)
c, Å	41.309(6)
α,°	90
β,°	90
γ,°	90
Volume, $Å^3$	6523.8(14)
Z	8
Density (calc), Mg/m^3	1.287
Abs. coefficient, mm^{-1}	1.841
F(000)	2672
Crystal size, mm^3	
Theta range, °	4.281 to 61.652
Reflections collected	22681
Indpt reflections (R_{int})	9262 (0.0522)
Completeness,%	85.7
Absorption correction	multi-scan
Max.- min. transmission	1.0 / 0.591
Refinement method	Full-matrix least-squares on F^2
Data /restraints/parameters	9262 / 1/ 798
Goodness-of-fit on F^2	1.066
R1, wR2 [I>2σ(I)]	0.0687, 0.1749
R1, wR2 (all data)	0.0788, 0.1838
Flack's parameter	0.32(3)
Residual density, $e.Å^{-3}$	1.128 /-0.455

$(L^5)Ni(NO_3)_2$

Identification code	$(L^5)Ni(NO_3)_2$
Empirical formula	$C_{39}H_{48}N_{10}Ni_{O.50}S_2$
Formula weight	1011.70
Temperature, K	163(2)
Wavelength, Å	0.71073
Crystal system	Triclinic
Space group	P-1
a, Å	9.7671(7)
b, Å	13.2342(12)
c, Å	19.3064(16)
α,°	101.620(5)
β,°	98.306(4)
γ,°	111.546(3)
Volume, $Å^3$	2207.3(3)
Z	2
Density (calc), Mg/m^3	1.522
Abs. coefficient, mm^{-1}	0.614
F(000)	1056
Crystal size, mm^3	0.620 x 0.470 x 0.250
Theta range, °	1.109 to 26.369
Reflections collected	54552
Indpt reflections (R_{int})	9019 (0.0509)
Completeness,%	99.6
Refinement method	Full-matrix least-squares on F^2
Data /restraints/parameters	9019 / 0 / 564
Goodness-of-fit on F^2	1.175
R1, wR2 [$I>2\sigma(I)$]	0.0575, 0.1386
R1, wR2 (all data)	0.0654, 0.1428
Residual density, $e.Å^{-3}$	0.926 /-0.622

$(\mathbf{L^5})Co(NO_3)_2$	
Identification code	$(\mathbf{L^5})Co(NO_3)_2$
Empirical formula	$C_{39}H_{48}N_{10}CoO_{10}S_2$
Formula weight	939.92
Temperature, K	173(2)
Wavelength, Å	0.71073
Crystal system	Triclinic
Space group	P-1
a, Å	9.930(3)
b, Å	13.237(5)
c, Å	19.527(7)
α,°	72.143(16)
β,°	81.775(15)
γ,°	68.686(15)
Volume, Å3	2274.6(14)
Z	2
Density (calc), Mg/m3	1.372
Abs. coefficient, mm-1	0.534
F(000)	982
Theta range, °	1.096 to 25.027
Reflections collected	54690
Indpt reflections (Rint)	8029 (0.0640)
Completeness,%	100.0
Refinement method	Full-matrix least-squares on F^2
Data /restraints/parameters	8029 / 0 / 564
Goodness-of-fit on F2	1.089
R1, wR2 [I>2σ(I)]	0.0457, 0.1237
R1, wR2 (all data)	0.0632, 0.1447
Residual density, e.Å-3	0.382 /-0.548

[(**L²**-2H)Fe](ClO_4)

Identification code	[(**L²**-2H)Fe](ClO_4)
Empirical formula	$C_{22}H_{18}F_{12}FeN_4O_2$, ClO_4
Formula weight	753.70
Temperature, K	180(2)
Wavelength, Å	0.71073
Crystal system	Monoclinic
Space group	P 21/c
a, Å	15.8631(3)
b, Å	11.0708(3)
c, Å	15.4138(3)
α,°	90
β,°	90.610(2)
γ,°	90
Volume, $Å^3$	2706.78(10)
Z	4
Density (calc), Mg/m^3	1.850
Abs. coefficient, mm^{-1}	0.787
F(000)	1508
Crystal size, mm^3	
Theta range, °	2.951 to 26.372
Reflections collected	13227
Indpt reflections (R_{int})	5517(0.0241)
Completeness,%	99.5
Absorption correction	Semi-empirical from equivalents
Max.- min. transmission	1.0 / 0.964
Refinement method	Full-matrix least-squares on F^2
Data /restraints/parameters	5517 / 0 / 415
Goodness-of-fit on F^2	1.038
R1, wR2 [I>2σ(I)]	0.0315, 0.0722
R1, wR2 (all data)	0.0407, 0.0770
Residual density, $e.Å^{-3}$	0.331 /-0.374

2.5. References

[1] (a) L. R. Widger, C. G. Davies, T. Yang, M. A. Siegler, O. Troeppner, G. N. L. Jameson, I. Ivanović-Burmazović, D. P. Goldberg, *J. Am. Chem. Soc.* **2014**, *136*(7), 2699–2702.
(b) D. Bansal, G. Kumar, G. Hundal, R. Gupta, *Dalton Trans.* **2014**, *43*(39), 14865–14875.
(c) H. Yamagishi, S. Nabeya, T. Ikariya, S. Kuwata, *Inorg. Chem.* **2015**, *54*(24), 11584–11586.
(d) M. L. Helm, M. P. Stewart, R. M. Bullock, M. R. DuBois, D. L. DuBois, *Science* **2011**, *333*(6044), 863–866.

[2] (a) R. Mas-Ballesté, L. Que, *J. Am. Chem. Soc.* **2007**, *129*(51), 15964–15972.
(b) O. Cussó, J. Serrano-Plana, M. Costas, *ACS Catal.* **2017**, *7*(8), 5046–5053.

[3] (a) Y. Watanabe, H. Nakajima, T. Ueno, *Acc. Chem. Res.* **2007**, *40*(7), 554–562.
(b) K. Neimann, R. Neumann, *Org. Lett.* **2000**, *2*(18), 2861–2863.
(c) M. C. White, A. G. Doyle, E. N. Jacobsen, *J. Am. Chem. Soc.* **2001**, *123*(29), 7194–7195.
(d) O. Cussó, I. Garcia-Bosch, X. Ribas, J. Lloret-Fillol, Costas, M. *J. Am. Chem. Soc.* **2013**, *135*(39), 14871–14878.
(e) O. Cussó, M. Cianfanelli, X. Ribas, R. J. M. Klein Gebbink, M. Costas, *J. Am. Chem. Soc.* **2016**, *138*(8), 2732–2738.
(f) G. Olivo, O. Cussó, M. Costas, *Chem. Asian J.* **2016**, *11*(22), 3148–3158.
(g) E. P. Talsi, K. P. Bryliakov, *Coord. Chem. Rev.* **2012**, *256*(13), 1418–1434.

[4] (a) M. C. Esmelindro, E. G. Oestreicher, H. Márquez-Alvarez, C. Dariva, S. M. S. Egues, C. Fernandes, A. J. Bortoluzzi, V. Drago, O. A. C. Antunes, *J. Inorg. Biochem.* **2005**, *99*(10), 2054–2061.
(b) R. A. Leising, R. E.; Norman, L. Que, *Inorg. Chem.* **1990**, *29*(14), 2553–2555.
(c) T. Kojima, R. A. Leising, S. Yan, L. Que, *J. Am. Chem. Soc.* **1993**, *115*(24), 11328–11335.

[5] Y. Li, X.-M. Lu, X. Sheng, G.-Y. Lu, Y. Shao, Q. *J.* Xu, *Incl. Phenom. Macrocycl. Chem.* **2007**, *59*(1), 91–98.

[6] W.-T. Lee, S. Xu, D. A. Dickie, J. M. Smith, *Eur. J. Inorg. Chem.* **2013**, *2013*(22–23), 3867–3873.

[7] F. Tang, Y. Zhang, N. P. Rath, L. M. Mirica, *Organometallics* **2012**, *31*(18), 6690–6696.

[8] (a) H. Sugimoto, K. Ashikari, S. Itoh, *Chem. Asian J.* **2013**, *8*(9), 2154–2160.
(b) T. W.-S. Chow, E. L.-M. Wong, Z. Guo, Y. Liu, J.-S. Huang, C.-M. Che, *J. Am. Chem. Soc.* **2010**, *132* (38), 13229–13239.

[9] N. Raffard, R. Carina, A. J. Simaan, J. Sainton, E. Rivière, L. Tchertanov, S. Bourcier, G. Bouchoux, M. Delroisse, F. Bans, J.-J. Girerd, *Eur. J. Inorg. Chem.* **2001**, *2001*(9), 2249–2254.

[10] W.-P. To, T. W.-S. Chow, C.-W. Tse, X. Guan, J.-S. Huang, C.-M. Che, *Chem. Sci.* **2015**, *6*(10), 5891–5903.

[11] P. Wang, G. Liang, C. L. Boyd, C. E. Webster, X. Zhao, *Eur. J. Inorg. Chem.* **2019**, *2019*(15), 2134–2139.

[12] (a) H. Noh, D. Jeong, T. Ohta, T. Ogura, J. S. Valentine, J. Cho, *J. Am. Chem. Soc.* **2017**, *139*(32), 10960–10963.
(b) Kim, B.; Jeong, D.; Cho, J. *Chem. Commun.* **2017**, *53*(67), 9328–9331.

[13] D. Jeong, T. Ohta, J. Cho, *J. Am. Chem. Soc.* **2018**, *140*(47), 16037–16041.

[14] (a) A. J. Wessel, J. W. Schultz, F. Tang, H. Duan, L. M. Mirica, *Org. Biomol. Chem.* **2017**, *15*(46), 9923–9931.
(b) E. A. Pedrick, J. W. Schultz, G. Wu, L. M. Mirica, *Inorg. Chem.* **2016**, *55*(11), 5693–5701.
(c) F. Tang, F. Qu, J. R. Khusnutdinova, N. P. Rath, L. M. Mirica, *Dalton Trans.* **2012**, *41*(46), 14046–14050.

[15] P. Guillo, J.-C. Daran, E. Manoury, R. Poli, *ChemistrySelect.* **2017**, *2*(8), 2574–2577.

[16] (a) B. Chakraborty, R. D. Jana, R. Singh, S. Paria, T. K. Paine, *Inorg. Chem.* **2017**, *56*(1), 359–371.
(b) A. Kejriwal, S. Biswas, A. N. Biswas, P. Bandyopadhyay, *J. Mol. Catal. A-Chem.* **2016**, *413*, 77–84.

[17] (a) A. M. Zima, Y. O. Lyakin, R. V. Ottenbacher, K. P. Bryliakov, E. P. Talsi, *ACS Catal.* **2017**, *7*(1), 60–69.
(b) B. Wang, Y.-M. Lee, M. Clémancey, M. S. Seo, R. Sarangi, J.-M. Latour, W. Nam, *J. Am. Chem. Soc.* **2016**, *138*(7), 2426–2436.

[18] (a) J. Du, C. Miao, C. Xia, Y.-M. Lee, W. Nam, W. Sun, *ACS Catal.* **2018**, *8* (5), 4528–4538.

[19] F. Bottino, M. Di Grazia, P. Finocchiaro, F. R. Fronczek, A. Mamo, S. Pappalardo, *J. Org. Chem.* **1988**, *53*(15), 3521–3529.

[20] C. Hureau, G. Blondin, M.-F. Charlot, C. Philouze, M. Nierlich, M. Césario, E. Anxolabéhère-Mallart, *Inorg. Chem.* **2005**, *44*(10), 3669–3683.

[21] S. J. Grant, P. Moore, H. A. A. Omar, N. W. Alcock, *J. Chem. Soc., Dalton Trans.* **1994**, 485–489.

[22] (a) C. M. Wallen, J. Bacsa, C. C. Scarborough, *Inorg. Chem.* **2018**, *57*(9), 4841–4848.
(b) C. M. Wallen, L. Palatinus, J. Bacsa, C. C. Scarborough, *Angew. Chem. Int. Ed.* **2016**, *55*(39), 11902–11906.
(c) C. M. Wallen, J. Bacsa, C. C. Scarborough, *J. Am. Chem. Soc.* **2015**, *137*(46), 14606–14609.

[23] G. S. Matouzenko, A. Bousseksou, S. A. Borshch, M. Perrin, S. Zein, L. Salmon, G. Molnar, S. Lecocq, *Inorg. Chem.* **2004**, *43*(1), 227–236.

[24] M. L. Turonek, P. Moore, H. J. Clase, N. W. Alcock, *J. Chem. Soc., Dalton Trans.* **1995**, 3659–3666.

[25] T. Ollevier, G. Lavie-Compin, *Tetrahedron Lett.* **2002**, *43*(44), 7891–7893.

[26] S. Lorenz, B. Plietker, *ChemCatChem* **2016**, *8*(20), 3203–3206.

[27] (a) M. E. Ahmed, S. Dey, M. Y. Darensbourg, A. Dey, *J. Am. Chem. Soc.* **2018**, *140*(39), 12457–12468.
(b) Y. Nicolet, A. L. de Lacey, X. Vernède, V. M. Fernandez, E. C. Hatchikian, J. C. Fontecilla-Camps, *J. Am. Chem. Soc.* **2001**, *123*(8), 1596–1601.
(c) A. Silakov, B. Wenk, E. Reijerse, W. Lubitz, *Physical Chemistry Chemical Physics* **2009**, *11*(31), 6592–6599.

[28] A. Berkessel, In *Modern Oxidation Methods*, John Wiley & Sons, Ltd, 2010; pp 117–145.

[29] A. Call, Z. Codolà, F. Acuña‐Parés, J. Lloret‐Fillol, *Chem. Eur. J.* **2014**, *20*(20), 6171–6183.

[30] J. R. Khusnutdinova, J. Luo, N. P. Rath, L. M. Mirica, *Inorg. Chem.* **2013**, *52*(7), 3920–3932.

[31] T. Shimoda, T. Morishima, K. Kodama, T. Hirose, D. E. Polyansky, G. F. Manbeck, J. T. Muckerman, E. Fujita, *Inorg. Chem.* **2018**, *57*(9), 5486–5498.

Chapter 3

Replacement of volatile acetic acid by solid SiO_2@COOH for the (ep)oxidation using Mn^{II} and Fe^{III} complexes containing BPMEN ligand.

Abstract: This chapter does describe the catalytic activity of Mn and Fe complexes bearing the BPMEN ligand. Mn and Fe BPMEN complexes were successfully synthesized, and as described previously in the literature, showed an excellent reactivity in catalytic oxidation reactions with a co-reagent (CH_3COOH) used in excess.[1] In the straight line of the research engaged in the group,[2] the aim has been to find a way to obtain a cleaner catalytic system, more atom economical, replacing the classical volatile acetic acid co-reagent by **SiO_2** Stöber silica particles on which pending carboxylic functions were added. The carboxylic containing beads were obtained following a two-steps method, starting by functionalization by pending nitrile functions (**SiO_2@CN**) that were hydrolyzed into carboxylic ones.[3] To access these final beads, named **SiO_2@COOH**, in the first step, **SiO_2** beads were synthesized in two different solvents (methanol or ethanol) since the solvent does influence the size of SiO_2 beads and as a consequence, the number of COOH pending functions. All BPMEN related complexes and silica beads were fully characterized by different methods (liquid and solid-state NMR, Infrared, DLS and TEM)

The replacement of CH_3COOH by **SiO_2@COOH** (100 times less on molar ratio) has been evaluated for the (ep)oxidation on several substrates of interest (cyclooctene, cyclohexene, cyclohexanol) and discussed. The difference of **SiO_2@COOH** size has been discussed and presented.

3.1. Introduction

Synthesis of epoxides is an interesting research field from fundamental to applicative point of view in different research areas of chemistry, being in organic synthesis or catalysis. Indeed, those organic compounds can be obtained using very simple organic oxidants (but quite tedious in the post-treatment procedure) like *m*-CPBA,[4] $NaIO_4$,[5] RCO_3H[6] …. They can also be obtained using metal catalysts and the use of an organic solvent is very often required.[7] It can be the case with several Mo complexes.[8] The use of chlorinated solvents such as DCE, a highly toxic solvent, has to be avoided.[9] Some processes have been found in the research group to be active without the use of organic solvent and several tridentate ligands, giving a first step towards a cleaner process.[2a,2b] The oxidant used in this case is TBHP in aqueous solution. In terms of atom economy, the epoxidation reaction could be even more improved using for example H_2O_2 as oxidant. For example, other processes interesting for selective epoxidation reactions have used as catalysts the $(BPMEN)Mn(OTf)_2$ [10] manganese complexes or, $(BPMEN)Fe(OTf)_2$ and $(Me_2PyTACN)Fe(OTf)_2$.[1d, 11] iron complexes. With those catalysts, the epoxidation of olefins using H_2O_2 as oxidant was performed in acetonitrile as organic solvent. The use of H_2O_2 as oxidant is very interesting in terms of atom economy. As detailed in Chapter 2, those Mn and Fe catalysts are only selective in favour of epoxides when acetic acid is added as co-reagent.[1c] Indeed, by blocking one of the labile sites on the metal center, the access to *cis*-diols is not possible.[12] Moreover, carboxylic acids play the role of proton relay, protonating the distal oxygen of the metal-hydroperoxo intermediate, favouring the heterolytic cleavage of its O-O bond and thus leading to the clean formation of a metal-oxo compound, the intermediate responsible for the selective oxidation of the olefin into epoxide[12b,13] When BPMEN is used as ligand, a very high quantity of acetic acid is used (14 equiv. relative to the substrate) this quantity being comparable in volume to the quantity of the organic solvent engaged in the reaction. An elegant way to replace the organic volatile carboxylic acid by recoverable objects can be the use of a solid reagent with COOH pending functions.[3,14] For this, it was interesting to take advantage to the sol-gel chemistry and the possibility of functionalization of silica - using trialkoxysilane precursors- to obtain pending acidic functions within the silica.[15] The use of silica was employed previously for different uses, especially to graft in a covalent way polydentate ligands and related complexes for catalysed reactions, or to trap heavy metals for depollution concerns. Those strategies used mainly mesoporous compounds[16] but scarcely non-porous silica beads. Few examples are related to the replacement of carboxylic function in oxidation reactions catalysed by Fe or Mn

complexes surrounded by tetradentate ligands. Notestein and coworkers reported mono- or di-nuclear Mn complexes of Me_3tacn (1,4,7-Trimethyl-1,4,7-triazacyclononane) partially grafted on functionalized mesoporous silica with pendant carboxylic functions. The functions were aimed to recover catalyst and to replace volatile reagents. Those systems showed interesting results in oxidation reaction on several substrates.[17]

In order to find an easy recoverable non-volatile acidic agent, we used functionalized silica beads instead of acetic acid. To prove the efficiency, the reactions were performed in similar conditions with several metal complexes based on BPMEN ligands. Metal complexes derived from BPMEN ligands are not reported as the most efficient catalysts for OAT reactions, but possess several advantages:

(i) they are well described in the literature.[1c,18]

(ii) their synthesis is straightforward.[1c]

(iii) they display well reported OAT reactivity.[18b]

The effect of the metal and/or counter ion in the catalysts was studied. The quantity of COOH functions was evaluated according to the size of the synthesized silica beads. Influence of reaction temperature and reaction time were studied as parameters. In the case of the most active complex, silica beads recovery and reuse have been tested.

3.2. Results and discussion

3.2.1. About the metal complexes of BPMEN ligand (BPMEN = L^3)

3.2.1.1. Synthesis

In order to study the influence of the counter anion during the catalytic experiments and more particularly with the use of the silica beads, three Mn(II) metal complexes, with different anions were synthetized according to Scheme 1. (L^3)$MnCl_2$ was obtained in 65% yield as a yellow powder by reaction between L^3 and $MnCl_2$,$4H_2O$ in acetonitrile.[19] Similarly, (L^3)$Mn(OTf)_2$ was obtained in 68% yield as a white powder.[1c] (L^3)$Mn(p\text{-}Ts)_2$ was obtained from (L^3)$MnCl_2$ *via* anion metathesis using silver para-toluenesulfonate. Precipitation of AgCl during the reaction confirmed the anion exchange and (L^3)$Mn(p\text{-}Ts)_2$ was isolated as a grey powder in 72% yield.

One Fe^{III} metal complex, [(L^3)$FeCl_2$]($FeCl_4$), determined by X-ray analysis (*vide infra*), was obtained in 73% yield by reaction between L^3 and 2 equivalents of $FeCl_3$,$6H_2O$ in acetonitrile. It has to be noted that the same reactivity has been observed from L^1 and L^2 (chapter 2) and previously described with other ligands in the literature.[20]

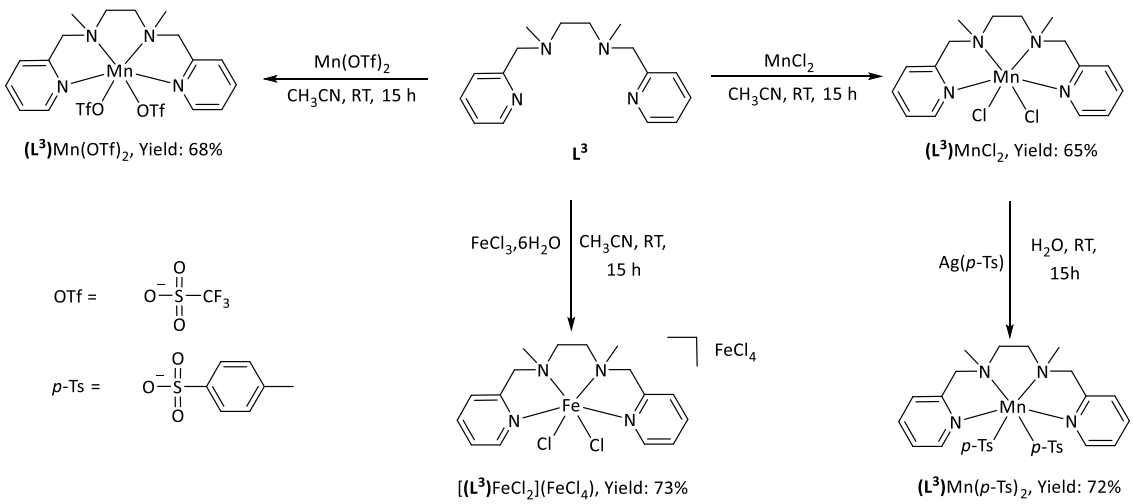

Scheme 1- Synthesis of metal complexes of **L³**.

3.2.1.2. X-ray diffraction characterization of the complexes

Suitable crystals for X-ray analysis have been obtained for all four metal complexes synthesized from **L³**. X-ray diffraction structures of (**L³**)$MnCl_2$[19] and (**L³**)$Mn(OTf)_2$[21] have been previously described in the literature and during the X-ray analysis, same crystallographic parameters were obtained, confirming the nature of the metal complexes described in scheme 1. Concerning (**L³**)Mn(*p*-Ts)$_2$ and [(**L³**)$FeCl_2$]($FeCl_4$), their X-ray structures are represented in Figure 1, and principal bond lengths and angles listed in Table 1.

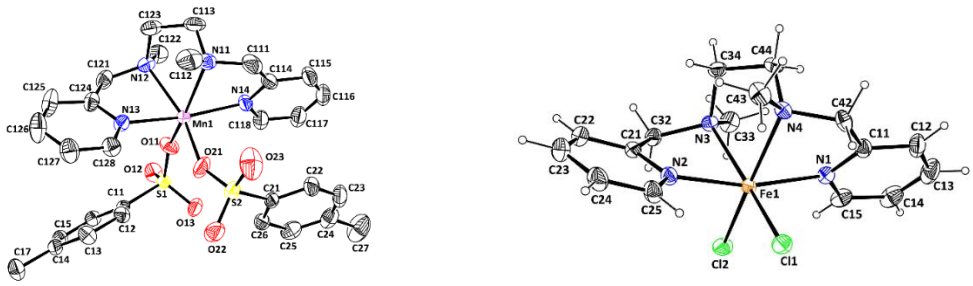

(**L³**)Mn(*p*-Ts)$_2$ [(**L³**)$FeCl_2$]($FeCl_4$)

Figure 1 - Molecular views of (**L³**)Mn(*p*-Ts)$_2$ and [(**L³**)$FeCl_2$]($FeCl_4$) with the atom labelling scheme. Ellipsoids are drawn at the 50% probability level. H atoms have been omitted for the sake of clarity for (**L³**)Mn(*p*-Ts)$_2$. For [(**L²**)$FeCl_2$]($FeCl_4$), $FeCl_4$ anion has been omitted for the sake of clarity.

Table 1- Selected bond distances (Å) and angles (deg.) for (**L³**)Mn(*p*-Ts)$_2$ and [(**L³**)$FeCl_2$]($FeCl_4$).

	(**L³**)Mn(*p*-Ts)$_2$	[(**L³**)$FeCl_2$]($FeCl_4$)
Bonds		
M - N_{py}	2.308(5) – 2.352(2)	2.1408(12) – 2.1556(12)
M - N_{amine}	2.249(2) – 2.283(2)	2.2233(11) – 2.2264(12)
Angles		
N_{amine}-M-N_{amine}	75.46(9) - 76.06(8)	79.70(4)
N_{Py}-M-N_{Py}	168.55(8) – 168.87(7)	166.17(5)

In both structures, the metal center is in a distorted octahedral environment. Several ligand-metal-ligand angle values in both metal complexes deviate significantly from the ideal values of a regular octahedron. However, all the angles measured fall in the range found for similar metal complexes in the literature, notably (L^3)$MnCl_2$[19] and (L^3)$Mn(OTf)_2$[21]. The metal centers are coordinated by the four nitrogen atoms of the L^3 ligand, and two anions. In both cases, the two anions are in *cis* positions and the two pyridine groups of L^3 *trans* to one another. Consequently, the L^3 ligand folds around the metal center using the *cis*-α conformation usually observed within this family of aminopyridine ligands.

3.2.2. About the SiO_2@COOH beads

3.2.2.1. Synthesis

The syntheses of **SiO_2@COOH** (nano)particles have been obtained, starting from SiO_2 beads obtained using a modified Stöber synthesis from TEOS as precursor in presence of aqueous ammonia solution and H_2O in alcohol (ethanol or methanol) as solvent (Scheme 2).[22] Before and after the grafting of any pending functions, those SiO_2 beads were analyzed by different techniques.

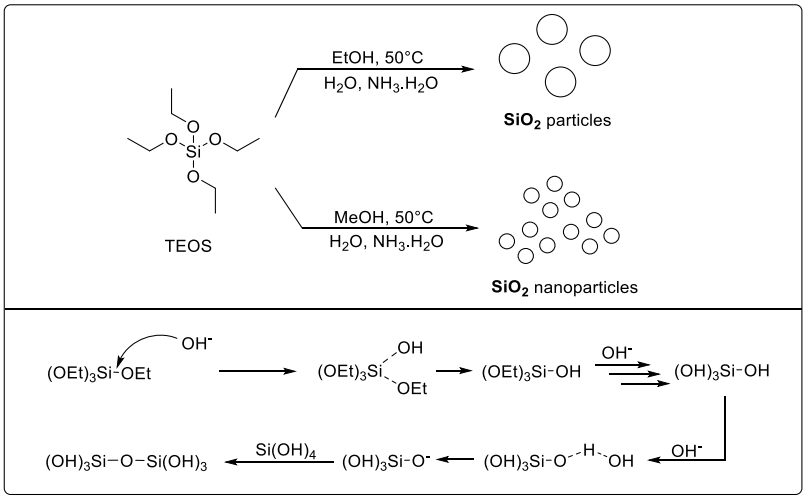

Scheme 2- Mechanism of **SiO_2** particles synthesis.

Influence of solvent,[23] quantity of water,[24] concentration of ammonia solution[25] and temperature[26] on the size of silica nanoparticles were already described in different articles.[27] (Nano)Particle size decreases when solvent polarity increases and viscosity decreases.[28] Two batches of silica particles with different sizes were then synthesized according to the nature of solvent used during the synthesis. Their reactivity will be compared in several catalyzed oxidation reactions.

The syntheses of **SiO_2@COOH** were performed in two steps (scheme 3). The first step is the functionalization of the surface of the SiO_2 nanoparticles by 3-(triethoxysilyl)propionitrile (TESPN) in order to obtain a silica bead with pending nitrile functions **SiO_2@CN**. The terminal nitrile functions have been in a second step hydrolyzed into carboxylic ones using H_2SO_4 (65 wt.%) to obtain the **SiO_2@COOH** beads. The last step, as we will see later, does remove a substantial part of "grafted" silanes.

All silica (nano) particles (**SiO_2**, **SiO_2@CN**, **SiO_2@COOH**) were characterized by DLS, TEM, multinuclear solid state NMR and the number of functions grafted quantified by ^{1}H NMR.

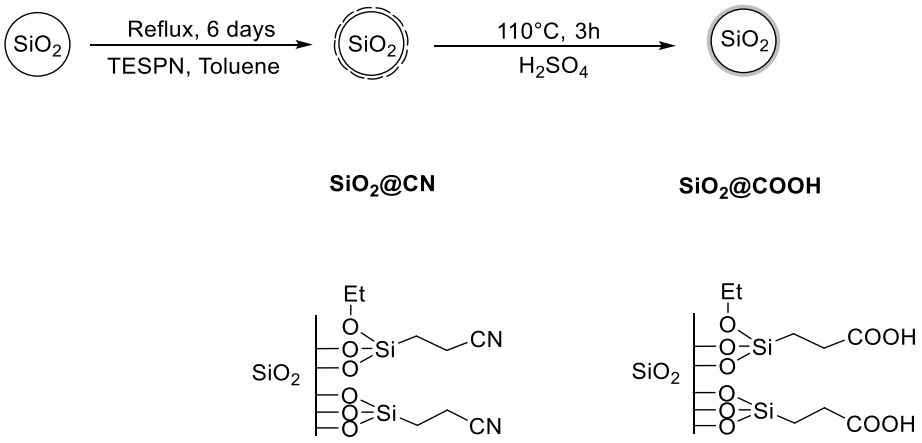

Scheme 3- Synthesis pathway of the functionalized SiO_2 nanoparticles.

3.2.2.2. Characterization

As described previously, several parameters can influence the size of SiO_2 particles. The purpose of the use of two different solvents for the synthesis of the starting **SiO_2** was the access to different beads sizes. Thus, different sized non-porous silica beads might lead to different specific surfaces (linked to the average diameter of the beads) and might influence the number of grafted functions per gram of silica beads. Thus, objects of different sizes can be added into the reaction media and might change the reactivity in the catalyzed oxidation reactions studied herein.

The characterization has been divided in three steps. The morphological study of these (nano)particles was done first by TEM and DLS to determine their sizes. The proof of the grafting was done using different spectroscopic methods (IR, solid NMR) and the quantification of the grafting through ^{1}H liquid NMR.

3.2.2.2.a. Morphological study

TEM Analysis

From the TEM pictures in the case of the **SiO_2** and **SiO_2@COOH** beads (Figure 2), it has been possible to prove the different sizes of silica beads according to the solvent used. For each step, quite monodisperse spherical beads have been obtained around 430-440 nm when done in ethanol and 62-66 nm when done in methanol.

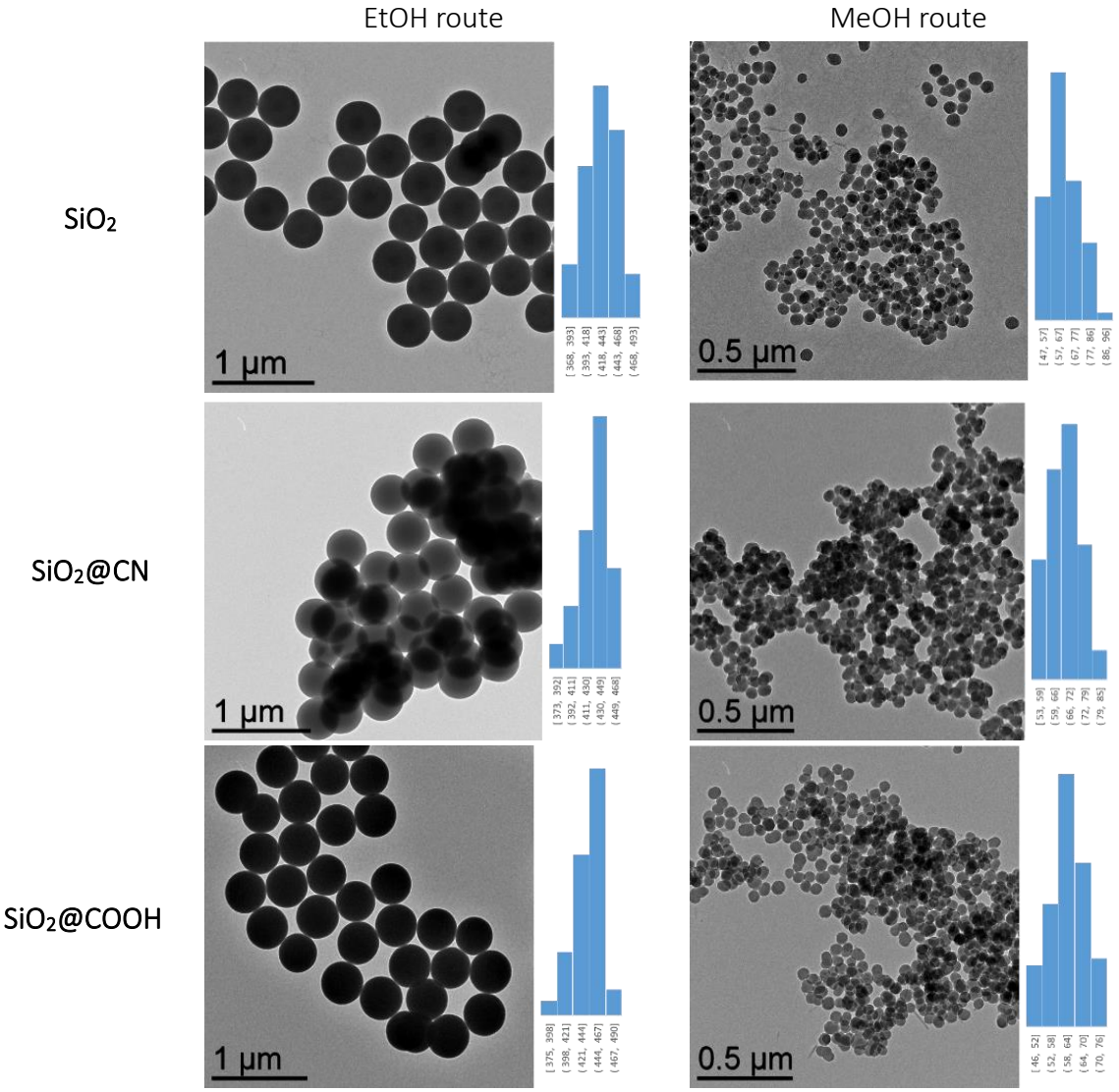

Figure 2- From up to down- TEM images and diameters distribution of **SiO_2**, **SiO_2@CN**, **SiO_2@COOH** beads from SiO_2 beads done in EtOH (left) and MeOH (right).

Dynamic Light Scattering (DLS) measurements

Monodispersity is an important parameter to characterize the homogeneity of size and to calculate function coverage of the non-porous **SiO_2@CN** and **SiO_2@COOH** beads. This parameter will ensure some reproducibility of the catalytic reactions. DLS is another practical and simple method that could determinate the hydrodynamic diameter distribution, intensity of distribution and number of distributions of silica particles.

The DLS measurements for the **SiO_2**, **SiO_2@CN** and **SiO_2@COOH** beads done in ethanol show a regular hydrodynamic diameter of the nanoparticles around 400-450 nm, very close to the ones found by TEM analysis. The diameters are very close since the additional functions do not modify strongly the beads sizes as the size of functions are negligible. A narrow distribution of number confirmed the monodispersity of the SiO_2 NPs. In the case of SiO_2 beads done in methanol, where the size is expected to be smaller, the DLS measurements (100 nm for **SiO_2**, 190 nm for **SiO_2@CN** and 68 nm for **SiO_2@COOH**) do not give data that correspond to the observations from TEM. This could be due to some aggregation phenomena or multilayers of silanes in the case of **SiO_2@CN**.

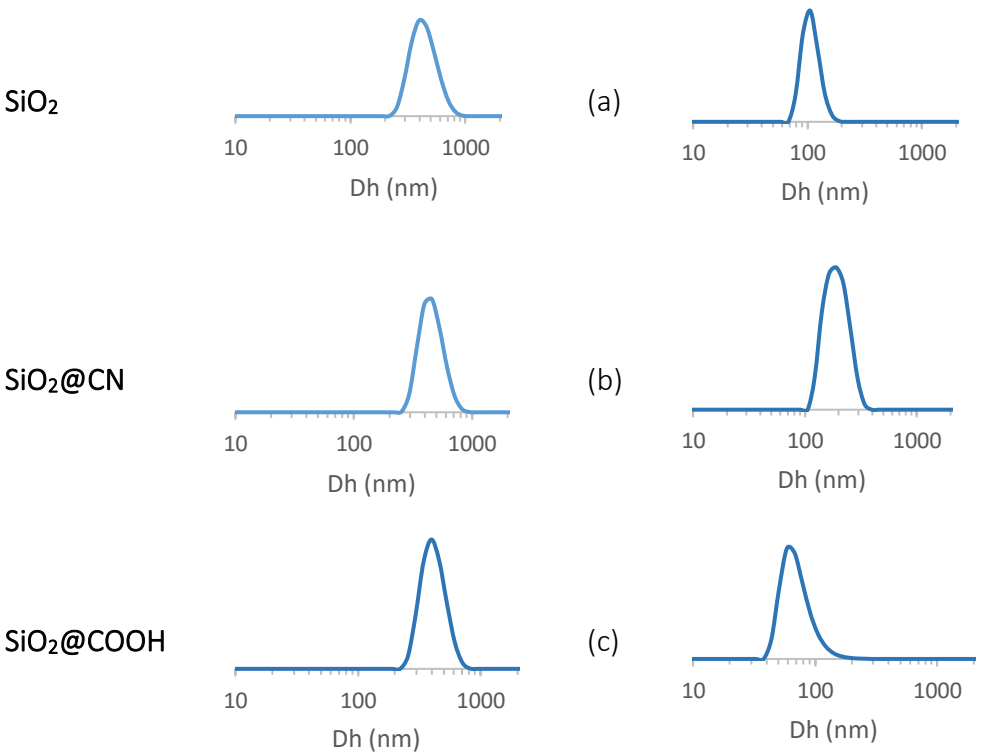

Figure 3 - From up to down - Size (hydrodynamic diameter) distribution (in number) obtained by DLS for **SiO_2** (a), **SiO_2@CN** (b), **SiO_2@COOH** (c) beads from SiO_2 beads done in EtOH (left) and MeOH (right).

3.2.2.2.b. Spectroscopic characterization of the grafting

Infrared spectroscopy

IR spectra of all studied silica nanoparticles (Figure 4) show typical vibration bands in accordance with **SiO_2** at 793 cm^{-1} for Si-O-Si symmetrical vibration, 945 cm^{-1} for Si-OH, 1060 cm^{-1} for Si-O-Si asymmetrical ones, 3700 cm^{-1}-2930 cm^{-1} for-OH in stretching mode. In the case of **SiO_2@CN** vibrations at 2250 cm^{-1} for-CN[29] and 2832 cm^{-1} for-CH stretching mode.[30] The presence of carboxylic functions could be detected *i.e.* C=O for **SiO_2@COOH** at 1712 cm^{-1}.[31]

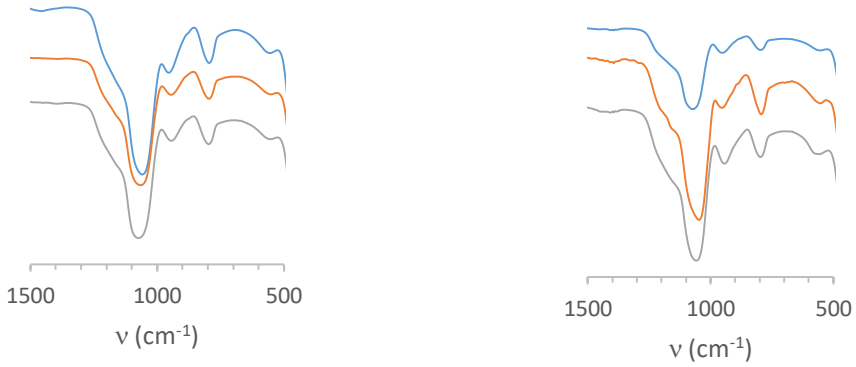

Figure 4- From up to down: Relevant IR vibration zones for **SiO_2**, **SiO_2@CN**, **SiO_2@COOH** beads from SiO_2 beads done in EtOH (left) and MeOH (right).

One interesting feature is that the nature of the starting **SiO_2** does give different intensities for the grafted fragments. Indeed, while it is very easy to observe the vibrations assigned to functions of the grafted organic part with the **SiO_2** beads obtained using methanol as solvent, it is less obvious in the case of ethanol. This phenomenon has to be linked to the size of the particles and the grafting rate.

Due to low loading of grafted functions in the case of **SiO_2@CN** and even lower in **SiO_2@COOH** done in EtOH, the vibrations corresponding to functional groups were observed with difficulty from raw spectra. Those vibrations were observed doing difference spectra between of **SiO_2@CN** and **SiO_2** OR between **SiO_2@COOH** and **SiO_2**, proving the existence of-CN (Figure 5) and-COOH (Figure 6) function groups.

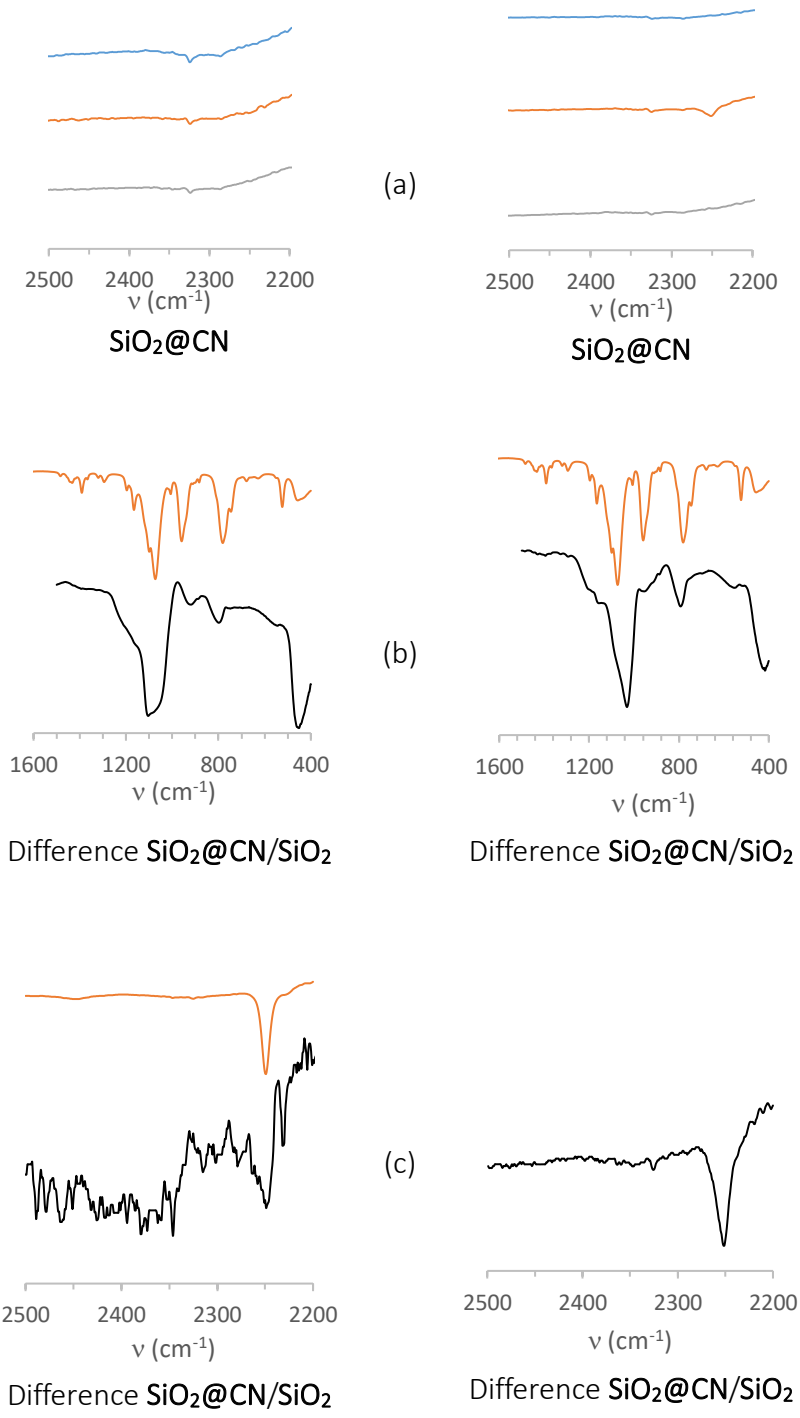

Figure 5 - (a) Raw IR spectrum of **SiO_2**, **SiO_2@CN**, **SiO_2@COOH** in the vibration area of CN for beads from SiO_2 beads done in EtOH (left) and MeOH (right). (b) and (c) Difference spectra (**SiO_2@CN** - **SiO_2**) on specific ranges (in blue). The spectrum of TESPN is indicated in orange in (b) and (c). Left (with SiO_2 done in EtOH), Right (with SiO_2 done in MeOH).

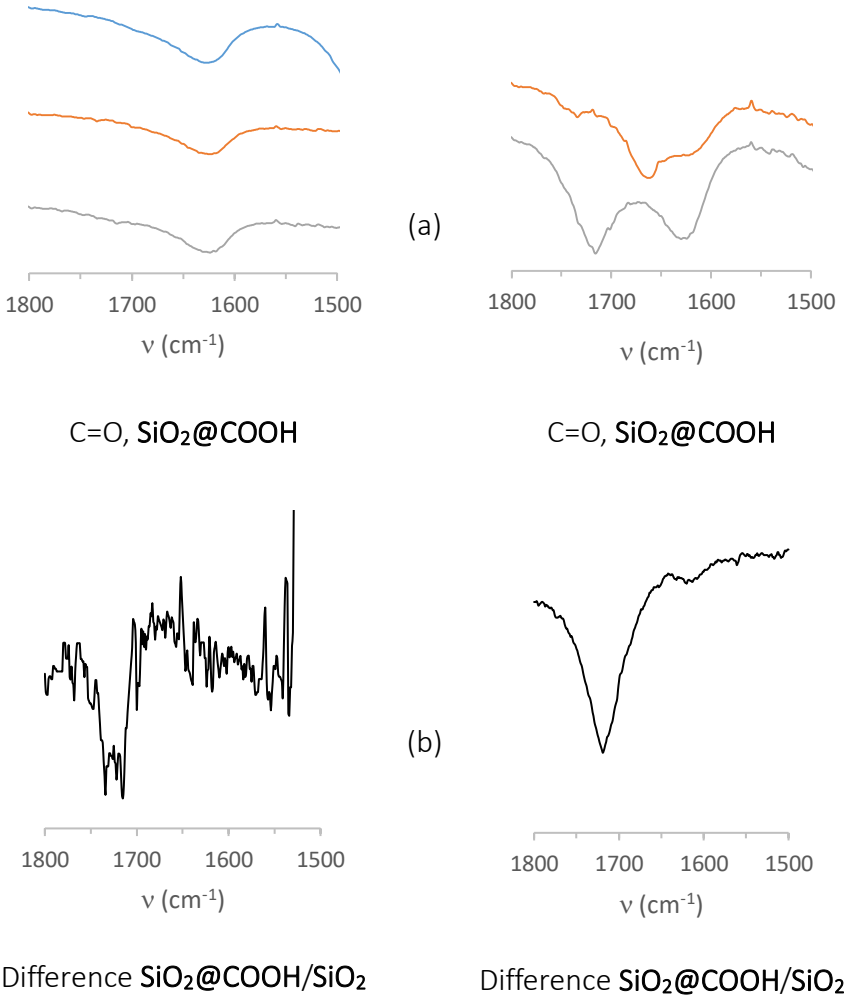

Figure 6 - (a) Raw IR spectrum of **SiO_2**, **SiO_2@CN**, **SiO_2@COOH** in the vibration area of COOH for beads from **SiO_2** beads done in EtOH (left) and MeOH (right). (b) Difference spectra (**SiO_2@COOH** - **SiO_2**) on specific ranges. Left (with **SiO_2** done in EtOH), Right (with **SiO_2** done in MeOH).

3.2.2.2.c. Solid State NMR

IR spectroscopy could give affirmative answers concerning the grafting, but it is not enough to ensure it. To increase the proof about it, Solid State NMR has been an efficient tool. Indeed, ^{1}H, ^{13}C and ^{29}Si are nuclei that can bring numerous interesting information. All data have been summarized in Table 1. Each relevant information will be discussed through nuclei.

^{1}H MAS NMR

The spectra have very large signals that correspond to the different groups on the silica beads, silanols and physiosorbed water molecules (3.5-5 ppm), ethoxy (3.3-3.6 ppm), and methoxy (1.1-1.3 ppm) as well as the CH_2 from the grafted units (0.7-0.9 (Si-CH_2), 6.5-6.8 (CH_2-N) 4.0-4.1 (CH_2)).[32] Unfortunately, signals are quite large and/or overlapped and spectra are simply indicative.

^{13}C CP-MAS NMR

The ^{13}C CP-MAS NMR spectra show the signals corresponding to the organic functions grafted on **SiO_2**, ethoxy functions are present in both **SiO_2** starting beads and also present after grafting. The signals corresponding to the silane with CN function are also visible, as well as for the COOH after the hydrolysis (see Table 1 and Figure 7).[33] This method does confirm the grafting and the transformation of the pending functions.

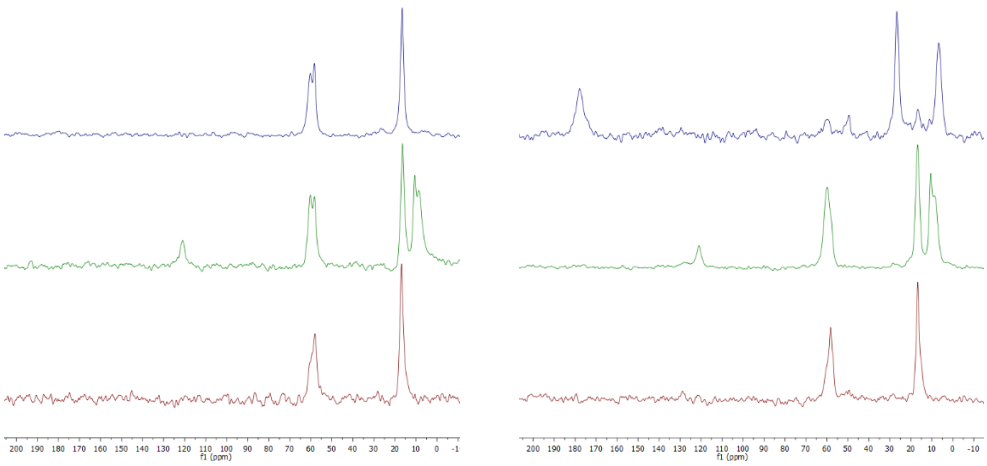

Figure 7 - ^{13}C CP-MAS NMR spectra of **SiO_2** (down), **SiO_2@CN** (middle) and **SiO_2@COOH** (up). For beads from SiO_2 beads done in EtOH (left) and MeOH (right).

Table 1 - Relevant solid-state NMR data.

	Solvent used for the starting beads					
	EtOH			MeOH		
	SiO_2	SiO_2@CN	SiO_2@COOH	SiO_2	SiO_2@CN	SiO_2@COOH
^{1}H MAS						
	6.1 4.7 3.5 1.12 0.05	8.0 7.6 6.8 4.6 4.2 3.5 1.12 0.07	7.4 4.7 4.3 3.6 1.15	0 5.5 3.5 1.0	7.0 4.7 3.6 1.1	6.0, 6.5 3.6 1.05
^{29}Si CP-MAS						
T_2		-62.2	-59.6		-64.7	-58.8
T_3		-70.4	-68.7		-70.5	-68.4
Q_2	-93.3 (5.7)	-92.8 (2.2)	-92.8 (3.5)	-93.3 (5.6)	-93.3 (6.3)	-91.9 (4.4)
Q_3	-101.9 (58.9)	-101.9 (64.5)	-101.9 (65.8)	-101.9 (55.7)	-102.4 (59.8)	-101.8 (66.1)
Q_4	-111.8 (35.4)	-111.9 (33.3)	-111.7 (30.7)	-111.7 (38.7)	-111.7 (33.9)	-111.6 (29.5)
^{29}Si MAS						
Q_2	-93.3 (8.5)	-92.0 (3.4)	-92.5 (2.0)	-93.0 (6.0)	-93.2 (2.5)	-93.7 (8.2)
Q_3	-101.4 (30.6)	-101.4 (25.6)	-101.4 (22.0)	-101.4 (28.7)	-102.5 (33.0)	-101.9 (28.9)
Q_4	-111.5 (60.9)	-111.3 (71.0)	-111.6 (76.0)	-111.8 (65.3)	-111.4 (64.5)	-111.5 (62.9)
^{13}C CP MAS						
CN		120.9			121.0	
COOH						177.9
CH_2O		60.2	60.0			
CH_2O	58.0	58.1	58.3	58.2	59.9	59.9
CH_2O						49.5
CH_3	16.9	16.4	16.6	16.7	16.8	16.7
CH_2Si		10.6			10.5	
CH_2Si		8.8			8.8	6.7

^{29}Si CP MAS NMR

The ^{29}Si CP MAS NMR spectra gave informations about the grafting (Table 1 and Figure 8). In all spectra, the signals at -93, -101 and -111 ppm corresponding to Q_2, Q_3 and Q_4 respectively (Q_n= $Si(OSi)_n(OH)_{4-n}$) are in accordance with SiO_2 core.[34] The grafting was proved by two signals at around -60 and -70 ppm (T_2 and T_3).[35] A change in the proportion of the signals was observed from **SiO_2** to **SiO_2@CN** and from **SiO_2@CN** to **SiO_2@COOH**, the trend being identical with the starting **SiO_2** beads, being done in ethanol or methanol. Since ^{29}Si CP MAS NMR spectra could not be used to quantify the Q_n, the deconvolutions were done on MAS spectra (Figure 9). The intensity distribution is summarized on table 1.

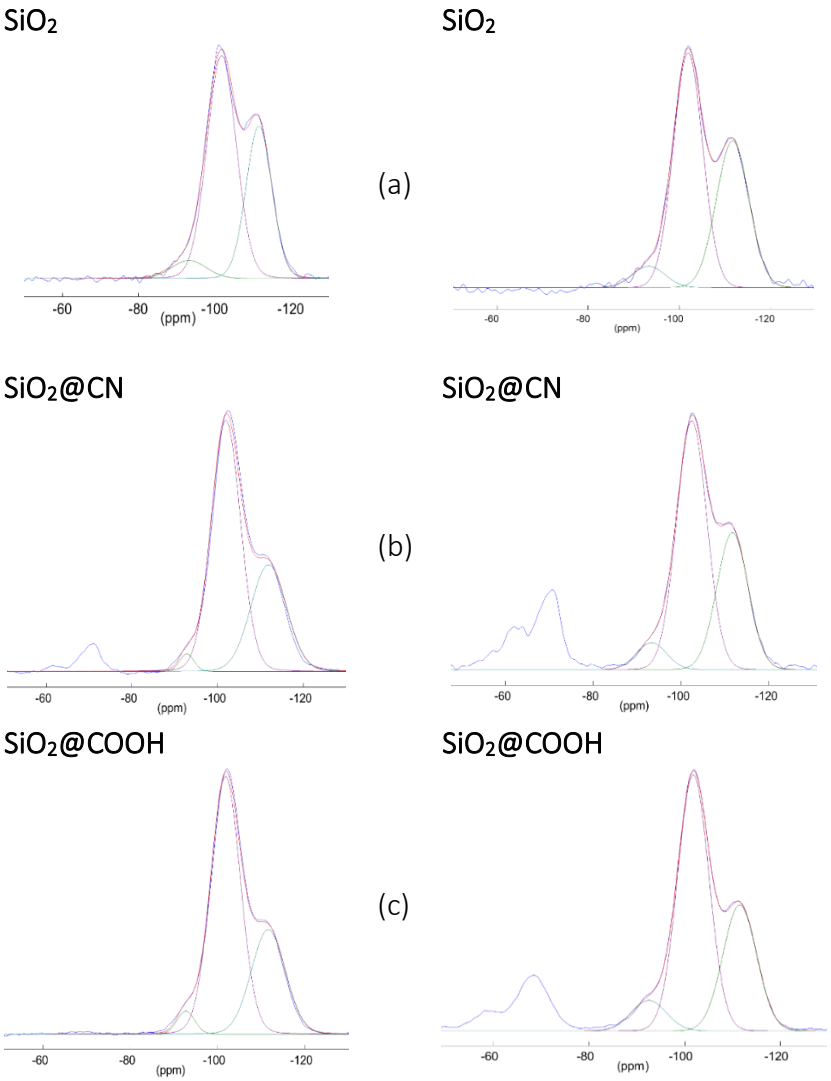

Figure 8 - ^{29}Si CP MAS NMR spectra of **SiO_2** (a) **SiO_2@CN** (b), **SiO_2@COOH** (c) from SiO_2 beads done in EtOH (left) and MeOH (right).

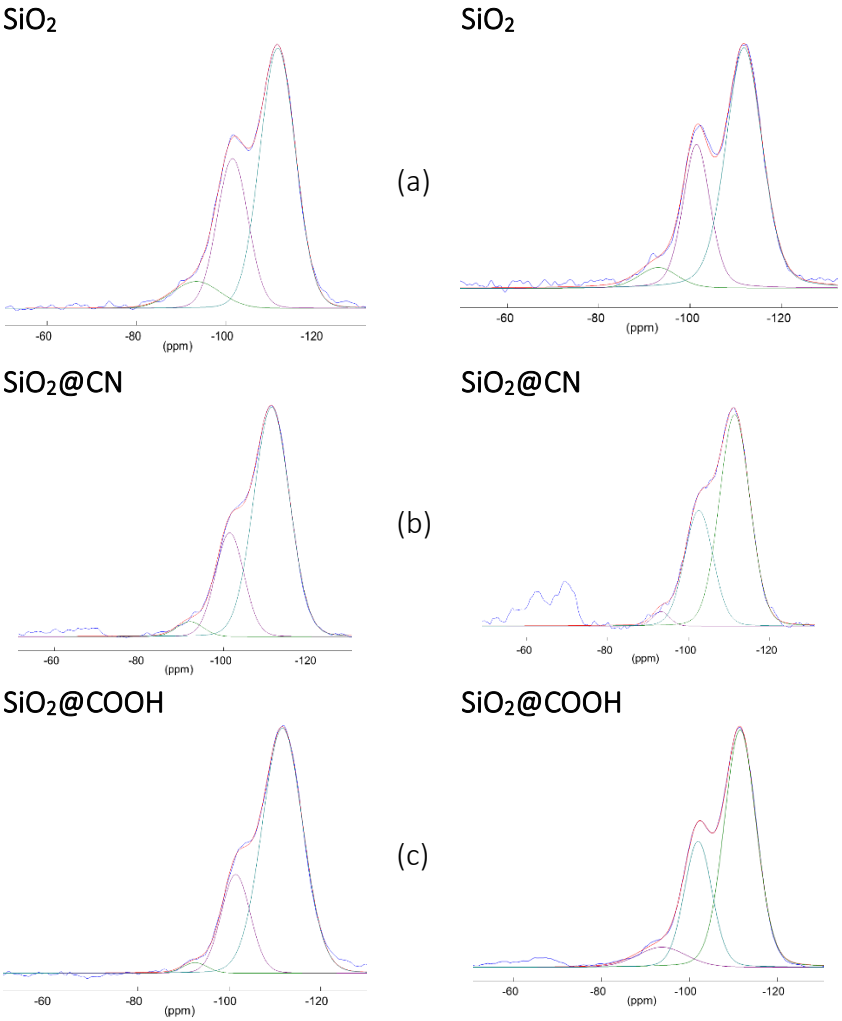

Figure 9 - ^{29}Si MAS NMR spectra of **SiO_2** (up) **SiO_2@CN** (middle), **SiO_2@COOH** (down) from SiO_2 beads done in EtOH (left) and MeOH (right).

The solid-state NMR showed that the **SiO_2** beads contain some ethoxy functions (although dried under vacuum) and those functions remain even when the grafting occurs. ^{29}Si NMR spectra exhibit a change of the nature of the silicon atoms, in relationship with the grafting. But, in order to use those beads in a more precise and quantitative way, it was important to quantify the nature of the grafted functions at the surface, having thus different parameters (surface coverage, etc.).

3.2.2.2.d. Quantification by NMR ^{1}H

Usually, elemental analysis can give the elemental composition of a sample. When systems are “unique” or simple, a simple analysis can give an accurate information. In the case of those silica beads, the system, as it has been showed in multinuclear MAS NMR, is more complicated and the elemental analysis would not give reliable results. One elegant method has been developed by one research group,[14a] taking into account that silica can be dissolved in very alkaline medium into silicates. By this method, the organic fragments remain untransformed and it is easy to quantify them by ^{1}H NMR in solution, using an internal standard (benzoic acid in this case, stable in very basic solution as benzoate and soluble in the solution)

Thus, a known mass of sample of silica beads was dissolved in strong alkaline deuterated aqueous solution (pH≈13) and analyzed by ^{1}H NMR using a known mass of benzoic acid as internal reference.

The comparison of the integrations could give a number of moles of functions per gram of silica beads.

This measurement has been done with **SiO_2**, **SiO_2@CN** and **SiO_2@COOH**.

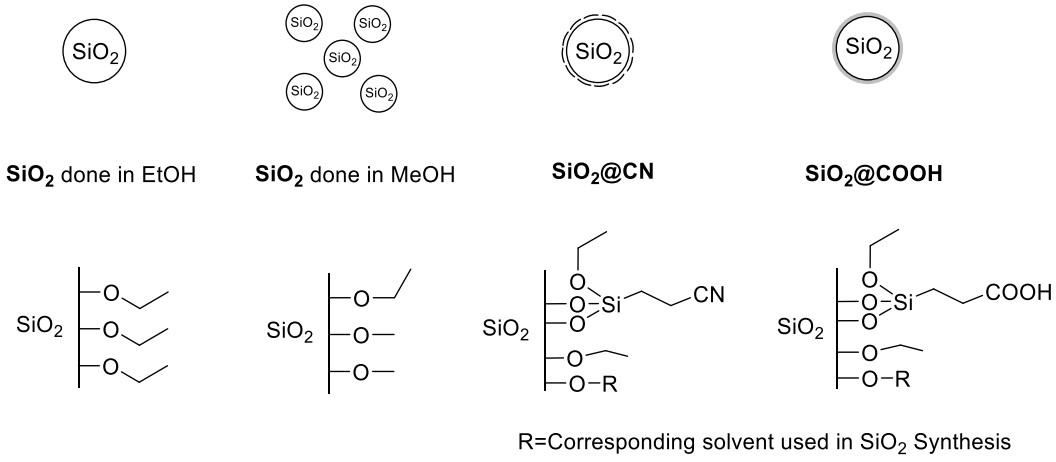

Scheme 4- Schematic functions on the silica beads.

In the basic solutions, signals corresponding to ethanol and methanol peaks are related to all the alkoxy functions present in the reaction media, from TEOS to TESPN. All the other CH_2 signals related to the non-alkoxy part of TESPN and the corresponding oxidized one. The ^{1}H NMR shifts have been presented in the Table 2.

Table 2- ^{1}H NMR chemical shifts (in ppm) observed with **SiO_2**, **SiO_2@CN** and **SiO_2@COOH** in D_2O/NaOH (pH=13) solution.

Solvent used in synthesis	S	EtOH		MeOH	$Si(CH_2)_2CN$		$Si(CH_2)_2COOH$	
		CH_2	CH_3	CH_3	CH_2	CH_2	CH_2	CH_2
Ethanol	**SiO_2**	3.3	0.9	-	-	-	-	-
	SiO_2@CN	3.4	1.0	-	0.4-0.6	1.9-2.3	-	-
	SiO_2@COOH	3.3	0.9		-	-	0.4	1.9
Methanol	**SiO_2**	3.4	0.9	3.1	-	-	-	-
	SiO_2@CN	3.4	1.0	3.1	0.4-0.6	1.9-2.3	-	-
	SiO_2@COOH	3.4	1.0	3.1	-	-	0.5	2.0

The number of functions n(f) has been calculated based on results of ^{1}H NMR integrations with presence of a known mass of internal standard, m(ref), here the benzoic acid. The calculation used the integration of protons signals from benzoic acid I(ref) and integration of specific signals I(f) coming from the organic parts grafted on **SiO_2**. From the n(f) value, the density of f functions per mass of sample ρ(f) was defined according to the mass of SiO_2 sample (m_S) using equation 1. Results were collected in Table 3.

$$\rho(f) = \frac{n(f)}{m_S} = \frac{I(f)}{m_S} \cdot \frac{n(ref)}{I(ref)} = \frac{I(f)}{m_S} \cdot \frac{m(ref)}{M(ref)} \cdot \frac{1}{I(ref)} \quad (1)$$

Table 3- number Functions (F) (mmol) per g sample, calculated by ^{1}H NMR.

Solvent used in synthesis	S	ρ(f) (mmol F/g S)			
		OCH_2CH_3	OCH_3	CN	COOH
Ethanol	**SiO_2**	0.43	-	-	-
	SiO_2@CN	0.64		0.29	
	SiO_2@COOH	0.45			0.04
Methanol	**SiO_2**	1.18	0.05	-	-
	SiO_2@CN	1.85	0.04	1.40	-
	SiO_2@COOH	0.08	0.05	-	039

The results showed, as it was observed in MAS NMR that-O-CH_2-CH_3 fragments were present on starting **SiO_2**, with higher content per gram of sample with the beads formed in MeOH (smaller size).[36] The functionalization was, for the same reason, higher per gram of sample in the case of **SiO_2@CN** when done in MeOH. From **SiO_2@CN** to **SiO_2@COOH**, the hydrolysis removed a substantial part of the "grafted" functions in both cases. Most of these functions might be destroyed/removed by high concentration of sulfuric acid (65 wt.%).

3.2.2.2.e. Determination function coverage of functionalized silica beads

Using several informations obtained through the different techniques, it is possible to calculate the function coverage density (in mol/nm^2) of the silica beads that will be an important parameter within the catalytic part. The parameter μ(f) can be defined in mmol/m^2 but the easiest representation is the number of groups per nm^2. It could be determined by the equation A[14a] According to the number of functions found in section 3.2.2.2.d. through the quantification method but adapted for the silica core only (equation 2) and the average radius of the **SiO_2** beads (r_{core}) deduced from TEM measurements, the formula was demonstrated with a core mass (m_{core}) of 1g.

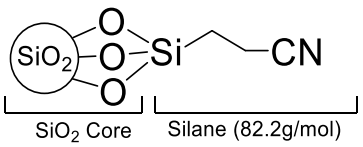

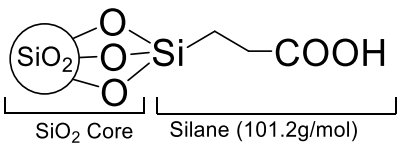

$$\rho'(f) = \frac{n(f)}{m_{core}} \ (mol.g^{-1}) \qquad (2)$$

The parameter to determine is μ_f , i.e. the number of molecules n_f present on 1g of the sample surface ΣS_{core} (in nm^2))

$$\mu(f) = \frac{n(f)}{\Sigma S_{core}} \times N_A \ (number\ f.nm^{-2}) \qquad (A)$$

The total surface (ΣS_{core}) (in nm^2) and volume (ΣV_{core}) (in nm^3) of 1 g of beads sample is related to the number of beads contained in one gram (N_{core}) multiplied by the surface (S_{core}), the volume (V_{core}) of a spherical bead of average radius (r_{core}) deduced from TEM measurements.

$$\Sigma S_{core} = N_{core}.S_{core} \qquad \Sigma V_{core} = N_{core}.V_{core}$$

$$S_{sph} = 4\pi r_{core}^2 \qquad V_{sph} = \frac{4}{3}\pi r_{core}^3$$

The number of spheres (N_{sph}) present in one gram of S can be extracted from the equation while the total volume of sample (ΣV_S) contained in 1g of sample S (expressed in nm^3) can be deduced from the density of non-porous SiO_2 (ρ_{SiO2}=1.6g.cm^{-3}).[37]

$$N_{core} = \frac{\Sigma V_{core}}{V_{core}}$$

$$\Sigma V_{core} = \frac{1}{\rho_{SiO_2}} \times 10^{+21}$$

The formula A can be completed

$$\mu(f) = \frac{n(f)}{\Sigma S_{core}} N_A = \frac{n(f)}{N_{core}.S_{core}} N_A = \frac{n(f)}{\frac{\Sigma V_{core}}{V_{core}} S_{core}} N_A = \frac{n(f).V_{core}}{\Sigma V_{core}.S_{core}} N_A$$

$$\mu(f) = \frac{\rho'(f).\frac{4}{3}\pi r_{core}^3}{\frac{10^{+21}}{\rho_{SiO_2}}.4\pi r_{core}^2} N_A = \frac{\rho'(f).r_{core}.\rho_{SiO_2}}{3\times 10^{+21}} \times N_A$$

$$\mu(f) = \frac{\rho'(f).r_{core}.\rho_{SiO_2}}{3\times 10^{+21}} \times N_A$$

The ρ'(f) does correspond to the number of functions grafted on the "naked" silica bead; Indeed, ρ(CN) (for **SiO_2@CN**) and ρ(COOH) (for **SiO_2@COOH**) do contain the mass of grafted silanes for **SiO_2@CN** and **SiO_2@COOH** in one gram sample.

$$\rho'(f) = \frac{n(f)}{m_{SiO_2}} = \frac{n(f)}{m_{SiO_2@f} - m_{silane}}$$

In the case of 1g of **SiO_2@f**

$$n(f) = \rho(f)\ (f = CN, COOH)$$

$$m_{silane} = \rho(f).M_{Silane}$$

$$\rho'(f) = \frac{n(f)}{m_{SiO_2}} = \frac{n(f)}{m_{SiO_2@f} - m_{silane}}$$

$$\rho'(f) = \frac{\rho(f)}{1 - \rho(f).M_{Silane}}$$

Using this formula, coverages of the beads by the CN and COOH containing fragments have been calculated and presented in Table 4. Concerning the **SiO_2@CN**, the μ(CN) value is very high (>17) and seems to confirm the multilayer deposition hypothesis. The μ(COOH) values found (around 3) for **SiO_2@COOH** are in agreement with what is expected with monolayers. This validates the different hypotheses assumed.

Table 4- number Function (mol) per nm² core (μ(f)).

Solvent used for SiO_2 synthesis	SiO_2@CN	SiO_2@COOH
Ethanol	20.6	2.8
Methanol	16.6	3.3

3.2.3. Oxidation catalysis with BPMEN (L^3) based metal complexes. Replacement of CH_3COOH by SiO_2@COOH

The BPMEN related complexes were tested on three different substrates (cyclooctene: CO, cyclohexene: CH, and cyclohexanol: CYol) and with two different co-reagents, CH_3COOH (in order to use the results as reference) or SiO_2@COOH under the same experimental conditions. The catalytic study presented herein will be divided according to the substrates.

Homogenous catalysis of L^3 complexes have been all tested under the classical homogeneous conditions (using acetic acid as co-reagent) and the influence of metal and anion has been studied. The reactivity under homogeneous conditions will be compared with the processes using SiO_2@COOH beads instead of acetic acid.
These complexes were tested in two types of catalyzed oxidations:

- olefin epoxidation
- alcohol oxidation

As these two reactions have two different mechanisms, it is very interesting to know the activity in both reactions. For this reason, cyclooctene (CO) was chosen as standard model for the epoxidation, while the study of the (ep)oxidation of cyclohexene (CH) and oxidation of cyclohexanol (CYol) were studied for their potential applied interest towards the synthesis of adipic acid, both being starting reagents in different processes.[11a-b,38]

Reaction conditions under homogeneous catalysis were already described in different articles.[10a, 39] To prevent the disproportionation [40] of H_2O_2 and Fenton reaction,[41] H_2O_2 was slowly added during two hours[42] (especially in the case of Fe complex)[43] and all reactions were performed at 0°C using CH_3CN as solvent. Therefore, in our case, the classical conditions (0°C Cat./Substrate/H_2O_2/CH_3COOH = 1/100/130/1400) have been slightly modified for all substrates (CO, CH, CYol) as followed

Cat./Substrate/H_2O_2/CH_3COOH = 1/100/150/1400

The reactions were stopped after 3 hours. The reaction was followed by GC-FID using acetophenone as internal standard.

3.2.3.1. Oxidation of cyclooctene

Role of acetic acid

To prove the need of carboxylic function as co-reagent in this catalysis, some tests with all complexes were done in absence of CH_3COOH. Results have been compiled in Table 5. While no CO conversion was observed with the [(**L**^{3})$FeCl_2$]($FeCl_4$), complexes (**L**^{3})$MnCl_2$, (**L**^{3})$Mn(OTf)_2$ and (**L**^{3})Mn(*p*-Ts)$_2$ were poorly active These results showed the necessity of carboxylic function for this reaction. All complexes were then tested in presence of a co-reagent, either acetic acid either the **SiO_2@COOH** (taking into account the bead sizes) under identical experimental conditions.

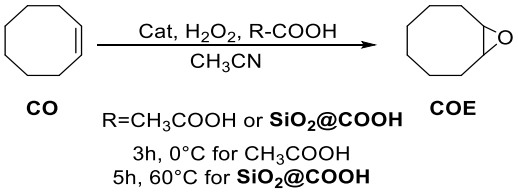

Scheme 5- Catalysis oxidation of cyclooctene.

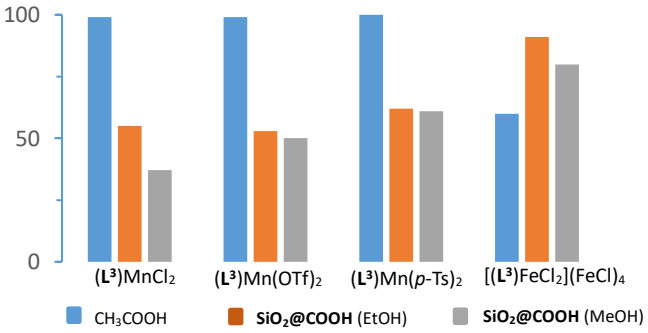

Figure 10 –Comparison of CO conversion between different catalysts and different conditions.

*CH_3COOH vs. **SiO_2@COOH***

In presence of the co-reagent, in all experimental conditions (Scheme 5), all catalysts could achieve conversion of the CO, the best conditions being in presence of acetic acid for all manganese complexes, while the conversion was better in presence of **SiO_2@COOH** in the case of the iron complex (Table 5 and Figure 10).

This lower conversion in presence of **SiO_2@COOH** beads for the manganese complexes seems to be due to the heterogeneous character of the reaction, phenomenon classically observed. COE was the only product observed by GC-FID. The low selectivity towards COE in presence of complexes (**L**^{3})$Mn(OTf)_2$, (**L**^{3})Mn(*p*-Ts)$_2$ and [(**L**^{3})$FeCl_2$]($FeCl_4$), might be due to the formation of cyclooctane-1,2-diol then the subsequent opening ring reaction conduct to suberic acid.[44] These two products could not be observed by GC-FID using the method we developed to follow this reaction.

Effect of anion with CH_3COOH as co-reagent

Using CH_3COOH as a co-reagent (Table 5 and Figure 10), similar results were found for complexes (L^3)$MnCl_2$ and (L^3)$Mn(OTf)_2$ than the ones found in literature.[1c] The manganese complexes (L^3)$MnCl_2$, (L^3)$Mn(OTf)_2$ and (L^3)Mn(*p*-Ts)$_2$ gave a conversion of CO > 99%. However, the selectivity towards COE with (L^3)$Mn(OTf)_2$ and (L^3)Mn(*p*-Ts)$_2$ were around 60%, lower than (L^3)$MnCl_2$ (81%). With those results, it can be concluded that the anion has an influence on the selectivity towards COE. It might due to the different acidity of the anion, the chloride being less basic than the two other ones. As pointed out previously, the ring opening might occur in presence of acid or base, and it is certainly what does happen here.

Table 5 - Relevant data for the catalyzed epoxidation of CO.[a]

Catalyst	RCOOH	CO	COE		TON[4]
		Conv[b]	Sel[c].	Yield[d]	TON[e]
(L^3)$MnCl_2$	no	1	-	-	-
	CH_3COOH	99	81	81	100
	SiO_2@COOH(MeOH)	37	9	4	38
	SiO_2@COOH(EtOH)	55	26	14	55
(L^3)$Mn(OTf)_2$	no	5	7	<1	3
	CH_3COOH	99	54	54	99
	SiO_2@COOH(MeOH)	50	45	23	50
	SiO_2@COOH(EtOH)	53	43	23	52
(L^3)Mn(*p*-Ts)$_2$	no	5	50	2.7	6
	CH_3COOH	100	62	62	100
	SiO_2@COOH(MeOH)	61	30	19	61
	SiO_2@COOH(EtOH)	62	28	23	62
[(L^3)$FeCl_2$]($FeCl_4$)	no	0	-	-	-
	CH_3COOH	60	21	13	60
	SiO_2@COOH(MeOH)	80	31	25	80
	SiO_2@COOH(EtOH)	91	25	23	91

[a] Experimental conditions: 0°C with CH_3COOH, 60°C with **SiO_2@COOH**.

Cat. /H_2O_2/CO/CH_3COOH=1/150/100/1400 for CH_3COOH, t=3h;

Cat. /H_2O_2/CO/-OOH=1/150/100/14 for **SiO_2@COOH**; t=5h.

[b] n CO converted/n_{CO} engaged (in%) at the end of the reaction.

[c] n COE formed/ n CO converted at the end of the reaction

[d] n COE formed /n CO engaged at the end of the reaction

[e] n CO transformed /n [cat] at the end of the reaction

*Effect of anion with **SiO_2@COOH** beads as co-reagent*

The use of **SiO_2@COOH** beads as co reagents gave in case of the manganese complexes a reverse effect (Table 5 and Figure 10). Indeed, the conversion follows the order *p*-Ts > OTf> Cl according to the anion, with a selectivity towards COE in favor of the triflate, followed by the *p*-Ts and finally the chloride salt. In the case of the two stronger coordinating anions, the effect of the bead size is negligible while a stronger difference is observed with the chloride salt, giving lower selectivity towards COE. This

could be explained by the effect of the anion. Indeed, the easily protonable anions might deprotonate easier the carboxylic functions present at the surface of the silica bead, promoting the mechanism towards the cyclooctene conversion. In addition, those anions are less linked to the metal than the chlorides, and this favors even better the reactivity.

3.2.3.2. Catalysis oxidation of cyclohexene

The cyclohexene (CH) is a very interesting substrate in terms of application since it can be one starting material for the synthesis of adipic acid.[38b] In addition, in terms of reactivity, at the difference with CO, the (ep)oxidation of CH is more complex. Indeed, according to the nature of the metal used within the reaction but also the nature of the cycle, two types of oxidations are possible: the allylic oxidation occurring on sp^3 C-H bonds and the epoxidation on the C=C double bond.[45] Other water addition and/or subsequent oxidation can occur and give a complex mixture. Several products such as cyclohexene oxide (CHO), cyclohexanediol (CHD), cyclohexene-1-ol (CHol) and cyclohexen-1-one (CHone) are the most common ones observed (see Scheme 6). The results in terms of conversion of CH, selectivity towards the substrates presented in Scheme 6 and TON have been compiled in Table 6 and Figure 11.

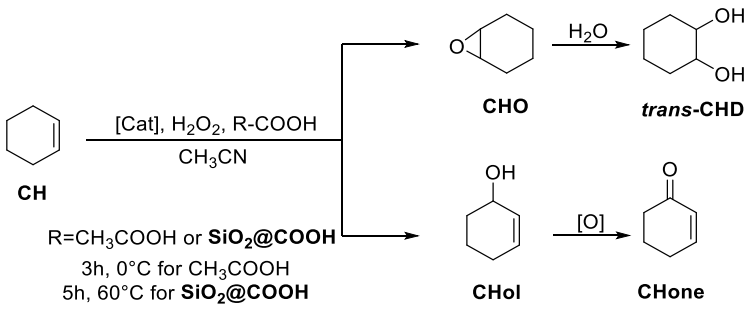

Scheme 6- catalysis oxidation of cyclohexene.

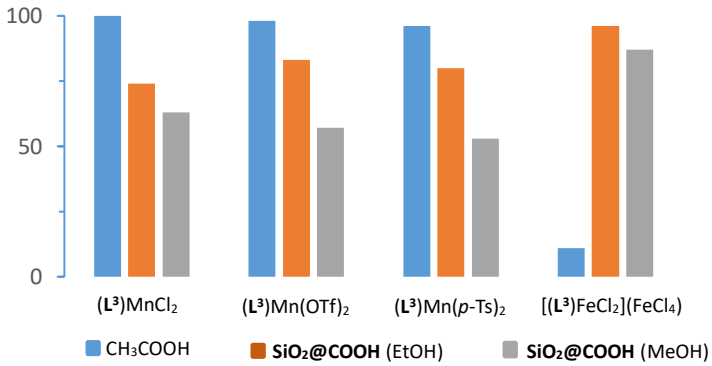

Figure 11 – Comparison of conversion of CH between different catalysts and different co-reagents. Reaction time: 3h with CH_3COOH, 5h with **SiO_2@COOH**.

*Manganese complexes- CH_3COOH vs. **SiO_2@COOH** / Effect of the anion*

All manganese complexes exhibited a high CH conversion in presence of CH_3COOH and the resulted products that could be analyzed are depending on the nature of the anion. While (L^3)$MnCl_2$ gave exclusively the epoxide (CHO) with a relative good selectivity (89%), the (L^3)$Mn(OTf)_2$ and (L^3)$Mn(p\text{-}Ts)_2$ gave a small quantity of CHD (due to CHO opening with water) and CHone (coming from allylic oxidation oxidation).

When **SiO_2@COOH** beads are used, the CH conversions are lower, CHO being the only product detected with (L^3)$Mn(OTf)_2$ and (L^3)$Mn(p\text{-}Ts)_2$. (L^3)$MnCl_2$ does show a part of ring opening (presence of CHD) with the beads done in EtOH and allylic oxidation (presence of CHol and Chone) with the beads done in MeOH.

From those observations, it seems that the presence of CH_3COOH or **SiO_2@COOH** have reverse effects in terms of selectivity according to the nature of the anion of the Mn complex. This has certainly to be linked to the mechanism occurring between the manganese complex and the co-reagent linked to the nature of the interaction between the anion and the "MnL" part.

Iron complex

With the [(L^3)$FeCl_2$]$FeCl_4$ complex, the mechanism seems to be radically different since the reaction with CH_3COOH as co-reagent did not give any expected product (although a slight conversion was observed). Surprisingly, the use of **SiO_2@COOH** as co reagent did improve the CH conversion but not in a selective way since products originating from epoxidation and allylic oxidation were observed in almost equal quantities.

Table 6 - Relevant data for the catalyzed (ep)oxidation of cyclohexene. [a]

Cat.	R-COOH	Conv[b].	Selectivity[c]				TON[d]
		CH	CHO	CHD	CHol	CHone	
(L^3)$MnCl_2$	CH_3COOH	100	89	0	0	0	100
	SiO_2@COOH(MeOH)	63	3.3	0	2	2	63
	SiO_2@COOH(EtOH)	74	14	23	0	0	74
(L^3)$Mn(OTf)_2$	CH_3COOH	98	57	3	0	1	98
	SiO_2@COOH(MeOH)	57	13	0	0	0	56
	SiO_2@COOH(EtOH)	83	27	0	0	0	83
(L^3)$Mn(p\text{-}Ts)_2$	CH_3COOH	96	68	2	0	2	96
	SiO_2@COOH(MeOH)	53	16	0	0	0	53
	SiO_2@COOH(EtOH)	80	28	0	0	0	80
[(L^3)$FeCl_2$]($FeCl_4$)	CH_3COOH	11	0	0	0	0	11
	SiO_2@COOH(MeOH)	87	9	23	6	17	86
	SiO_2@COOH(EtOH)	96	4	5	0	9	96

[a] Conditions: 0°C for the case with CH_3COOH, 60°C for the case with **SiO_2@COOH**.

Cat. /H_2O_2/CH/CH_3COOH=1/150/100/1400 for CH_3COOH, t=3h;

Cat. /H_2O_2/CH/-OOH=1/150/100/14 for **SiO_2@COOH**; t=5h.

[b] n CH converted/n CH engaged (in%) after 3h. for CH_3COOH, 5h for **SiO_2@COOH**. [c] n product formed/ n CH converted at 3h. for CH_3COOH, 5h for **SiO_2@COOH**. [d] n CH transformed /n[Cat] at 3h. for CH_3COOH, 5h for **SiO_2@COOH**.

3.2.3.3. Catalysis oxidation of cyclohexanol.

The cyclohexanol (CYol) is also a very interesting substrate in terms of application since it can be one starting material of the KA oil used for the synthesis of adipic acid.[46] In addition, in terms of reactivity, at the difference with CH, the oxidation of CYol is very simple and only one product is expected, i.e. cyclohexanone (CYone) (see scheme 7). Catalyzed oxidation of cyclohexanol followed the same procedure than catalytic oxidation of CO and CH. Results have been compiled in Figure 12 and Table 7.

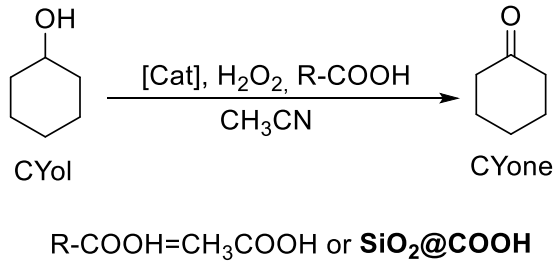

R-COOH=CH_3COOH or **SiO_2@COOH**

Scheme 7- Catalysis oxidation of cyclohexanol.

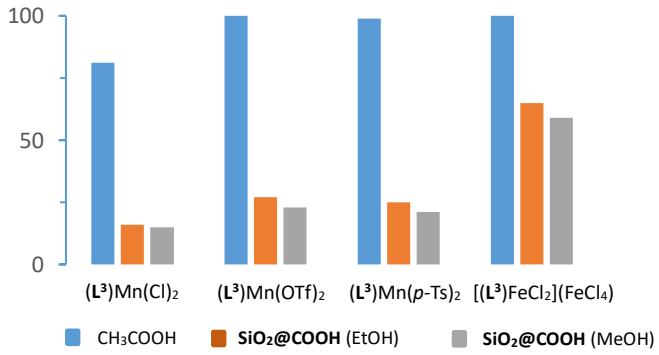

Figure 12 - Comparison of CYol conversion between different catalysts and different co-reagents. Reaction time: 3h with CH_3COOH, 5h with **SiO_2@COOH**.

CH_3COOH vs. ***SiO_2@COOH*** */ Effect of the anion*

With all studied complexes, in presence of CH_3COOH, the conversion of CYol was very high with a very high selectivity towards CYone (the only product observed in GC).[47] (L^3)Mn(OTf)$_2$ and (L^3)Mn(*p*-Ts)$_2$ complexes are more active than (L^3)$MnCl_2$. It might be due to the strength of metal – anion bond and/or to the acid strength of the anion, according to the postulated mechanisms described in literature. The free coordination site in (L^3)Mn(OTf)$_2$ and (L^3)Mn(*p*-Ts)$_2$ being more accessible than (L^3)$MnCl_2$, peroxide and carboxylic function might reach easier the metal center.

Due to the heterogeneous nature of the **SiO_2@COOH** reagent, the conversion in its presence is lower in all the cases. Some differences appear in terms of selectivity, that could be due to the nature of the anion within the complexes (in the case of the manganese complexes) and/or to the nature of the metal in the case of the iron complex.

Table 7 - Relevant data for the catalysed oxidation of cyclohexanol. [a]

Catalyst	R-COOH	CYol	CYone		TON[e]
		Conv[b]	Sel[c].	Yield[d]	
	CH_3COOH	81	91	74	81
(L^3)$MnCl_2$	**SiO_2@COOH**(MeOH)	15	46	7	15
	SiO_2@COOH(EtOH)	16	90	14	16
	CH_3COOH	100	79	79	100
(L^3)$Mn(OTf)_2$	**SiO_2@COOH**(MeOH)	23	90	21	23
	SiO_2@COOH(EtOH)	27	87	24	27
	CH_3COOH	99	85	85	99
(L^3)$Mn(p\text{-}Ts)_2$	**SiO_2@COOH**(MeOH)	21	97	21	21
	SiO_2@COOH(EtOH)	25	87	22	25
	CH_3COOH	100	79	79	99
[(L^3)$FeCl_2$]($FeCl_4$)	**SiO_2@COOH**(MeOH)	59	45	27	59
	SiO_2@COOH(EtOH)	65	36	23	65

[a]Conditions: 0°C for the case with CH^3COOH, 60°C for the case with **SiO_2@COOH**

Cat. /H_2O_2/CYol/CH_3COOH=1/150/100/1400 for CH_3COOH, t=3h;

Cat. /H_2O_2/ CYol/-OOH=1/150/100/14 for **SiO_2@COOH**; t=5h.

[b] n CYol converted/n CYol engaged (in%) after 3h. for CH_3COOH, 5h for **SiO_2@COOH**.

[c] n CYone formed/ n CYol converted at 3h. for CH_3COOH, 5h for **SiO_2@COOH**.

[d] n CYone formed/ n CYol engaged at 3h. for CH_3COOH, 5h for **SiO_2@COOH**.

[e] n CYol transformed /n[Cat] at 3h. for CH_3COOH, 5h for **SiO_2@COOH**.

3.3. Conclusion

It has been possible to replace acetic acid by silica beads with carboxylic functions in the reaction of epoxidation of olefins. The study showed lower activity with the silica beads with Mn complexes in the case of cyclooctene and cyclohexene and selectivity seems to be linked to the nature of the ion of the complex. With cyclohexene, the activity with beads is higher relatively to cyclooctene. However, for the Fe complex, the beads are more active than with acetic acid. With cyclohexanol, the process works much better with acetic acid. The size of the bead does seem to have no relevant effect in terms of efficiency, except that the quantity of carboxylic functions brought in the reaction is 100 times less that the quantity of acetic acid. It has to be noticed that under lower quantity of acetic acid, the reaction did not work. Although less active, this method is the first step towards the replacement of an organic volatile reagent.

3.4. Experimental part

3.4.1. Materials

All manipulations were carried out under air. Distilled water was used directly from a Milli-Q purification system (Millipore). Acetonitrile, ethanol, methanol (synthesis grade, Aldrich) were used as solvents and employed as received. Tetraethyl orthosilicate (TEOS, 98% Aldrich), Ammonium hydroxide solution (25%, Aldrich), 3-(Triethoxysilyl)propionitrile (97%, Aldrich), *cis*-cyclooctene (95%, Alfa Aesar), cyclooctene oxide (99%, Aldrich), cyclohexene (99%, Acros), cyclohexene oxide (98%, Aldrich), 2-cyclohexen-1-ol (95%, TCI), 2-cyclohexen-1-one (96%, TCI), *cis*-1,2-cyclohexanediol (99%, Acros), cyclohexanol (99%, Alfa Aesar), cyclohexanone (99.8%, Acros) and TBHP (70% in water, Aldrich) were used as received.

3.4.2. Methods

Dynamic Light Scattering: Preparation sample: in order to be able to obtain repetitive and correct data analysis, particle samples were prepared at 0.1 wt.% in water. A sonication of the particles suspension was made before DLS analysis during 5 min at 350 W (FB705 Fisherbrand Ultrasonic Processor), facilitating the dispersion of Silica Particles. Hydrodynamic diameters of the particles in suspension were obtained with a ZetaSizer Nano-ZS (Malvern Instruments Ltd). This equipment uses a laser (He-Ne at λ=633 nm, under voltage of 3 mV) and the detector is located at 173° to analyse the scattered intensity fluctuations. 10 mg of particles were dispersed inside 20 mL of water with the ultrasonic processor40 (5 min, 350 W) prior to the measurement performed at a temperature of 25 °C.

TEM: Particles morphology were performed with a JEOL JEM1011 transmission electron microscope equipped with 100 kV voltage acceleration and tungsten filament (Service Commun de Microscopie Electronique TEMSCAN, Centre de Microcaractérisation Raimond Castaing, Toulouse, France). A drop of sonicated particles solution (at 0.1 wt.% in water) was disposed on a formvar/carbon-coated copper grid (400 mesh) and dried in air for 48 h.

Infrared spectroscopy: Fourier Transform infrared (FTIR) spectres were recorded by Spectrum two – PerkinElmer.

Solid state NMR: NMR experiments were recorded on Bruker Avance 400 III HD spectrometers operating at magnetic fields of 9.4 T. Samples were packed into 4mm zirconia rotors. The rotors were spun at 8 kHz at 293K. ^{1}H MAS was performed with DEPTH pulse sequence and a relaxation delay of 3 s. For ^{29}Si MAS single pulse experiments, small flip angle of 30° were used with a recycle delays of 60 s. ^{13}C CP and ^{29}Si CP MAS spectra were recorded with a recycle delay of 2 s and contact times of 3 ms and 4 ms, respectively. Chemical shifts were referenced to TMS. All spectra were fitted using the DMfit software.

Liquid state NMR: ^{1}H-NMR and ^{13}C-NMR spectres were recorded on Bruker NMR III HD 400 MHz spectrometers. 400 MHz for ^{1}H-NMR, and 101 MHz for ^{13}C-NMR.

Quantification of the number of functions per gram of grafted silica through ^{1}H NMR in solution: 7 mg of SiO_2@R (R= CN, COOH) was added in 4 mL of D_2O/NaOH solution (pH≈13) in an NMR tube. The mixture was heated until the powder completely dissolved. A known amount of benzoic acid (ca. 4 mg) was added as internal standard. Then the NMR proton data were collected immediately.

Elemental analysis: Elemental analyses were performed by the microanalysis service of the LCC

Centrifugation: The silica beads were collected by centrifugation on a Fisher 2-16P with a 11192 rotor (Max. rpm 4500, Sigma).

Gas Chromatography: The catalytic reactions were followed by gas chromatography on an Agilent 7820A chromatograph equipped with an FID detector, a DB-WAX capillary column (30m × 0.32mm × 0.5µm) and autosampler. Authentic samples of reactants (cyclooctene, cyclohexene, cyclohexanol) and some potential products (cyclooctene oxide, cyclohexene oxide, 2-cyclohexen-1-ol, *cis*-1.2-cyclohexanediol, 2-cyclohexen-1-ol, and cyclohexanone) were used for calibration. The conversion and the formation were calculated from the calibration curves (r^2 = 1) and an internal standard.

3.4.3. Synthesis

- Synthesis of metal complexes

- Synthesis of (L^3)$MnCl_2$ [19]

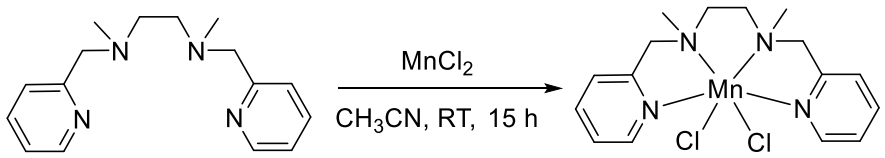

L^3 (L^3)$MnCl_2$

$MnCl_2$,$4H_2O$ (0.48 g, 2.4 mmol) was added to a solution of L^3 (0.54 g, 2mmol) in 3 mL of acetonitrile at room temperature. The mixture was stirred at room temperature for 15 h and the solvent was removed under vacuum. The grey powder obtained was washed twice by diethyl ether and after recrystallization by diffusion of diethyl ether into a solution of the product in an acetonitrile-ethanol mixture, (L^3)$MnCl_2$ (0.52 g, 65% yield) was obtained as a white powder.

Anal. Calc. for $C_{16}H_{22}Cl_2MnN_4 \cdot 0.5EtOH$: C, 48.70; H, 6.01; N, 13.36. Found: C, 49.02; H, 5.98; N, 13.40.

- Synthesis of (L^3)$Mn(OTf)_2$ [1c].

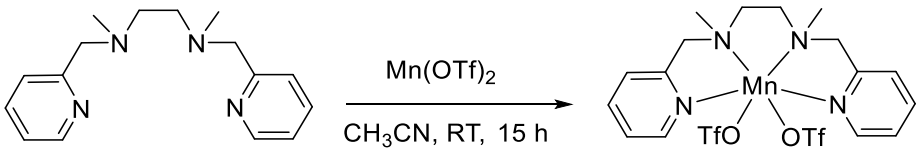

L^3 (L^3)$Mn(OTf)_2$

$Mn(OTf)_2$ (0.875 g, 2.4 mmol) was added to a solution of L^3 (0.54 g, 2 mmol) in 3 mL of acetonitrile at room temperature. The mixture was stirred at room temperature for 15 h and the solvent was removed under vacuum. The light grey powder obtained was washed twice by diethyl ether and after recrystallization by diffusion of diethyl ether into a solution of the product in acetonitrile, (L^3)$Mn(OTf)_2$ (0.85 g, 68% yield) was obtained as a white powder.

Anal. Calc. for $C_{18}H_{22}F_6MnN_4O_6S_2$: C, 34.68; H, 3.56; N, 8.99. Found: C, 34.68; H, 3.42; N, 8.95.

- Synthesis of ($\mathbf{L^3}$)Mn(*p*-Ts)$_2$

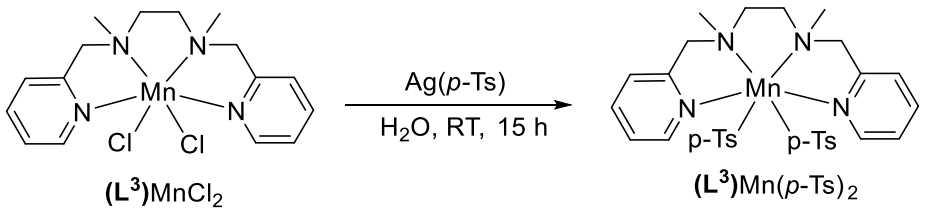

($\mathbf{L^3}$)$MnCl_2$ ($\mathbf{L^3}$)Mn(*p*-Ts)$_2$

A solution of silver paratoluenesulfonate (Ag(*p*-Ts)) (1.34 g, 4.8 mmol) in 5 mL of H_2O was added to a solution of ($\mathbf{L^3}$)$MnCl_2$ (0.79 g, 2 mmol) in 5 mL of H_2O and the mixture was stirred at room temperature for 15 h. After removal of AgCl, that has precipitated, by filtration, the solvent was removed under vacuum. Recrystallization of the crude product in absolute ethanol afforded ($\mathbf{L^3}$)Mn(*p*-Ts)$_2$ (0.96 g, 72% yield) as a grey solid.

Anal. Calc. for $C_{30}H_{36}MnN_4O_6S_2$: C, 53.97; H, 5.43; N, 8.39. Found: C, 53.82; H, 5.50; N, 8.36.

- Synthesis of [($\mathbf{L^3}$)$FeCl_2$]($FeCl_4$)

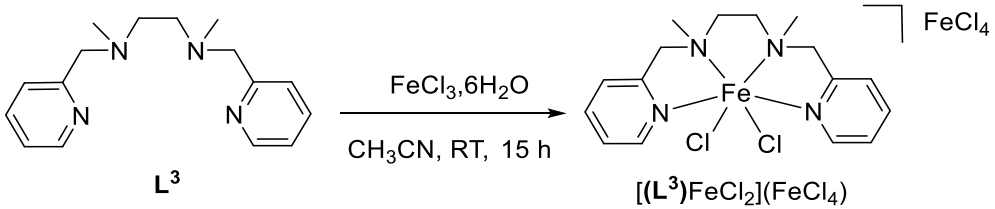

$\mathbf{L^3}$ [($\mathbf{L^3}$)$FeCl_2$]($FeCl_4$)

$FeCl_3$,6H_2O (1.08 g, 4 mmol) was added to a solution of $\mathbf{L^3}$ (0.54 g, 2 mmol) in 5 mL of acetonitrile. After 15 minutes, a red precipitate appeared and the mixture was stirred for 15 h at room temperature. After filtration of the red solid recrystallization in CH_3CN afforded [($\mathbf{L^3}$)$FeCl_2$]($FeCl_4$) (0.93 g, 73% yield) as a red solid.

Anal. Calc. for $C_{16}H_{22}Cl_6Fe_2N_4$: C, 32.31; H, 3.73; N, 9.42. Found: C, 32.39; H, 3.16; N, 9.33.

- Synthesis of silica particles

- Synthesis of Stöber $\mathbf{SiO_2}$ nanoparticles in EtOH (SiO_2(EtOH))[25]

72 mL (4 mol) of H_2O, 60 mL of ammonic solution (28%wt) were mixed in 630 mL (10.79 mol) of absolute ethanol at room temperature. 40 mL (0.18 mol) of tetraethylorthosilicate (TEOS) were added into the solution. A white suspension appeared. The mixture was stirred at 50°C for 6 hours. Then the solid was washed by absolute ethanol 5 times and collected by centrifugation. $\mathbf{SiO_2}$ nanoparticles were dried under vacuum at 120°C overnight. A white powder was obtained.

SiO_2: ^{1}H NMR (400 MHz, D_2O/NaOH-Benzoic acid) δ 7.57 (m, 2H, Ar-H), 7.21 (m, 3H, Ar-H), 3.31 (q, *J* = 7.1 Hz, 0.3H, CH_2), 0.86 (t, *J* = 7.1 Hz,.0.43H, CH_3). Anal. Found: C, 1.09; H, 0.67. ^{29}Si CP MAS-NMR:-93.3 ppm (Q^2),-101.9 ppm (Q^3),-111.8 ppm (Q^4). ^{13}C CP MAS-NMR: 58.0 ppm (CH_2O), 16.9 ppm (CH_3). IR (ATR, ν(cm^{-1})): 3710-2935 (OH), 1059 (Si-O-Si), 949 (Si-OH), 790 and 438 (Si-O-Si).

- Synthesis of **SiO_2@CN** particles from SiO_2(EtOH)[29]

10 g of **SiO_2**(EtOH) particles were mixed with 25 mL of TESPN (0.11 mol) in 150 mL of toluene under stirred at 110°C for 6 days. Then the **SiO_2@CN** particles were washed 5 times by toluene and were collected by centrifugation. Finally, the **SiO_2@CN** particles were dried under vacuum at 120°C for overnight and obtained as a white powder.

^{1}H NMR (400 MHz, D_2O/NaOH-Benzoic acid) δ 7.66 (m, 2H, Ar-H), 7.29 (m, 3H, Ar-H), 3.42 (q, *J* = 7.1 Hz, 0.36H, CH_2), 2.15 (m, 0.23H, CH_2), 0.96 (t, *J* = 7.1 Hz, 0.54H, CH_3), 0.54 (m, 0.24H, CH_2). ^{29}Si CP MAS-NMR:-62.2 ppm (T^2),-70.4 ppm (T^3),-92.8 ppm (Q^2),-101.9 ppm (Q^3),-111.9 ppm (Q^4). ^{13}C CP MAS-NMR: 120.9 ppm (CN), 60.2 ppm (CH_2O), 58.1 ppm (CH_2O), 16.4 ppm (CH_3), 10.6 ppm (CH_2Si), 8.8 ppm (CH_2Si). IR (ATR, ν(cm^{-1})) :3712-2937 (OH), 2248 (CN), 1073 (Si-O-Si), 943 (Si-OH), 795 and 442 (Si-O-Si). ρ(CN) =0.29 mmol/g. μ(CN)= 20.6 functions/nm^2

- Synthesis of **SiO_2@COOH** particles[3]

5 g of **SiO_2@CN**(EtOH) were added into 50 mL of H_2SO_4 (65%wt, 0.52 mol) and the solution was heated at 150°C under stirring for 4 hours. A grey powder was found in suspension. Then the powder was washed by H_2O until pH=7. The product was collected by centrifugation and was dried under vacuum at 120°C. A light grey powder was obtained.

^{1}H NMR (400 MHz, D_2O/NaOH-Benzoic acid) δ 7.58 (m, 2H, Ar-H), 7.21 (m, 3H, Ar-H), 3.33 (q, *J* = 7.1 Hz, 0.16H, CH_2), 1.91 (m, 0.02H, CH_2), 0.87 (t, *J* = 7.1 Hz, 0.23H, CH_3), 0.54 (m, 0.03H, CH_2). ^{29}Si CP MAS-NMR:-59.6 ppm (T^2),-68.7 ppm (T^3),-92.8 ppm (Q^2),-101.9 ppm (Q^3),-111.7 ppm (Q^4).^{13}C CP MAS-NMR: 60.0 ppm (CH_2O), 58.8 ppm (CH_2O), 16.6 ppm (CH_3). IR (ATR, ν(cm^{-1})) :3709-2933 (OH), 1737-1716 (C=O), 1073 (Si-O-Si), 943 (Si-OH), 794 and 446 (Si-O-Si) ρ(COOH) =0.04 mmol/g. μ(COOH)= 2.8 functions/nm^2.

- Synthesis of Stöber SiO_2 nanoparticles in methanol (**SiO_2**(MeOH)

72 mL (4 mol) of H_2O, 60 mL of ammonia solution (28 wt.%) were mixed in 630 mL (15.57 mol) of methanol at room temperature. 40 mL (0.18 mol) of tetraethyl orthosilicate (TEOS) were added into the solution. A suspension of a white solid appeared. The mixture was stirred at 50 °C for 6 hours. Then the solid was washed by

absolute ethanol 5 times and was collected by centrifugation. **SiO_2** nanoparticles were dried under vacuum at 120°C overnight. A white powder was obtained.

^{1}H NMR (400 MHz, D_2O/NaOH-Benzoic acid) δ 7.62 (m, 2H, Ar-H), 7.25 (m, 3H, Ar-H), 3.06 (s, 0.04H, CH_3). ^{29}Si CP MAS-NMR:-93.3 ppm (Q^2),-101.9 ppm (Q^3),-111.7 ppm (Q^4). ^{13}C CP MAS-NMR: 58.2 ppm (CH_2O), 16.7 ppm (CH_3).IR (ATR, ν(cm^{-1})): 3732-2850 (OH), 1062 (Si-O-Si), 945 (Si-OH), 784 and 443 (Si-O-Si).

- Synthesis of **SiO_2@CN** particles from **SiO_2**(MeOH)

10 g of **SiO_2** particles were mixed with 25 mL of TESPN (0.11 mol) in 150 mL of toluene at 110°C under stirring for 6 days. Then the **SiO_2@CN** particles were washed 5 times by toluene and were collected by centrifugation. The **SiO_2@CN** particles were dried under vacuum at 120°C for overnight and a white powder was obtained.

^{1}H NMR (400 MHz, D_2O/NaOH-Benzoic acid) δ 7.66 (m, 2H, Ar-H), 7.30 (m, 3H, Ar-H), 3.43 (q, *J* = 7.1 Hz, 3.16H, CH_2), 3.12 (s, 0.06H, CH_3), 2.20 (m, 1.98H, CH_2), 0.96 (t, *J* = 7.1 Hz, 4.76H, CH_3) 0.54 (m, 2.02H, CH_2). ^{29}Si CP MAS-NMR:-64.7 ppm (T^2),-70.5 ppm (T^3),-93.3 ppm (Q^2),-102.4 ppm (Q^3),-111.7 ppm (Q^4). ^{13}C CP MAS-NMR: 121.0 ppm (CN), 59.9 ppm (CH_2O), 16.8 ppm (CH_3), 10.5 ppm (CH_2Si), 8.8 ppm (CH_2Si). IR (ATR, ν(cm^{-1})) :3721-2903 (OH), 2253 (CN), 1065 (Si-O-Si), 941 (Si-OH), 788 and 425 (Si-O-Si). ρ(CN) =1.40 mmol/g. μ(CN)= 16.6 functions/nm^2

- Synthesis of **SiO_2@COOH** particles from **SiO_2@CN**(MeOH)

5 g of **SiO_2@CN** were added into 50 mL of H_2SO_4 (65%wt, 0.52 mol) and the solution was heated at 150°C under stirring for 4 hours. A grey powder was found in suspension. Then the powder was washed by H_2O until pH=7. Then the product was collected by centrifugation and was dried under vacuum at 120°C. A light grey powder was obtained.

^{1}H NMR (400 MHz, D_2O/NaOH-Benzoic acid) δ 7.66 (m, 2H, Ar-H), 7.29 (m, 3H, Ar-H), 3.42 (q, *J* = 7.1 Hz, 0.03H, CH_2), 3.12 (s, 0.03H, CH_3), 1.99 (m, 0.12H, CH_2), 1.02 (t, *J* = 7.1 Hz, 0.04H, CH_3), 0.46 (m, 0.13H, CH_2). ^{29}Si CP MAS-NMR:-58.8 ppm (T^2),-68.4 ppm (T^3),-91.9 ppm (Q^2),-101.8 ppm (Q^3),-111.6 ppm (Q^4). ^{13}C CP MAS-NMR: 177.9 ppm (COOH), 59.9 ppm (CH_2O), 49.5 ppm (CH_2O), 16.7 ppm (CH_3), 6.7 ppm (CH_2Si).IR (ATR, ν(cm^{-1})) :3709-2852 (OH), 1717 (C=O), 1046 (Si-O-Si), 932 (Si-OH), 785 and 450 (Si-O-Si). ρ(COOH) =0.31 mmol/g. μ(COOH)= 3.2 functions/nm^2.

3.4.4. Catalytic experiments

- General procedure of catalysis with CH_3COOH

1 mmol of substrate (CO, CH. CYol), 0.84g (14 mmol) of CH_3COOH, 0.01 mmol of complexes (($\mathbf{L^3}$)$MnCl_2$, ($\mathbf{L^3}$)$Mn(OTf)_2$, ($\mathbf{L^3}$)Mn(*p*-Ts)$_2$, [($\mathbf{L^3}$)$FeCl_2$]($FeCl_4$)) and some drops of an internal standard (acetophenone) were mixed in 2 mL of CH_3CN at room temperature. 0.13 mL of H_2O_2 (35 wt.% in H_2O) diluted into 0.87 mL of CH_3CN were slowly added into the mixture during 2h at 0°C. The mixture was left for 1h at 0°C.

- General procedure of catalysis with $\mathbf{SiO_2@COOH}$

1 mmol of substrate (CO, CH, CYol), 300 mg of $\mathbf{SiO_2@COOH}$(EtOH) (33.5mg for $\mathbf{SiO_2@COOH}$(MeOH) (0.14 mmol of carboxylic function), 0.01 mmol of complexes (($\mathbf{L^3}$)$MnCl_2$, ($\mathbf{L^3}$)$Mn(OTf)_2$, ($\mathbf{L^3}$)Mn(*p*-Ts)$_2$, [($\mathbf{L^3}$)$FeCl_2$]($FeCl_4$)) and some drops of an internal standard (acetophenone) were mixed in 2 mL of CH_3CN at room temperature. 0.13 mL of H_2O_2 (35 wt.% in H_2O) diluted in 0.87 mL of CH_3CN were slowly added into the mixture during 3h at 50°C. Then the mixture was left at 60°C for 2 hours.

3.5. References

[1] (a) R. Mas-Ballesté, L. Que, *J. Am. Chem. Soc.* **2007**, *129* (51), 15964–15972.
(b) M. C. White, A. G. Doyle, E. N. Jacobsen, *J. Am. Chem. Soc.* **2001**, *123* (29), 7194–7195.
(c) S. Lorenz, B. Plietker, *ChemCatChem*, **2016**, 8 (20), 3203–3206.
(d) E. A. Duban, K. P. Bryliakov, E. P. Talsi, *Eur. J. Inorg. Chem.* **2007**, 2007 (6), 852–857.

[2] (a) W. Wang, D. Agustin, R. Poli, *Mol. Catal.* **2017**, *443*, 52–59.
(b) W. Wang, J.-C. Daran, R. Poli, D. Agustin, *J. Mol. Catal. A: Chem.* **2016**, *416*, 117–126.
(c) D. Cvijanović, J. Pisk, G. Pavlović, D. Šišak-Jung, D. Matković-Čalogović, M. Cindrić, D. Agustin, V. Vrdoljak, *New J. Chem.* **2019**, *43* (4), 1791–1802.
(d) C. Cordelle, D. Agustin, J.-C. Daran, R. Poli, *Inorg. Chim. Acta*, **2010**, *364* (1), 144–149.
(e) J. Morlot, N. Uyttebroeck, D. Agustin, R. Poli, *ChemCatChem*, **2013**, *5* (2), 601–611.

[3] M.-Y. Yao, Y.-B. Huang, X. Niu, H. Pan, *ACS Sustainable Chem. Eng.* **2016**, *4* (7), 3840–3849.

[4] (a) N. N. Schwartz, J. H. Blumbergs, *J. Org. Chem.* **1964**, *29* (7), 1976–1979.
(b) R. N. McDonald, R. N. Steppel, J. E. Dorsey, *Org. Synth.* **1970**, 50, 15– 18.

[5] E. Brulé, Y. R. de Miguel, *Tetrahedron Lett.* **2002**, *43* (47), 8555–8558.

[6] (a) D. R. Burfield, A.-H. Eng, *Polym*. **1989**, *30* (11), 2019–2022.
(b) V. G. Dryuk, *Russ. Chem. Rev.* **1985**, 54 (10), 986–1005
(c) D. Swern in *Org. Peroxides, Vol. 2 (Ed.: D. Swern), Interscience, New York*, NY, **1971**, pp. 355–533.

[7] (a) Y. Shen, P. Jiang, P. T. Wai, Q. Gu, W. Zhang, *Catalysts*, **2019**, *9* (1), 31.
(b) K. Srinivasan, P. Michaud, J. K. Kochi, *J. Am. Chem. Soc.* **1986**, *108* (9), 2309–2320.
(c) J. Rudolph, K. L. Reddy, J. P. Chiang, K. B. Sharpless, *J. Am. Chem. Soc.* **1997**, *119* (26), 6189–6190.

[8] (a) S. Kobayashi, K. Tahara, (*Jpn. Kokai Tokkyo Koho)* JP 2007230908 A2020070913, **2007**.
(b) M. Bagherzadeh, L. Tahsini, R. Latifi, L. K. Woo, *Inorg. Chim. Acta,* **2009**, *362* (10), 3698–3702.
(c) K. Dallmann, R. Buffon, W. Loh, *J. Mol. Catal. A: Chem.* **2002**, *178* (1), 43–46.
(d) M. Yamazaki, H. Endo, M. Tomoyama, Y. Kurusu, *Bull. Chem. Soc. Jpn*. **1983**, *56* (11), 3523–3524.
(e) J. C. Anderson, N. M. Smith, M. Robertson, M. S. Scott, *Tetrahedron Lett.* **2009**, *50* (38), 5344–5346.

[9] J. Sherwood, *Angew. Chem. Int. Ed.* **2018**, 57, 14286 – 14290.

[10] (a) C. Miao, B. Wang, Y. Wang, C. Xia, Y.-M. Lee, W. Nam, W. Sun, *J. Am. Chem. Soc.* **2016**, 138 (3), 936–943.
(b) R. V. Ottenbacher, D. G. Samsonenko, E. P. Talsi, K. P. Bryliakov, *ACS Catal.* **2016**, 6 (2), 979–988.
(c) J. Du, C. Miao, C. Xia, Y.-M. Lee, W. Nam, W. Sun, *ACS Catal.* **2018**, 8 (5), 4528–4538.

[11] (a) D. Clemente-Tejeda, F. A. Bermejo, *Tetrahedron* **2014**, 70 (49), 9381–9386.
(b) D. Clemente-Tejeda, A. López-Moreno, F. A. Bermejo, *Tetrahedron,* **2013**, 69 (14), 2977–2986.
(c) D. Clemente-Tejeda, *Tetrahedron,* **2012**, 68 (45), 9249–9255.
(d) E. A. Duban, K. P. Brylyakov, E. P. Talsi, *Kinet Catal,* **2008**, 49(3), 379–385.
(e) S. Taktak, S. V. Kryatov, T. E. Haas, E. V. Rybak-Akimova, *J. Mol. Catal. A: Chem.* **2006**, 259 (1), 24–34.

[12] (a) K. Chen, L. Que. Jr, *Angew. Chem. Int. Ed.* **1999**, *38* (15), 2227–2229.
(b) O. Cussó, I. Garcia-Bosch, X Ribas, J. Lloret-Fillol, M. Costas, *J. Am. Chem. Soc.* **2013**, *135* (39), 14871–14878.

[13] J. Bautz, P. Comba, C. Lopez de Laorden, M. Menzel, G. Rajaraman, *Angew. Chem. Int. Ed.* **2007**, *46* (42), 8067–8070.

[14] (a) C. I. C. Crucho, C. Baleizão, J. P. S. Farinha, *Anal. Chem.* **2017**, 89(1), 681–687.
(b) R. Cohen, C. N. Sukenik, Colloids Surf., A, **2016**, *504*, 242–251.
(c) A. Feinle, F. Leichtfried, S. Straßer, N. Hüsing, *J. Sol-Gel Sci. Technol.* **2017**, *81* (1), 138–146.

[15] (a) A. Boullanger, G. Gracy, N. Bibent, S. Devautour‐Vinot, S. Clément, A. Mehdi, *Eur. J. Inorg. Chem.* **2012**, *2012* (1), 143–150.
(b) F. A. Ghaida, S. Clément, A. Mehdi, Heterogenized Catalysis on Metals Impregnated Mesoporous Silica. In *Novel Nanoscale Hybrid Materials*; John Wiley & Sons, Ltd, 2018; pp 323–349.
(c) N. Touisni, N. Kanfar, S. Ulrich, P. Dumy, C. T. Supuran, A. Mehdi, J.-Y. Winum, *Chem. Eur. J.* **2015**, *21* (29), 10306–10309.
(d) Y. Chen, Y. Zhou, H. Pi, G. Zeng, *RSC Adv.* **2019**, *9* (6), 3469–3478.

[16] (a) S. Atta, M. Fatima, A. Islam, N. Gull, M. Sultan, *Key Eng. Mater.* **2018**, *778*, 316–324.
(b) M. Yadav, T. Akita, N. Tsumori, Q. Xu, *J. Materials Chem.* **2012**, *22* (25), 1258–12586.
(c) R. van den Berg, T. E. Parmentier, C. F. Elkjær, C. J. Gommes, J. Sehested, S. Helveg, P. E. de Jongh, K. P. de Jong, *ACS Catal.* **2015**, *5* (7), 4439–4448.
(d) W. Yantasee, R. D. Rutledge, W. Chouyyok, V. Sukwarotwat, G. Orr, C. L. Warner, M. G. Warner, G. E. Fryxell, R. J. Wiacek, C. Timchalk, et al. *ACS Appl. Mater. Interfaces*, **2010**, *2* (10), 2749.
(e) J.-S. Kim, S. Chah, J. Yi, *Korean J. Chem. Eng.* **2000**, *17* (1), 118–121.

[17] (a) P. A. A. Ignacio-de Leon, C. A. Contreras, N. E. Thornburg, A. B. Thompson, J. M. Notestein, *Appl. Catal. A: Gen.* **2016**, *511*, 78–86.
(b) N. J. Schoenfeldt, Z. Ni, A. W. Korinda, R. J. Meyer, J. M. Notestein, *J. Am. Chem. Soc.* **2011**, *133* (46), 18684–18695.

[18] (a) R. V. Ottenbacher, E. P. Talsi, K. P. Bryliakov, *Catal. Today*, **2016**, *278*, 30–39.
(b) O. Cussó, J. Serrano-Plana, M. Costas, *ACS Catal.* **2017**, *7* (8), 5046–5053.

[19] C. Hureau, G. Blondin, M.-F. Charlot, C. Philouze, M. Nierlich, M. Césario, E. Anxolabéhère-Mallart, *Inorg. Chem.* **2005**, *44*, 3669-3683.

[20] (a) T. W.-S. Chow, E. L.-M. Wong, Z. Guo, Y. Liu, J.-S. Huang, C.-M. Che, *J. Am. Chem. Soc.* **2010**, *132* (38), 13229–13239.
(b) W.-P. To, T. W.-S. Chow, C.-W. Tse, X. Guan, J.-S. Huang, C.-M. Che, *Chem. Sci.* **2015**, *6* (10), 5891–5903.

[21] A. Murphy, G. Dubois, T. D. P. Stack, *J. Am. Chem. Soc.* **2003**, *125*, 5250-5251

[22] W. Dexuan, L. Guian, H. Qingyan, W. Ziqiang, P. Liping, Z. Zhongyue, Z. Hairong, *J. Nanosci Nanotechnol.* **2016**, 16(4), 3821-3826.

[23] M. A. Bourebrab, D. T. Oben, G. G. Durand, P. G. Taylor, J. I.Bruce, A. R. Bassindale, A. Taylor, *J. Sol-Gel Sci. Technol.* **2018**, 88(2), 430–441.

[24] (a) D. L. Green, S. Jayasundara, Y.-F. Lam, M. T. Harris, *J. Non-Cryst. Solids,* **2003**, 315(1), 166–179.
(b) T. Suratwala, M. L. Hanna, P. Whitman, *J. Non-Cryst. Solids*, **2004**, 349, 368–376.

[25] W. Stöber, A. Fink, E. Bohn, *J. Colloid Interface Sci.* **1968**, 26(1), 62–69.

[26] X.-D. Wang, Z.-X. Shen, T. Sang, X.-B. Cheng, M.-F. Li, L.-Y. Chen, Z.-S. Wang, *J. Colloid Interface Sci.* **2010**, 341 (1), 23–29.

[27] D. L. Green, J. S. Lin, Y.-F. Lam, M. Z.-C. Hu, D. W. Schaefer, M. T. Harris, *J. Colloid Interface Sci.* **2003**, 266 (2), 346–358.

[28] (a) O. Malay, I. Yilgor, Y. Z. Menceloglu, *J. Sol-Gel Sci. Technol.* **2013**, 67 (2), 351–361.

(b) S. Sadasivan, A. K. Dubey, Y. Li, D. H. Rasmussen, *J. Sol-Gel Sci. Technol.* **1998**, *12* (1), 5–14.

[29] J. Bu, R. Li, C. W. Quah, K. J. Carpenter, *Macromolecules,* **2004**, 37 (18), 6687–6694.

[30] K. S. Aneja, S. Bohm, A. S. Khanna, H. L. Mallika Bohm, *Nanoscale,* **2015**, 7 (42), 17879–17888.

[31] (a)D. Das, Y. Yang, J. S. O'Brien, D. Breznan, S. Nimesh, S. Bernatchez, M. Hill, A. Sayari, R. Vincent, P. Kumarathasan, *J. Nanomater.* **2014**, *2014*, 1-12

(b) S. C. Feifel, F. Lisdat, *J. Nanobiotechnol.* **2011**, *9* (1), 59.

[32] J. Trébosc, J. W. Wiench, S. Huh, V. S.-Y. Lin, M. Pruski, *J. Am. Chem. Soc.* 2005, 127, 3057-3068.

[33] R. Mouawia, A. Mehdi, C. Reyé, R. Corriu, *J. Mater. Chem.* **2007**, *17*, 616–618.

[34] R. K. Sharma, S. Sharma, S. Gulati, A. Pandey, *Anal. Methods*, **2013**, 5, 1414.

[35] S.O. Ribeiro, C.M. Granadeiro, P. L. Almeida, J. Pires, M. C. Capel-Sanchez, J. M. Campos-Martin, S. Gago, B. de Castro, S. S. Balula, *Catal. Today,* **2019,** 333, 226–236

[36] (a) J. S. Park, J. Hah, S. M. Koo, Y. S. Lee, *J. Ceram. Process. Res.* **2006**, 7(1), 83–89.

(b) A. Beganskienė, V. Sirutkaitis, M. Kurtinaitienė, R. Juškėnas, A. Kareiva, *Mater. Sci. (Medžiagotyra)*. **2004**, 10, 287-290.

[37] (a) S. Li, Q. Wan, Z. Qin, Y. Fu, Y. Gu, *Langmuir* **2015**, 31 (2), 824–832.

(b) A. Labrosse, A. Burneau, *J. Non-Cryst. Solids*, **1997**, 221(2), 107–124.

(c) Q. Wan, C. Ramsey, G. Baran, *J. Therm. Anal. Calorim.* **2010**, 99 (1), 237–243.

(d) V. M. Masalov, N. S. Sukhinina, E. A. Kudrenko, G. A. Emelchenko, *Nanotechnology*, **2011**, 22(27), 275718.

(e) D. N. Mangos, T. Nakanishi, D. A. Lewis, *Sci. Technol. Adv. Mater.* **2014**, 15 (1).

[38] (a) S. V. de Vyver, Y. Román-Leshkov, *Catal. Sci. Technol.* **2013**, *3* (6), 1465–1479.

(b) F. Cavani, S. Alini, *Sustainable Industrial Processes*, Weinheim, Germany, **2009**, *pp.* 367–425.

[39] K. Chen, M. Costas, J. Kim, A. K. Tipton, L. Que, *J. Am. Chem. Soc.* **2002**, *124* (12), 3026–3035.

[40] A. Gelasco, A. Askenas, V. L. Pecoraro, *Inorg. Chem.* **1996**, *35* (6), 1419–1420.

[41] H. J. H. Fenton, *J. Chem. Soc. Trans*. **1894**, *65*, 899-910.

[42] F. Jaouen, J.-P. Dodelet, *J. Phys. Chem. C*, **2009**, *113(34)*, 15422-15432

[43] K. Sengupta, S. Chatterjee, A. Dey, *ACS Catal.* **2016**, 6 (3), 1382–1388.

[44] (a)M. Nourian, F. Zadehahmadi, R. Kardanpour, S. Tangestaninejad, M. Moghadam, V. Mirkhani, I. Mohammadpoor-Baltork, *Appl. Organomet. Chem.* **2018**, *32* (1), e3957.

(b) J. Y. Wang, M. D. Zhou, Y. G. Yuan, N. H. Fu, S. L. Zang, *Russ. J. Gen. Chem.* **2015**, 85 (10), 2378–2385.

[45] J. Chen, M. Chen, B. Zhang, R. Nie, A. Huang, T. W. Goh, A. Volkov, Z. Zhang, Q. Ren, W. Huang, *Green Chem.* **2019**, *21* (13), 3629–3636.

[46] (a) S. A. Chavan, D. Srinivas, P. Ratnasamy, *J. Catal.* **2002**, *212* (1), 39–45.

(b) U. Schuchardt, D. Cardoso, R. Sercheli, R. Pereira, R. S. da Cruz, M. C. Guerreiro, D. Mandelli, E. V. Spinacé, E. L. Pires, *Appl. Catal. A: Gen.* **2001**, *211* (1), 1–17.

[47] (a) D. Shen, C. Miao, D. Xu, C. Xia, W. Sun, *Org. Lett.* **2015**, *17* (1), 54–57.

(b) N. Kasi, S.-J. Kim, I. Kim, M. Sook Seo, Y. Kim, S.-J. Kim, J. Kim, W. Nam, *Chem. Commun.* **2007**, *44*, 4623–4625.

Chapter 4

Organic solvent-free olefins and alcohols (ep)oxidation using recoverable catalysts based on $[PM_{12}O_{40}]^{3-}$ (M= Mo or W) ionically grafted on amino functionalized silica nanobeads.

Abstract: Catalyzed organic solvent-free (ep)oxidation reactions were achieved using $H_3PM_{12}O_{40}$ (M= Mo or W) complexes ionically grafted on APTES-functionalized nano-silica beads obtained from straightforward method. Those catalysts have been extensively analysed through morphological studies (DLS, TEM) and several spectroscopic qualitative (IR, multinuclear solid-state NMR) and quantitative (^{1}H and ^{31}P solution NMR) methods. Interesting catalytic results were obtained for the epoxidation of cyclooctene, cyclohexene, limonene and oxidation of cyclohexanol with a lower [POM]/olefin ratio. The catalysts were found to be recyclable and reused during three runs with similar catalytic performances.

4.1. Introduction

Oxidation of olefins and alcohols are important reactions in organic chemistry, with fundamental and applicative interest of those chemical transformations.[1] Indeed, epoxides can be obtained using very efficient organic oxidants (m-CPBA,[2] NaClO,[3] RCO_3H[4]) but with procedures needing long workup, detrimental for eco-logical and economical purposes. Those issues can be diminished using metal-based catalysts, but some drawbacks of those processes come from the use of (toxic) metals and/or the use of (toxic) organic solvent(s). As examples for epoxidation, several Mo complexes used in industrial plants need the use of chlorinated solvents[5] such as DCE, a highly toxic solvent that has to be avoided.[6] An elegant way to circumvent those issues, in straight line with the principles of green chemistry,[7] is to diminish/suppress the use of organic solvent within the oxidation process. We demonstrated it in some processes we published with active (pre)catalysts (Mo, V or W based, complexes with tridentate ligands and/or polyoxometalates), giving a first step towards a cleaner process.[8] In term of efficient greener process, the best oxidant found was TBHP in aqueous solution for the epoxidation since the "waste", tBuOH is potentially recycled.[9] In terms of atom economy, the oxidation reactions could be even more improved using for example H_2O_2 as oxidant. Although advantageous, some of those cited processes could not allow an easy separation of the catalysts from the media. One strategy we employed to recover the POM catalyst was to graft the catalyst on Merrifield resin.[10] Other supports do worth to be explored. Mesoporous silica as support was tried by several research groups in order to retain the POMs within the pores.[11] Although the compounds were active (under organic solvent conditions mainly), the disadvantage of mesoporous supports is the potential incomplete accessibility of the POMs present in the material for a catalytic process and thus a loss of efficiency. For this, it was interesting to take advantage to the known sol-gel chemistry and Stöber process, and the possibility of functionalization of silica - using trialkoxysilane precursors - to obtain pending ammonium functions only on the surface of the silica beads.[12] This strategy was employed for different uses, in order to graft in a covalent way polydentate ligands and related complexes or POMs for catalyzed reactions,[13] luminescence properties,[14] analytical purposes,[15] to trap heavy metals for depollution[16] concerns or organic molecules for controlled release,[17] mainly on mesoporous compounds[18] but scarcely with non-porous silica beads.[19] In order to find an easy recoverable catalyst, those functionalized silica beads played the role of countercations of the anionic polyoxometalate. The influence of the metal (Mo vs. W) was studied on different substrates. In the case of the most active complex, the silica beads were recovered and reused three times.

4.2. Results and discussion

4.2.1. Synthesis of the catalytic objects.

The synthesis of the catalytic objects is a three-step method (Scheme 1), starting from the synthesis of non-porous **SiO_2** beads according to a modified Stöber method using $Si(OEt)_4$ (TEOS) and ammonia in MeOH.[20] The second step, i.e. the grafting of aminopropyltrietoxysilane (APTES) at the surface of **SiO_2**, has been performed under classical conditions in toluene,[21] the grafted species with pending NH_2 functions (named here **$SiO_2@NH_2$**) being isolated as white powder. The final step consists into the ionic grafting of the POM catalysts on **$SiO_2@NH_2$** simply by mixing in water **$SiO_2@NH_2$** beads and the corresponding Keggin heteropolyacids $H_3PM_{12}O_{40}$ (M=Mo or W) in water, in a POM/NH_2 functions ratio of 1/3. The final solids **$SiO_2@PMo$** and **$SiO_2@PW$** were isolated as powders. In the case of molybdenum, the powder was slightly blue, indicating an interaction with ammonium.[22] The mixture with the tungsten gave a white powder.

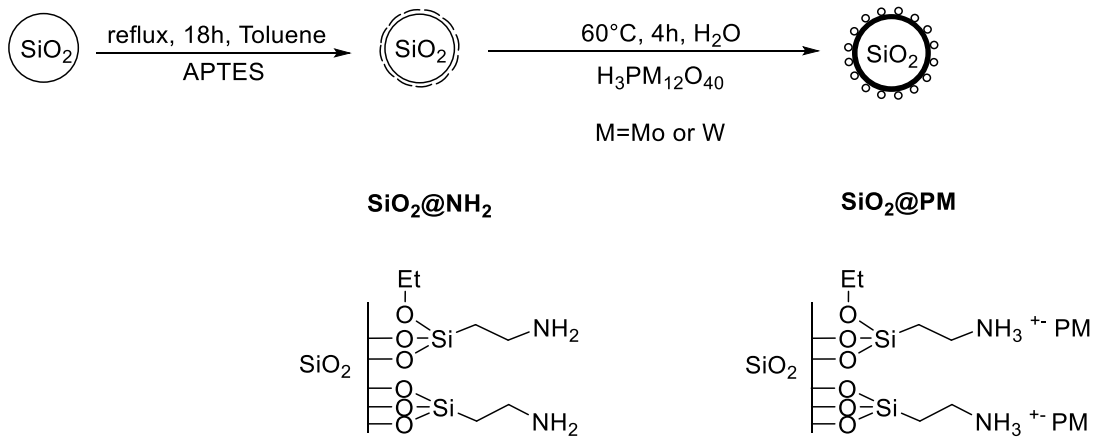

Scheme 1 - Schematic synthetic pathway of the different silica particles.

Amorphous nature, as well as the sizes and morphologies of the isolated objects **SiO_2**, **$SiO_2@NH_2$**, **$SiO_2@PMo$** and **$SiO_2@PW$** were analysed before the catalytic experiments by PXRD, DLS and TEM. Accurate analysis of the functional content has been performed using IR and multinuclear solid-state NMR. Qualitative studies were performed through elemental analysis and ^1H and ^{31}P solution NMR.

4.2.2. Morphological Characterization of the silica beads

4.2.2.1. Analysis by PXRD

The amorphous state of isolated **SiO_2@PM** beads has been characterized through powder X-ray diffraction (Figure 1) and does correspond to what is expected with 2θ=23°.[15,23] At the difference with POMs grafted in a similar way in mesoporous SBA-15,[24] no diffraction peaks corresponding to the starting heteropolyacids (Fig. 2) could be detected (in comparison with the PXRD spectra of the starting materials), certainly indicating that POMs have been grafted but do not remain agglomerated in a crystalline way.

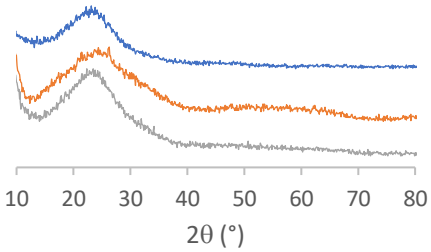

Figure 1 - Powder X-ray diffraction diagrams of **SiO_2** (blue), **SiO_2@PW** (orange) and **SiO_2@PMo** (grey) particles.

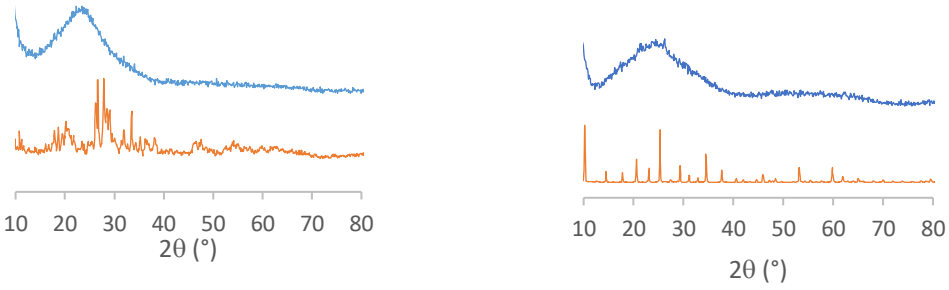

(a) (b)

Figure 2 - Comparison of Powder X-ray diffractions of (a) $H_3PMo_{12}O_{40}$ (orange) and **SiO_2@PMo** (blue) and (b) $H_3PW_{12}O_{40}$ (orange) and **SiO_2@PW** (blue). The intensities of **SiO_2@PMo** and **SiO_2@PW** were magnified 10 times.

4.2.2.2. Dynamic Light Scattering Analysis

The DLS measurements are usually performed to determine the hydrodynamic diameter of colloidal particles. As described previously with the silica particles obtained by Stöber method,[20] we considered the objects as spherical. This technique can give a perfect size (hydrodynamic diameter D_h) of the particles when enough dispersed in the suspension and that no time depending aggregation phenomena do occur.[25] Measurements have been performed with **SiO_2**, **SiO_2@NH_2**, **SiO_2@PW** and **SiO_2@PMo**. The results have been graphically indicated in Figure 3.

- *Case of SiO_2*

As for the SiO_2 from Chapter 3, The DLS measurements gave stable measurements within the time range for the SiO_2 beads only (Figure 3a), the D_h found being around 70 nm in suspension in water.

- *Case of $SiO_2@NH_2$*

The $SiO_2@NH_2$ beads show a different behavior (Figure 3b). Within the time, the size distribution is changing and aggregation seems to occur, the diameter evolving from 190 nm at the first measurement (implicating some small association of the beads under the conditions of the measurements if we consider that the starting beads used for the grafting are the SiO_2 presented previously) to even bigger aggregation with higher Dh values, i.e. 340 nm after a longer time. This might be due to the nature of the pending NH_2 functions and the possibility of hydrogen bonds.

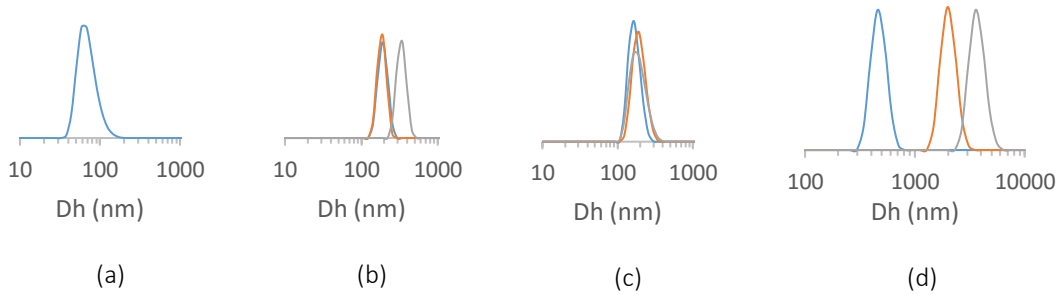

Figure 3 - Size (hydrodynamic diameter) distribution (in number) obtained by DLS for the SiO_2 (a) $SiO_2@NH_2$ (b) $SiO_2@PW$ (c) and $SiO_2@PMo$ (d) beads. The time dependent size increase (case b-d) has been indicated by the different colors (blue-orange-grey).

- *Case of $SiO_2@PM$*

Addition of the POMs to the $SiO_2@NH_2$ beads did profound changes to the DLS measurements according to the nature of the POM. With $SiO_2@PW$, the starting measured size is around 190 nm (as for the $SiO_2@NH_2$) and evolve to 220 nm (Fig. 3c). In the case of the $SiO_2@PMo$ beads (Fig. 3d), the starting value is huge from 450 nm to 3900 nm between the different time measurements. This is a proof of a time–dependent rearrangement of the beads. DLS did not give information for the hydrodynamic radii of the single particles in this case but pointed out an aggregation phenomenon due to the nature of the surrounding of the silica particles, once the grafting was done. Interactions with the POMs (and protonation of the pending NH_2) might change the pH value and favor the aggregation.[26] Such phenomenon was observed with thiolated silica particles interacting with different concentrations of hydroxyethylcellulose.[27]

4.2.2.3. TEM analysis

TEM measurements gave the proof of narrow dispersity of the silica beads (Fig.4). The beads have an average diameter of 75.9 nm for SiO_2 and $SiO_2@NH_2$ and around 80.6 and 82.9 nm for the $SiO_2@PW$ and $SiO_2@PMo$ ones respectively, indicating that the structure of the SiO_2 core is maintained during the three steps. The coverage of $SiO_2@NH_2$ with POMs could be proven in addition by a textural change of the surface of the beads.

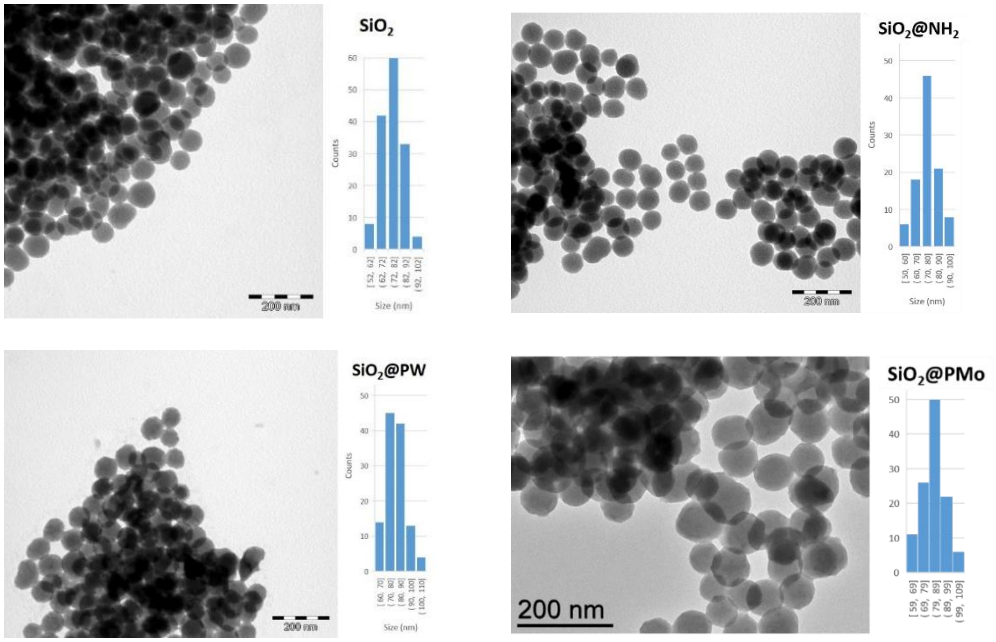

Figure 4- TEM images and diameters distribution of SiO_2, $SiO_2@NH_2$, $SiO_2@PW$ and $SiO_2@PMo$ beads.

Interesting observations could be done concerning the interactions between particles in case of $SiO_2@PW$ and $SiO_2@PMo$. The contrast at the contact area between particles in TEM pictures (Figure 5) seem to indicate contacts between the beads, stronger than with SiO_2 or $SiO_2@NH_2$ with angles that seem to be not due to a simple packing.

This feature could be similar to the one observed with Europium-containing POMs entrapped within SiO_2[28] on which fusing could be possible since silica covered the POMs, but the situation described herein is reverse since POMs cover the surface of the silica beads. The first possible explanation could be that the surface of the beads is rearranged in presence of acidic POM (and water media) twinning the silica nanoparticles. The surface of silica could be corroded and react again, fusing on contact points. This explanation could be valid since this phenomenon does need the presence of POMs and it is not observed in the case of $SiO_2@NH_2$. The fusing was proved by Greasley and al. using SiO_2 particles and CaO at temperatures higher than the ones used herein.[29] Another explanation could be that POMs are "agglomerated" between SiO_2

beads (but not in a crystalline arrangement since no peaks of the POMs have been observed in XRD spectra of **SiO_2@PM**) and favour a simple ionic contact/fusing between the beads. This plausible explanation looks like silica beads functionalized with cyclodextrin and G1 adamantly PPI dendrimers (H-bond interactions)[30] or gold nanoparticles decorated with POMs (ionic interactions).[31] Due to the nature of the silica part in **SiO_2@PM** beads (positively charged in surface through ammonium functions), a complex association composed of POM/ammonium attractions and ammonium/ammonium repulsions might favour electrostatic interactions with specific angles corresponding to superficial contacts, the closest contact between three beads giving a triangular aspect.

Thus, an explanation of the observed phenomenon in TEM seems to be situated between beads fusing and/or strong inter-bead electrostatic interactions. Both phenomena being possible in the aqueous media, it might be concluded that ionic rearrangements can occur when the species are mixed in water. Although TEM does give an image of a dried sample, the time dependent aggregation phenomena observed in solution through DLS seems to corroborate those assumptions.

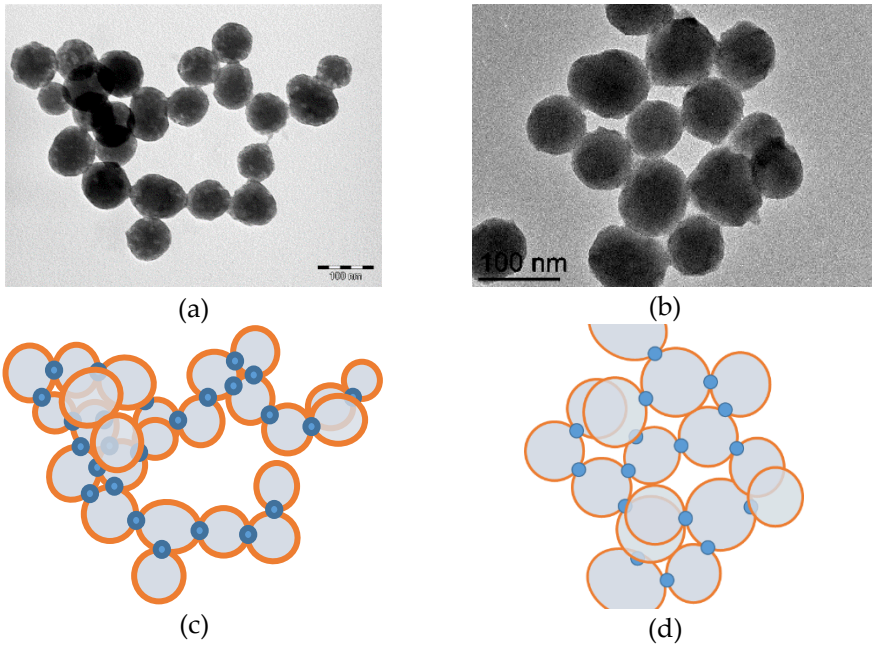

Figure 5 - TEM images of **SiO_2@PW** (a) and **SiO_2@PMo** (b). Relative schematic potential interactions (c) and (d) are represented with blue circles.

4.2.3. Qualitative Functional Characterization of the silica beads

4.2.3.1. Infrared Spectroscopy

IR spectra of all studied silica nanoparticles (Figure 6) show typical vibration bands with **SiO_2** at 793 cm^{-1} $(Si\text{-}O\text{-}Si)_{sym}$, 945 cm^{-1} (Si-OH), 1060 cm^{-1} $(Si\text{-}O\text{-}Si)_{asym}$, and 3700 cm^{-1}-2930 cm^{-1} for -OH stretching mode. With **SiO_2@NH_2** and **SiO_2@PM** vibrations are observed at 1495 cm^{-1} for CH_2 and 2832 cm^{-1} for -CH stretching mode.[32] Very small vibrations corresponding the NH_2 at 3700 cm^{-1}-2930 cm^{-1} for -NH stretching mode and 1485 cm^{-1} for NH_2 bending mode were observed for **SiO_2@NH_2**.[33]

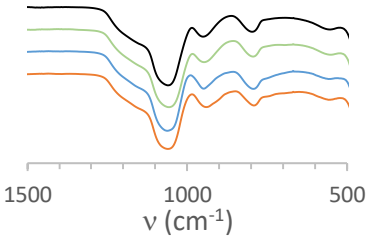

Figure 6- From up to down: Relevant IR vibration zones for **SiO_2**, **SiO_2@NH_2**, **SiO_2@PW**, **SiO_2@PMo**.

At the difference with mesoporous silica-based materials,[34] the content of APTES and PMs on non-porous silica beads is very low (only onto the surface of non-porous silica beads). Thus, it is not obvious to determine directly through IR if some APTES and PMs were grafted on the surface of **SiO_2** and **SiO_2@NH_2** respectively. Some shouldering could be seen in **SiO_2@PMo** and **SiO_2@PW** at 950 cm^{-1} for P-O, 870 cm^{-1} for Mo=O and 805 cm^{-1} for Mo-O-Mo in case of **SiO_2@PMo**, 1083-1092 cm^{-1} for P-O, 979-982 cm^{-1} for W=O, 897-901 cm^{-1} and 810-814 cm^{-1} for W-O-W in case of **SiO_2@PW**.[24,35] Those absorptions could correspond to the presence of polyanions. In addition, typical vibrations corresponding to Keggin units are overlapped with the ones of **SiO_2**.[36] An elegant method to prove the grafting is to do difference spectra between **SiO_2@NH_2** and **SiO_2** (Figure 7) or **SiO_2@PM** and **SiO_2@NH_2** (Figure 8). Very small changes can be observed at 2926 and 1450-1700 cm^{-1} that could give a proof of the presence of the grafted APTES on **SiO_2**. (Figure 6)

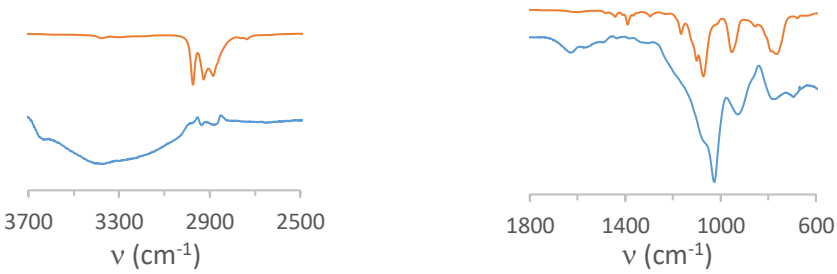

Figure 7 - Difference spectra (**SiO_2@NH_2** - **SiO_2**) on specific ranges (in blue). The spectrum of APTES is indicated in orange.

After addition of POMs, the difference spectra show vibrations corresponding to the POM backbone at 1060 cm^{-1} (P=O), 981 (W=O) and 873 cm^{-1} (W-O-W) for **SiO_2@PW**, or 944 (Mo=O) and 879 cm^{-1} (Mo-O-Mo) for **SiO_2@PMo** with small shifts in comparison to pure POMs [18b] (Figure 7). MAS NMR gave direct proofs of the grafting.

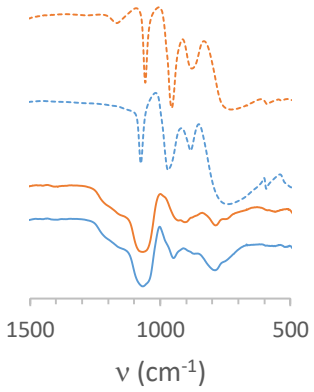

Figure 8 - From up to down: Relevant IR vibration area for $H_3PMo_{12}O_{40}$, $H_3PW_{12}O_{40}$, and difference spectra (**SiO_2@PMo** - **SiO_2@NH_2**), (**SiO_2@PW** - **SiO_2@NH_2**).

4.2.3.2. Multinuclear Solid-state NMR

Because IR did not give strongly affirmative answers concerning the nature of the functions surrounding the beads, solid state NMR has been an efficient tool. Indeed, ^{1}H, ^{13}C, ^{29}Si and ^{31}P are nuclei that can bring several information. All data have been summarized in Table 1.

^{1}H MAS NMR

The *^{1}H MAS NMR* spectra exhibits very large signals attributed to different groups on silica beads, silanols and physisorbed water molecules (3.5-5 ppm), ethoxy (3.3-3.6 ppm), and methoxy (1.1-1.3 ppm) as well as the CH_2 from the grafted silane (0.7-0.9 (Si-CH_2), 6.5-6.8 (CH_2-N) 4.0-4.1 (CH_2)). [37] Unfortunately, large and/or overlapped signals are simply indicative.

^{13}C MAS NMR

The ^{13}C MAS NMR spectra show signals corresponding to the organic functions grafted on **SiO_2** and slight changes when POMs are added (see Figure 9 and Table 1).[38] This method does confirm the silane and POM grafting.

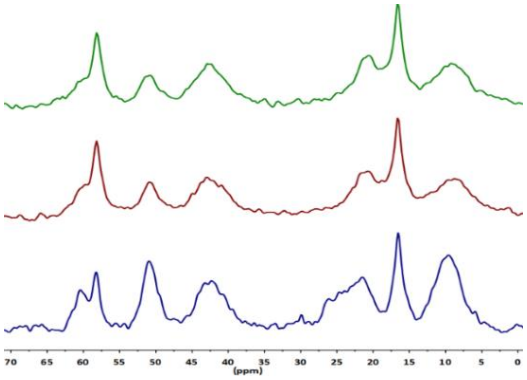

Figure 9- ^{13}C MAS NMR spectra of **SiO_2@PW** (top), **SiO_2@PMo** (middle) and **SiO_2@NH_2** (bottom).

^{29}Si NMR (CP-MAS and MAS)

The ^{29}Si CP MAS NMR (Figure 10 and Table 1) spectra gave additional information about the grafting on the silica bead itself. In all spectra, the signals at -93, -102 and -111 ppm corresponding to Q_2, Q_3 and Q_4 respectively (Q_n= $Si(OSi)_n(OH)_{4-n}$) are in accordance with SiO_2 core.[15] The silane grafting was proved by two signals around -60 and -68 ppm (T_2 and T_3).[39] A change of signals proportion was observed from **SiO_2** to **SiO_2@NH_2** and from **SiO_2@NH_2** to **SiO_2@PM**, the trend being identical when both POMs were added.

Since ^{29}Si CP MAS NMR could not quantify the Q_n, deconvolutions on SiO_2 cores only were done on ^{29}Si MAS NMR spectra, the relative intensity of the signals being indicated in parenthesis in table 1. The stronger differences observed in ^{29}Si CP-MAS (due to cross-polarisation) is not so pronounced in ^{29}Si MAS. (Figure 11) Those effects could be linked to the interactions between the ionic POMs and the **SiO_2@NH_2** beads, once the proton exchange is performed.

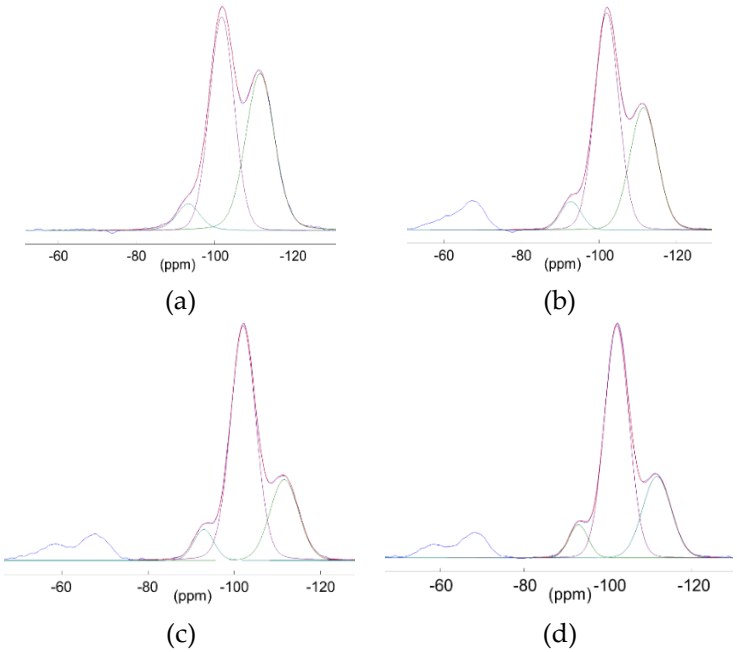

Figure 10- ^{29}Si CP MAS NMR spectra of **SiO_2** (a) **SiO_2@NH_2** (b), **SiO_2@PW** (c) and **SiO_2@PMo** (d).

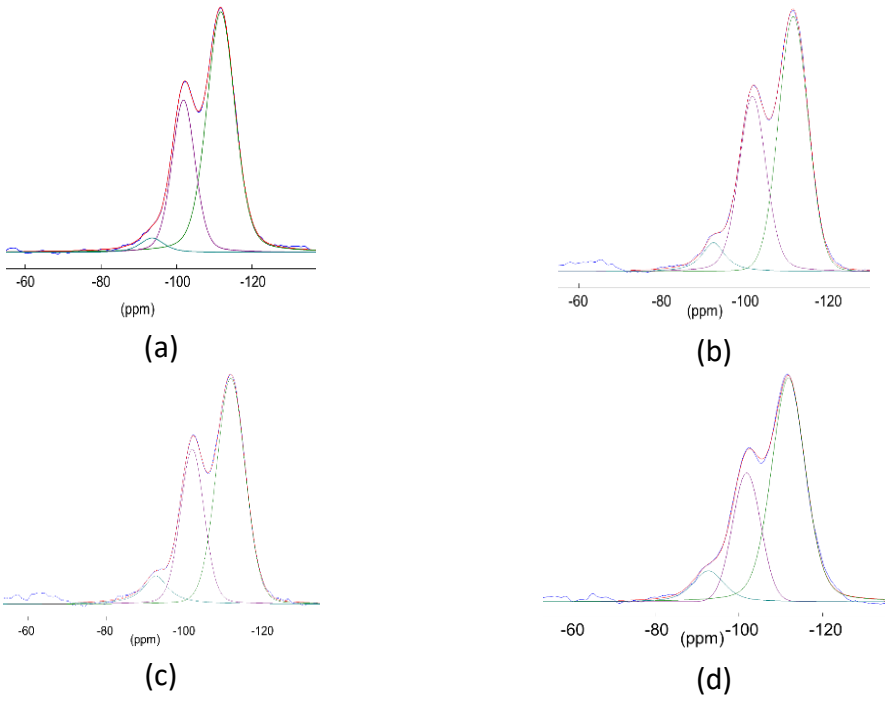

Figure 11 - ^{29}Si MAS NMR spectra of **SiO_2** (a) **SiO_2@NH_2** (b), **SiO_2@PW** (c) and **SiO_2@PMo** (d).

^{31}P MAS NMR

Added POMs covering the **SiO_2@NH_2** beads, different environments can be found, according to ionic interactions between charged POMs and pending ammonium, as well as H-interactions with silanol surfaces. [40] ^{31}P MAS NMR signals of the grafted ones (Table 1) are shifted comparing to the value of the free POMs (the one used for the grafting) and relatively close to some referenced in the literature in ^{31}P MAS for "$PW_{12}O_{40}$" [24,41] and $PMo_{12}O_{40}$"[42] backbones.

Table 1 - Relevant solid-state NMR data.

	SiO_2	SiO_2@NH_2	SiO_2@PW	SiO_2@PMo
		^{1}H MAS		
	3.4- 5.8-	0.9 1.2 2.2 3.6 5.1	0.8 3.3 4.0 6.5	0.8 3.4 4.0 6.8
		^{13}C CP MAS		
CH_2O		60.4	59.9	59.9
CH_2O		58.2	58.2	58.2
CH_2N		50.9	50.8	50.9
CH_2N		42.3	42.8	42.9
CH_2		21.5	20.6	20.7
CH_3		16.5	16.6	16.6
CH_2Si		9.6	9.2	8.8
		^{29}Si CP-MAS (deconvolution is in parenthesis)		
T_2		-62.1	-58.3	-58.6
T_3		-67.7	-67.9	-68.2
Q_2	-93.3 (7)	-92.8 (6)	-93.0 (7)	-93.0 (7)
Q_3	-101.9 (49)	-102.0 (57)	-102.1 (67)	-102.1 (66)
Q_4	-111.8 (44)	-111.5 (37)	-111.7 (26)	-111.7 (27)
		^{29}Si MAS (deconvolution is in parenthesis)		
Q_2	-93.5 (4)	-92.4 (7)	-92.6 (9)	-92.8 (9)
Q_3	-101.9 (32)	-101.8 (37)	-101.9 (33)	-101.9 (27)
Q_4	-111.8 (64)	-111.6 (56)	-111.7 (58)	-111.6 (64)
		^{31}P CP MAS (value of free POMs are in parenthesis)		
			-12.8 (-15.8)	-1.5 (-4.3,-5.0)
		^{31}P MAS (value of free POMs are in parenthesis)		
			-13.4 (-15.4,-15.8)	-1.5,-4.7,-6.7 (-4.3)

4.2.4. Quantitative Functional Characterization of the silica beads

4.2.4.1. Quantification by elemental analysis

From the nitrogen content (%N) found in elemental analysis, it is possible to calculate the number of moles of grafted aminosilane ρ(NH_2) and POM grafted (ρ(PM)) per gram of sample S. The values can be compared to the one found using ^{1}H liquid NMR. The number of moles of nitrogen atoms found in a sample S being equivalent to the number of NH_2 fragments, the formula can be defined as follows in equation 1. According to the Scheme 2, ρ(PM) can be calculated from the elemental analysis since we can postulate that the mixture of **SiO_2@NH_2** with POM does proton exchange from POM to the pending NH_2 functions and no other modifications. ρ(NH_2) and ρ(PM) are gathered in Table 2.

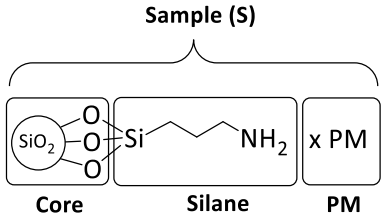

Scheme 2 - Schematic representation of the **SiO_2@NH_2** and **SiO_2@PM** beads.

$$\rho(NH_2) = \frac{n_{NH_2}}{m_S} = \frac{n_N}{m_S} = \frac{m_N}{m_S . M_N} = \frac{\%N}{M_N} \quad (1)$$

$$\rho(PM) = \frac{n_{PM}}{m_{SiO_2@PM}} = x . \rho(NH_2), \quad (2)$$

In order to find the x value, the important parameter is the mass of the SiO_2 core within **SiO_2@NH_2**, obtained from %N values that corresponds to the number of grafted APTS fragments. This number is supposed to be unchanged after addition of POM, the variation observed in %N for **SiO_2@PMo** and **SiO_2@PW** will depend on the quantity of POMs retained by the beads (equation 3)

$$\%N_{SiO_2@PM} = \frac{M_N}{M_{SiO_2@NH_2} + x . M_{PM}} \quad (3)$$

M(**SiO_2@NH_2**) can be found using the N% of **SiO_2@NH_2** (equation 4)

$$\%N_{SiO_2@NH_2} = \frac{M_N}{M_{SiO_2@NH_2}} \quad (4)$$

Then, injecting in equation 3, the x can be obtained from simple data using equation (5).

$$x = \frac{M_N}{M_{PM}} \left(\frac{1}{\%N_{SiO_2@PM}} - \frac{1}{\%N_{SiO_2@NH_2}} \right) \quad (5)$$

x will give the number of POM vs N within the sample. According to the equation, the calculated data have been compilated in Table 2.

Table 2 - POM/NH_2 molar ratio (x) obtained through EA data.

	SiO_2@NH_2	SiO_2@PW	SiO_2@PMo
N (%)	0.74	0.43	0.58
x	0	0.47	0.29

The ideal x value would have been 0.33, i.e. one POM retained by 3 NH_2 functions. This can be due to the fact the some NH_2 functions are "free" and the POM in the complete deprotonated form in the case of SiO_2@PMo while in the case of SiO_2@PW, the POM is not completely deprotonated.

4.2.4.2. Quantification of grafted functions and retained POM by liquid NMR

Multinuclear liquid NMR (^{1}H, and ^{31}P) was used for this purpose with SiO_2@NH_2, SiO_2@PMo and SiO_2@PW beads. Silica beads and POMS can be destroyed in alkaline medium, giving silicates for the silica part, and tungstates/molybdates and phosphates for the POMs.

^{1}H NMR in solution for the quantification of functions present on the silica surface.

It was proved that quantification could be done through the dissolution of the silica in aqueous solution in alkali medium.[43] The organic backbone was maintained and could be quantified using an internal standard with ^{1}H NMR. Using this method, the number of APTS fragments ρ(NH_2) could be evaluated per gram of sample (Table 3).

^{31}P NMR in solution for the quantification of POM.

Using the same methodology than the ^{1}H NMR, the SiO_2@PM were dissolved in very basic solution (pH=13), in order to isolate the PO_4^{3-}. The ^{31}P NMR signals obtained with the beads were quantified using an external calibration curve with different aqueous solutions of H_3PO_4 at pH=13. The parameter found through this method (Table 3), ρ(PM), was relatively close to the one found through elemental analysis.

Table 3 - Calculated ρ(NH_2) and ρ(PM) data and Surface coverage μ(NH_2).

Sample	ρ(NH_2)[1] (^{1}H NMR)	ρ(PM)[1] (^{31}P NMR)	ρ(NH_2)[1] (EA)	ρ(PM)[1] (EA)	μ(NH_2)[2]
SiO_2@NH_2	0.52	-	0.53	-	6.8
SiO_2@PW	0.33	0.15	0.31	0.14	6.8
SiO_2@PMo	0.40	0.12	0.41	0.12	6.7

[1] in mmol functions/g sample [2] in number functions/nm^2.

4.2.4.3. Surface coverage of the beads

Considering the number of functions present on one bead and the average size of the beads, using the classical density of SiO_2, we could evaluate the surface coverage in number of functions per nm^2. The demonstration of equation A is given in this part.

$$\mu(NH_2) = \frac{\rho'(NH_2).\, r_S.\, \rho_{SiO_2}}{3 \times 10^{+21}} \times N_A \quad (A)$$

Determination function coverage of functionalized silica beads

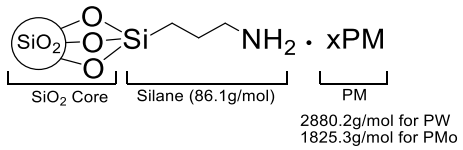

$\mu(NH_2)$,[43] the function coverage density (in molecules/nm^2) of cores, is the number of silane molecules grafted on the surface ΣS_{core} of 1 gram SiO_2 cores (equation 1).

$$\mu(NH_2) = \frac{n(NH_2)}{\Sigma S_{core}} \cdot N_A \quad (1)$$

Determination of ΣS_{core}

The total surface ΣS_{core} (nm^2) of cores is related to the number of cores contained in one gram (N_{core}) multiplied by the surface of those cores (S_{core}).(equation 2)

$$\Sigma S_{core} = N_{core}.\, S_{core} \quad (2)$$

N_{core} present in one gram of cores can be extracted from the equation 3

$$N_{core} = \frac{\Sigma V_{core}}{V_{core}} \quad (3)$$

- ΣV_{core} (nm^3) = volume of 1g cores deduced from non-porous SiO_2 density (ρ_{SiO2} = 1.6 $g.cm^{-3}$).[44] (Equation 4)

$$\Sigma V_{core} = \frac{1}{\rho_{SiO_2}} \cdot 10^{+21} \quad (4)$$

- V_{core} (nm^3) = volume of spherical bead, r_{core} being deduced from TEM measurements. (equation 5)

$$V_{core} = \frac{4}{3}\pi r_{core}^3 \quad (5)$$

S_{core} is obtained from r_{core}. (equation 6)

$$S_{core} = 4\pi r_{core}^2 \quad (6)$$

Thus

$$\Sigma S_{core} = N_{core} . S_{core} = \frac{\Sigma V_{core}}{V_{core}} \cdot S_{core} = \frac{1}{\rho_{SiO_2}} \cdot 10^{+21} \cdot \frac{4\pi r_{core}^2}{\frac{4}{3}\pi r_{core}^3} = \frac{3 \cdot 10^{+21}}{r_{core} \cdot \rho_{SiO_2}}$$

$$\Sigma S_{core} = \frac{3 \cdot 10^{+21}}{r_{core} \cdot \rho_{SiO_2}} \quad (7)$$

Determination of $n(NH_2)$

$n(NH_2)$ can be deduced from known data. Since $\mu(NH_2)$ is according to the SiO_2 core (scheme 1), it can be deduced from the $\rho'(NH_2)$ parameter

$$\rho'(NH_2) = \frac{n(NH_2)}{m_{core}} \quad (8)$$

on a complete sample, it is known that

$$m_S = m_{core} + m_{silane} + m_{PM} \quad (9)$$

$\rho'(NH_2)$ does correspond to the naked silica bead. (equation 10)

$\rho(NH_2)$ for **SiO_2@NH_2**, **SiO_2@PMo** and **SiO_2@PW** does contain the mass of grafted silanes and PMs **SiO_2@NH_2**, **SiO_2@PMo** and **SiO_2@PW**. This parameter does consider 1 g of complete bead (m_S). For $\rho'(NH_2)$, it has to consider the silica core only and not the complete sample (Scheme 2).

$$\rho'(NH_2) = \frac{n(NH_2)}{m_{core}} = \frac{n(NH_2)}{m_S - m_{silane} - m_{PM}} \quad (10)$$

$$\rho'(NH_2) = \frac{n(NH_2)}{m_{core}} = \frac{\frac{n(NH_2)}{m_S}}{\frac{m_S - m_{silane} - m_{PM}}{m_S}}$$

$$\rho'(NH_2) = \frac{n(NH_2)}{m_{core}} = \frac{\rho(NH_2)}{1 - \frac{m_{silane} + m_{PM}}{m_S}}$$

$$\rho'(NH_2) = \frac{n(NH_2)}{m_{core}} = \frac{\rho(NH_2)}{1 - \left(\frac{m_{silane}}{m_S} + \frac{m_{PM}}{m_S}\right)} \quad (11)$$

Using equation 12 and 13, equation 11 can be simplified into equation 14.

$$m_{silane} = n_{silane} * M_{silane} = n(NH_2) \cdot M_{silane} \quad (12)$$

$$m_{PM} = n_{PM} * M_{PM} = x * n(NH_2) \cdot M_{PM} \quad (13)$$

$$\rho'(NH_2) = \frac{n(NH_2)}{m_{core}} = \frac{\rho(NH_2)}{1 - \left(\frac{n(NH_2) \cdot M_{silane}}{m_S} + \frac{x \cdot n(NH_2) \cdot M_{PM}}{m_S}\right)}$$

$$\rho'(NH_2) = \frac{\rho(NH_2)}{1 - \rho(NH_2).(M_{Silane} + x.M_{PM})} = \frac{1}{\frac{1}{\rho(NH_2)} - (M_{Silane} + x.M_{PM})} \quad (14)$$

the formula was demonstrated with a mass core (m_{core}) of 1g

$$\rho'(NH_2) = \frac{n(NH_2)}{m_{core}} = n(NH_2)$$

The final formula can be written as in equation A

$$\mu_f = \frac{n(NH_2)}{\Sigma S_S} N_A = \frac{n(NH_2)}{\frac{3 \cdot 10^{+21}}{r_{core} \cdot \rho_{SiO_2}}} N_A = \frac{\rho'(NH_2).r_{core}.\rho_{SiO_2}}{3 \times 10^{+21}} \times N_A$$

$$\mu(NH_2) = \frac{\rho'(NH_2).r_{core}.\rho_{SiO_2}}{3 \cdot 10^{+21}} \cdot N_A \quad (A)$$

Using those calculations, results (Table 3) indicated a relatively constant $\mu(NH_2)$ value around 6.8 functions per nm^2.

4.2.5. Catalysis

Homogenous catalysis with commercial POMs (especially $H_3PW_{12}O_{40}$ and $H_3PMo_{12}O_{40}$) has showed excellent activity in oxidation reaction.[45] Several examples have proven to be effective and the composition of the POMs can be modified for better selectivity.[8d,10,] In most of published experiments, organic solvent was needed, and the catalyst could not be recovered. Few examples described grafted POMs using Merrifield resins,[10] polymeric quaternary ammonium salts,[46] mesoporous supports,[47] MOFs [48] or carbonaceous supports.[49]

Mesoporous supports are interesting, but POMs entrapped within zeolites might be not all accessible. The advantage of the present process lies on complete accessibility of all POMs since only at the surface of the support. One drawback could be the lack of selectivity, but the reactions studied being quite simple, selectivity is not such a big issue. Following the grafting concept, **SiO_2@PM** (M= Mo or W) were studied herein to achieve activity, recovery and reuse. Low ratio of POMs *vs*. substrate was tested. The **SiO_2@PM** objects were recycled and used during three runs, with aqueous TBHP as oxidant. The activity of the catalysts was tested on four model substrates.

Cyclooctene (CO) is known to give essentially the cyclooctene oxide (COE) and few by-products. Cyclohexene (CH) gives cyclohexene oxide (CHO) and more products due to ring opening. Limonene (Lim) is a good biomass-issued substrate to study with different useful by-products. Cyclohexanol (CHol) is also interesting since its oxidation gives normally cyclohexanone, useful for the adipic acid synthesis. Relevant points are the low POM/substrate ratio used in the experiments (see tables) and no added organic solvent. This last point is something important towards the quest of chemical process tending to diminish the Green House effect.[50]

4.2.5.1. Cyclooctene epoxidation.

CO is interesting because the corresponding epoxide, cyclooctene oxide (COE) is known to be relatively stable towards ring-opening reactions.[51] Although not frequent, hydrolysis and subsequent ring-opening might respectively lead to cyclooctanediol and suberic acid. The oxidant (CO/TBHP ratio being 1:1.5) is added once the temperature reached 80°C.[8d] It must be pointed out that no organic solvent was added. The engaged mass of functionalized silica was identical but, due to different POM/SiO_2 grafting ratio between Mo and W experiments, the POM/substrate ratio differ. Relatively low POM/substrate ratio (0.070% and 0.058% for $H_3PW_{12}O_{40}$ and $H_3PMo_{12}O_{40}$ respectively) was added, among the lowest observed in the literature. Catalysts were recovered by centrifugation and reused under the same experimental conditions to test the activity persistence. Test with non-grafted POMs have been performed for comparison. Results have been compiled in Table 4.

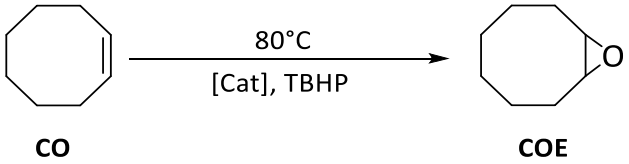

Scheme 3 - catalyzed epoxidation of CO.

Table 4 - Relevant data for the catalyzed epoxidation of CO.[1]

Catalyst	Run	CO Conv.[2]	COE Sel.[3]	TON[4]
$H_3PW_{12}O_{40}$	1	64	14	807
SiO_2@PW	1	72	41	981
	2	75	38	987
	3	77	37	968
$H_3PMo_{12}O_{40}$	1	99	44	1712
SiO_2@PMo	1	98	71	1693
	2	96	72	1620
	3	93	69	1598

[1] Conditions: 80°C. POM/TBHP/CO=0.070/150/100 for W, 0.058/150/100 for Mo; *t*=24h.

[2] n CO converted/n CO engaged (%) after 24h.

[3] n COE formed/ nCO converted (%) at 24h.

[4] n CO transformed /nPOM at 24h.

Although the activity of SiO_2@PM is slower during the first 6 hours, CO conversions are almost the same than free POMs after 24 hours but more selective towards COE in the case of the grafted POMs. (Figure 10) The higher selectivity might be due to less acidic media with SiO_2@PM. The SiO_2@PMo catalyst is more active than SiO_2@PW_{12}, giving better CO conversion and higher selectivity towards COE. This trend was also observed with the free POMs.

An interesting fact was the reuse of SiO_2@PM. For both metals, catalytic performances were close during two extra runs (Figure 11) (with average TON values around 950 and 1640 for W and Mo respectively).

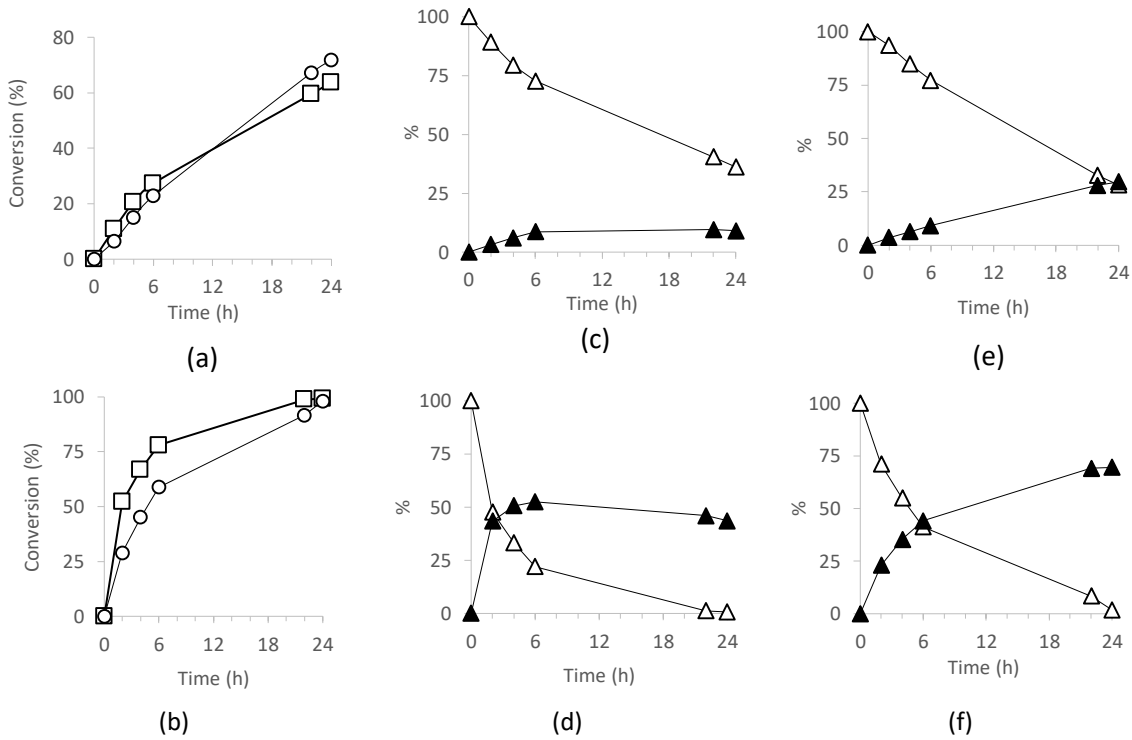

Figure 10 - Comparison of CO conversion between (a) $H_3PW_{12}O_{40}$ (□) and **SiO_2@PW** (○), (b) $H_3PMo_{12}O_{40}$ (□) and **SiO_2@PMo** (○). Evolution of CO (△) and COE (▲) with (c) $H_3PW_{12}O_{40}$, (d) $H_3PMo_{12}O_{40}$, (e) **SiO_2@PW** (Run 1) and (f) **SiO_2@PMo** (Run 1).

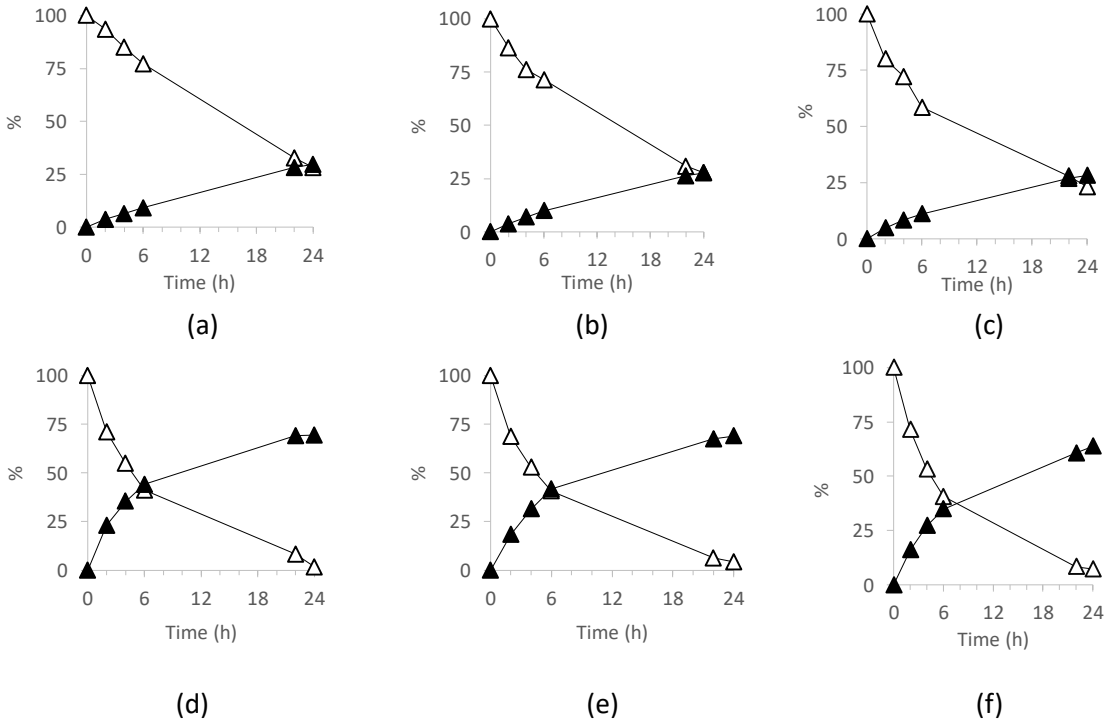

Figure 11 - Evolution of CO (△) and COE (▲) with **SiO_2@PW** (Run 1 (a), Run 2 (b) and Run 3 (c)) and **SiO_2@PMo** (Run 1 (d), Run 2 (e) and Run 3 (f)).

4.2.5.2. Cyclohexene (CH) (ep)oxidation

(Ep)oxidation of CH, precursor of adipic acid [10] and simplified version of limonene, competes between epoxidation (CHO and the ring opening CHD) and allylic oxidation (CHol and CHone). The studies were done with the same TBHP ratio than for CO but with a 5 times lower catalyst charge than for CO (i.e. POM/CH ratio of 0.014% and 0.0116% for $H_3PW_{12}O_{40}$ and $H_3PMo_{12}O_{40}$ respectively) in order to exhibit the high activity of the catalysts. (Scheme 4) As we observed previously with Mo tridentate compounds,[8k] the epoxidation is the main reaction when TBHP was used as oxidant.

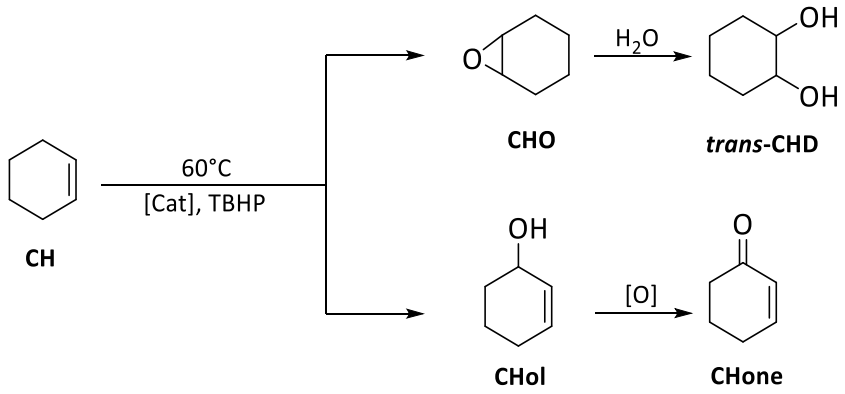

Scheme 4- oxidation reaction of CH.

Table 5 - Relevant data for the catalyzed (ep)oxidation of cyclohexene[1]

Catalyst	Run	CH Conv[2]	CHO Sel[3]	CHD sel[3]	CHol sel[3]	CHone sel[3]	TON[4]
$H_3PW_{12}O_{40}$	1	31	< 1	4	3	3	11307
SiO_2@PW	1	45	1	2	4	5	21458
	2	43	1	2	2	3	20649
	3	26	3	3	7	7	12373
$H_3PMo_{12}O_{40}$	1	91	< 1	40	3	2	52728
SiO_2@PMo	1	80	13	26	5	2	46732
	2	74	15	22	6	3	42487
	3	60	26	20	4.9	2	36345

[1]Conditions: 60°C. POM/TBHP/CH=0.014/150/100 for W, 0.0116/150/100 for Mo; *t*=48h.
[2]nCH converted/nCH engaged (%) after 48h. [3]n product formed/ nCH converted (%) at 48h.
[4]nCH transformed /nPOM at 48h.

After 48h at 60°C, as for CO substrate, SiO_2@PMo is much more active than SiO_2@PW_{12}. (Table 4) The free H_3PMo_{12} favoured the epoxidation and the ring opening of the epoxide. The allylic oxidation seems to be the preferred pathway with W containing species but not with a high difference towards Mo ones, showing that allylic oxidation does work without catalyst. (Figure 12) The reuse of the SiO_2@PM exhibits interesting durability during two runs and the third started to show lower activity. (Figure 13)

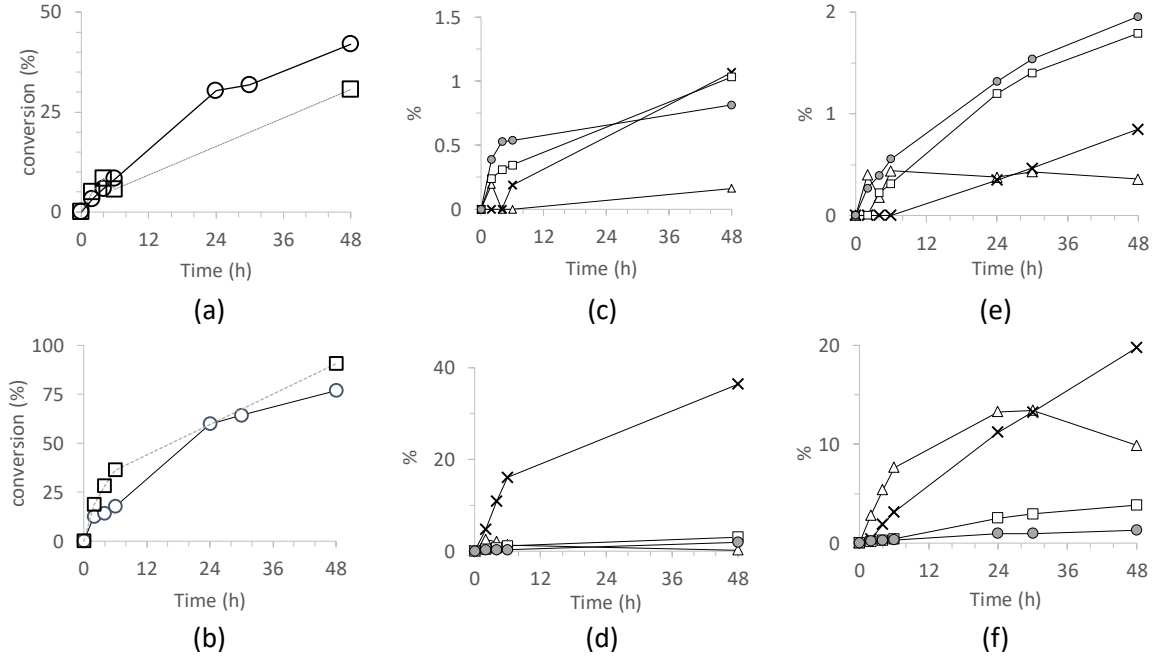

Figure 12 - Comparison of conversion of CH between (a) $H_3PW_{12}O_{40}$ (□) and **SiO_2@PW** (○), (b) $H_3PMo_{12}O_{40}$ (□) and **SiO_2@PMo** (○). Evolution of CHO (△), CHD (×), CHol (□) and CHone (●) with (c) $H_3PW_{12}O_{40}$, (d) $H_3PMo_{12}O_{40}$, (e) **SiO_2@PW** (Run 1) and (f) **SiO_2@PMo** (Run 1).

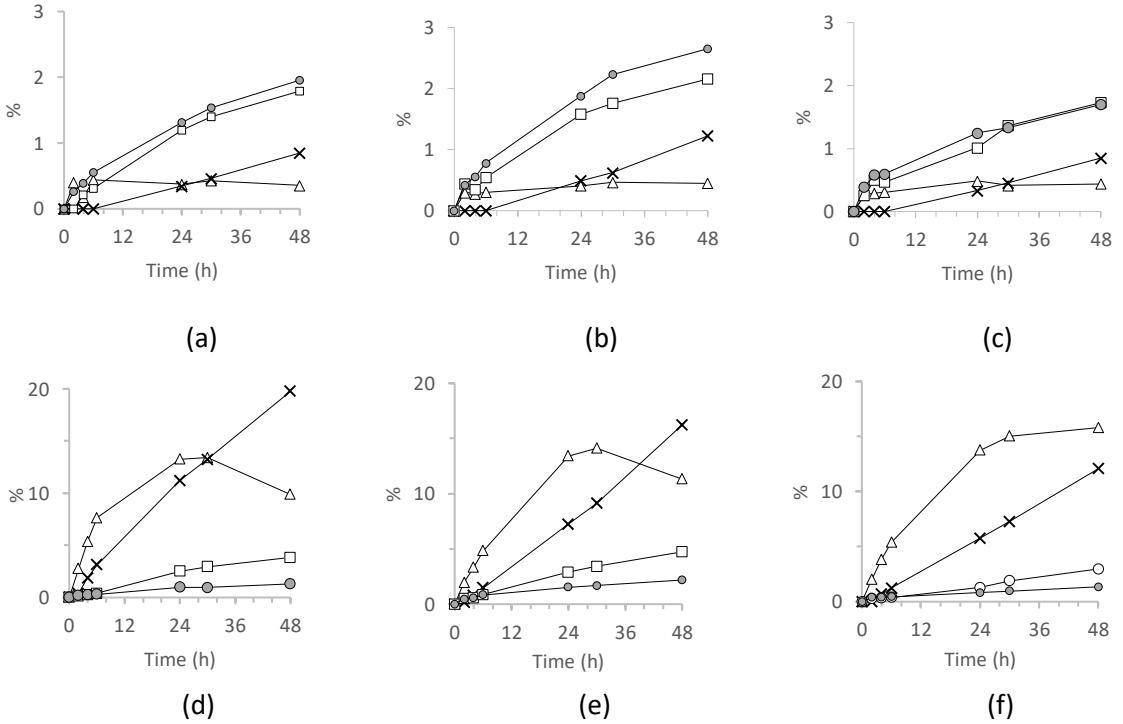

Figure 13 - Evolution of CHO (△), CHD (×), CHol (□) and CHone (●) with **SiO_2@PW (**Run 1 (a), Run 2 (b) and Run 3 (c)) and **SiO_2@PMo (**Run 1 (d), Run 2 (e) and Run 3 (f)).

4.2.5.3. Catalysis oxidation of limonene

Oxidation reaction of limonene could lead to several different products corresponding to epoxidation with LO (cis and trans) and epoxide opening LD (ax and eq) and allylic oxidation (carveol C^{ol}, and carvone C^{one}).

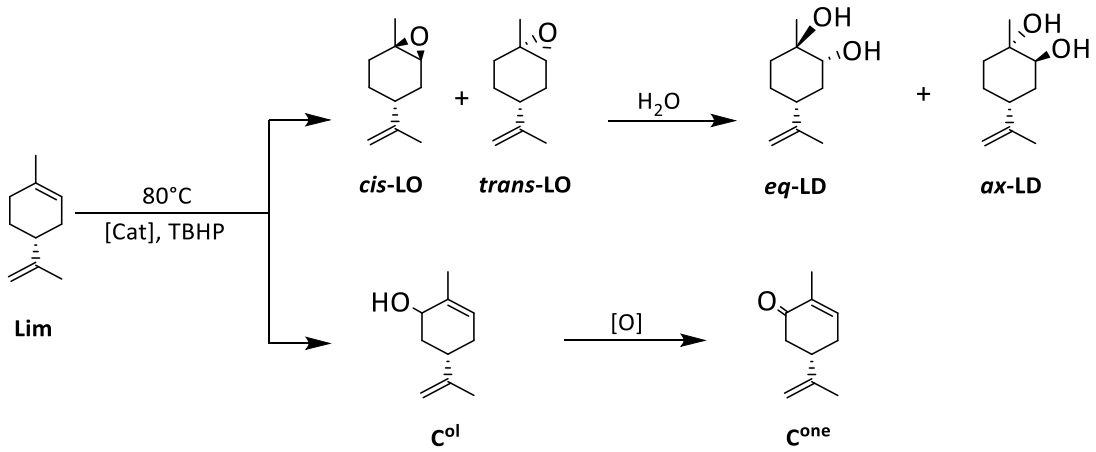

Scheme 5- Oxidation reaction of limonene.

Under the same conditions than for CO, results have been complied in Table 5 (and Figure 14). The results are strongly depending to the nature of the catalysts. Major product observed were *ax*- and *eq*-LD for SiO_2@PMo, and carveol and carvone for SiO_2@PW_{12}. This observation goes in straight line with observations done with CH.

Activity of SiO_2@PMo is higher than SiO_2@PW after each run (Fig. 15). This can be also assumed by the absence of LO with Mo after 24h, (but present at 6 hours) and the presence of LDs. This was previously observed with other type of complexes.[8m] Catalysts have very weak influence on allylic oxidation which could explain the similar selectivity of carveol and carvone. Durability of SiO_2@PM were also proved by recycling with average TONs of 110 and 228 for SiO_2@PW and SiO_2@PMo respectively.

Table 6 - Relevant data for the catalysed oxidation of limonene.[1]

Catalyst	Run	Lim Conv[2]	*cis*-LO sel[3]	*trans*-LO sel[3]	*ax*-LD sel[3]	*eq*-LD sel[3]	C^{ol} sel[3]	C^{one} sel[3]	TON[4]
$H_3PW_{12}O_{40}$	1	67	0	0	5	3	1	4	1287
SiO_2@PW	1	58	0	3	13	1	8	8	754
	2	59	0	3	13	1	10	8	768
	3	62	0	2	12	2	11	8	754
$H_3PMo_{12}O_{40}$	1	99	0	0	18	10	1	2	1859
SiO_2@PMo	1	91	0	0	36	11	4	3	1721
	2	86	0	0	32	8	6	7	1626
	3	81	0	< 1	20	5	6	6	1526

[1] Conditions: 80°C. POM/TBHP/Lim=0.070/150/100 for W, 0.058/150/100 for Mo; *t*=24h.

[2] nLim converted/nLim engaged (%) after 24h. [3] n product formed/ nLim converted at 24h.

[4] nLim transformed /nPOM at 24h.

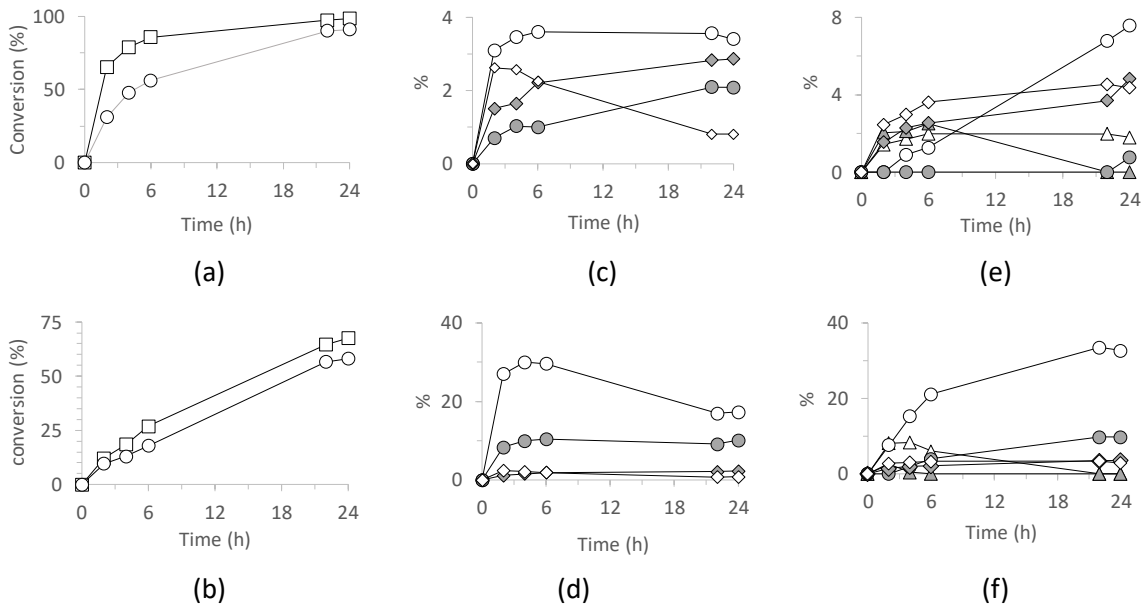

Figure 14 - (a) Comparison of Lim conversion between (a) $H_3PW_{12}O_{40}$ (□) and **SiO_2@PW** (○), (b) $H_3PMo_{12}O_{40}$ (□) and **SiO_2@PMo** (○). Evolution of *trans*-LO (△), *cis*-LO CHD (▲), eq-LD (●), ax-LD (○), C^{ol} (◇) and C^{one} (◆) with (c) $H_3PW_{12}O_{40}$, (d) $H_3PMo_{12}O_{40}$, (e) **SiO_2@PW** (Run 1) (f) **SiO_2@PMo** (Run 1).

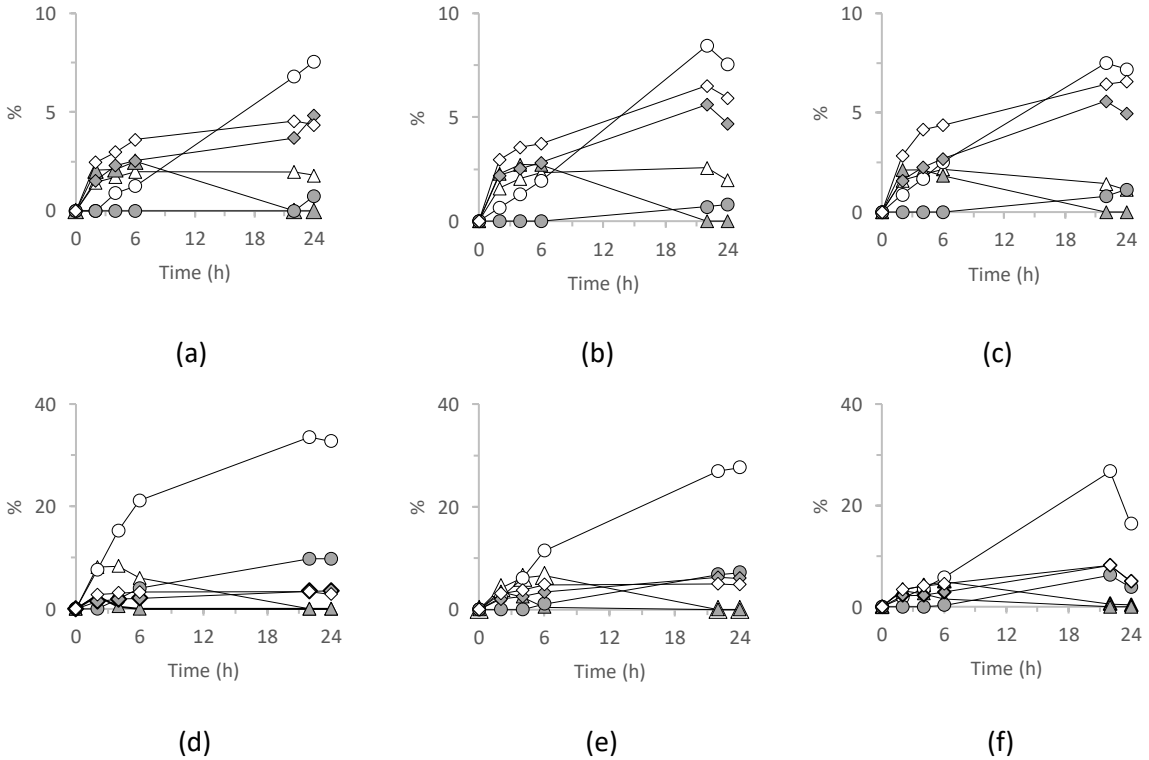

Figure 15 - (a) Evolution of *trans*-LO (△), *cis*-LO CHD (▲), eq-LD (●), ax-LD (○), C^{ol} (◇) and C^{one} (◆) with **SiO_2@PW** (Run 1 (a), Run 2 (b) and Run 3 (c)) and **SiO_2@PMo** (Run 1 (d), Run 2 (e) and Run 3 (f)).

4.2.5.4. Catalysis oxidation of cyclohexanol

Cyclohexanol (CYol), is a precursor of adipic acid, i.e. one component of KA oil. Cyclohexanone (CYone) was the only oxidation product that was observed. Under same catalytic conditions than for CO and Lim, results have been compiled in Table 7 and Fig. 15.

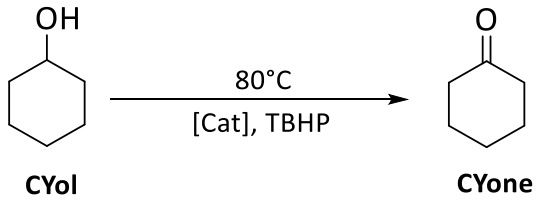

Scheme 6 - Catalyzed oxidation of CYol.

Table 7 - Relevant data for the catalysed oxidation of cyclohexanol after 24 hours.[1]

Catalyst	Run	CYol Conversion[2]	CYone Selectivity[3]	TON[4]
$H_3PW_{12}O_{40}$	1	44	34	525
SiO_2@PW	1	11	51	137
	2	8	97	101
	3	7	87	92
$H_3PMo_{12}O_{40}$	1	58	54	728
SiO_2@PMo	1	18	76	228
	2	17	90	207
	3	20	75	249

[1] Conditions: 80°C. POM/TBHP/CYol=0.070/150/100 for W, 0.058/150/100 for Mo; *t*=24h.

[2] n CYol converted/n CYol engaged (%) after 24h.

[3] n CYone formed/ nCYol converted (%) at 24h.

[4] n CYol transformed /nPOM at 24h.

Both grafted catalysts have low conversion, **SiO_2@PMo** being more active than **SiO_2@PW_{12}** (with average conversion of 10 and 18% respectively) but with moderate activity compared to the free POMs. Although slow, the processes are more selective when grafted. Recycling of the catalyst was interesting with similar conversions within the time. (Fig. 16)

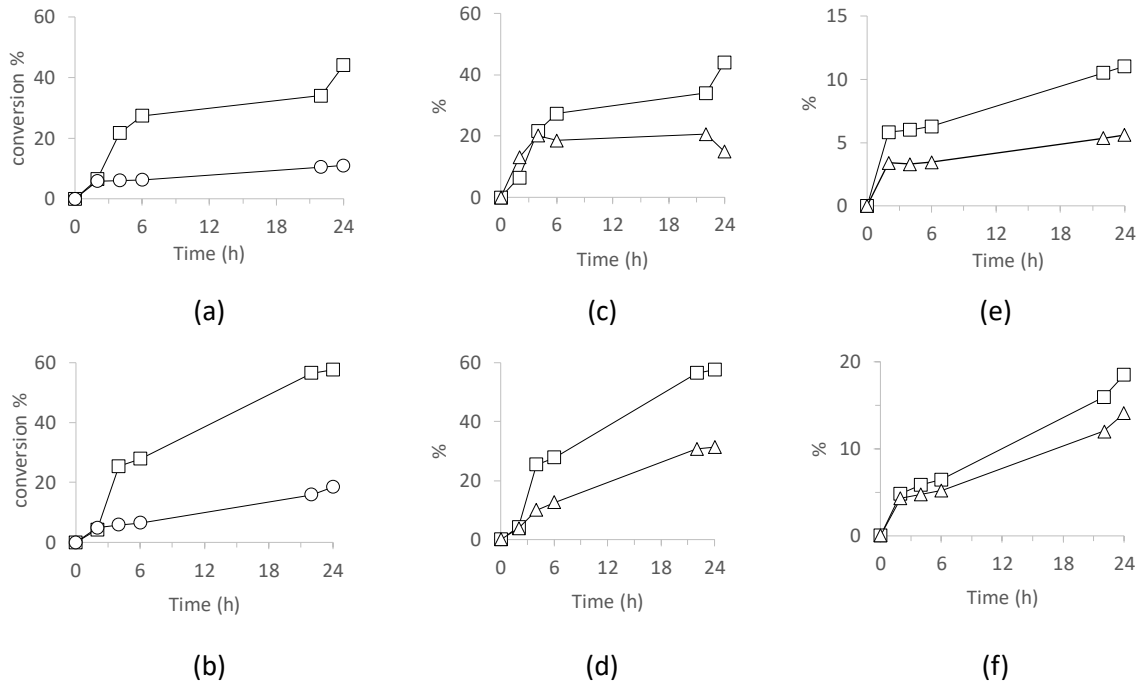

Figure 15 - Comparison of CYol conversion between (a) $H_3PW_{12}O_{40}$ (□) and **SiO_2@PW** (O), (b) $H_3PMo_{12}O_{40}$ (□) and **SiO_2@PMo** (O). Conversion of CYol (□) and formation of CYone (△) with (c) $H_3PW_{12}O_{40}$, (d) $H_3PMo_{12}O_{40}$, (e)**SiO_2@PW** (Run 1) and(f) **SiO_2@PMo** (Run 1).

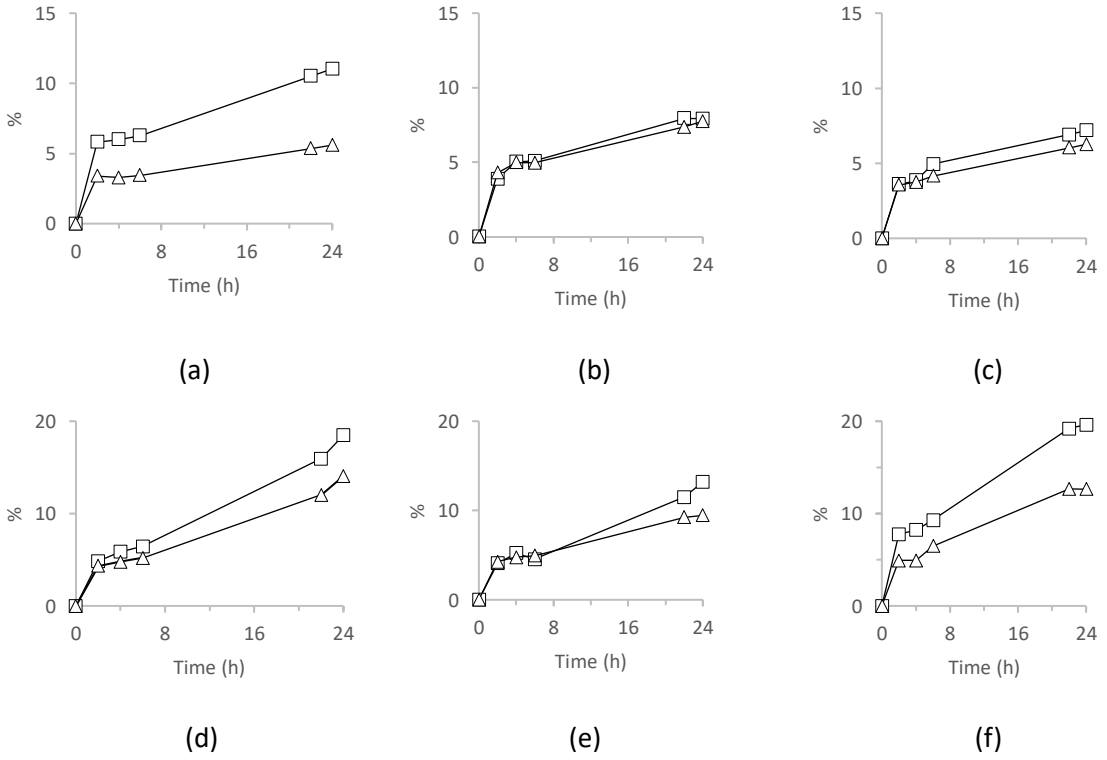

Figure 16 - Conversion of CYol (□) and formation of CYone (△) with **SiO_2@PW (**Run 1 (a), Run 2 (b) and Run 3 (c)) and **SiO_2@PMo** (Run 1 (d), Run 2 (e) and Run 3 (f)).

4.3. Conclusion

Ionic immobilization of POMs on silica beads functionalized by APTES has led to the development of new catalytic materials (SiO_2@PM) used for organic solvent-free (ep)oxidation reactions, showing with the studied substrates better selectivity than the corresponding free POMs. Morphological (DLS and TEM) studies of the SiO_2@PM objects exhibited interesting behavior with ionic interactions going to dynamic particles agglomeration. This phenomenon seems to ensure the stability of non-monolithic recoverable catalytic objects, interesting in terms of potential industrial use. This methodology of catalysis uses *organic solvent-free process*, *smoother oxidant, minimal catalyst loading and catalyst recyclability* in straight line with some principles of green chemistry. This environmentally benign protocol with a new type of catalytic materials can be easily modulated (other functionalization on beads, other grafted catalysts, other catalyzed reactions) and does open a new field of future investigations.

4.4. Experimental part

4.4.1. Materials

All manipulations were carried out under air. Distilled water was used directly from a Milli-Q purification system (Millipore). Acetonitrile, ethanol, methanol, diethyl ether (synthesis grade, Aldrich) were used as solvents and employed as received. Tetraethyl orthosilicate (TEOS, 98% Aldrich), Ammonium hydroxide solution (25%, Aldrich), 3-Aminopropyltriethoxysilane (APTES, 99%, Aldrich), *cis*-cyclooctene (CO, 95%, Alfa Aesar), cyclooctene oxide (COE, 99%, Aldrich), cyclohexene (CH, 99%, Acros), cyclohexene oxide (CHO, 98%, Aldrich), 2-cyclohexen-1-ol (CHol, 95%, TCI), 2-cyclohexen-1-one (CHone, 96%, TCI), *cis*-1,2-cyclohexanediol (CHD, 99%, Acros), limonene (Lim, 98%, Aldrich), limonene oxide (LO *cis*/*trans* mixture, 97%, Aldrich), (1S, 2S, 4R)-(+)-limonene-1,2-diol (*ax*-LD, 97%, Aldrich), L-carveol (C^{ol} *cis*/*trans* mixture, 95%, Aldrich), (R)-(-) Carvone (C^{one} 98%, Aldrich), cyclohexanol (CYol, 99%, Alfa Aesar), cyclohexanone (CYone, 99.8%, Acros), Phosphotungstic acid hydrate (reagent grade, Aldrich), molybdatophosphoric acid hydrate (reagent grade, Merck), and TBHP (70% in water, Aldrich) were used as received. The pure *cis*-LO, *trans*-LO and *eq*-LD were synthesized according to literature procedures. [52]

4.4.2. Methods

Powder X-Ray diffraction: The solids were analysed by X-ray diffraction (XRD) with a Bruker D2 X'Pert PRO diffractometer using Cu Kα radiation (40 kV and 40 mA).

Dynamic Light Scattering: in order to be able to obtain repetitive and correct data analysis, particle samples were prepared at 0.1wt.% in water. - Sonication of particles suspension was made before DLS analysis during 10 min at 350 W (FB705 Fisherbrand Ultrasonic Processor) and using an ice bath, facilitating the dispersion of Silica Particles. - Hydrodynamic diameters of the particles in suspension were obtained with a ZetaSizer Nano-ZS (Malvern Instruments Ltd) at 25°C. This equipment uses a laser (He-Ne at λ=633 nm, under voltage of 3 mV) and the detector is located at 173 ° to analyse the scattered intensity fluctuations.

TEM: Particles morphology were performed with a JEOL JEM1011 transmission electron microscope equipped with 100 kV voltage acceleration and tungsten filament (Service Commun de Microscopie Electronique TEMSCAN, Centre de Microcaractérisation Raimond Castaing, Toulouse, France). A drop of sonicated particles solution (at 0.1wt.% in water) was disposed on a formvar/carbon-coated copper grid (400 mesh) and dried in air for 48 h.

Infrared spectroscopy: Fourier Transform infrared (FTIR) spectra were recorded by Spectrum two – PerkinElmer.

Solid state NMR: NMR experiments were recorded on Bruker Avance 400 III HD spectrometers operating at magnetic fields of 9.4 T. Samples were packed into 4mm zirconia rotors. The rotors were spun at 8 kHz at 293K. ^{1}H MAS was performed with DEPTH pulse sequence and a relaxation delay of 3s. For ^{29}Si MAS single pulse experiments, small flip angle of 30° were used with a recycle delays of 60 s. ^{13}C CP and ^{29}Si CP MAS spectra were recorded with a recycle delay of 2s and contact times of 3ms and 4ms, respectively. Chemical shifts were referenced to TMS. All spectra were fitted using the DMfit software.

Solution NMR: ^{1}H-NMR, ^{13}C-NMR and ^{31}P-NMR spectra were recorded on Bruker NMR III HD 400 MHz spectrometers. 400 MHz for ^{1}H-NMR, 101 MHz for ^{13}C-NMR and 162 MHz for ^{31}P-NMR.

Quantification of the number of functions per gram of grafted silica through ^{1}H NMR in solution: 7 mg of SiO_2@R (R= NH_2, PM) were added in 4 mL of D_2O/NaOH solution (pH≈13) in an NMR tube. The mixture was heated until the powder completely dissolved. A known amount of benzoic acid (ca. 4 mg) was added as internal standard. Then the NMR proton data were collected immediately.

Quantification of the number of POMs per gram of grafted silica through ^{31}P NMR in solution: 7 mg of SiO_2@PM was added in 4 mL of D_2O/NaOH solution (pH≈13) in an NMR tube. The mixture was heated until the powder completely dissolved. The PM amount per gram of SiO_2@PM sample were calculated from calibration curves (r^2 = 0.999) obtained with different concentrations on phosphates at the same pH.

Elemental analysis: Elemental analyses (EA) were performed by the LCC microanalysis service

Centrifugation: The silica beads were collected by centrifugation on a Fisher 2-16P with 11192 rotor (Max. rpm 4500, Sigma).

Gaz Chromatography: The catalytic reactions were followed by gas chromatography (GC) on an Agilent 7820A chromatograph equipped with an FID detector, a DB-WAX capillary column (30m × 0.32mm × 0.5µm) and autosampler. Authentic samples of reactants (cyclooctene, cyclohexene, limonene, cyclohexanol) and some potential products (cyclooctene oxide, cyclohexene oxide, 2-cyclohexen-1-ol, *cis*-1.2-cyclohexanediol, 2-cyclohexen-1-ol, L-carveol, R-carvone, limonene oxide, limonene-diol and cyclohexanone) were used for calibration. The Lim conversion and the formation of LimOs and limDs were calculated from the calibration curves (r^2 = 1) and an internal standard.

4.4.3. Synthesis

- Synthesis of Stöber **SiO_2** nanoparticles.

72 mL (4 mol) of H_2O, 60 mL of ammonic solution (28%wt) were mixed in 630 mL (15.57 mol) of methanol at room temperature. 40 mL (0.18 mol) of tetraethyl orthosilicate (TEOS) were added into the solution. A suspension of a white solid appeared. The mixture was stirred at 50°C for 6 hours. Then the solid was washed by absolute ethanol 5 times and was collected by centrifugation. SiO_2 nanoparticles were dried under vacuum at 120°C overnight. A white powder was obtained.

SiO_2:
^{1}H NMR (400 MHz, D_2O/NaOH-Benzoic acid) δ 7.65 (m, 2H, Ar-H), 7.29 (m, 3H, Ar-H), 3.10 (s, 3H, CH_3).
^{29}Si CP MAS-NMR: -93.3 ppm (Q^2), -101.9ppm (Q^3), -111.8 ppm (Q^4).
Elem. Anal. Found: C, 1.09; H, 0.67.
IR (ATR, ν(cm^{-1})): 3707-2930 (OH), 1053 (Si-O-Si), 942 (Si-OH), 795 and 434 (Si-O-Si).

- Synthesis of **SiO_2@NH_2** particles.

3.5 g of **SiO_2** particles were mixed with 12.08 mL (51.6 mmol) of APTES in 87.5 mL (823.3 mmol) of toluene. The mixture was refluxed under stirring for 18h. The product was washed by toluene (5x40 mL) and collected by centrifugation. The collected powder was dried under vacuum at 120°C overnight.

SiO_2@NH_2:
^{1}H NMR for the quantification (400 MHz, D_2O/NaOH-Benzoic acid) δ 7.6 (m, 2H, Ar-H), 7.25 (m, 3H, Ar-H), 3.33 (q, *J*=7.1Hz, 0.07H, CH_2), 3.03 (s, 0.09H, CH_3), 2.25 (t, *J*=7.0Hz 0.21H, CH_2), 1.18 (m, 0.23H, CH_2), 0.87 (t, *J*=7.1Hz 0.1H, CH_3), 0.08 (m, 0.23H, CH_2).
^{29}Si CP MAS-NMR : -62.1 ppm (T^2), -67.7 ppm (T^3), -92.8 ppm (Q^2), -102.0 ppm (Q^3), -111.5 ppm (Q^4).
^{13}C CP MAS-NMR : 60.4 ppm (CH_2O), 58.2 ppm (CH_2O), 50.9 ppm (CH_2N), 42.3 ppm (CH_2N), 21.5 ppm (CH_2), 16.5 ppm (CH_3), 9.6 ppm (CH_2Si).
EA. Found: C, 3.74; H, 1.32; N, 0.74%.
IR (ATR, ν(cm^{-1})) :3700-2969 (OH and NH), 1485 (CH_2 and NH_2), 1049 (Si-O-Si), 939 (Si-OH), 785 and 429 (Si-O-Si).
ρ(NH_2) (mmol/g) = 0.52 (^{1}H NMR), 0.53 (EA).

- Syntheses of **SiO_2@PM** objects

500 mg of **SiO_2@NH_2** and 0.32 g (0.1 mmol) of $H_3PW_{12}O_{40}$-$15H_2O$ (0.23 g for $H_3PMo_{12}O_{40}$-$26H_2O$) were mixed in 10 mL of H_2O at 60°C and stirred for 24 hours. The product was washed by H_2O (3x40 mL), collected by centrifugation as a powder and dried under vacuum at 120°C overnight.

SiO_2@PW:

^{1}H NMR for the quantification (400 MHz, D_2O/NaOH-Benzoic acid) δ 7.66 (m, 2H, Ar-H), 7.31 (m, 3H, Ar-H), 3.41 (q, *J*=7.1Hz, 0.11H, CH_2), 3.10 (s, 0.09H, CH_3), 2.33 (t, *J*=7.0Hz, 0.18H, CH_2), 1.26 (m, 0.18H, CH_2), 0.94 (t, *J*=7.1Hz, 0.16H, CH_3), 0.17 (m, 0.19H, CH_2).

^{29}Si CP MAS-NMR : -58.3 ppm (T^2), -67.9 ppm (T^3), -93.0 ppm (Q^2), -102.1 ppm (Q^3), -111.7 ppm (Q^4).

^{13}C CP MAS-NMR : 59.9 ppm (CH_2O), 58.2 ppm (CH_2O), 50.8 ppm (CH_2N), 42.8 ppm (CH_2N), 20.6 ppm (CH_2), 16.6 ppm (CH_3), 9.2 ppm (CH_2Si).

^{31}P CP MAS-NMR: -12.8 ppm.

IR (ATR, ν(cm^{-1})) :3700-2969 (-OH and -NH), 1485 (CH_2 and NH_2), 1065 (P-O),1067 (Si-O-Si), 981 (W-O), 873 (W-O-W), 785 and 429 (Si-O-Si).

EA. Found: C, 2.99; H, 0.89; N, 0.43%.

ρ(NH_2) (mmol/g) = 0.33 (by ^{1}H NMR), 0.31 by elemental analysis.

ρ(PW_{12}) (mmol/g) = 0.15 (by EA), 0.14(by ^{31}P NMR).

SiO_2@PMo:

^{1}H NMR for the quantification (400 MHz, D_2O/NaOH-Benzoic acid) δ 7.65 (m, 2H, Ar-H), 7.30 (m, 3H, Ar-H), 3.41 (q, *J*=7.1Hz, 0.16H, CH_2), 3.10 (s, 0.13H, CH_3), 2.33 (t, *J*=7.0Hz, 0.25H, CH_2), 1.26 (m, 0.28H, CH_2), 0.94 (t, *J*=7.1Hz, 0.23H, CH_3), 0.17 (m, 0.27H, CH_2).

^{29}Si CP MAS-NMR : -58.6 ppm (T^2), -68.2 ppm (T^3), -93 ppm (Q^2), -102.1 ppm (Q^3), -111.7 ppm (Q^4).

^{13}C CP MAS-NMR : 59.9 ppm (CH_2O), 58.2 ppm (CH_2O), 50.9 ppm (CH_2N), 42.9 ppm (CH_2N), 20.7 ppm (CH_2), 16.6 ppm (CH_3), 8.8 ppm (CH_2Si).

^{31}P CP MAS-NMR: -1.5 ppm.

IR (ATR, ν(cm^{-1})) :3700-2969 (-OH and -NH), 1485 (CH_2 and NH_2), 1065 (P-O),1068 (Si-O-Si), 944 (Mo-O), 879 (Mo-O-Mo), 785 and 443 (Si-O-Si).

Elem. Anal. Found: C, 2.49; H, 1.29; N, 0.59%.

ρ(NH_2) (mmol/g) = 0.40 (^{1}H NMR), 0.41 (EA).

ρ(PMo_{12}) (mmol/g) =0.12 (EA), 0.12 (^{31}P NMR).

4.4.4. Catalytic experiments

- Epoxidation of cyclooctene

1.09 g (9.89 mmol) of cyclooctene, a quantity of catalyst (24.6 mg (7.8 µmol) of $H_3PW_{12}O_{40}$-$15H_2O$ or 13.2 mg (5.7 µmol) of $H_3PMo_{12}O_{40}$-$26H_2O$ or 50 mg of **SiO_2@PM** (7.7 µmol for PW_{12} 5.7 µmol for PMo_{12})) and 0.35 mL (2.83 mmol) of acetophenone (internal standard) were mixed in a 25 mL flask. 2.05 mL (14.84 mmol) of TBHP (70wt.% in H_2O) were added into the mixture when the temperature was stabilized at 80°C. The reaction mixture was heated at 80 °C under stirring for 24h. The reaction was followed by GC-FID.

- Epoxidation of cyclohexene

With free-POM: 5 g (60.9mmol) of cyclohexene were mixed with 26.9 mg (8.5 µmol) $H_3PW_{12}O_{40}$. $15H_2O$ (or 15.4mg (6.7 µmol) for $H_3PMo_{12}O_{40}.26H_2O$) and 0.7 mL (5.66 mmol) of acetophenone (internal standard). 12.5 mL (91.3mmol) of TBHP (70wt.% in H_2O) were added into the mixture at 60°C and the solution was left under stirring for 48h. The reaction was followed by GC-FID.

With ***SiO_2@POM***: 6.3 g (77 mmol) of cyclohexene, 75 mg **SiO_2@PM** (11.5 mol for PW_{12}, 8.14 µmol for PMo_{12}) and 0.7 mL (5.66 mmol) of acetophenone (internal standard) were mixed in a 50 mL flask. 15.2 mL (111.3 mmol) of TBHP (70 wt.% in H_2O) were added into the mixture at 60°C and left under stirring for 48h. The reaction was followed by GC-FID.

- Epoxidation of limonene

2 g (14.9 mmol) of limonene, 33.3 mg (10.4 µmol) of $H_3PW_{12}O_{40}.15H_2O$ or 19.6 mg (8.6 µmol) of $H_3PMo_{12}O_{40}.26H_2O$) or 75 mg of **SiO_2@PM** (11.5 µmol for PW_{12}, 8.6 µmol for PMo_{12}) and 0.7 mL (5.66 mmol) of acetophenone (internal standard) were mixed in a 50 mL flask. 3.05 mL (22.3 mmol) of TBHP (70 wt.% in H_2O) were added into the mixture at 80°C. Then the mixture was heated at 80°C under stirring for 24h. The reaction was followed by GC-FID.

- Oxidation of cyclohexanol

With free-POM: 2 g (20 mmol) of cyclohexanol, 49.7 mg (14 µmol) of $H_3PW_{12}O_{40}$-$15H_2O$ (23.5 mg (11.6 µmol) for $H_3PMo_{12}O_{40}$-$26H_2O$) and 0.35 mL (2.83 mmol) of acetophenone (internal standard) were mixed in a 50 mL flask. 4.1 mL (29.9 mmol) of TBHP (70 wt.% in H_2O) were added into the mixture at 80°C. Then the mixture was heated at 80°C under stirring for 24h. The reaction was followed by GC-FID.

With ***SiO_2@PM***: 1.46 g (14.6 mmol) of cyclohexanol were mixed with 75 mg of **SiO_2@POM** (11.52 µmol of POM for **SiO_2@PW**, 8.6 µmol of POM for **SiO_2@PMo_{12}**) and 0.35 mL (2.83 mmol) of acetophenone (internal standard). Then 3 mL (21.9 mmol) of TBHP (70 wt.% in H_2O) were added into the mixture at 80°C. Then the mixture was stirred at 80°C for 48h. The reaction was followed by GC-FID.

- Recycling of **SiO_2@PM**

SiO_2@PM was recycled by centrifugation (Fisher 2-16P with 11192 rotor, Sigma) at 4500rpm for 30 minutes. Then, the precipitated solid was washed 3 times with absolute ethanol. The powder was collected and dried at 120°C under vacuum.

4.5. References

[1] (a) I.M. Pastor, M. Yus, *Curr. Org. Chem.* **2005**, *9*, 1–29.
(b) P.L. Matlock, W.L. Brown, N.A. Clinton, *Chem. Ind.* **1999**, *77*, 159–193.
(c) Z.S. Petrovic, *Polym. Rev.* **2008**, *48*, 109–155.
(d) S. D. McCann, S. S. Stahl, *Acc. Chem. Res.* **2015**, *48*, 1756-1766.
(e) S. E Davis, M. S. Ide, R. J. Davis, *Green Chem.* **2013**, *15* (1), 17–45.
(f) R. Ciriminna, V. Pandarus, F. Béland, Y.-J. Xu, M. Pagliaro, *Org. Process Res. Dev.* **2015**, *19*, 1554-1558.
(g) C. Parmeggiani, C. Matassini, F. Cardona, *Green Chem.* **2017**, *19*, 2030-2050.
(h) R. A. Sheldon, *Catal. Today* **2015**, *247*, 4-13.
(i) L. Marais, A. J. Swarts, *Catalysts,* **2019**, *9*, 395.
(j) X. Bai, X. Huang, L. Wen, N. Song, J. Zhang, Y. Zhang, Y. Zhao, *Chem. Commun.* **2019**, *55* (25), 3598–3601.

[2] R. N. McDonald, R. N. Steppel, J. E. Dorsey, *Org. Synth.* **1970**, 50, 15–18.

[3] E. Rose, B. Andrioletti, S. Zrig, M. Quelquejeu-Ethève, *Chem. Soc. Rev.* **2005**, *34* (7), 573–583.

[4] (a) D. Swern, in Organic Peroxides, Vol. 2, Wiley-*Interscience*, *New York*, *NY*, ***1971***, *pp*. *355-533*.
(b) B. Plesnicar, *Organic Chemistry, Part C; Trahanovsky, W. C., Ed.; Academic Press: New York, San Francisco, London,* **1978**; pp 211−294.

[5] *S. Kobayashi, K. Tahara, (Jpn. Kokai Tokkyo Koho) JP 2007230908A 2020070913,* ***2007****.*

[6] J. Sherwood, *Angew. Chem. Int. Ed.* **2018**, 57, 14286 – 14290.

[7] (a) R. A. Sheldon, I. Arends, U. Hanefeld, *Green Chemistry and Catalysis, Wiley - VCH,* Weinheim, **2007**.
(b) P. Anastas, J. Warner, *Green Chemistry: Theory and Practice, Oxford University Press,* New York, **1998**.
(c) P. Tundo, P. Anastas, D. S. Black, J. Breen, T. Collins, S. Memoli, J. Miyamoto, M. Polyakoff, W. Tumas, *Pure Appl. Chem.* **2000**, 72, 1207–1228.

[8] (a) J. Pisk, D. Agustin, V. Vrdoljak, R. Poli, *Adv. Synth. Catal*. **2011**, 353(16), 2910-2914.
(b) J. Pisk, B. Prugovecki, D. Matkovic-Calogovic, R. Poli, D. Agustin, V. Vrdoljak, *Polyhedron,* **2012**, 33(1), 441-449.
(c) J. Morlot, N. Uyttebroeck, D. Agustin, R. Poli, *ChemCatChem,* **2013**, 5(2), 601-611.
(d) B. Guerin, D. Mesquita Fernandes, J-C. Daran, D. Agustin, R. Poli, *New J. Chem.* **2013**, 37(11), 3466-3475.
(e) C. Cordelle, D. Agustin, J-C. Daran, R. Poli, *Inorg. Chim. Acta.* **2010**, 364(1), 144-149.
(f) M. Loubidi, D. Agustin, A. Benharref, R. Poli, *C.R. Chim*. **2014**, 17(6), 549-556.
(g) J. Pisk, B. Prugovecki, D. Matkovic-Calogovic, T. Jednacak, P. Novak, D. Agustin, V. Vrdoljak, *RSC Adv.* **2014**, 4(73), 39000-39010.
(h) W. Wang, T. Vanderbeeken, D. Agustin, R. Poli, *Catal. Commun.* **2015**, 63, 26-30
(i) V. Vrdoljak, J. Pisk, D. Agustin, P. Novak, J. Parlov Vukovic, D. Matkovic-Calogovic, *New J. Chem.* **2014**, 38(12), 6176-6185.
(j) W. Wang, T. Guerrero, S. R. Merecias, H. Garcia-Ortega, R. Santillan, J-C. Daran, N. Farfan, D. Agustin, R. Poli, *Inorg. Chim. Acta.* **2015**, 431, 176-183.
(k) W. Wang, J-C. Daran, R. Poli, D. Agustin, *J. Mol. Cat. A.: Chem.* **2016**, 416, 117-126.
(l) V. Vrdoljak, J. Pisk, B. Prugovecki, D. Agustin, P. Novak, D. Matkovic-Calogovic, *RSC Adv.* **2016**, 6(43), 36384-36393.
(m) W. Wang, D. Agustin, R. Poli, *Mol. Catal.* **2017**, 443, 52-59.
(n) J. Pisk, M. Rubcic, D. Kuzman, M. Cindric, D. Agustin, V. Vrdoljak, *New J. Chem.* **2019**, 43(14), 5531-5542.
(o) D. Cvijanovic, J. Pisk, G. Pavlovic, D. Sisak-Jung, D. Matkovic-Calogovic, M. Cindric, D. Agustin, V. Vrdoljak, *New J. Chem.* **2019**, 43(4), 1791-1802.

(p) V. Vrdoljak, M. Mandaric, T. Hrenar, I. Djilovic, J. Pisk, G. Pavlovic, M. Cindric, D. Agustin, *Cryst. Growth & Des.* 2019, 19(5), 3000-3011
(q) M. Cindric, G. Pavlovic, R. Katava, D. Agustin, *New J. Chem.* 2017, 41(2), 594-602.
(r) J. Pisk, J-C. Daran, R. Poli, D. Agustin, *J. Mol. Cat. A.: Chem.* 2015, *403*, 52-63.
(s) V. Damjanović, J. Pisk, D. Kuzman, D. Agustin, V. Vrdoljak, V. Stilinović, M. Cindrić, *Dalton Trans.* 2019, *48 (27)*, 9974–9983.

9 R. Landau, G. A. Sullivan, D. Brown, *Chemtech* 1979, 9, 602–607.

10 J. Pisk, D. Agustin, R. Poli, *Molecules*, 2019, 24(4), 783.

11 (a) R. Richards, U. Kortz, L. Bi, K. Zhu, A. Suchopar, L. Cheng, *Patent*, WO 2007/142727
(b) S. S. Balula, L. Cunha-Silva, I. C. M. S. Santos, A; C. Estrada, A. C. Fernandes, J. A. S. Cavaleiro, J. Pires, C. Freire, A. M. V. Cavaleiro, *New J. Chem.*, 2013, 37, 2341
(c) V. N. Panchenko, I. Borbath, M. N. Timofeeva, S. Gobolos, *J. Mol. Cat. A.: Chem.* 2010, 319, 119-125.
(d) X. Li, P. Jiang, Z. Wang, Y. Huang, *Catalysts,* 2016, *6* (1), 2.
(e) R. Neumann, H. Miller, *J. Chem. Soc., Chem. Commun.* 1995, 2277-2778.

12 (a) A. Simon, T. Cohen-Bouhacina, M. C. Porte, J. P. Aime, C. Baquey, *J. Colloid Interface Sci.* 2002, 251,278–283.
(b) F. Cuoq, A. Masion, J. Labille, J. Rose, F. Ziarelli, B. Prelot, J.-Y. Bottero, *Appl. Surf. Sci.* 2013, 266, 155– 160.
(c) B. Qiao, T.-J. Wang, H. Gao, Y. Jin, *Appl. Surf. Sci.* 2015, 351, 646–654.

13 (a) N. M. Okun, T. M. Anderson, C. L. Hill, *J. Am. Chem. Soc.* 2003, 125, 3194-3195.
(b) N. M. Okun, T. M. Anderson, C. L. Hill, *J. Mol. Cat. A.: Chem.* 2003, 197, 283–290

14 (a) W-J. Wu, J. Wang, M. Chen, D-J. Qian, M. Liu, *J. Phys. Chem. C,* 2017, 121, 2234−2242
(b) J. Wang, Q. Hao, *J. Alloys Compd.* 2009, 482, 235–239.

15 R. K. Sharma, S. Sharma, S. Gulati, A. Pandey, *Anal. Methods*, 2013, 5, 1414-1426.

16 J. H. Lee, J. H. Kim, K. Choi, H. G. Kim, J. A. Park, S. H. Cho, S. W. Hong, J. Lee, J. H. Lee, S.-J. Lee, S. Y. Lee, J. Lee, W. *Sci. Rep.* 2018, *8* (1), 12078.

17 J. Goscianska, A. Olejnik, I. Nowak, *Colloids Surf., A,* 2017, *533*, 187–196.

18 (a) L. S. Nogueira, S. Ribeiro, C. M. Granadeiro, E. Pereira, G. Feio, L. Cunha-Silva, S. S. Balula, *Dalton Trans.* 2014, 43, 9518–9528
(b) N. M. Okun, M. D. Ritorto, T. M. Anderson, R. P. Apkarian, C. L. Hill, *Chem. Mater.* 2004, *16*, 2551-2558.

19 (a) A. Naz, S. Arun, S.S. Narvi, M.S. Alam, A. Singh, P. Bhartiya, P.K. Dutta, Int. *J. Biol. Macromol.* 2018, 110, 215–226.

(b) K. Talreja, I. Chauhan, A. Ghosh, A. Majumdar, B.S. Butola, *RSC Adv.* 2017, 7(78), 49787–49794.

(c) R. van den Berg, T. E. Parmentier, C. F. Elkjær, C. J. Gommes, J. Sehested, S. Helveg, P. E. de Jongh, K. P. de Jong, *ACS Catal*. 2015, 5(7), 4439–4448.

(d) M. Sándor, C.L. Nistor, G. Szalontai, R. Stoica, C.A. Nicolae, E. Alexandrescu, J. Fazakas, F. Oancea, D. Donescu, *Materials* 2016, 9(1), 34.

20 W. Stöber, A. Fink, E. Bohn, *J. Colloid Interface Sci.* 1968, *26* (1), 62–69.

21 J. Bu, R. Li, C. W. Quah, K. J. Carpenter, *Macromolecules*, 2004, *37* (18), 6687–6694.

22 A. Dolbecq, E. Dumas, C. R. Mayer, P. Mialane, *Chem. Rev.* 2010, *110* (10), 6009–6048.

23 (a) T. Gholami, M. Salavati-Niasari, M. Bazarganipour, E. Noori, *Superlattices Microstruct.* 2013, 61, 33–41
(b) S. Azarshin, J. Moghadasi, Z. A Aboosadi, *Energy Explor. Exploit.* 2017, 35(6), 685–697

24 W. Cai, Y. Zhou, R. Bao B. Yue, H. He, *Chin. J. Catal*., 2013, 34(1) 193-199

[25] J. Stetefeld, S. A. McKenna, T. R. Patel *Biophys Rev,* **2016**, 8,409–427

[26] M. Kobayashi, F. Juillerat, P. Galletto, P. Bowen, M. Borkovec, *Langmuir*, **2005**, 21, 5761-5769

[27] E. D. H. Mansfield, Y. Pandya, E. A. Mun, S. E. Rogers, I. Abutbul-Ionita, D. Danino, A. C. Williams, V. V. Khutoryanskiy, *RSC Adv.*, **2018**, 8, 6471-6478.

[28] C. S. Neves, C. M. Granadeiro, L. Cunha-Silva, D. Ananias, S. Gago, G. Feio, P. A. Carvalho, P. Eaton, S. S. Balula, E. Pereira, *Eur. J. Inorg. Chem.* **2013**, 2877–2886

[29] S. L. Greasley, S. J. Page, S. Sirovica, S. Chen, R. A. Martin, A. Riveiro, J. V. Hanna, A. E. Porter, J. R. Jones, *J. Colloid Interface Sci.* **2016**, 469, 213–223

[30] V. Mahalingam, S. Onclin, M. Peter, B. Jan Ravoo, J. Huskens, D. N. Reinhoudt, *Langmuir,* **2004**, *20*, 11756-11762.

[31] S. Martín, Y. Takashima, C-G. Lin, Y-F. Song, H. N. Miras, L. Cronin *Inorg. Chem*. **2019** 58 (7), 4110-4116.

[32] K. S. Aneja, K. S. Bohm, A. S. Khanna, H. L. Mallika Bohm, *Nanoscale* **2015**, 7 (42), 17879–17888.

[33] (a) T. Karimpour, E. Safaei, B. Karimi, Y.-I. Lee, *ChemCatChem* **2018**, 10 (8), 1889–1899.

(b) S. Tighadouini, S. Radi, A. Elidrissi, M. Zaghrioui, Y. Garcia, *Eur. J. Inorg. Chem.* **2019**, *2019* (27), 3180–3186.

[34] X. Luo, C. Yang, *Phys. Chem. Chem. Phys.* **2011**, *13* (17), 7892–7902.

[35] D. Kumar, C. C. Landry, *Microporous Mesoporous Mater.* **2007**, *98* (1), 309–316.

[36] M. Misono, N. Mizuno, K. Katamura, A. Kasai, Y. Konishi, K. Sakata, T. Okuhara, Y. Yoneda, *Bull. Chem. Soc. Jpn.* **1982**, *55* (2), 400–406.

[37] J. Trébosc, J. W. Wiench, S. Huh, V. S.-Y. Lin, M. Pruski, *J. Am. Chem. Soc.* 2005, 127, 3057-3068.

[38] J. C. Hicks, C. W. Jones, *Langmuir*, **2006**, *22* (6), 2676–2681.

[39] S. O. Ribeiro, C. M. Granadeiro, P. L. Almeida, J. Pires, M. C. Capel-Sanchez, J. M. Campos-Martin, S. Gago, B. de Castro, S. S. Balula, *Catal. Today,* **2019**, 333, 226–236

[40] (a) F. Bentaleb, O. Makrygenni, D. Brouri, C. Coelho Diogo, A. Mehdi, A. Proust, F. Launay, R. Villanneau, *Inorg. Chem*.**2015**, *54*, 7607–7616.
(b) C.-Y. Cheng, K.-J. Lin, M.R. Prasad, S.-J. Fu, S.-Y. Chang, S.-G. Shyu, H.-S. Sheu, C.-H. Chen, C.-H. Chuang, M.-T. Lin, *Catal. Commun.* **2007**, *8*, 1060–1064.
(c) Y. Xiao, D. Chen, N. Ma, Z. Y. Hou, M.B. Hu, C. H. Wang, W. Wang, *RSC Adv.* **2013**, *3*, 21544–21551.
(d) N. Mizuno, K. Yamaguchi, K. Kamata, *Catal Surv Asia*, **2011**, *15* (2), 68–79.

[41] I. V. Kozhevnikov, K. R. Kloetstra, A. Sinnema, H. W. Zandbergen, H. van Bekkum, *J. Mol. Catal. A: Chem.* **1996**, 114, 287-298

[42] R. Canioni, C. Roch-Marchal, F. Secheresse, P. Horcajada, C. Serre, M. Hardi-Dan, G. Ferey, J.-M. Greneche, F. Lefebvre, J.-S. Chang, Y.-K. Hwang, O. Lebedev, S. Turnerf, G.S Van Tendeloo, *J. Mater. Chem.* **2011**, 21, 1226–1233

[43] C. I. C. Crucho, C. Baleizão, J. P. S. Farinha, *Anal. Chem.* **2017**, 89(1), 681–687

[44] (a) S. Li, Q. Wan, Z. Qin, Y. Fu, Y. Gu, *Langmuir* **2015**, 31 (2), 824–832.
(b) A. Labrosse, A. Burneau, *J. Non-Cryst. Solids*, **1997**, 221(2), 107–124.
(c) Q. Wan, C. Ramsey, G. Baran, *J. Therm. Anal. Calorim.* **2010**, 99 (1), 237–243.
(d) V. M. Masalov, N. S. Sukhinina, E. A. Kudrenko, G. A. Emelchenko, *Nanotechnology*, **2011**, 22(27), 275718.
(e) D. N. Mangos, T. Nakanishi, D. A. Lewis, *Sci. Technol. Adv. Mater.* **2014**, 15 (1).

[45] (a) M. Carraro, A. Sartorel, M; Ibrahim, N. Nsouli, C; Jahier, S. Nlate, U. Kortz, M. Bonchio, Polyoxometalate as Homogeneous Oxidation Catalysts in *Innovative Catalysis in Organic*

Synthesis: Oxidation, Hydrogenation, and C-X Bond Forming Reaction, Ed: P. Andersson, John Wiley & Sons, 2012; pp. 3–24.
(b) R. Neumann, Applications of Polyoxometalates in Homogeneous Catalysis. *In Polyoxometalate Molecular Science*, Borrás-Almenar, J. J., Coronado, E., Müller, A., Pope, M., Eds.; NATO Science Series; Springer Netherlands: Dordrecht, 2003; pp 327–349.
(c) E. Rafiee, S. Eavani, *Curr. Org. Chem.* 2017, 21(9), 752-778
(d) D. Duprez, F. Cavani, Handbook of Advanced Methods And Processes In Oxidation Catalysis: From Laboratory To Industry; World Scientific, Imperial College Press, London, United Kingdom, 2015
(e) M. Carraro, G. Fiorani, A. Sartorel, M. Bonchio, In Handbook of Advanced Methods and Processes in Oxidation Catalysis; Imperial College Press, London, United Kingdom, 2011; pp 586–630.
(f) O. A. Kholdeeva, N. V. Maksimchuk, G. M. Maksimo, *Catal. Today*, 2010, *157*, 107–113.

46 L. Zhang, S. Song, N. Yang, X. Tantai, X. Xiao, B. Jiang, Y. Sun, *Ind. Eng. Chem. Res.* 2019 58(9), 3618-3629

47 (a) M. Masteri-Farahani, M. Modarres, *J. Mol. Catal. A: Chem*. 2016, 417, 81–88.
(b) X. Song, W. Zhu, K. Li, J. Wang, H. Niu, H. Gao, W. Gao, W. Zhang, J. Yu, M. Jia, *Catal. Today,* 2015, 259, 59–65.
(c) Z. Karimi, A.R. Mahjoub, S.M. Harati, *Inorg. Chim. Acta*, 2011, 376, 1–9.

48 (a) W. Gao, X. Sun, H. Niu, X. Song, K. Li, H. Gao, W. Zhang, J. Yu, M. Jia, *Microporous Mesoporous Mater.* 2015, 213, 59-67.
(b) X. Song, D. Hu, X. Yang, H. Zhang, W. Zhang, J. Li, M. Jia, J. Yu, *ACS Sustainable Chem. Eng.* 2019 7 (3), 3624-3631.

49 M. Mohammadi, A. Khazaei, A. Rezaei, Z. Huajun, S. Xuwei, *ACS Sustainable Chem. Eng.* 2019 7 (5), 5283-5291

50 C. Jiménez-González, A. D. Curzons, D. J. C. Constable, V. L. Cunningham, *Clean Technol. Environ. Policy.* 2004, *7* (1), 42–50.

51 J. Y. Wang, M. D. Zhou, Y. G. Yuan, N. H. Fu, S. L. Zang, *Russ. J. Gen. Chem.* 2015, *85* (10), 2378–2385.

52 (a) M. Blair, P. C. Andrews, B. H. Fraser, C. M. Forsyth, P. C. Junk, M. Massi, K.L. Tuck. *Synthesis* 2007, 1523-1527
(b) M. J. van der Werf, H. Jongejan, M. C. R. Franssen. *Tetrahedron Lett*., 2001, 42, 5521-5524
(c) D. Steiner, L. Ivison, C. T. Goralski, R. B. Appell, J. R. Gojkovic, B. Singaram. *Tetrahedron: Asymmetry,* 2002, 13, 2359-2363

General conclusions and perspectives

Conclusions

During this work, different strategies have been explored to obtain new oxidation catalysts in the straight lines with some Principles of Green Chemistry.

The first strategy was based on the introduction of a second coordination sphere on metal complexes previously described as efficient catalysts for Oxygen Atom Transfer (OAT) reactions with H_2O_2 as oxidant. The aim was to obtain more efficient catalysts and mechanistic information during H_2O_2 activation notably. To create H-bond network with H_2O_2, fluoroalcohol groups have been introduced on pyridinophane tetradentate N_4-donor ligand. Corresponding metal complexes (Fe^{III}, Mn^{II}, Co^{II}, Ni^{II}) have been synthetized and fully characterized. Iron and manganese metal complexes were inefficient for epoxidation of cyclooctene with H_2O_2 as oxidant. The coordination on metal of the deprotonated free alcohol from ligand might explain the lack of reactivity. Ni^{II} and even more Co^{II} metal complexes without second sphere modification have shown interesting catalytic activity for hydrogen photoproduction using an iridium photosensitizer and Et_3N as sacrificial electron donor. The fluoroalcohol functions were introduced to **remove** acetic acid, a volatile co-reagent that favors the exclusive formation of epoxides during epoxidation reactions.

In a second part of the work, in order to **replace** the *volatile* acetic acid from the process, silica nanobeads functionalized with pendant COOH functions have been synthetized and characterized by different techniques including DLS, TEM, NMR. The silica beads were aimed to be *solid* versions of acetic acid. During the catalytic experiments, reasonable conversion of the substrates was observed but the selectivity was lower than using acetic acid. However, it has to be noted that the number of COOH functions was 100 times less with nanobeads than with acetic acid. When using acetic acid in the same conditions that nanobeads functionalized with COOH functions, no selectivity was observed. These results confirmed the effect of the silica nanobeads on the catalytic efficiency of the system. These systems are interesting, but the catalyst and the additive are still not recoverable.

Finally, with the will to **recover** the catalyst, silica nanobeads functionalized with amine pendant functions have been used as supports for commercially available Mo

and W polyoxometalates (POM) described as efficient catalysts for *organic solvent-free* (ep)oxidation reactions using TBHP as oxidant. These POM have been anchored by ionic interactions on the beads and fully characterized by different techniques such as DLS, TEM, solid state NMR. Under catalytic conditions, these catalysts were efficient for the oxidation of cyclooctene, cyclohexene, limonene and cyclohexanol. In comparison to their homogeneous analogs, better selectivity in favor of epoxides were observed. Maybe more importantly, these systems were *recyclable* and up to 3 recycling processes have been realized without significant loss of activity.

Perspectives

Based on these results in which **remove**, **replace** and **recover** were highlighted, several perspectives are possible.

Concerning the molecular part, in order to have a better understanding of the role of the second coordination sphere in oxidation reactions, new ligands are envisioned and efforts will be devoted to introduce the fluoroalcohol groups on better positions in the ligand to prevent the coordination of the alcoholate on the metal center of metal complexes. Moreover, as presented in the manuscript, Fout group has developed systems in which ligand tautomerization occurs during the activation of the oxidant to stabilize the oxidizing species. This aspect might be important to have a system able to accommodate different oxidation states by modulating the electronic charge between the ligand and the metal. Introduction of fluoroketone groups on a pyrrolide ligand able of tautomerization is envisioned. From this point, catalytic tests on classical substrates will be done.

In order to obtain more efficient processes replacing the acetic acid, it is aimed to develop other types of silica beads with sulfonic acid pending functions, since it has been shown that acetic acid could be replaced by strong acids. At this point, it will be interesting to develop different series of beads sizes, in order to evaluate the best size for a simple and efficient process, *i.e.* not too small beads since hard to recycle, not too big ones in order to diminish the charge in the reaction. Those sulfonic functions could be interesting anionic part (when deprotonated) to graft cationic entities at the surface (complexes or oxoclusters)

The strategy with the POMs and the silica beads will be further developed towards more challenging organic molecules, especially those issued from biomass

source. It is possible through this simple method to develop process with easily recoverable catalysts. Changing the catalysts by vanadium POMs could give the possibility to use O_2 as oxidant and cover other aspects, as the benzene oxidation. The facility of fabrication and handling such catalytic objects is promising in terms of fundamental studies but also for future applications. Indeed, continuous flow-reactions can be thought using those systems.

The work with the silica beads opens a large palette of applications. Building "hairy" beads (with long aliphatic chains grafted on beads) would bring the possibility to work under organic solvent-free process, the solvent being replaced by those beads that could mimic solvents. This could give the possibility to work on the oxidation of solid substrates (high molecular weight, like synthetic or natural polymers) that cannot be transformed without solvent in order to obtain high value oxidation products.

From a general point of view, all those aspects are in favor to cleaner processes, using less volatiles, simple objects and the assumed choice to create simple procedures.

Résumé

Afin de développer une chimie plus respectueuse de l'environnement, l'accès à de nouveaux procédés est nécessaire. Plus spécifiquement, dans le domaine de l'oxydation, l'utilisation d'oxydants toxiques doit être bannie, l'utilisation de solvants limitée et l'utilisation de catalyseurs recyclables développée. Dans ce contexte, deux approches « vertes » ont été explorées.

La première d'entre elle consiste à éliminer ou remplacer l'acide acétique, additif qui, en présence de H_2O_2 et de complexes de Mn ou de Fe, favorise la formation exclusive d'époxydes lors d'oxydation d'alcènes. Pour cela, deux stratégies ont été testées. La première consiste à introduire dans la seconde sphère de coordination de complexes de Fe(III) et de Mn(II) des fonctions fluoroalcools devant faciliter l'activation d'H_2O_2. Comparés aux complexes analogues non modifiés, aucune amélioration de l'activité catalytique pour l'oxydation de cyclooctène n'est observée. Cependant, des complexes de Ni(II) et de Co(II) à ligands non modifiés ont démontré une activité catalytique élevée pour la photoproduction d'hydrogène. La seconde stratégie est basée sur le remplacement de l'acide acétique. Pour cela, en utilisant des billes de silice fonctionnalisées par des fonctions COOH (SiO_2@COOH) comme co-réactif, une sélectivité significative en faveur de l'époxyde est observée lors de l'oxydation d'alcènes en présence de complexes de Mn(II) et de Fe(III) à ligand BPMEN.

La seconde approche concerne des réactions d'(ép)oxydation sans solvant et utilisant des catalyseurs recyclables à base de polyoxométallates (POMs). Les catalyseurs SiO_2@PMo et SiO_2@PW, respectivement obtenus par greffage ionique de $H_3PMo_{12}O_{40}$ ou $H_3PW_{12}O_{40}$ sur des billes de silices fonctionnalisées par des fonctions pendantes NH_2 (SiO_2@NH_2). Avec une faible charge catalytique, les deux catalyseurs sont efficaces lors de réactions d'oxydation avec une meilleure sélectivité que les POM libres. De plus, les deux catalyseurs réutilisés ont donné des conversions et des sélectivités similaires après deux recyclages.

Mots clés : Chimie verte, Catalyse, (Ep)oxydation, Recyclage du catalyseur par greffage, Nanoparticule, Procédé sans solvant organique, Métaux non toxique, eau oxygénée, Valorisation de la biomasse.

Abstract

In order to develop a chemistry more respectful of the environment, access to sustainable processes is mandatory. More specifically, in the field of oxidation chemistry, use of toxic oxidants has to be banished, use of solvents limited and reusable catalysts developed. In this context, two types of greener approaches have been explored.

The first approach concerns removal or replacement of acetic acid, an additive- in association with H_2O_2, favoring exclusive formation of epoxides with Mn and Fe metal complexes as catalysts. For this objective, two strategies have been explored. The first one consists in introducing fluoroalcohol functions in the second coordination sphere of metal complexes with pyridinophane-based ligand to easily activate H_2O_2. Those complexes did not enhance the catalytic activity for cyclooctene oxidation reactions in comparison to analogous Mn(II) and Fe(III) complexes with unmodified ligands. However, Ni(II) and Co(II) metal complexes with unmodified ligands display interesting catalytic activity for H_2 photoproduction. The second strategy aimed to replace acetic acid. Using silica beads functionalized with COOH pendant arms (**SiO_2@COOH**) as additive and H_2O_2 as oxidant, catalytic epoxidation reactions catalyzed by Mn(II) and Fe(III) metal complexes with BPMEN ligand displayed significant selectivity towards epoxide.

The second approach concerns organic-solvent free (ep)oxidation processes with catalysts based on polyoxometalates (POMs). Catalysts **SiO_2@PMo** and **SiO_2@PW**, respectively obtained by ionic grafting of $H_3PMo_{12}O_{40}$ or $H_3PW_{12}O_{40}$ on silica beads functionalized with NH_2 pending functions (**SiO_2@NH_2**), have been fully characterized. With low catalyst loading, both catalysts displayed efficient oxidation activity and better selectivity than the free POMs. Moreover, recovered beads gave similar conversion and selectivity after two recycling processes.

Key words: Green chemistry, Catalysis, (Ep)oxidation, Catalyst recycling through grafting, Nanoparticle, organic solvent-free process, non-toxic metals, Hydrogen peroxide, Valorization of biomass.